POLYMER MODIFICATION STRATEGIES TO DEVELOP NEW BIOACTIVE STRUCTURES FOR GUIDED TISSUE REGENERATION

ADARSH R.K.

Ph.D. Thesis
2022

SREE CHITRA TIRUNAL INSTITUTE FOR MEDICAL SCIENCES AND TECHNOLOGY

TRIVANDRUM

POLYMER MODIFICATION STRATEGIES TO DEVELOP NEW BIOACTIVE STRUCTURES FOR GUIDED TISSUE REGENERATION

A THESIS PRESENTED BY

ADARSH R.K.

TO

SREE CHITRA TIRUNAL INSTITUTE FOR
MEDICAL SCIENCES AND TECHNOLOGY
TRIVANDRUM
INDIA

IN PARTIAL FULFILLMENT OF THE REQUIREMENTS
FOR THE AWARD OF

DOCTOR OF PHILOSOPHY

2022

DECLARATION

I, **Adarsh R.K.**, hereby declare that I have personally carried out the work depicted in the thesis entitled ***"Polymer modification strategies to develop new bioactive structures for guided tissue regeneration"*** except where due acknowledgment has been made in the text. No part of the thesis has been submitted for the award of any other degree or diploma prior to this date.

Adarsh R.K.

Reg. No. 2016/PhD/12

20. 09. 2022

TRIVANDRUM

श्री चित्रा तिरुनाल आयुर्विज्ञान एवं प्रौद्योगिकी संस्थान, त्रिवेंद्रम, जैवचिकित्सकीय प्रौद्योगिकी स्कंध
पूजप्पुरा, तिरुवनन्तपुरम - 695 012, केरल, भारत
SREE CHITRA TIRUNAL INSTITUTE FOR MEDICAL SCIENCES AND TECHNOLOGY, TRIVANDRUM
BIO MEDICAL TECHNOLOGY WING
POOJAPPURA, THIRUVANANTHAPURAM - 695 012, KERALA, INDIA
(एक राष्ट्रीय महत्व का संस्थान, विज्ञान एवं प्रौद्योगिकी विभाग, भारत सरकार)
(An Institution of National Importance, Department of Science and Technology, Government of India)
टेलीफॉन नं./Telephone No.: 0471-2340801/ 2520450 फैक्स/Fax: 0471-2341814
ई-मेल/E-mail: sct@sctimst.ac.in वेबसाइट/Website: www.sctimst.ac.in

Dr Manoj Komath PhD,
Scientist G and in Charge,
Division of Bioceramics,
Dept. of Biomaterial Science and Technologies.
BMT Wing, SCTIMST.

CERTIFICATE

This is to certify that **Adarsh R.K.** in the Division of Bioceramics, Dept. of Biomaterial Science and Technology of this Institute has fulfilled the requirements prescribed for the Ph. D. degree of Sree Chitra Tirunal Institute for Medical Sciences and Technology, Trivandrum.

The thesis entitled, ***"Polymer modification strategies to develop new bioactive structures for guided tissue regeneration"*** was carried out under my direct supervision. No part of the thesis was submitted for the award of any degree or diploma prior to this date.

Date: 20. 09. 2022
Place: TRIVANDRUM

Dr. MANOJ KOMATH, PhD
Scientist G & In-charge, Bioceramics Division
Dept. of Biomaterials Science and Technology
Biomedical Technology Wing, SCTIMST
Poojappura, Thiruvananthapuram - 695 012

The Thesis Entitled

POLYMER MODIFICATION STRATEGIES TO DEVELOP NEW BIOACTIVE STRUCTURES FOR GUIDED TISSUE REGENERATION

Submitted By

Adarsh R K

For the award of

Doctor of Philosophy

of

SREE CHITRA TIRUNAL INSTITUTE FOR
MEDICAL SCIENCES AND TECHNOLOGY
TRIVANDRUM

is evaluated and approved

By

(*Research Guide*)

Dr. MANOJ KOMATH, Ph.D
Scientist G & HOD,
Dept of Biomaterials Science & Technology
Biomedical Technology Wing, SCTIMST
Poojappura, Trivandrum - 695012

Examiner

Professor Biman B Mandal
IIT Guwahati, Assam

Table of Contents

ACKNOWLEDGEMENTS

With deep sense of gratitude, I take this opportunity to thank all who contributed in one or the other way towards the success of this study.

First and foremost I express my sincere gratitude and respect to my Guide Dr. Manoj Komath, Scientist G and Head, Division of Bioceramics, SCTIMST for his continuous advice and encouragement throughout the course of my study. He was always accessible and took significant effort for the successful completion of this endeavor.

My sincere gratitude to the Director, SCTIMST; the Head, BMT Wing; the Dean, Registrar, Associate Dean and all the staffs of Academic Division and Administration for their help and support throughout the course. I express my profound gratitude to all the faculty members for the course work and seminars conducted.

I sincerely thank the members of my Doctoral Advisory Committee – Dr. Maya Nandkumar A., Scientist G and Head, Division of Microbial Technology, Dr. Lizymol P.P., Scientist F and Head, Division of Dental Products and Dr. Rekha M.R., Scientist F and Head, Division Of Biosurface Technology for their timely suggestions, ideas and comments which helped in improvement of quality of my work.

I am greatly indebted to the Department of Science and Technology (DST), Government of India for providing me funding for carry out this work.

My wholehearted thanks to all members (former and present) of the Division of Bioceramics : Dr. Francis Boniface Fernandez , Dr. Suresh Babu, Dr. Nishad K. V., Dr. Remya K. R. Mrs. Susan Mani, Mr. Jijo P. T., Mr. Sajin Raj, Dr. Nimmy Mohan, Dr. Eva C. Das, Dr. Beena G. Mohan, Mrs. Sreekala Balan, Ms. Gayatry G., Mrs. Ganga Anand, Ms. Saranya S. S., Mr. Sreekanth P. J., Mrs. Anchu R., Dr. Poornima, Ms. Archana, Mrs. Swathy, Mrs. Malini for their constant support, encouragement and friendship.

I am very much grateful to Dr. Muthu Jayabalan (former HOD, Polymer Division) and Dr. Shivaram Selvam (Inspire Faculty) for training me in polymer synthesis and cell culture experiments. I express my sincere thanks to all the members of Polymer Division Dr. Sunitha Prem Victor, Dr. Vineeth Vijayan, Dr. Remya Komeri, Mr. Shamon, Dr. Jibin, Mrs. Girija Seetharaman, Mrs. Gayatri, Mr. Sam and Dr. Reesha K V for their friendship and support.

I thank Dr. H.K. Varma, former Head, Division of Bioceramics for his motivation and support which helped me in my PhD tenure.

I owe my sincere thanks to Dr. P. R. Anilkumar, Scientist F and In-charge, Division of Tissue culture for granting me permission to conduct in vitro cell culture experiments at tissue culture laboratory. I extend my special appreciation to Dr. Eva C. Das for in vitro cell culture experiments and for all the help and support which helped me to improve the quality my work.

I am thankful to Dr. Prabha D. Nair, for her valuable suggestions and comments and I also express my thanks to Dr. Lynda V. Thomas for helping me with the water contact angle measurements. I thank Dr. Amritha Natarajan, Dr. Rahul & all lab members of DTERT for their friendship and timely help.

I thank Dr. Roy Joseph, Mrs. Jasmin Joseph and Dr. Chandra Shekhar Nayak of Division of Polymeric Medical Devices for helping me with mechanical testing using UTM; Dr. Anilkumar T.V. for permitting me to use their freezer dryer facility and all the lab members of Experimental Pathology for their friendship and support; Dr. Renjith and Mrs. Nimi for GPC analysis and Mr. Willi Paul for Confocal Raman Spectroscopy. I would also like to acknowledge Dr. Harikrishnan Bhatt & Mrs. Soumya of NIIST, Thiruvananthapuram for NMR spectroscopy analysis and RGCB, Thiruvananthapuram for confocal imaging.

I have no words to express gratitude to my family members who provided the most precious support. I am indebted to my parents and my wife Gopika V. Gopan for their unconditional love, support and encouragement.

ADARSH R.K.

LIST OF ABBREVIATIONS

^{1}H- Nuclear Magnetic Resonance spectroscopy	^{1}H- NMR
5.5 '-dithiobis(2-nitrobenzoic acid)	DTNB
American Society For Testing Materials	ASTM
Analytical Reagent	AR
Bone-marrow-derived human mesenchymal stromal cells	hBMSCs
Carbon dioxide	CO_2
Chitosan	CS
Confocal Laser Scanning Microscopy	CLSM
Diels Alder	DA
Energy-dispersive X-ray spectroscopy	EDAX
Environmental Scanning Electron Microscopy	ESEM
Expanded Polytetrafluoroethylene	ePTFE
Fourier transform infrared spectroscopy	FTIR
Gel permeation chromatography	GPC
Glycidyltrimethylammonium chloride	GTMAC
Guided bone regeneration	GBR
Guided tissue regeneration	GTR
human Periodontal Ligament Cells	hPDLC
Hyaluronic acid	HA
Hydrochloric acid	HCl
Hydroxyapatite	HA
Laboratory Reagent	LR
N-(3-Dimethylaminopropyl)-N′-ethylcarbodiimide hydrochloride	EDC
N,N,N-trimethyl chitosan iodide	TMC
N,N′-Dicyclohexylcarbodiimide	DCC
Phosphate buffer saline	PBS
Poly-DL-Lactic Acid	PDLLA
Polyethylene glycol	PEG
Polyethylene glycol diacrylate	PEGDA

Polyglycolic acid	PGA
Polylactic acid	PLA
Poly-Lactic-Glycolic Acid	PLGA
Polyvinyl Alcohol	PVA
Quaternary ammonium salts	QAS
Quaternized chitosan	QC
Quaternized chitosan – Strontium hydroxyapatite	QC-SA
Quaternized chitosan- calcium phosphate	CPQC
Scanning Electron Microscopy	SEM
Sodium borohydride	$NaBH_4$
Sodium cyanoborohydride	$NaBH_3CN$
Strontium apatite	SA
Sulfuric acid	H_2SO_4
Thioglycolic acid	TGA
Thiolated Chitosan	TCS
Thiolated Polyvinyl Alcohol	TPVA
Thiolated Polyvinyl Alcohol - Thiolated Chitosan-Hydroxyapatite	TPVA-TCS-HA
Thiolated PVA - hydroxyapatite	TPVA-HA
Titanium	Ti
Tricalcium phosphate	TCP
Trimethylene Carbonate	TMC
X ray diffraction	XRD

LIST OF NOTATIONS

%	Percentage
µg	Microgram
µL	Microliter
µm	Micrometer
cm	Centimeter
cm^2	Centimeter square
g	Gram
h	Hour
M	Molar
mg	Milligram
min	Minute
mL	Milliliter
mm	Millimeter
$^{\circ}C$	Degree Celsius

LIST OF FIGURES

List of tables

SYNOPSIS

The thesis entitled "**Polymer modification strategies to develop new bioactive structures for guided tissue regeneration**", deals with the structural and functional modification of polymeric materials for tissue regeneration applications. It explores the ways of making bioactive implantable structures from affordable polymers, natural as well as synthetic, through state of the art chemical techniques so that they can be used for regenerating damaged tissues. The major requirement of such biomaterial structures is in "guided tissue regeneration" technique in which hard and soft tissues are appropriately guided to reinstate the functional and structural features of the host site.

Tissue structures in human body can get impaired by several problems like birth defects, diseases, trauma, malignancies and atrophy, or lost in surgical interventions. Human body has an innate ability to repair the lost tissue, within a certain biological limits. In most of the cases, the defects or damages will be significant and need to be managed with grafting, appending and fixing techniques. In addition, certain 'tissue guidance' structures are used to ensure the effectiveness of the repair process. The use of tissue guide membranes is most essential in the case of loss of periosteum in orthopedics or damage in periodontium in dentistry, wherein the interference of local soft tissues causes delay or impairment in bone remodeling. Placing the guide membranes help to regain the local hard tissue architecture and hence called guided tissue regeneration or guided bone regeneration (GBR/GTR) technique.

The basic requirements of GBR/GTR materials are mechanical strength, porous structure, biocompatibility, degradability, bioactivity and affordability. Various kinds of membranes have been developed for the purpose. Currently, the most popular GBR/GTR membranes are made of collagen. The biodegradation rate of collagen remains

unpredictable and it has immunogenicity risks. Alternative products made with polylactic acid (PLA) and polyglycolic acid (PGA) are very expensive. Other candidate materials like polycaprolcatone (PCL), chitosan and derivatives of alginate and cellulose are in the research stage. Generally the lack of physiological degradation and low level of bioactivity are ailing problems for such materials. None of them satisfy the ideal requirement of GBR/GTR material and hence there is a need for new materials with high reliability in clinical performance.

The approach of the present work is to select highly affordable materials which satisfy the mechanical requirements, and make them biocompatible, degradable and bioactive through state-of-the-art chemical modification/functionalization techniques for GBR/GTR applications.

Two polymeric materials, one of natural origin (chitosan) and the other of synthetic origin (Polyvinyl Alcohol) were selected for the work. They were structurally and functionally modified adopting techniques like quaternization and thiolation. For enhancing the bioactivity, novel apatitic materials were incorporated using appropriate material synthesis techniques.

The work is based on the hypothesis: ‘‘Chemical functionalization of the modified structures based on chitosan and polyvinyl Alcohol is capable of enhancing their bioactivity and degradability making them better suited for guided tissue regeneration applications”.

The aims of the work are:

- To modify chitosan to impart higher solubility and make composite structure with calcium phosphate based minerals to achieve bioactivity.

- To modify polyvinyl alcohol to a cross linkable polymer and make graded composite structure with calcium phosphate based minerals to achieve bioactivity.
- To make combinational materials containing modified chitosan and modified polyvinyl alcohol, with functionally graded structure satisfying the essential requirements of guided tissue regeneration membranes.

In order to achieve the aims, the following objectives were set for the work:

- Preparation of quaternized chitosan (QC) using Glycidyltrimethylammonium-chloride.
- Fabricating composites based on QC and its blend with strontium doped hydroxyapatite by freeze drying method.
- Fabrication of composites based on QC and its blend with *in situ* precipitated calcium phosphate by freeze drying method followed by pH adjustment.
- Physical, chemical and *in vitro* cytotoxicity evaluation of composites to ensure the material meets the essential requirements for GBR/ GTR application.
- Synthesis of thiolated Polyvinyl Alcohol (TPVA) by acid mediated esterification reaction.
- Fabricating graded composites based on TPVA with hydroxyapatite (HA) by click crosslinking technique with dialkene followed by freeze drying.
- Physical, chemical and *in vitro* cytotoxicity evaluation of composites to ensure the material meets the essential requirements for GBR/ GTR application.
- Synthesis of thiolated chitosan (TCS) by the 1-Ethyl-3-(3-dimethyl aminopropyl) carbodiimide (or EDC) mediated amide coupling with thioglycolic acid.
- Fabricating composites based on TPVA and TCS with HA by click crosslinking technique with dialkene followed by freeze drying.

- Physical, chemical and *in vitro* cytotoxicity evaluation of composites to ensure the material meets the essential requirements for GBR/ GTR application.

The work is presented in six chapters. The chapter 1 begins with an introduction to the Guided Bone Regeneration (or Guided Tissue Regeneration) concept, current treatment modalities and challenges in bone defect management. It also briefly introduces the structural, mechanical and biocompatibility requirements for an ideal GBR/GTR material and various compositing methods as well as various approaches to attain a functionally graded system.

Chapter 2 carries an exhaustive literature review, concentrating on the current status of GBR/GTR materials and techniques used for orthopedic and dental applications. The topics reviewed include history of GBR/GTR, various polymer modifications done on chitosan and polyvinyl alcohol, composite fabrication techniques, functional grading techniques, click crosslinking method and bioactivity enhancement methods in materials.

In chapter 3, the experimental design in order to achieve the proposed objectives of the study is presented. This includes detailed description of the materials used, experimental protocols, instruments utilized, composite preparation techniques and preliminary cytotoxicity assays. The first section in this chapter describes essential chemicals and modification strategies utilized for the study. Section 2 deals with the material development which is divided into purification of chitosan, quaternization of purified chitosan, preparation of strontium doped hydroxyapatite, composite fabrication with strontium doped hydroxyapatite, various characterization plans for the study. This section also includes the preparation of *in situ* calcium phosphate composite from quaternized chitosan (CPQC), preparation of thiolated Polyvinyl Alcohol (TPVA), preparation of thiolated chitosan (TCS), preparation of hydroxyapatite (HA), fabrication of TPVA-HA graded composite and fabrication of TPVA-TCS-HA graded composite.

Section 3 deals with various test and analysis methods, which include estimations (ICP-OES, Potentiometric titrations, Gel permeation chromatography and Ellman assay), instrumental methods (FTIR, FT-Raman, ^{1}HNMR, ^{13}C NMR, X-ray Diffraction and Scanning Electron Microscopy) and various physicochemical tests like optimization of gelling parameters, mechanical tests, *in vitro* properties like water uptake, degradation, bioactivity and cytotoxicity tests.

Chapter 4 presents the results of the studies, represented using figures, tables and graphs. The purified chitosan was characterized in terms of molecular weight using Gel permeation chromatography, degree of deacetylation via potentiometric methods and ^{1}H NMR, heavy metal analysis using ICP-OES. The synthesized QC, QC-SA composite and the *in situ* composite CPQC were characterized using ^{1}HNMR, FTIR techniques for chemical structure, XRD for the confirmation of calcium phosphate in the composite and SEM for the surface microstructure. The incorporation of calcium phosphate improved the surface wettability, biodegradability as well as mechanical properties of QC scaffolds. Comparative evaluation of both physical and cytotoxic properties of QC and calcium phosphate containing QC suggested that CPQC composite would be the better, owing to its enhanced mechanical properties, bioactivity, enhanced biodegradability and non-cytotoxicity. The synthesized TPVA was characterized using GPC for molecular weight, by ^{1}HNMR, FTIR and FT Raman for chemical structure, and the cross linked TPVA-HA, cross-linked TPVA-TCS-HA composites were characterized by XRD for the confirmation of calcium phosphate phase in the composite and by SEM for surface microtopography, along with bioactivity evaluation. The immobilization of calcium phosphate in graded pattern via click crosslinking improved the surface wettability, biodegradability as well as mechanical properties of TPVA sheets. Comparative evaluation of both physical and *in vitro* cytotoxic behaviour of TPVA, cross-linked TPVA-HA and cross-linked TPVA-TCS-

HA composites suggested that the TPVA-TCS-HA composites would be the best in terms of mechanical properties, bioactivity, biodegradability and non-cytotoxicity.

In Chapter 5, results are discussed and analyzed with the aid of current literature. The concept of GBR/GTR and its requirements were compared with the data obtained with above mentioned four composites. The *in situ* incorporation of calcium phosphate in quaternized chitosan makes the material more bioactive and one of the essential requirements of the GBR material was thus satisfied. The PVA modification via thiol groups offered a better possibility to generate graded composites. Crosslinking through thiol-ene reaction of TPVA-HA dispersion using PEGDA paved the way to create ceramic graded composite from TPVA-HA as well as TPVA-TCS-HA. The TPVA and TPVA-TCS based systems thus meet another requirement ideal GBR membranes, i.e., functional grading.

Chapter 6 summarizes the results and conclusions which are drawn from the study on four systems QC-SA, CPQC, TPVA-HA and TPVA-TCS-HA. Studies with QC-SA and CPQC showed that the CPQC will be best among the two systems. Studies with TPVA-HA and TPVA-TCS-HA showed that the TPVA-TCS-HA will be the best to be used as new generation GBR/GTR material. These materials could be made as a membrane and animal trials could be done for applications like periosteal substitutes and barrier membranes for periodontal defects.

CHAPTER 1

INTRODUCTION

The present work deals with the structural and functional modification of polymeric biomaterials for tissue regeneration applications. It explores the ways of making bioactive and resorbable structures from affordable polymers, natural as well as synthetic, through state-of-the-art chemical techniques so that they can be used for regenerating damaged tissues. The major requirement of such biomaterial structures is in "guided tissue regeneration" technique in which hard and soft tissues are appropriately guided to reinstate the functional and structural features of the host site.

This introduction chapter explores the development of biomaterials for tissue regeneration, the need for bone tissue regeneration, challenges in bone defect healing in orthopedics and dentistry, the concept of guided bone tissue regeneration (GBR/GTR), the current status of GBR/GTR approach and the scope of developing new materials for GBR/GTR technique.

1.1 Biomaterials for Tissue Regeneration

Biomaterials signify the merger of Materials Science with Physiology and Clinical Science. The term 'biomaterials' generally refers to those materials compatible with body, used as single, or in combination, modified or designed as a device. These are used for replacement of diseased or damaged parts, to assist in tissue healing, to improve function, to correct abnormalities, to aid diagnosis and to aid treatments. Products based on biomaterials have taken a significant role in enhancing the quality of life of mankind through the past half-century. This field has consistently generated novel materials for different biomedical applications [Ratner., 2019].

The scientific understandings of biomaterials got evolved in definite phases of time. This has been realized through extensive tests and analysis undertaken to identify the composition, physico-chemical properties, mechanical properties, and biological response of materials. Each level of understanding generated novel biomaterials and innovative device designs for the unmet clinical needs existed at each point of time. The development of the various biomaterials could be chronologically plotted as different generations [Ratner., 2019].

The first generation was bioinert materials and the second was resorbable materials. The third-generation materials started appearing from the early years of the 21st century, which combine the bioactivity and resorbability, in order to enable tissue regeneration. [Hildebrand., 2013; Ratner., 2019]. These materials were designed to stimulate specific cellular responses at the level of biomolecules. The basic aim was to direct cell proliferation, differentiation and extracellular matrix (ECM) production and organization. This generation represents the convergence of bioactivity and resorbability. These third-generation biomaterials made significant role in the progress of Regenerative Medicine. Engineered tissue-mimicking constructs were designed at research level that can adapt to the physiological environment and provide repair or replacement [Hench and Polak., 2002].

1.2 Bone Tissue Regeneration

Biomaterials, throughout its history, have been highly successful in bone tissue regeneration. Treating of defects in bone is a routine need in day-to-day healthcare, which arise out of trauma, tumors, osteoporosis and infections. Bone is the hard tissue with a woven structure comprising of collagen and calcium phosphate mineral, created out of cellular activity in the body. Body has the ability to repair small defects in bone through a process comprised of a well-organized sequence of biological events. The repair process

involves specific cell types, various signaling pathways both intracellular and extracellular, in order to restore the skeletal function [Einhorn., 1998; Cho et al., 2002].

The bone healing sequence in a typical fracture case starts with inflammatory response to injury followed by fibrin clot and fracture hematoma formation as result of bleeding from surrounding soft tissue and fractured area. An initial soft callus is formed at the site by angiogenesis and mesenchymal progenitor cell proliferation. These two processes get completed within 2 weeks of injury. The second stage of healing starts with the resorption of bone from broken end. Along with the bone resorption, mesenchymal progenitor cell differentiation occurs to get converted to chondrocytes. Thereafter callus of cartilaginous type is formed from the fracture, when the bone-laying cells '*osteoblasts*' inhabits the area. During the final stage, hard callus is formed by endochondral ossification and slowly converted to mature bone. This whole sequence of events is known as '*Bone Remodeling*' [Stewart et al., 2015].

The clinical management of bone defects is mainly based on remodeling principle. Small fractures or defects lesser than the critical size (normally less than 1cm) are fixed using metallic devices and immobilized temporarily and allowed to heal naturally [Owston et al.,2020]. In case of larger defects or significant bone loss, the defect will be grafted to regain the mechanical integrity. The autogenous cancellous bone graft is considered as gold standard for bone defect repair due to its inherent properties of osteoinduction, osteoconduction and osteogenesis [Sen Miclau., 2007; Nauth et al., 2011]. The harvest site for cancellous bone described in literature includes anterior iliac crest, posterior iliac crest, distal femur, proximal tibia, and distal tibia. In case, when a good quality autograft is not available in the required quantity, synthetic bioceramics grafts are used [Ratner., 2019].

1.3 Challenges in bone defect healing

1.3.1 Bone defects in orthopedics

The present day orthopedics is highly evolved in surgical techniques as well as in implant materials, and therefore, simple fractures below the critical size are handled successfully. However, larger defects, especially segmental bone loss, and infections are still problematic. Delayed healing and non-union of bone often pose challenge in orthopedics [Elliott et al., 2016]. Non-unions are characterized by the failure of bone to completely heal even after 6-8 months from the time of treatment [Bell et al., 2016]. Various reasons are identified for this condition, like the extent of bone loss or periosteum (outermost layer of bone) loss, the location, presence of infection, soft-tissue envelope condition, inadequate mechanical stability, as well as patient's health condition [Owston et al.,2020].

Periosteum plays a significant role in the initiation and maintenance of the bone remodeling process. Immediately after the trauma, periosteum undergoes inflammation and periosteal cells proliferate and results in the periosteum thickening [Lu et al., 2005]. It is also reported that the increased population of mesenchymal progenitor cells from periosteum greatly influence the formation of cartilage and bone within the callus. The contribution of periosteal cells towards the callus formation is of critical importance towards the vascularization and remodeling of the bone grafts since there is no contribution of cell from endosteum towards callus formation due to their inability to migrate [Zhang et al., 2005; Colnot., 2009; Zhang et al., 2012]. In addition, for the proper healing of bone defect via regeneration, it is necessary to avoid the in-growth of faster growing fibrous tissues into the defect spaces, which can be prevented by an intact periosteum [Aaboe et al., 1993; Queiroz et al., 2006]. Thus, periosteal loss lead to multiple

issues like limited biological environment for healing and invading of fibrous tissues to the healing site.

1.3.2 Bone defects in Dentistry

Bone defects in Dentistry mainly refer to the loss of alveolar bone structure which anchors the teeth and gives mechanical support for mastication. The periodontal bone loss occurs due to periodontitis (or the infective condition) in which the inflammatory response to infection progressively destroys alveolar bone and the associated tissue structure. This damage, owing to its specific manifestation, is not reversible and pocket formation can lead to tooth loss [Chapple et al., 2015]. In addition, traumatic injuries can do considerable damage to tooth structure and periodontal bone [Petti et al., 2018; DiAngelis et al.,2012].

The management of periodontal diseases is carried out by routine scaling and root planning procedures in the mild cases. In moderate to severe periodontitis in which bony pockets are formed around the root, grafting can be done using allogenic bone chips or ceramic granules. The bone graft need to be covered with a barrier membrane so as to guard against gingival epithelial overgrowth into the area [Villar and Cochran., 2010]. After periodontal surgery, the type of cell that repopulates near the exposed defect site will determine the nature of attachment [Nyman et al., 1982]. The in-growth of epithelial cells will result in the formation of a weak epithelial attachment (othrewise called long junction epithelium) attachment rather than strong collagen fibre attachment between the alveolar bone and the tooth root [Listgarten and Rosenberg.,1979 ; Bowers et al.,1989; Caton et al.,1980; Lindhe et al.,1984]. The key idea of using the barrier membrane is to stop the migration of epithelial cells into the wound area, thereby permitting the selective repopulation of periodontal ligament cells to form new periodontal attachment. Apart from barrier property to exclude cells, the barrier safeguards the blood clot during the early stages of healing and ensures space maintenance in the defect area for the proper

periodontal bone ingrowth [Villar and Cochran., 2010].This is proved to be successful and the technique, better known as Guided Tissue Regeneration (or GTR), is an accepted practice in periodontal bone defect treatment [Nyman et al.,1980; Karring et al.,1980; Karring et al.,1985; Melcher et al.,1987].

1.4 The concept of Guided Bone Tissue Regeneration

The challenges in bone defect healing in orthopedics and dentistry necessitates additional measures for bone regeneration so as to reinstate the structure and function of the defective area. In orthopedics, delayed healing and non-union are the main challenges whereas in periodontal repair, regaining the alveolar bone around the tooth root is of concern. Though the bone healing requirements are structurally and functionally different in both cases, a common strategy of guiding the tissue regeneration by using a membrane will apparently work out.

The use of 'Guided Bone Regeneration'/'Guided Tissue Regeneration' (GBR/GTR) membranes is most essential in the case of loss of periosteum in orthopedics or damage in periodontium in dentistry, wherein the interference of local soft tissues causes delay or impairment in bone remodeling. Placing the membranes help to regain the local hard tissue architecture [Owston et al., 2020]. This concept is schematically represented in Figure 1A. For periodontal defect management, a thin barrier membrane of adequate mechanical strength is placed after filling the defect with graft material. It functions as a space-maintainer for alveolar bone growth, and a barrier by inhibiting the migration of epithelial tissue. The concept is represented in Figure 1B.

In orthopedics, the technique of substitution of periosteum is called 'Guided Bone Regeneration' (GBR), as the main concern is the healing of defective bone. In Dentistry, the technique of using barrier membrane is known as 'Guided Tissue Regeneration' (GTR) because the aim is to regenerate the whole periodontia structure (consisting of

alveolar bone, periodontal ligament and cementum) by allowing selective infiltration of cells. Therefore, the concept of using membranes for tissue regeneration can be termed in common as GBR/GTR.

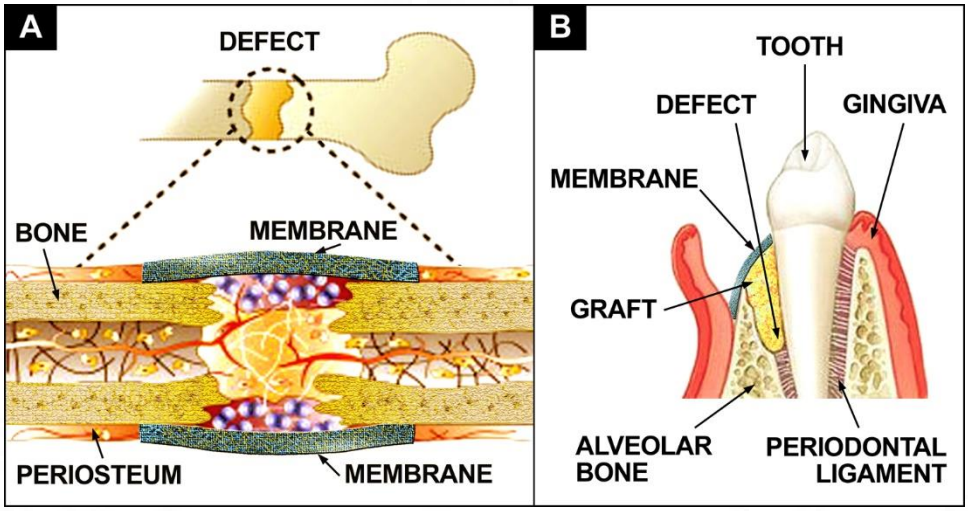

Figure 1: The basic concept of guided bone regeneration in orthopedics and dentistry. Picture A shows a large segmental defect in long bone managed with membranes substituting the lost periosteum. Picture B represents the grafted periodontal bone defect is covered with a barrier membrane. In both the cases, the membranes give space and environment for bone regeneration to happen.

1.5 The current status of GBR/GTR approach

The idea of GBR/GTR has been in place for more than 3 decades [Dahlin et al., 1988; Dahlin et al.,1990]. This has become an accepted surgical practice in periodontal treatment and several products have appeared in the market. The basic requirements of GBR/GTR materials to achieve the goal are now clearly defined. They include biocompatibility, mechanical strength, porous structure, degradability and bioactivity. Additional features like affordability is an added advantage. Various kinds of membranes have been developed for the purpose. The first GTR membranes developed were non-resorbable membranes based on cellulose and expanded polytetrafluoroethylene (ePTFE) which acted just for space maintaining [Jacob and Amudha., 2017]. These were soon gone unpopular because a second surgical procedure was required for the removal of these non-

resorbable membranes [Florjanski et al., 2019]. Next generation of biodegradable guided bone regeneration material were developed to solve this issue, mainly based on collagen and polyglycoside based synthetic copolymers [Buser., 2009]. Collagen based products became very popular because of the material compatibility and affordability. It is the main component of connective tissues and well tolerated by the body. Other properties of collagen include hemostasis, chemotaxis and ease of manipulation in membrane form. It undergoes natural degradation upon implantation [Wang and Carroll., 2001; Pitaru et al.,1989]. However, the biodegradation rate of collagen remains unpredictable and it has immunogenicity risks. The resorption of collagen depends on the form in which it is used; cross-linked collagens using formaldehyde last for 6 to 8 weeks maintains their structural integrity, whereas the structural integrity of uncrosslinked collagen will last for only 7days [Blumenthal.,1988]. Alternative products made with polylactic acid (PLA) and polyglycolic acid (PGA) are degradable, but very expensive. Their degradation products have limited tissue compatibility. Other candidate materials like polycaprolactone (PCL), chitosan, derivatives of alginate and cellulose are in the research stage. Generally, the lack of physiological degradation and low level of bioactivity are ailing problems for such materials. None of them satisfy the ideal requirement of GBR/GTR material and hence there is a need for new materials with high reliability in clinical performance.

There are non-resorbable and resorbable barrier membranes available commercially in the international market. Among the non-resorbable material PTFE is well accepted. Brands based on Expanded-PTFE (Gore-Tex from WL Gore and Associates, USA) and Dense- PTFE (Cytoplast from WL Gore and Associates, USA and TefGen FD form Lifecore Biomedical, USA) are available. Titanium mesh also is used (Ti-Micromesh from ACE Surgical Supply, USA, and Tocksystem Mesh, from Tocksystem, Italy).

Resorbable barrier membranes are made of different material components with varying properties. The essential details are given as a chart below:

Commercial name	***Company***	***Component***	***Tensile strength***	***Resorption rate***
Resolute	WL Gore and Associates, USA	Poly-DL lactide/ co-glycolide	_____	10 weeks
EpiGuide	Kensey Nash Corporation, USA	Poly-DL lactic acid	_____	6-12 weeks
OsseoQuest	WL Gore and Associates, USA	Hydrolyzable Polyester	_____	8 weeks
Vivosorb	Polyganics B.V., Netherlands	PCL	_____	16-42 weeks
Vicryl	Jhonson & Jhonson, USA	Polyglactin 910 Polyglicolide	_____	4-12 weeks
Biofix	Bioscience, Tampere, Finland	Polyglycolic acid	_____	24-48 weeks
Bio-Gide®	Geistlich Biomaterials, Baden-Baden, Germany	collagen	4.8 MPa	24 weeks
Collprotect®	Botiss Biomaterials, Italy	collagen	13.1 MPa	8-12 weeks
Jason®	Botiss Biomaterials, Italy	collagen	13 MPa	12-24 weeks
OSSIX Plus	OraPharma Inc.,USA	collagen	5.13 MPa	4-6 months

1.6 Scope of new materials for GBR/GTR technique

Initial literature search shows that the present biomaterials available for tissue engineering are not fully compatible with the requirement of ideal GBR/GTR material. The approach of the present work is to select highly affordable materials which satisfy the mechanical requirements, and make them biocompatible, degradable and bioactive through state-of-the-art chemical modification/functionalization techniques for GBR/GTR applications.

Two polymeric materials, one of natural origin (chitosan) and the other of synthetic origin (polyvinyl alcohol), were selected for the work. They were structurally and functionally modified adopting techniques like quaternization and thiolation. For enhancing the bioactivity, novel apatitic materials were incorporated using appropriate material synthesis techniques.

CHAPTER 2

REVIEW OF LITERATURE

The introductory exploration indicates the scope of developing bioactive graded polymer composite structures from chemically modified natural and synthetic polymeric platform for the use as guided tissue / bone regeneration membranes for both orthopedic and dental applications. A thorough understanding of the past and current developments in the area of guided tissue / bone regeneration is necessary in order to make an ideal material suitable for these applications. This chapter discuss in detail about the concept and evolution of guided tissue/bone regeneration materials in orthopedics and dentistry, its current status, various polymer modification techniques carried out on chitosan and polyvinyl alcohol to render it more bioactive and biodegradable, the different fabrication techniques, and strategies to introduce bioactivity in biomaterials. This chapter also details the new click chemistry approach and its significance in developing new functional materials. The background of the work, experimental design and work strategies are deduced with the aid of published literature to develop the research hypotheses and set the aims and objectives of the thesis.

2.1 Guided tissue/bone regeneration

The success of the repair of a bone defect depends on various factors like the extent of bone or periosteum (outermost layer of bone) loss, the location of the defect, presence of infection, soft tissue envelope condition, provision of adequate mechanical stability, as well as patient related factors, like age and co-morbidities [Owston et al.,2020]. In classic clinical approach of surgical repair, the lost portion will be grafted after bone debridement if needed. Autograft (patient's own bone) is the gold standard for

grafting, yet in case good quality bone is not available, synthetic graft materials are used. Vascularization of the grafted area is very crucial for fast and effective healing [Menger et al., 2020]. If the periosteum in the defect region is damaged or lost, it will hamper the vascularization and supply of progenitor cells to the area, leading to delayed healing or bone non-union. Another hindrance for healing is the presence of soft tissues enveloping the area.

The need for physical separation of the overlying soft tissue from the bone defect is known 6 decades back. In a report of 1959, it has been hypothesized that "osteo synthesis" in the spine can be rapidly and effectively achieved when the paraspinal muscles were separated from the defect part with the aid of bone graft' and it was tested in rabbit's femur [Hurley et al., 1959]. Similarly, experiments of maxillofacial reconstruction in dogs in which cellulose acetate was used to exclude the fibrous tissue from the defect site was observed to create optimal environment for bone regeneration [Boyne., 1969]. The idea of 'guided bone regeneration' originated out of these experiences, which proposes to use a template of biodegradable membrane to stimulate and guide endogenous bone regeneration [Owston et al., 2020].

2.1.1 Guided tissue/bone regeneration in orthopedics

The use of membranes for healing bone defects have become common for the past 3 decades [Dahlin et al., 1988; Dahlin et al.,1990]. According to the studies done by Wang et al, Ritsila et al and Roberto et al on the role of periosteum on facture healing, studies have shown that the risk of non-union increases in case of complete removal or compromising of the periosteum [Wang et al.,2015; Ritsila et al.,1994; Roberto et al.,2015]. In case of periosteal loss, the artificial or natural materials in membrane form that resemble the periosteum were to be created in order to pave the way for healing. Nielsen et al tried to heal the 1 cm segmental, osteoperiosteal defects produced in rabbit

radius, by covering with a biodegradable polyurethane membrane formed as a tube. Healing was analyzed by radiographic and histologic studies after 5 weeks. The membrane-treated defects consistently healed by forming callus external to the membrane fusing the bone fragments. Presumably, the membrane has served as a scaffold for regenerating periosteum [Nielsen et al.,1992]. The regeneration path in the bone defect site in presence of membrane was studied by Schenk et al by observing the healing pattern of bone regeneration in canine mandible where defects were protected with a membrane [Schenk et al.,1994]. According to Nyman et al, in large bone defect additional bone graft material with osteogenic and osteoinductive potential is needed for lamellar bone formation. In the absence of this bone grafting material, bone formation only occurs at the marginal zone with central zone of loose connective tissue [Nyman et al., 1995].

Caridade et al has evaluated a free-standing membrane impregnated with BMP-2 on a chitosan and alginate layer-by-layer fabricated membrane to resemble the biomimetic system of the periosteum. The layers between the membrane crosslinked with 1-Ethyl-3-(3-dimethylaminopropyl) carbodiimide (EDC) coupling and the myogenic and osteogenic potentials assessed *in vitro* using BMP-2 responsive skeletal myoblasts and osteoinductive properties *in vivo* were also studied [Caridade et al.,2015]. In a recent study done by Chou et al using biodegradable drug eluting poly ([D, L]-lactide-co-glycolide) (PLGA) nanofibrous membrane as a substitute for periosteum to cover femoral fracture in *in vivo* rabbit suggested that drug eluting periosteal substitute exhibited statistically significant healing and better preclinical performance compared with the rabbits without the artificial periosteum [Chou et al.,2016]. Another *in vitro* study done by osteogenic differentiation in stem cells originating from human exfoliated deciduous teeth by Su et al using dexamethasone containing polyvinyl alcohol nano fiber periosteal substitute showed that

after 21 days of induced culture there is significant increase in the expression of alkaline phosphatase activity and calcium mineralization [Su et al.,2016].

2.1.2 Guided tissue/bone regeneration in dentistry

The GBR/GTR concept is more prevalent in dentistry because of the regular occurrence of periodontal bone defects and ease of surgical procedures. GTR is a clinically established technique in dentistry, for which barrier membranes are available commercially.

The preliminary *in vivo* studies to evaluate the efficacy of material assisted guided bone regeneration was done by using non-resorbable membranes. The experiments in Sprague – Drawly rats to heal a surgically created bone defect using Gore-Tex® (porous PTFE) membrane showed significant increase in bone regeneration on the membrane side as compared to the control (defect side without membrane) [Dahlin et al.,1988]. They also extended the principles of guided regeneration to regenerate bone in rabbit's tibia at the exposed part to titanium implant by placing a PTFE membrane over the test fixtures, covering the threads. Later the muscles and periosteum were replaced and sutured. The histological examination of the defect part from 6 week of post-surgery time showed better bone regeneration near the titanium implants covered with PTFE membrane compared with those kept as control (without membrane). Based on the observation he concluded that the usage of a barrier membrane with appropriate pore size will avoid the migration of undesired cells to defect site to maintain the space for bone regeneration [Dahlin et al., 1990]. The need for second surgery during the usage of non-resorbable membranes led to the use of resorbable membranes. Collagen based membranes were used and was able to prevent the migration of epithelium to periodontal defect site of canine models and guided in the regeneration [Pitaru et al., 1988].

2.2. Current status of GBR/GTR materials

The guided bone regeneration techniques earlier utilized non resorbable titanium meshes or expanded polytetrafluoroethylene (ePTFE) barrier membranes to allow for selective repopulation of the bone defect area with the most appropriate host cells to promote proper regeneration. These non-resorbable materials needed an additional barrier retrieval surgery, which necessitated an unwanted surgical intervention. This disadvantage led to the development of the second generation resorbable membranes consisting mainly of collagen [Zitzmann et al., 1997].

Barrier membranes are advantageous for guided bone regeneration in long bone defects to prevent the in-growth of fibrous connective tissue components that can result in scar tissue formation. Fibrous connective tissue tends to interfere with or delay the natural regeneration of long bones through osteoblast cells. This is especially significant when there is destruction of periosteum, which acts as a natural barrier and a source of osteoblast progenitor cells [Aaboe et al., 1993] Collagen membranes are ideal resorbable membranes as periosteal substitutes and barrier membranes in guided bone regeneration procedures for long bone defects along with bone grafts or engineered constructs [Guda et al., 2013].

Collagen, although a versatile barrier material, lacked the mechanical strength and durability, along with allergic reactions in sensitive individuals. The early resorption of collagen membranes by collagenase enzymes also leads to the collapse of the barrier membranes. This led to the use of synthetic aliphatic polyester based resorbable membranes made of polylactic acid (PLA), polyglycolic acid (PGA), polylactic-co-glycolic acid (PLGA) etc. as GBR barrier membranes. Different permutations and combinations of suitable biomaterials and fabrication techniques such as electrospinning,

freeze drying etc. are studied upon to develop ideal barrier membranes and periosteal substitutes for guided bone regeneration [Hutmacher et al., 1996].

With the advent of tissue engineering and additive manufacturing techniques, it is possible to fabricate intricate scaffolds that can mimic the host tissue ECM and promote regeneration. These scaffolds utilize graded porosities and functional molecules in a tunable spacio temporal arrangement to promote selective cell homing and regeneration. Novel synthetic-natural polymer combinations are invaluable in the fabrication of functional scaffolds for GBR/GTR procedures [Bottino et al., 2017].

2.3 Polymer modification techniques

The present work explores the possibility of modifying polymers, natural as well as synthetic, so as to make them fit for tissue regeneration applications. Essentially, the modification is directed towards making the material biocompatible (safety in implantation inside the body) and bioactive (interact with the surrounding tissues and lead to the repair of damaged structures). In addition, the modified material should satisfy the mechanical and structural requirements of the application. Two materials are identified as potential polymers for the intended investigation – Chitosan, from among the natural polymers and polyvinyl alcohol, from among the natural polymers. The following subsections give the details of these materials and the scope of modifications.

2.3.1 Modification of Chitosan

2.3.1.1 Chitin and Chitosan

Chitosan is a polysaccharide based natural polymer widely exploited in the areas of medicine and pharmaceutics, due to its biocomaptibility, availability, biodegradability and ease of functionalization. Its natural form has been identified early in 1811 when

Braconnot isolated a fibrous subtance from marine products that dissolves in concentrated acidic solvents such as orthophosphoric acid (H_3PO_4), hydrochloric acid (HCl), sulphuric acid (H_2SO_4) and amide/Lithiumchloride (LiCl) systems (N,N-dimethylacetamide/LiCl and N-methyl-2-pyrrolidone/LiCl) [Knaul et al., 1999]. Later in 1823, it was named as 'chitin' which means 'envelope' in Greek. 70 years later Seyle made the deacetylted derivative of the polymer which got the name 'chitosan'. It's polymeric chain is composed of β-1,4-linked 2-amino-2-deoxy β –D-glucopyranose. The main advantage of chitosan is its solublity in mild acidic solutions like dilute acetic acid. By mid 1900's the chitosan gained much interest in the area of medicine [Miyazaki et al., 1981], with unique applications as antioxidant, antimicrobial, anti-inflammatory, mucoadhesive etc. [Wenshui et al.,2011].

2.3.1.2 Chitosan derivatives

Chitosan chain mainly contains three types of reactive moieties: a primary amine group at C_2 carbon, primary alcohol at C_6 carbon and secondary alcohol at C_3 carbon. The modified chitosan derivatives include quaternized Chitosan, N-Alkyl Chitosan, Carboxy Alkyl Chitosan, Acyl Chitosan, Thiolated Chitosan, Sulfated Chitosan, Phosphorylated Chitosan and so on, which show certain useful properties. Quaternized chitosan is an interesting material for biomedical applications because of its biodegradability in aqueous solutions.

The first reported quaternized chitosan was prepared by Muzzareli et al, through N-alkylation using methanol followed by reduction by using sodium borohydride and finally methylation by methyl iodide to form N,N,N-trimethyl chitosan iodide (TMC) [Muzzareli et al.,1985]. The method introduced by Muzzareli *et al* is time consuming and utilizes multi-step reactions. Later, Domards method was introduced in which quaternized chitosan was prepared by reductive methylation of chitosan using methyliodide in basic

condition [Domard et al.,1986]. The disadvantages of using methyl iodide as quaternization agent is their volatile and toxic nature. Also, methyl iodide is expensive and after the reaction it is difficult to remove the halide ions from the solution. This issue led to the development of new reaction methods and finally methyliodide was replaced by dimethylsuplhate. Being a methylating agent, the dimethyl sulphate had several advantages like lower cost, less toxicity, low volatility and higher efficiency comapred to methyliodide [Britto and Assis., 2007].

Apart from the direct quaternization of amine groups in chitosan, indirect binding methods were also utilized. This is achieved by reacting chitosan with glycidyltrimethylammonium chloride (GTMAC) to yield water soluble soluble N[(2-hydroxy-3-trimethylammonium)propyl] chitosan chloride (HTCC) [Loubaki et al., 1991]. The amine groups and hydroxyl groups can act as nucleophile for the attack of epoxide ring GTMAC; the author claimed that the N-substitution will be preferred by GTMAC in water medium.

The key idea of preparing N-alkyl chitosan is that the primary amino groups of chitosan can be covalently bonded to aldehydes and ketones via Schiff reaction to yield aldimines and ketimines. This can be later converted to N-alkyl derivative by reduction reaction of imines by sodium borohydride ($NaBH_4$) or sodium cyanoborohydride ($NaBH_3CN$) [Tsui-Chu et al., 2005]. Acyl chitosan also showed better water solubility and are commonly prepared by the reaction of chitosan with acid chloride in presence of organic solvent. In 1995, Min et al has done acylation using various cyclic acid anhydrides on chitosan and showed the improvement in water solubility by reducing the hydrogen bond interaction with in the polymer during acylation [Min and Shigehiro., 1995]. As a method to increase the water solubility and mucoadhesive nature of chitosan, Kast and Bernkop prepared thiol derivative of chitosan by EDC mediated amide coupling between

the primary amine groups and the carboxylic groups of thioglycolic acid [Kast and Bernkop., 2001]. Initially the thiolated chitosan was prepared to be used as a drug carrier due to the enhance mucoadhesive nature; later other potentials of chitosan thiol were explored, as an excipient in drug delivery system and as a potential antibacterial agent. The other applications are tissue engineering and gene delivery [Kast et al., 2003; Martien., 2007; Bernkop-Schnürchetal.,2003; Geisberger et al., 2013].

2.3.1.3 Biological properties of modified chitosan

The use of chitosan as a bone regeneration scaffold has gained much interest. Chitosan being a natural biodegradable polymer can enhance healing as well as bone regeneration. Park et al., in 2000 showed that chitosan sponges loaded with platelet derived growth factors were osteoconductive and induce bone formation [Park et al., 2000]. Shin et al has done biological evaluation of chitosan nanofiber membrane for guided bone regeneration and found that the nanofiber based membrane were biocompatible and non-inflammatory with bone regeneration potential [Shin et al., 2005]. The use of cross-linked chitosan using NaOH, $Na_5P_3O_{10}$ and Na_2SO_3 for guided tissue regeneration was done by Kuo et al. A critical sized defect was made in the skull of adult rats and then the defect site was covered using chitosan membranes. After 4 weeks of recovery, chitosan membrane covered regions showed a good healing, cell infiltration and osteogenesis of bone [Kuo et al., 2006]. Lee et al showed the efficacy of a chitosan-silica zerogel composite membrane on its potential ability to regenerate bone in rat's calvarial defect. The composite membrane showed improvement in mechanical as well as *in vitro* / *in vivo* properties compared to the bare chitosan. The rapid deposition of calcium phosphate under *in vitro* conditions proved the excellent bioactivity of the material and further proof was obtained from the *in vivo* studies on calvarial defect [Lee et al., 2009]. Chitosan-hydroxyapatite composite for guided bone regeneration was prepared by the co-

precipitation method followed by dynamic filtration and freeze drying process by Teng et al and showed the effect of the hydroxyapatite content on enhancing the tensile strength and alkaline phosphatase activity of the composite [Teng et al.,2009]. Cui et al has done *in vitro* and *in vivo* evaluation of chitosan-β-glycerol phosphate material having thermosensitive sol–gel transition behavior for guided bone regeneration and found that even with mild inflammatory responses, the material is suited for GBR application. The presence of β-glycerol phosphate adds osteogenic bioactivity to the material and the preparation processes are simple. The incorporation of osteogenic factors makes the material an active guide for bone regeneration rather than merely a passive barrier [Cui et al., 2014].

2.3.2 Polyvinyl Alcohol (PVA)

2.3.2.1 Synthesis and properties of PVA

Polyvinyl Alcohol (PVA) is a fully synthetic polymer first synthesized in 1924 by Hermann and Haehnel by the saponification of poly vinyl ester using caustic soda solution [Halima., 2016]. Unlike other polymers, PVA is not prepared by the polymerization of vinyl alcohol units. The physicochemical, mechanical properties of PVA is greatly influenced by the number of hydroxyl groups (degree of hydrolysis) in the polymeric chain [Tubbs., 1966]. As polyvinyl alcohol is considered, its chemical versatility finds potential applications in the pharmaceutical and biomedical area. It is a water soluble polymer with high degree of biocompatibility. Apart from this, it has good chemical resistance, mechanical property, and film forming property [Shi et al., 2008]. As PVA structure is considered, it has a long hydrocarbon chain with pendant hydroxyl groups in the alternate carbon atoms.

2.3.2.2 Derivatives of PVA

The chemical modifications of PVA are similar to that in the case of alcohol and the introduction of chemical groups is to improve its properties. Theoretically any compound capable of reacting with hydroxyl groups can react with OH groups of PVA to form modified PVA or crosslinked PVA [Gohil et al.,2006].The chemical modifications through hydroxyl groups includes esterification, etherification and acetylation of the hydroxyl groups [Gaina et al., 2012]. PVA reacts with di-aldehydes to form acetal cross-linked PVA and this reaction occur at acidic pH. The most common dialdehyde used for crosslinking PVA is gluteraldehyde [Mansour et al., 2008]. PVA reacts with carboxylic acid in acid catalyzed (H_2SO_4 or HCL) esterification or Steglich esterification (DCC/ DMAP mediated) to form esters [Dicharry et al., 2006; Wu et al., 2017]. Etherification of PVA is mainly done via Williamson ether synthesis in which PVA was made to react with an alkyl halide containing alkene or arene at another end [Liou et al., 2001; Agusti et al., 2015]

2.3.2.3 Biological properties of PVA

PVA is widely studied in the development of ophthalmic materials, drug delivery devices, microspheres, tissue engineering constructs etc. [Teodorescu et al., 2019]. In the area of guided bone regeneration, PVA based materials are not much explored. PVA-nano hydroxyapatite composite membrane was prepared by Zeng et al using solvent casting and evaporation method. The physico-chemical characterization, cell attachment and cytotoxicity studies suggest the composite membrane has the potential to be used for GBR application [Zeng et al., 2011]. The interest in magnetic biodegradable biomimetic scaffolds led to the development of Fe_3O_4/chitosan/polyvinyl alcohol nanofibrous membranes via electrospinning for bone regeneration application. The preliminary cytocompatibility tests showed good cell adhesion and proliferation and suggests it as a

promising material for osteogenesis [Wei et al., 2011]. Ba Linh et al tried a combination of PVA, biphasic calcium phosphate (BCP) and gelatin (GE) in the form of a nano fiber mat for bone regeneration in rat calvarial defects. The out- come of the work showed that the PVA/GE fibers mat containing 50 % BCP most optimal in mechanical properties, cell attachment, growth, protein expression and *in vivo* bone formation in calvarial defect of rat models [Ba Linh et al., 2013]. when using cross-linked PVA for any biomedical application including for GBR purpose, toxic residues could be present in the final product [Hassan and Peppas., 2000] so the crosslinking chemistry which avoids free radical initiators will be beneficial.

2.4 Membrane fabrication techniques

Nature has given a well oragnised hierarchial architecture from basic cells to tissues to organs to the whole body. While keeping up the physiological requirement of maintaining life, this structure satisfies the biomechanical requirements of body functions. Nature inspired structure has attracted a lot in developing functionl materials for tissue engineering application because these structures will facilitate cell distribution, proliferation as well as their growth in three dimensional space [Suresh et al., 2020]. Such scaffolds will help in the regeneration of the defect area to the original architecture, as closely as possible. Commonly used techniques for fabricating scaffolds are as follows.

2.4.1 Solvent casting

Solvent casting is one of the simple, easy and inexpensive technique for polymeric scaffold preparation. In this technique a polymer is dissolved in a suitable solvent and cast into mould of desired shape and the solvent is allowed to evaporate [Mikos et al., 2004]. The main draw back of this technique is the toxicity produced by residual solvents. As a solution to this problem, prolonged drying can be done in vaccum condition, but it is time

consuming. Usually, particulate leaching is combined along with solvent casting for the fabrication of membranes [Mikos et al., 1993].

2.4.2 Particulate-leaching techniques

Particulate leaching is an efficient method to develop tissue engineering materials with desired pores and channels of interest. In this technique, a porogen of appropriate dimension usually salt, wax or sugar is added along with polymer in solution and casted into moulds of specific shape. The dry scaffold obtained after solvent evaporation is subjected to porogen leaching in suitable solvent to form porous membrane. The process is easy and pore size as well as distribution depends solely on the size and the amount of porogen added [Plikk et al., 2009].

2.4.3 Gas foaming

Gas foaming technique utilizes CO_2 at high pressure to generate porous structure. Briefly the porosity depends on the amount of CO_2 dissolved in the polymer. The highly porous polymer material is exposed to gas at very high pressure, results in phase seperation of CO_2 and expands the polymer matrix to increase volume and decrease density. The initial porosity of the material is controlled by using a variety of porogens. A mixture of polymer and porogen are exposed to CO_2 at high pressure until saturation with carbon dioxide is attained. This is followed by foaming process and porogen removal results in highly interconnected pore structure [Huang & Mooney., 2005].

2.4.4 Freeze drying

One of the simple technique used for the generation of three dimensional porous polymer membrane is the sublimation of solvent from frozen solvent polymer mix in vaccum [Schoof et al., 2001]. The technique is more preferable for water soluble polymers and this technique is used to fabricate polymeric membrane with high porosity and

interconnectivity [Mandal & Kundu., 2009]. The freeze drying technique has been widely utilized for generating scaffolds from silk proteins, chitosan, collagen, etc.[Altman et al., 2003; Kim and Lee., 2011; Matsumoto et al., 1999]. The pore size of freeze dried membranes is mainly controlled by freezing rate; a fast freezing rate produces smaller pores. For generating homogenous three dimensional pore structures, controlled directional freezing is adopted [Schoof et al., 2001]. The benefit of this technique is that degradation issues of polymers associated with high temperature can be avoided. One of the drawbacks found for this method is low pore diameter and long processing time [Boland et al., 2004].

2.4.5 Electrospinning

Electrospinning depends on the electrostatic force for the generation of polymeric fibers in which fibre thickness ranges between nano to micro size. It applies high voltages to create an electrically charged jet of polymer solution which forms polymer fiber after drying. This dried polymer fibres are deposited on collector [Reneker and Chun., 1996]. Since the introduction of electrospinning for scaffold preparation, numerous polymers were used for spinning, including silk fibroin [Sukigara et al., 2003], collagen [Mathews et al., 2002], chitosan [Ohkawa et al., 2004], gelatin [Ma et al., 2005] etc. The membranes generated via elctrospinning have structural architecture feasible for cell growth and subsequent tissue organisation. These architectures are suitable for directed or specific cellular growth *in vitro* / *in vivo* since they influence the cell adhesion, cell expression and the transportation of oxygen and nutrients to the cells [Li & Tuan., 2009; Leong et al., 2008].

2.5 Functionally graded materials

Functionally graded composite materials are basically heterogeneous systems graded in their composition or structure or properties (physicochemical as well as biological), so as to suit tissue engineering applications [Tarlochan., 2012]. Functional gradation is a characteristic feature of nature and functionally graded structures include spongy trabecular structures of bone, human skin or local tissue variation in seashells etc. [Fratzl and Weinkamer., 2007]. Considering bone as an example, design changes from a dense stiff external structure to a porous internal structure showing a functional gradation formed by biological adaptation. This graded structure is to optimize the material's response to the load acting on it. Similarly depending on the site of application, the artificial graft or scaffold material should show similar structural as well as functional gradation [Pompe et al.,2003].

For bone regeneration, Liao et al developed a three-layered porous graded membrane using nano-carbonated hydroxyapatite, collagen and polylactic-co-glycolic acid by layer by layer casting approach. The bottom porous layer with 8% nano-carbonated hydroxyapatite/collagen/poly(lactic-co-glycolic acid), the top layer contains PLGA nonporous layer and middle layer of 4% nano-carbonated hydroxyapatite/collagen/ poly(lactic-co-glycolic acid) layer. The membranes showed high degree of cytocompatibility when evaluated using osteoblastic MC3T3-E1 cells as well as mechanical properties suited for practical medical application [Liao et al., 2005]. Tang et al in 2013 prepared a porous graded hydroxyapatite scaffold which mimics natural bone by less porous compact structure on outer side and a highly porous internal structure, fabricated by partial melting–recrystallization across the sides by a two-step freeze casting method. The prepared material has a compressive strength of 22.2±4.1 MPa, 42% porosity and 2 mm outer thickness [Tang et al., 2013]. Giannitelli et al made an attempt to fabricate

graded porous polyurethane foam based material for the treatment of oro-maxillary bone defects. Polyisocyanate and polyester diol were used to generate with a dense shell and a porous core suggested to be used as an osteoconductive scaffold. Mechanical tests along with cytocompatibility assessment with bone-marrow-derived human mesenchymal stromal cells (hBMSCs) proved the suitability for guided bone regeneration applications [Giannitelli et al., 2015]. In an attempt to increase the strength of a layered functionally graded composite membrane for guided bone regeneration in orthopedics, Jamuna-Thevi et al fabricated a three layered composite membrane comprising of poly(lactic-co-glycolic) acid, nanoapatite and lauric acid using thermally induced phase separation technique and was able to significantly increase the tensile strength [Jamuna-Thevi et al., 2016]. Fu and coworkers reported a novel functionally graded bilayer membrane composite using poly (lactic-co-glycolic acid) and nano-hydroxyapatite for GBR application. The properties like surface morphology, mechanical strength, degradability, barrier function and *in vitro* osteogenic bioactivity were evaluated. Depending on the amount of nano hydroxyapatite in the matrix, different essential properties can be achieved. A quantity of 5% nano hydroxyapatite in dense layer shows excellent barrier function and meets the requirement of mechanical strength, where as 30% nano hydroxyapatite in porous layer is essential for good physical and chemical properties. Also, this composition was observed to enhance the *in vitro* mineralization, superior capabilities of cell adhesion, proliferation and differentiation [Fu et al., 2017].

2.6 Bioactivity enhancement methods in biomaterials

Bioactivity of a biomaterial is its ability to trigger a specific biological response at the material interface which results in the formation of union between tissue and the material of choice [Hench et al., 1971]. For any GBR/GTR material, the interface between

material and host tissue plays a crucial role in bone bonding. When the bioactive material is implanted, an environment favorable for bone growth is generated by the *in vivo* deposition of carbonated hydroxyapatite on the material surface and resulted in the connection between the host and implanted material [Cao and Hench., 1996]. Several calcium based phosphates, silicates and its composite with polymers are known to show bioactivity *in vivo*. The most used method to induce bioactivity to polymer scaffold is compositing it with calcium phosphates or bioglass. The most popular bioactive materials are the two forms of calcium phosphates - hydroxyapatite (HA) and tricalcium phosphate (TCP). The bioactive nature arises out of their similarity with bone mineral in terms of chemical composition and crystallographic structure. TCP and HA are implanted in ceramic form and they greatly differ in their resorption rate, where TCP is fast resorbing than HA *in vivo* [Hench., 1991].

2.7 Click approach for developing functional materials

Tissue engineering utilizes the contributions from material science, engineering and biology in a symbiotic manner for the development of new scaffolds for treating diseases and tissue damages. Due to resemblence with extracellular matrix and its tunable property, hydrogels and hydrogel-intermediates will be ideal candidates for tissue engineering applications [Saul and Williams., 2013]. Both synthetic and naturally derived polymeric hydrogels are commonly used for tissue engineering. The commonly used synthetic polymers are based on polyethylene glycol and polyvinyl alcohol while the popular naturally derived polymeric material includes proteins (collagen, geltain and fibrin) and polysaccharides (chitosan, hyaluronic acid and gellan gum) [Saul and Williams., 2013; Yu et al., 2013]. Hydrogels are usually preapared by both covalent and noncovalent crosslinking methods, which includes free radical initated, hydrogen bonding

etc. [Saul and Williams., 2013]. The introduction of click chemistry for polymer modification as well as crosslinking facilitated the ease fabrication of hydrogels for tissue engineering application. The main click approches includes Diels-Alder reactions, azide-alkyne cycloaddition and thiol-ene reactions.

Click hydrogels were first reported by Hilborn et al., in 2006, where PVA-azide and PVA-alkyne in presence of copper catalyst produced gels with high elastic moduli [Ossipov and Hilborn.,2006]. Similar hydrogel preparation was done by Hawker et al. using PEG alkyne and PEG azide via Cu-catalysed alkyne-azide click reaction [Malkoch et al., 2006]. One of the major limitations of copper catalyzed alkyne-azide click is the potential cytotoxicity of copper ions and reactive oxygen species generated by copper ions when extended for biomedical application [Lallana et al., 2011]. This led to the use of copper-free click reaction in fabricating hydrogel. Song et al., reported a biodegradable hydrogels system via strain promoted alkyne-azide cycloaddition click under physiological conditions using azide containing PEG-co-poly(5,5-bis(azidomethyl)-1,3-dioxan-2-one) and dibenzocyclooctyne functionalized PEG. The resultant material showed higher viability towards bone marrow stromal cells [Xu et al., 2011]. Zheng et al also reported that hydrogels from Dibenzocyclooctyne (DBCO) functionalized PEG and three-arm glycerol ethoxylate triazide utilizing strain promoted alkyne-azide cycloaddition showed high viability towards human mesenchymal stem cells [Zheng et al., 2012]. Even though the strain promoted alkyne-azide cycloaddition is advantageous in constructing hydrogel for tissue engineering application, the overall yield and tedious steps for the preparation of cyclooctyne makes this strategy unsuitable for large-scale preparation.

Another click reaction which is highly selective is [4+2] cycloaddition between a diene and a dienophile is Diels–Alder (DA) reaction without any catalyst or byproduct. Shoichet et al. prepared hyaluronic acid (HA) hydrogels by crosslinking furan-modified

HA with dimaleimide-PEG via DA click. The cell attachment and viability assessed using MDA-MB-231 cells showed more than 98% viability and majority of cells began to adopt a flattened morphology suggesting cell attachment [Nimmo et al., 2011]. As thiol-michael addition reactions are considered, it is a versatile technique to prepare hydrogels with high chemical yield, speed, tolerance to a variety of functional groups [Chatani et al., 2013, Hoyle, et al., 2010]. It involves the addition of thiol groups to double bonds in acrylate, vinyl sulfone, or maleimide to form thio ethers with or without the help of a basic catalyst [Mather et al., 2006]. Compared to acrylates, vinyl sulfone is far more reactive in the thiol-Michael reaction, due to its higher electron withdrawing property of sulfone part [Chatani et al., 2013]. The maleimide-thiol Michael reaction is selective and quantitative and highly selective since the C=C in maleimide is more reactive towards SH groups [Pounder et al., 2008]. The thiol-ene Michael addition reaction to construct a step growth hydrogel was first demonstrated by Elbert et al, by reacting PEG multi acrylate with PEG dithiol, dithiothreitol as well as thiol containing peptides. They also showed that the gelling rate was influenced by factors like precursor concentration, catalyst and local ionic condition [Elbert et al., 2001; Metters and Hubbell., 2005]. Later the development of various thiol Michael addition gels like chitosan-PEG for smooth muscle encapsulation, fibronectin- hyaluronic acid-PEG hydrogel for wound repair, gelatin-PEG hydrogels for neovascularization and re-epithelialization in full thickness skin wounds in Sprague dawley rats were reported [Kim et al., 2007; Yu et al., 2011; Ghosh et al.,2006; Xu et al.,2013]. Hydrogel systems based on thiolated hyaluronic acid, thiolated gelatin and PEG diacrylate were effective in the repair of ischemic myocardial infarcts and osteochondral defects [Cheng et al., 2012; Toh et al., 2010].

2.8 Background of the work

The literature review gives an insight into the development, application and the state-of-the-art of GBR/GTR materials. The basic requirements of the materials needed for guided bone regeneration applications are stringent and no material currently available in the market satisfies the clinical needs completely. Several modified material are experimented but do not appear in market due to various limitations. The most common GTR material is collagen which is fast resorbing and lacking bioactivity. Other materials like PLA and PGA are expensive. Another polymer candidate PCL does not satisfy mechanical strength requirements. In short, the known materials and their composite forms do not serve the requirements of GBR/GTR to a satisfactory level.

It will be a wise and workable strategy to select cost-effective biocompatible materials and modify them to satisfy the needs. The literature review gives a number of novel modification techniques at our disposal to make a bioactive and degradable material as per our requirement. Therefore, two such materials were selected – Chitosan and polyvinyl alcohol. Both are cost-effective, as well as easily modifiable for inducing bioactivity and degradability. Also there are scopes for making graded materials and tune them for the required application.

The substitution of strontium (Sr) instead of calcium in hydroxyapatite (HA) crystals greatly affects the physiochemical properties. It is already reported that Sr substitution in HA enhances bone regeneration through the stimulation of osteoblasts and inhibition of osteoclasts [Capuccini et al., 2009]. Since the ionic diameter of Sr is larger than Calcium, the incorporation of strontium ions into HA crystal leads to an increase in lattice spacing (higher Sr-OH distance than that of Ca-OH), thereby introducing strain in the lattice energy and reducing the crystallinity [Li et al., 2007]. These result in enhancement of solubility and acceleration of biological properties [Krishnan et al.,2016].

Doping of Sr at lower doses have promising advantages like increase in bone formation, decrease in bone resorption, relaxing bone pain, alleviating bone cancer and so on. Several studies are available in the literature confirming the improvement in biocompatibility, osteoconduction, bioactivity, degradation rate, mechanical property etc., when a part of Ca ions in HA is replaced with Sr [Guo et al., 2013].

2.9 Research Question and Hypothesis

2.9.1 Research question

Whether chemical functionalization of polymers can influence bioactivity and biodegradability and make them suitable for guided tissue regeneration applications?

2.9.2. Hypothesis

"Chemical functionalization of the modified structures based on chitosan and polyvinyl alcohol is capable of enhancing their bioactivity and degradability making them better suited for guided tissue regeneration applications".

2.10 Aim and Objectives

2.10.1 Aim

The aim of the study is to develop modified polymers, of both natural and synthetic origin, in order to construct bioactive and functionally graded structures for the use as guided tissue regeneration membranes.

2.10.2 Objectives

To prove the above hypothesis and achieve the aims, the study was designed with the following objectives, with each objective is attained by a series of carefully planned experiments.

i. To modify chitosan to impart higher solubility and make composite structure with calcium phosphate-based minerals to achieve bioactivity.

ii. To modify polyvinyl alcohol and make graded composite structure with calcium phosphate-based minerals to achieve bioactivity.

iii. To make combinational materials containing modified chitosan and polyvinyl alcohol, with functionally graded structure satisfying the essential requirements of guided tissue regeneration membranes.

CHAPTER 3

MATERIALS AND METHODS

The basic approach of this work is to develop modified polymers, of both natural and synthetic origin, in order to construct bioactive structures, preferably in membrane form for the use as guided tissue regeneration, mainly the defective bone. Certain modification strategies are planned so as to arrive at materials which overcome the limitations of current materials used in tissue engineering. Four modified material systems are developed during the work – (i) Quaternized Chitosan-Strontium doped Hydroxyapatite composite (QC-SA); (ii) Quaternized Chitosan-Calcium phosphate *in situ* composite (CPQC); (iii) Cross-linked Thiolated PVA graded porous composite containing Hydroxyapatite (TPVA-HA) and (iv) Thiolated Polyvinyl Alcohol - Thiolated Chitosan-Hydroxyapatite composite (TPVA-TCS-HA).

3.1. Essential Chemicals and Modification Methods

3.1.1. Chemicals and purchases

Chitosan powder of approximately 85% deacetylation was purchased from India Sea Foods, Kochi. The chemicals used for polymer synthesis and modifications includes Glacial acetic acid (AR grade), sodium hydroxide (AR grade), Thioglycolic acid of AR grade, Methanol of AR grade, Hydrochloric acid AR grade (35% w/v), Phosphoric acid (AR grade), Tris- buffer , Sodium acetate (AR grade) and Sodium chloride (AR grade) were purchased from Merck, India. Glycidyl trimethyl ammonium chloride (GTMAC, AR grade, 80% (v/v) solution in water), Polyvinyl alcohol of number average molecular weight 98 kDa, Polyethylene glycol diacrylate (PEGDA) of number average molecular

weight 700 Da, 5.5 '-dithiobis (2-nitrobenzoic acid) (DTNB) were purchased from Sigma Aldrich. The chemicals Calcium nitrate tetra hydrate (LR 98%), Ammonium dihydrogen orthophosphate (LR 98%), Strontium nitrate (LR 99%) and aqueous Ammonia (25 v/v%) used for the synthesis of hydroxyapatite and strontium-substituted hydroxyapatite were procured from Rankem chemicals, India.

Chitosan was chosen for the study considering its lower cost, ease of availability, acceptable biocompatibility and inherent bacteriostatic properties which make it attractive for diverse applications in biomedical field. Chitosan is prepared by the partial deacetylation of chitin, a natural polymer mainly obtained from the shells of crustaceans and shrimps. Since chitosan is of natural origin, it is important to ensure its purity prior to its application for biomedical purpose.

Polyvinyl Alcohol a linear polymer of vinyl alcohol units is conventionally prepared by the saponification of polyvinyl acetate. Polyvinyl acetate is obtained by the suspension polymerization of vinyl acetate monomer. PVA is widely used in medical devices due to its antifouling nature, biocompatibility and high solubility in water. Common medical uses include soft contact lenses, eye drops, tissue adhesion barriers, artificial cartilage etc.

3.1.2 Modifications

3.1.2.1 Quaternization

Quaternization is an effective approach to induce positive charges in polymers. This involves introduction of positively charged active groups such as biguanide, quaternary ammonium salts (QAS), quaternary pyridinium or phosphonium salts, alkyl trimethyl ammonium halide or alkyl halides on to the polymer so as to render it cationic. The quaternized derivative has excellent properties than the parent polymer, especially the

water solubility and antibacterial properties. Chitosan is a natural polymer containing randomly distributed D-glucosamine and N-acetyl-D-glucosamine linked via β-(1→4) linkage. The solubility of chitosan in acidified water is due to the protonation of amino groups of chitosan. The pKa value of amine group in chitosan varies between 6.51 - 6.39, depending on the degree of deacetylation. The poor solubility of chitosan at physiological pH limits its potential applications which can be overcome by its chemical modification of amino group or hydroxyl groups. These chemical modifications will not change their fundamental skeletal structure and indeed they retain and improve their inherent physicochemical and biological properties. Quaternization of chitosan is a promising approach which involves introduction of permanent positively charged quaternary ammonium groups on chitosan or by simply converting the amino groups in chitosan to quaternary amine which enhances its water solubility and antimicrobial efficacy. The antimicrobial property of quaternized chitosan can be well explored in the area of biomaterial assisted biomedical devices where bacterial infection is a major concern. These antimicrobial materials can also find extensive application in biomedical field such as coatings on biomedical devices, wound dressing materials, drug delivery and tissue engineering applications.

3.1.2.2 Thiolation

Thiolation of polymers is the process of conjugating thiol bearing simple molecules such as mercaptoethanoic acid, mercaptopropanoic acid, cysteine, cystamine etc., into a polymeric backbone. These molecules are usually immobilized by acid catalyzed esterification, EDC coupling, dicyclohexyl carbodiimide (DCC) coupling reactions. Thiol groups immobilized on a polymer act like a second active site for further functionalization through simple chemical reactions. The thiolated polymers finds potential application in preparation of cross-linked nano particles, supramolecules,

dendrimers, self-cross-linked structures as well as hydrogel based system via thiol-ene as well as thiol-yne crosslinking reactions. Thiolated polymers find extensive application in biomedical field as drug delivery systems owing to their mucoadhesive properties, topical application formulations due to *in situ* gelling properties and as injectable hydrogel scaffolds for tissue engineering applications.

3.1.2.3 Click chemistry

In polymer modification approaches, click chemistry refers to a class of reaction which allows the joining of polymers of choice with specific molecules. The term Click Chemistry was introduced by K. B. Sharpless to describe reactions that are easy to perform, stereospecific, high yielding, create only by-products that can be removed without chromatographic techniques. Click reactions include Copper (I)-catalyzed alkyne-azide cycloaddition, Strain-promoted alkyne-azide cycloaddition, Strain-promoted alkyne–nitrone cycloaddition, Alkene and azide [3+2] cycloaddition, thiol-ene click reactions etc. Among these reactions, thiol-ene reaction was selected for PVA modification as modification using alkyne and alkene group reduces its solubility in water. Therefore the PVA was modified using thioglycolic acid via ester linkage through an acid catalyzed esterification reaction.

Click chemistry approach paves a new way for the novel innovations in the biomedical field in the area of nanoparticle research, targeted drug delivery, bioconjugation for developing biofunctional molecules, *in situ* forming crosslinking hydrogel system which could be for tissue engineering, drug delivery, gene delivery,3D bioprinting, wound healing, antimicrobial and cancer research applications.

3.1.2.4. In situ precipitation

In situ precipitation reactions involve precipitation of dissolved ions in solution to form insoluble solid via chemical reaction inside a reaction mixture. This way of *in situ* method for synthesis of polymer-ceramic composite preparation is often advantageous as it is quite simple, cost effective and better integration of ceramic with the polymer. In the present work, the *in situ* precipitation of calcium phosphate in quaternized chitosan has been done for making composite with improved physico-mechanical properties.

3.1.2.5. Functional grading

In material perspective, functional grading is characterized by both by structural and composition variation in a given volume of material. This results in graded properties throughout the material. These types of materials are constructed for specified function and application. In order to generate such type of materials the common techniques utilized includes layer by layer processing, melt processing etc. In the present work, graded membranes with four layers were made with combination of polymer and different weight percentage of ceramic. The first layer consist of polymer with 10 wt.% ceramic followed by the second layer having polymer with 5 wt.% ceramic, third layer with 2.5 wt.% and the fourth layer consist of polymer alone.

3.1.2.6. Lyophilization

Lyophilization or freeze drying is a low temperature dehydration process carried out through different steps. It includes the freezing of solution to solid form, lowering the pressure and finally sublimation of ice. For polymer solutions, freeze drying can generate highly porous structure in desired shape. The pores are generated by the sublimation of ice and hence structure has great importance here. The freeze drying technique offers advantages like shape maintenance, quality of product etc.

3.2 Materials Development

3.2.1 Quaternized chitosan – Strontium doped hydroxyapatite composite (QC-SA)

Quaternized chitosan-strontium hydroxyapatite composites were prepared with aim for using it as a bone regenerative material.The polymer quaternized chitosan and the bioactive ceramic strontium hydroxyapatite were synthesized and characterized.The QC-SA composites were fabricated by freeze drying method and characterized for its physicomechanical properties and cytocompatibility.The fabricated composite sheets is expected to be biocompatible and biodegradable with suffcient mechanical properties to be used as guided tissue/bone regeneration membranes.

3.2.2 Purification of chitosan

Chitosan was purified as per ASTM standard (ASTM F 2103). For purification, about one liter of 0.5% w/v solution of the crude chitosan powder was prepared in 1% v/v solution of acetic acid by constant stirring for about 24 h to ensure complete dissolution and filtered to remove insoluble impurities. To the solution at stirring condition, 5% w/v solution of sodium hydroxide was added drop wise till the pH value hits above 7. The precipitate was then collected by centrifugation and washed several times with distilled water till the pH of the washing drops to 7. The precipitate was again resuspended in 500 mL distilled water and about 0.5 mL of 10% w/v sodium dodecyl sulphate (SDS) was added, stirred for 30 min followed by addition of 3 mL of 5% w/v Ethylenediaminetetraacetic acid (EDTA) solution. The stirring was then continued for 2 h. Finally the precipitate was again collected by centrifugation and washed several times with distilled water till washing is free from SDS and EDTA. The residue was then collected and dried in a vacuum oven at 60°C to obtain purified chitosan which was designated as CS.

3.2.3 Preparation of quaternized chitosan (QC)

Quaternized chitosan was prepared by modifying the procedure reported in literature [Loubaki et al., 1991; Zou et al., 2015]. About 2% w/v purified chitosan solution was prepared in 2% v/v acetic acid solution and stirred overnight for complete dissolution. Prior to quaternisation step, the solution was heated to 80°C, to which about 0.75 mL (4.47 mmol) glycidyl trimethyl ammonium chloride (GTMAC) was added with stirring and maintained at 80°C for 7 h. It was then cooled to room temperature and the resulting solution was poured into three fold excess acetone (150 mL) to precipitate out quaternized chitosan (QC).The precipitate was then filtered, washed twice with methanol, centrifuged and further purified by dialyzing against distilled water using 3.5 kDa dialysis bag. This was continued for 24 h with change of media in between, to obtain the purified QC solution and polymer recovered by freeze drying.

3.2.4 Synthesis of strontium substituted hydroxyapatite (SA)

Strontium containing apatite was prepared through a co-precipitation method described in literature [Krishnan et al., 2016]. Calcium nitrate tetrahydrate and strontium nitrate were mixed in a ratio having the strontium content of 10 mol% with respect to calcium, and made into a solution. The amount of second ingredient, ammonium dihydrogen orthophosphate, was adjusted so that the (Ca+Sr) /P molar ratio is 1.67, the theoretical Ca/P ratio of the bone mineral in ‘apatite’ form. Solution of ammonium dihydrogen orthophosphate was prepared; and the pH was maintained above 10 using liquid ammonia and it was kept stirring at a temperature of 80°C. The nitrate solution was then added drop-wise to it so that that the strontium-containing apatite (SA) is precipitated. Being a nano-suspension, centrifuging was done to isolate the precipitate. It was then washed in distilled water multiple times and centrifuged to remove the reaction

by-products. The final slurry obtained was spray-dried to obtain fine, free-flowing powder of strontium doped hydroxyapatite.

3.2.5 Preparation of QC-SA

The purified quaternized chitosan was made into 1% w/v solution in distilled water by stirring it for 24 h. Composite membranes were made by blending the strontium-containing apatite (SA) with quaternized chitosan (QC) solution. The definite quantity of SA powder was dispersed in minimum amount of de-ionized water by stirring for 2 h. It was then added drop wise to QC solution, so as to contain a few milligrams of SA per millilitre volume. A homogenous mixture was made by subjecting it to vigorous stirring for 2 h and was transferred to flat plastic containers. Overnight freezing and subsequent lyophilization for 24 h gave spongy, thin sheets. The area and thickness of the sheets could be manipulated by the size of the container and the quantity of the poured solution. Samples containing 1.5 mg/mL and 2 mg/mL concentrations of SA were prepared for the present study, which are designated as QC-SA-1.5 and QC-SA-2.0 respectively. Membranes of bare QC were also prepared as control for comparison (QC-0).

3.2.6 Characterization plan for QC-SA composites

3.2.6.1 Purified chitosan

The crude chitosan powder after purification was analyzed for heavy metal content using Inductively Coupled Plasma Optical Emission Spectrometer (ICP-OES), degree of deacetylation by potentiometric titration, number average molecular weight by gel permeation chromatography.

3.2.6.2 Quaternized Chitosan

The conjugation of GTMAC via amine groups of chitosan was confirmed by using spectroscopic techniques like Infrared spectrophotometer (FTIR) spectra and ^{1}H- Nuclear Magnetic Resonance spectra (^{1}HNMR). The surface wettability analysed by water contact angle measurements. The phase analysis of the prepared Strontium doped hydroxyapatite was done using X-ray diffraction analysis.

The characterization of QC-SA composite includes

(a) Morphological analysis using Scanning Electron microscopy

(b) Mechanical property evaluation by measuring the tensile and suture pull out strength of material in membrane form

(c) *In vitro* biodegradation analysis by measuring weight loss in PBS and *in vitro* swelling by measuring the weight gain at different time points when kept in PBS

(d) *In vitro* cytocompatibility evaluation by MTT analysis and direct contact test using human periodontal ligament cells (hPDL cells)

3.2.7 Quaternized chitosan- calcium phosphate in situ composite (CPQC)

Quaternized chitosan-calcium phosphate *in situ* composites (acronymed as CPQC) were fabricated by freeze drying method for using it as a bone regenerative material.The CPQC composites were characterised for its physicomechanical properties and cytocompatibility. The fabricated composite sheets is expected to be biocompatible and biodegradable with suffcient mechanical properties to be used as guided tissue/bone regeneration membranes.

3.2.7.1 Preparation of CPQC

The purified quaternized chitosan was made into 1% w/v solution in distilled water by stirring it for 24 h and was mixed with $Ca(NO_3)_2.4H_2O$ and 1 M H_3PO_4 solution in the

Ca/P ratio 1.67. The calcium nitrate and phosphoric acid was added in such a weight ratio that the precipitated calcium phosphate will be 10% m/m of the weight of the membrane. The solution was then poured into petriplates of diameter 6 cm and frozen at -20°C overnight and freeze dried. Blank was prepared in the same manner avoiding calcium nitrate and phosphoric acid and was designated as QC (quaternized chitosan). The freeze dried membranes with calcium and phosphate ions are further immersed in 1 M ammonium hydroxide solution for calcium phosphate precipitation and after that the membranes were thoroughly washed to remove residual ions and dried in vacuum. The dried membranes were designated as CPQC.

3.2.7.2 Characterization plan for CPQC

The material characterization of CPQC includes

(a) Phase identification of *in situ* precipitated calcium phosphate using X-ray diffractometer

(b) Surface Morphological analysis using scanning electron microscope

(c) Mechanical property evaluation by measuring the tensile and suture pull out strength of material in membrane form

(d) *In vitro* biodegradation analysis by measuring weight loss in PBS and *in vitro* swelling by measuring the weight gain at different time points when kept in PBS

(e) *In vitro* bioactivity evaluation of material by immersing membrane in stimulated body fluid and subsequent surface feature analysis by SEM and elemental analysis by EDS and phase identification of deposited material by XRD

(f) *In vitro* cytocompatibility evaluation by MTT analysis, direct contact test using L929 cells and cell adhesion and spreading using hPDL cells

3.2.8 Cross-linked Thiolated PVA graded composite containing hydroxyapatite (TPVA-HA)

Thiolated PVA graded composite containing hydroxyapatite were prepared with aim for using it as a bone regenerative material. The polymer thiolated PVA and the bioactive ceramic hydroxyapatite were synthesized and characterized. The TPVA-HA composites were fabriacted by freeze drying in a layer by layer method (four layered) with polymer and different weight percentage of ceramic combination. The composites were characterised for their physicomechanical properties and cytocompatibility.The fabricated composite sheets is expected to be biocompatible and biodegradable with suffcient mechanical properties to be used as GBR/GTR membranes.

3.2.8.1 Material preparation from synthetic polymer Polyvinyl Alcohol

Polyvinyl Alcohol (PVA) is a hydrophilic biocompatible polymer that has been extensively used in diverse areas of biomedical field. PVA is water soluble and its solubility is primarily governed by degree of hydrolysis, molecular weight and crystallinity. As PVA is very sensitive towards moisture, PVA based membranes exhibit poor mechanical properties which are strongly undesirable for biomedical applications. Therefore, modification of PVA through its hydroxyl groups opens new domains of applications in the biomedical field. The esterification reaction of polyvinyl alcohol (PVA) with thioglycolic acid (TGA) in the presence of acid as a catalyst offers an attractive route to develop thiolated functional biomaterial.

3.2.8.2 Preparation of Thiolated Polyvinyl Alcohol (TPVA)

Thiolated Polyvinyl Alcohol (PVA) was prepared by acid catalyzed esterification of polyvinyl alcohol using thioglycolic acid (TGA) in aqueous medium [Gupta et al., 2013]. Briefly, about 5% (m/v) solution of polyvinyl alcohol was made in water by adding

10 g of polyvinyl alcohol to 50 mL boiling distilled water under stirring condition. It was then stirred for 12 h to ensure complete dissolution and after that temperature was reduced to 60°C followed by addition of 1.2 mL (13.98 mmol) concentrated HCl and 8.6 mL (123 mmol) thioglycolic acid in drop wise manner for 10 minutes. After the complete addition of reagents, the solution was maintained in stirring condition for 12 h at 60°C. After the reaction, the solution was cooled to room temperature and poured drop wise into three fold excess methanol. The precipitate was collected and washed two times in methanol. Finally the precipitated product was vacuum dried and stored at -20°C. The final purified product was named as TPVA.

3.2.8.3 Preparation of TPVA gel

TPVA gel is prepared by the thiol-ene click reaction. For the preparation of TPVA hydrogel, the thiolated polymer was made into 5% (m/v) solution in water at 60°C. After dissolution, the polymer solution was cooled to room temperature and pH adjusted from 4 to 7 using sodium bicarbonate. About 400 µL of this polymer solution was added to a 24-well tissue culture plate. 100 µL PEGDA solution at a concentration of 50 mmol percent to the total number of thiol groups in the solution was added and mixed thoroughly. After 1 min, the disc-shaped hydrogels can be scooped out using a spatula

3.2.8.4 In-house synthesis of hydroxyapatite (HA)

Hydroxyapatite was synthesized through a wet chemical precipitation method [Krishnan et al., 2016]. Calcium nitrate tetrahydrate and ammonium dihydrogen orthophosphate in the (Ca/P) molar ratio is 1.67 were made to react at aqueous alkaline (pH > 10) condition at 80°C. The calcium nitrate solution was added drop-wise to ammonium dihydrogen orthophosphate to precipitate hydroxyapatite. Centrifugation was done to isolate the precipitate and washed several time till the precipitate is free from

residual impurities. The final slurry obtained was spray-dried to obtain fine, free-flowing powder of hydroxyapatite.

3.2.8.5 Preparation of TPVA-HA composites

Polymeric composite TPVA-HA with a graded composition of hydroxyapatite was prepared by layer by layer casting of polymer-ceramic-crosslinker pre-gel suspension in petriplates. The composition of the HA was adjusted in a concentration 0 to 10% (m/m) to the dry weight of TPVA polymer. The method of gelation was similar to that discussed in section 3.2.8.3.The exception is, instead of TPVA solution, a mixture of TPVA-HA was used. The layered gel was casted as four layer with first layer having HA 10% m/m to polymer (TPVA-HA_{10}), second layer having HA 5% m/m to polymer (TPVA-HA_5), third layer having HA 2.5% m/m to polymer (TPVA-$HA_{2.5}$)and final fourth layer having HA 0% m/m to polymer (TPVA-HA_0). After complete gelation, the plates containing Gel was cooled to -20°C and freeze dried. The porous membrane thus obtained is designated as TPVA-HA. The control material is also prepared in the same manner by avoiding HA, and is designated as TPVA-$HA_{0.}$

3.2.8.6 Characterization plan for TPVA-HA

The structural changes of PVA by esterification was identified and confirmed by characterization techniques like

(a) Fourier transform Infrared spectrophotometer (FTIR) spectra

(b) FT Raman spectra

(c) ^{1}H- Nuclear Magnetic Resonance spectra (^{1}H NMR)

(d) ^{13}C-Nuclear Magnetic Resonance spectra (^{13}CNMR

(e) Molecular weight analysis (GPC)

(f) Estimation of thiol content by Ellman assay and Energy dispersive X-ray spectroscopy (EDS)

The gel formation by thiol-ene crosslinking was confirmed using FTIR and FT Raman analysis. The effect of parameters like pH, polymer concentration, cross-linker concentration vs. time was evaluated. The TPVA-HA composite was then subjected to analysis like

(a) Presence of HA in the composite X ray diffraction analysis

(b) Morphological analysis using Scanning Electron microscopy

(c) Mechanical property evaluation by measuring the tensile and suture pull out strength of material in membrane form

(d) *In vitro* biodegradation analysis by measuring weight loss in PBS medium and *in vitro* swelling by measuring the weight gain and dimension change at different time points when kept in PBS

(e) *In vitro* bioactivity evaluation of material by immersing membrane in stimulated body fluid and subsequent surface feature analysis by SEM and elemental analysis by EDS

(f) *In vitro* cytocompatibility evaluation by MTT analysis, Direct contact test and cell adhesion and spreading using hPDL cells

3.2.9 Thiolated Polyvinyl Alcohol –Thiolated Chitosan - Hydroxyapatite composite (TPVA-TCS-HA)

Thiolated PVA - thiolated chitosan graded composite containing hydroxyapatite were prepared with aim for using it as a bone regenerative material.The polymer thiolated PVA and thiolated chitosan, bioactive ceramic hydroxyapatite were synthesized and characterized.The TPVA-HA composites were fabricated by freeze drying in a layer by

layer method (four layered) with different weight percentage of polymer thiolated chitosan (10 & 5 wt.%) and ceramic HA combination. The composites were characterised for its physicomechanical properties and cytocompatibility.The fabricated composite sheets is expected to be biocompatible and biodegradable with suffcient mechanical properties to be used as GBR/GTR membranes.

3.2.9.1 Preparation of thiolated chitosan (TCS)

Thiolated chitosan (TCS) was prepared by EDC coupling reaction between the amine group of chitosan and the carboxylic acid group of thioglycolic acid [Geisberger et al.,2013; Esquivel et al.,2015]. Briefly a 1% (m/v) solution chitosan solution was prepared by dissolving 500 mg medium molecular weight chitosan in 50 mL morpholine ethane sulphonic acid (MES) buffer. To the chitosan solution in stirring condition, added a mixture of 0.38 mL Thioglycolic acid (5.43 mmol), 1.2 g 1-Ethyl-3-(3-dimethylaminopropyl)carbodiimide hydrochloride (6.26 mmol) and 0.720 g N-Hydroxysuccinimide (6.26 mmol) in drop wise fashion. The reaction mixture was stirred at room temperature for 12 h, followed by dialysis in dialysis bag of molecular cutoff of 3.5 kDa for 4 days. The dialysis media was changed twice a day and media used are as follows: 5 mM HCl (day 1), 5 mM HCl containing 1% (m/v) NaCl (day 2 and 3) and finally 1 mM HCl (Day 4). Finally the purified product was recovered by lyophilization and named as TCS.

3.2.9.2 Preparation of TPVA-TCS-HA

TPVA-TCS-HA polymeric composite membrane with a graded composition of hydroxyapatite was prepared by layer by layer casting of polymer- ceramic-cross linker pre gel solution in petri plates. The composition of the HA was adjusted in a concentration 0 to 10% (m/m) to the dry weight of TPVA polymer. The method of preparing graded

membrane is similar to that explained in the section 3.2.8.5. In addition to TPVA and HA, thiolated chitosan solution of two different concentrations (TCS_5 and TCS_{10}) was also incorporated. The weight ratio between TPVA and TCS was kept as constant in each layer. The layered gel was casted as four layer with first layer having HA 10% (m/m) to polymer (TPVA-TCS-HA_{10}), second layer having HA 5% (m/m) to polymer (TPVA-TCS-HA_5), third layer having HA 2.5% (m/m) to polymer (TPVA-TCS-$HA_{2.5}$) and finally fourth layer having HA 0% (m/m) to polymer (TPVA-TCS-HA_0). After complete gelation, the plates containing Gel was cooled to -20°C and freeze dried. The porous membranes thus obtained were designated as TPVA-TCS_5-HA and TPVA-TCS_{10}-HA. The control material used for the comparison is TPVA-HA.

3.2.9.3 Characterization plan for TPVA-TCS-HA

The structural changes of chitosan by EDC coupling reaction with TGA was identified and confirmed by characterization techniques like

(a) Fourier transform Infrared spectrophotometer (FTIR)spectra

(b) ^{1}H- Nuclear Magnetic Resonance spectra (^{1}HNMR)

(c) Estimation of thiol content (Ellman assay)

The combinatorial composite of TPVA-TCS-HA for biomedical application was evaluated for

(a) Presence of HA in the composite X ray diffraction analysis

(b) Morphological analysis using Scanning Electron microscopy

(c) Mechanical property evaluation by measuring the tensile and suture pull out strength of material in membrane form

(d) *In vitro* biodegradation analysis by measuring weight loss in PBS medium and *in vitro* swelling by measuring the weight gain and dimension change at different time points when kept in PBS

(e) *In vitro* bioactivity evaluation of material by immersing membrane in simulated body fluid and subsequent surface feature analysis by SEM, Elemental analysis by EDS.

(f) *In vitro* cytocompatibility evaluation by MTT analysis, Direct contact test and cell adhesion and spreading using hPDL cells

3.3. Tests and analysis methods

3.3.1 Estimations

Prior to modification of any polymer, it is important to identify and quantify the functional groups present in it. As chitosan is considered, its properties like solubility, bacteriostatic property, biocompatibility etc., are influenced by its molecular weight as well as the degree of deacetylation. For the determination of molecular weight, general technique like GPC analysis was conducted. Since chitosan is of natural origin, it is important to ensure the heavy metal content is below the permissible limit and for that purpose ICPOES will be a best method. For the determination of degree of deacetylation, techniques like ^{1}H NMR and potentiometric titration are commonly used. To quantify the sulfhydryl groups immobilized on PVA, commonly used technique is Ellman assay.

3.3.1.1 Degree of deacetylation of chitosan (CS) by Potentiometric titration.

The percentage of amino groups present per chain (Degree of deacetylation [DD]) of purified chitosan was calculated by potentiometric titration. For analysis, (0.1%) CS solution in standard HCl solution (0.106 M) was used. About 50 mL of the above solution was titrated against standard NaOH (0.254 M) solution. The potential of solution corresponding to each addition of a definite volume of NaOH is also measured.The potential of solution corresponding to the volume of NaOH was then plotted against

volume of NaOH added. Later a derivative graph was plotted by dE/dV in y axis the volume of NaOH added along the x axis. There will be two peaks in the graph; the difference in volume corresponds to the NaOH required for the neutralization of protonated amines.

3.3.1.2 Molecular weight of chitosan and quaternised chitosan

Molecular weight of the purified chitosan was evaluated using GPC. The technique involves the flow of pressurized liquid solvent containing sample through a column of adsorbent material. Based on the molecular weight difference each component interacts differently with the adsorbent material results in shift of flow rates for the different components. Components are eluted based on the pore size of the adsorbent material and volume of sample injected into the column. In general, low molecular weight components have longer retention times compared to high molecular weight one. Molecular weight change after reaction was determined using the Waters GPC system 600 series pump with Waters Ultra hydrogel column. Briefly chitosan and quaternised chitosan solutions of concentration 0.1 m/mL were prepared in the acetic acid-sodium acetate buffer (0.3M HAc +0.2 M NaAc). The same buffer was used as mobile phase.

3.3.1.3 Analysis of heavy metals in purified chitosan by ICP-OES

A known quantity of the sample was digested in acid mixture and then diluted to a known volume in de-ionized water and analyzed as per the work procedure for ICP-OES Analysis. The concentration of the element in the solution was determined from the calibration plot obtained by analyzing standard solutions. The results were recorded and processed using Win Lab 32 software.

3.3.1.4 Estimation of thiol content (Ellman assay)

Free thiol groups immobilized on PVA can be determined by spectrophotometry using Ellman reagent [5.5 '-dithiobis (2-nitrobenzoic acid)] (DTNB). Initially a standard curve was drawn using cystein as standard and from the standard curve the thiol group per gram of the polymer was calculated. PVA solution of same concentration was used as blank. Briefly DTNB 2 mM stock solution was prepared in 50 mM sodium acetate solution. Tris solution of final concentration of 1 M and pH 8.0 was also prepared. A series of cysteine standard solution were prepared starting at 2.5 mM to 1000 mM. 10 μL cysteine solution, 50 μL DTNB solution, 100 μL solution of Tris, and remaining water were mixed to a final volume of 1000 μL. Solution was mixed thoroughly and incubated at room temperature for 5 minutes, and then absorbance was measured at a wavelength of 412 nm. Absorbance obtained was plotted against concentration of thiol to obtain the regression equation.

Sample solution was prepared in water at concentrations of 10, 5, 2.5 and 1.5 m/v% of TPVA in 10 mL of water. Absorbance of sample was measured by adding 10 μL of sample instead of standard. Absorbance obtained was substituted into the regression equation of standard curve and thiol content in the polymer was determined.

3.3.2 Instrumental Methods

A chemical modification of polymer results in the addition of certain groups into the polymer backbone via specific linkages or by removal of groups to generate new functional groups. The simple and easiest technique for functional group evaluation is FTIR spectroscopy. It is an easy technique to identify chemical linkages. The ultimate proof for chemical modification will be obtained from ^{1}H NMR and ^{13}C NMR data along with FTIR. During the conversion of polymer to polymer ceramic composites, the phase of the ceramic filler in the matrix can be confirmed from X-ray diffraction analysis. Since

most of the polymers are amorphous in nature, the sharp peaks of the ceramic material will be predominant in the spectra of final composite. During the synthesis of a polymer or its modification it is important to identify the molecular weight of the final modified polymer. GPC is an effective technique to identify number average, weight average molecular weight of polymer and also it give an idea about its poly dispersive index.

3.3.2.1 Fourier Transform Infrared spectrophotometer (FTIR) spectra

FTIR analysis was done using Thermo-Nicolet 5700 spectrometer in attenuated total internal reflection (ATR) mode for sample in freeze dried form in the range from 4000 cm^{-1} to 600 cm^{-1} at resolution of 4 cm^{-1}. For samples in powder form, diffuse reflectance (drift) mode was utilized. The spectra were recorded in the range 4000 cm^{-1} to 400 cm^{-1} at resolution of 4 cm^{-1}. For samples in drift mode, spectrum was converted to absorbance spectrum by performing Kubelka –Munk mathematical transform on the data.

3.3.2.2 Fourier Transform Raman spectra (FT Raman)

The functional group in TPVA and cross-linked TPVA were evaluated using Raman spectroscopy analysis with the confocal Raman microscope (Witec Inc. alpha300R). The samples were used in lyophilized sheet and the Raman spectral measurements using frequency doubled Nd:YAG dye laser [output power 40 mW at 532 nm].

3.3.2.3 ^{1}H- Nuclear Magnetic Resonance spectra (^{1}HNMR)

A proton nuclear magnetic resonance (^{1}H-NMR) spectrometer (Bruker Advance DPX-300) was used to record the NMR spectra of all polymers and modified polymer samples using deuterated solvents.

3.3.2.4 ^{13}C- Nuclear Magnetic Resonance spectra (^{13}C NMR)

A ^{13}C magnetic resonance (^{13}C-NMR) spectrometer (Bruker Advance DPX-300) was used to record the NMR spectra of all polymer and modified polymer samples using deuterated solvents.

3.3.2.5 X ray diffraction (XRD) analysis

The phase analysis of the strontium doped hydroxyapatite, spray dried hydroxyapatite and the *in situ* calcium phosphate precipitate was characterized using X-ray powder diffraction (XRD) analysis. XRD was done in Bruker D8 Advance Diffractometer with Cu Kα radiation generated at a voltage of 40 kV and a current 30 mA. The spectra were recorded in the 2θ range of 10–50° at a rate of 4°/min. The diffraction data was then compared with the standard ICDD data to identify the phase of calcium phosphate.

3.3.2.6 Scanning Electron Microscopy (SEM)

The micromorphology of all composite membranes was investigated using scanning electron microscope (Hitachi, S-2400). The samples were dried and sputter-coated with gold before loading in SEM. For samples after bioactivity test, dried samples were directly visualized under SEM.

3.3.2.7 Contact angle studies

i. Static Contact Angle Measurements

Surface wettability of the QC, PVA, TPVA, TCS, TPVA-TCS, QC-SA and CPQC materials in the form of thin sheet (n=6) were estimated with Goniometer (Data Physics OCA 15 plus Germany). A drop of distilled water was automatically dropped onto a thin

film of the material adhered on a glass and the image was immediately captured and sent to the computer via camera and analyzed using Imaging SCA20 software.

ii. Dynamic contact angle measurements

Surface wettability of the PVA, TPVA, TPVA-HA and TPVA-TCS-HA materials in the form of thin sheet was estimated in water using Wilhelmy method using KSV sigma 701 tensiometer. The scaffolds in the dimension 4cm x 1.5 cm were cut off in n= 6 and the contact angle was determined. The immersion depth and speed was set to 10 mm and 5 mm/min. Six measurements were recorded for each sample and the average of three consecutive values for each sample is taken.

3.3.2.8 Molecular weight analysis (GPC)

GPC is a chromatographic technique for determining the molecular weight of polymers. The technique involves the flow of pressurized liquid solvent containing sample through a column of adsorbent material. Based on the molecular weight difference each component interacts differently with the adsorbent material results in shift of flow rates for the different components. Components are eluted based on the pore size of the adsorbent material and volume of sample injected into the column. In general, low molecular weight components have longer retention times compared to high molecular weight one. Molecular weight change after reaction was determined using the Waters GPC system 600 series pump with Waters Ultra hydrogel column.

3.3.3 Physicochemical tests

While considering gel based materials for graded systems, factors that control the gelling has to be optimized, this includes polymer concentration, pH of medium, cross linker concentration and time for gelling.

3.3.3.1 Optimization of Gelling parameters

i. Effect of pH of the medium on gelation

In order to evaluate the effect of pH on gelation, a 5% (m/v) solution of TPVA polymer was made in water. The polymer concentration was kept as constant and the polymer solution was divided into 7 equal portions. The pH of each solution was then adjusted to range of 4-10 using sodium bicarbonate and pH was measured using portable pH meter. 400 µL of each solution was collected in triplicate to a 24 well tissue culture plate and added 100 µL 10% (v/v) PEGDA solution to each well and stirred.

ii. Effect of polymer concentration on gelation

In order to evaluate the effect of polymer concentration on gelling, a 10% (m/v) stock solution of TPVA polymer in water was prepared. The pH of the solution was then adjusted to 7 using sodium bicarbonate. Different dilutions of the stock solution were prepared starting from 10 to 0.25% (m/v). To 400 µL of each concentration collected in triplicate into a 24 well tissue culture plate, then 100 µL 10% (v/v) PEGDA solution was added and stirred well.

iii. Effect of cross linker concentration (mmol % to SH) on gelation

In order to evaluate the effect of cross linker (PEGDA) concentration on gelling, 5% (m/v) stock solution of TPVA polymer in water was prepared and pH adjusted to 7 using sodium bicarbonate. About 400 µL of solution was collected to a 24 well tissue culture plate. To each well, 100 µL of PEGDA with concentration ranging from 100 to 3.125 mmol% to SH group in solution was added in triplicate. It was then thoroughly mixed and gelling time was recorded.

iv. Cross linker concentration Vs Time of gelation

In order to evaluate the time Vs cross linker concentration on gelling, a 5% (m/v) stock solution of TPVA polymer in water was prepared and pH adjusted to 7 using sodium bicarbonate. 400 µL of solution was collected a 24 well tissue culture plate. To each well about 100 µL of PEGDA with concentration ranging from 100 to 3.125 mmol% to SH group in solution was added in triplicate. It was the thoroughly mixed for gelation and gelling time is noted.

3.3.3.2 Thickness

The thickness of the polymer-calcium phosphate composite in membrane form was measured using a digital vernier caliper (Mitutoyo, Japan). Measurements were taken at five random positions and the mean thickness was determined.

3.3.3.3 In vitro degradation

In vitro degradation studies were carried out to identify and quantify the potential degradation products associated with materials intended to be used as implantable devices for biomedical applications. These tests are carried out as per ISO 10993-9 and are applicable for materials that are designed to degrade inside the body (degradable) and materials that are not intended to degrade (non-degradable).These degradation products associated with the materials has to be assessed prior to *in vivo* studies to get a better understanding of the material behavior.

In vitro degradation of polymer- calcium phosphate composite in the form of membrane was tested over a period of 4 weeks by immersing in phosphate buffered saline (PBS) having a pH of 7.4. The samples were cut into 10 mm × 10 mm size, (n = 6) for each composition, and weighed after 2 h drying in vacuum oven. Cell culture plates (6-well) were used for the experiment, with 5 mL PBS in each well. The samples were placed

in the wells and each was coded. The plates were loaded in an incubator maintained at 37 ± 0.5°C and taken out after the stipulated time period. Each sample was then washed with deionized water, dried in vacuum oven and weighed. This was repeated until constant weight is attained. The percentage weight loss (the ratio of the measured weight loss to the initial weight, multiplied by 100) at the time period was estimated. The samples were then placed back to the respective wells and the process was continued. The first measurement was done after 1 day and it was repeated at the interval of 4 days, till the 29th day. The *in vitro* degradation in terms of weight loss was calculated using the formulae,

$$\%\ \boldsymbol{weight\ loss} = \frac{(\boldsymbol{w_i} - \boldsymbol{w_f})}{\boldsymbol{w_i}} * \mathbf{100}$$

Where W_i and W_f are initial and final weight of the sample.

3.3.3.4 In vitro swelling studies

The swelling studies are carried out to measure the extent of swelling of the material when used for specific applications. The swelling can be measured by measuring the water uptake and dimensional changes (volumetric).

i. Water uptake

In vitro swelling studies of polymer- calcium phosphate composite in the form of membrane were analyzed in PBS saline (pH 7.4) at a temperature of 37 ± 0.5°C. Pre-weighed membranes of dimension 2 × 2 cm was kept immersed in 5 mL of 1 X PBS and taken out at different time point (0, 0.25, 0.5, 1, 24, 48 h). Surface water is wiped out using tissue paper and weight gain in the membrane was measured. The percentage swelling in terms of water uptake was calculated using the formulae,

$$\%\ \boldsymbol{Swelling\ by\ weight} = \frac{(\boldsymbol{w_f} - \boldsymbol{w_i})}{\boldsymbol{w_i}} * \mathbf{100}$$

Where W_i and W_f are initial and final weight of the sample.

ii. Volume swelling based on dimensional change

In vitro swelling studies based on dimension change of samples in membrane form were done in PBS saline (pH 7.4) at a temperature of 37 ± 0.5°C. Membranes of dimension 1 cm × 1cm × 0.05 cm was kept immersed in 5 mL of 1 X PBS and taken out at different time point (0, 0.25, 0.5, 1, 24, 48, 72, 96 h). Surface water was removed by using tissue paper and dimensions (length, breadth and thickness) were measured. The percentage change in the dimension based on volume was then calculated using the formula.

$$\%\ \boldsymbol{Swelling\ by\ volume} = \frac{(\boldsymbol{V_f} - \boldsymbol{V_i})}{\boldsymbol{V_i}} * \mathbf{100}$$

Where $\mathbf{V}_i$ is initial volume of membrane; $\mathbf{V}_f$ is the final volume of membrane.

3.3.3.5 Mechanical testing

For the use of polymer- Calcium Phosphate composite for GBR/GTR application, it should sufficient strength to withstand the forces experience over it. Strength of the material was test in terms of tensile strength and suture pull out strength.

i. Tensile strength

The tensile test was performed using universal testing machine (UTM model, Instron 3345, UK) as per the standard ISO 527-3. Samples of average thickness 0.5 mm were cut into size 5cm × 1cm (n=12), fitted using appropriate fixtures and subjected to tensile force vertically at the speed of 10 mm/min for chitosan based system and 20 mm/min for PVA based systems. Measurements were done using a load cell of 100 N up to the point of sample failure. The tensile strength and elongation of samples were determined from the data.

ii. Suture pull out strength

The suture pull out strength represents the tear off limit when a suture thread passed across the membrane is pulled out. Samples of size 10 mm width and 45 mm length (n=12) were cut out and the bottom end was gripped on to the lower jaw of the UTM. A single suture was tied on the top end with monofilament silk suture thread, at 5 mm down from the top edge along the middle line. The suture ends were folded and gripped to the upper jaw of the UTM fixture and pulled at a rate of 10 mm/min. The tearing off of the membrane was taken as the end point.

3.3.3.6 In vitro bioactivity

In GBR application, the ability of a material to generate bone-like apatite on its surface is of key importance during the physical and chemical processes leading to bone regeneration. The ability of a material to initiate apatite deposition is evaluated by *in vitro* bioactivity test using simulated body fluid. *In vitro* bioactivity test of all composites were carried out in membrane form by immersing the pre-weighed membrane (1.5cm x1.5 cm) in 10 mL SBF. Samples were done in triplicate. It was maintained at 37 ± 0.5°C for 3 days and 7 days with replacing SBF medium every 2 days. The membranes were removed at definite time period, washed thoroughly with deionized water and dried over silica gel till a constant weight is obtained.

The bioactivity was then confirmed by characterization techniques like X ray diffraction analysis over deposited layer, scanning electron microscopy and EDS analysis on the deposited layer. The dried samples were analyzed under Scanning electron microscope in 1000X and 3000X magnification. Energy dispersive spectroscopy (EDS) was done on deposited layer during the imaging using EDAX Genesis XM 4 integrated with the ESEM to find the ratio between Ca and P in the deposited layer.

3.3.3.7 In vitro cytocompatibility studies

In vitro cytocompatibility studies are cell culture assays carried out to assess the potential toxic effects of the developed materials under physiological conditions. These are the first line screening tests for a material prior to its use for further *in vitro* and *in vivo* studies. These tests are carried out using appropriate mammalian cell line as per the standard ISO-10993-5. The test involves exposing the cultured cells to the sample directly as in direct contact assay and measuring the viability of cells microscopically (qualitative method) or exposing the cells to the extract of the material as in MTT assay, a colorimetric method to determine cell viability quantitatively.

The cytocompatibility of the samples were evaluated through direct contact method and MTT assay using L929 mouse fibroblasts. The cells were cultured in α-MEM, 10% FBS containing the antibiotics penicillin, streptomycin (100 IU) and amphotericin B (0.25 mg/100 mL) in a humidified incubator at 5% CO_2 at 37 ± 0.2°C. The cells were characterized prior to direct contact test and MTT assay. The confluent monolayer was sub-cultured and maintained for further studies. Samples (4 mm disc shape cut from 0.5 mm thick membranes) were sterilized by autoclaving before the analysis.

The cytocompatibility of the samples were also evaluated through direct contact method and MTT assay using human periodontal ligament (hPDL) cells. The cells were isolated from human periodontal ligament tissues collected from anonymous discarded extracted teeth following Institutional Ethical Committee guidelines. The cells were cultured in α-MEM, 10% FBS containing the antibiotics penicillin, streptomycin (100 IU) and amphotericin B (0.25 mg/100 mL) in a humidified incubator at 5% CO_2 at 37 ± 0.2°C. The cells were characterized prior to direct contact test and MTT assay. The confluent monolayer was sub-cultured and maintained for further studies. Samples (4 mm disc shape cut from 0.5 mm thick membranes) were sterilized by autoclaving before the analysis.

i. Direct contact test using L929 mouse fibroblasts

The cytotoxicity of the polymer -calcium phosphate composites were evaluated *in vitro*, using L929 mouse fibroblasts. L929 cells were seeded onto the wells of 24 well plate (Nunc, Thermofischer) at a density of 3×10^4 cells/well and cultured in α-MEM, 10 % FBS for 24 h. After 24 h, the culture medium was discarded and test sample (TPVA and TPVA-HA) discs of 4 mm diameter were carefully placed over the cell monolayer, in direct contact with the cells. Organotin stabilized PVC discs which are toxic were placed over the cell monolayer as positive (toxic) control. The L929 cells cultured in the absence of biomaterials was taken as negative control (cell control). The cells were cultured for 24 h in α-MEM, 10% FBS and phase contrast images were taken (Nikon). Cytotoxicity was graded based on the morphology, cell lysis, cell detachment and vacuolization of the cells around the material (0 – Non-cytotoxic, 1 - Slight cytotoxic, 2 - Mild cytotoxic, 3 - Moderate cytotoxic and 4 - Severe cytotoxic).

ii. MTT assay using L929 cells

The cytocompatibility of polymer-calcium phosphate composites were evaluated by 3-(4,5-dimethylthiazol-2-yl)-2,5-diphenyltetrazolium bromide (MTT) reduction assay using L929 mouse fibroblasts. L929 cells were seeded onto the wells of 24 well plate (Nunc, Thermofischer) at a density of 3×10^4 cells/well and cultured in α-MEM, 10% FBS for 24 h. After 24 h, the culture medium was discarded and polymer and polymer-calcium phosphate composite discs of 4mm diameter were carefully placed in contact with the cells. L929 cells alone were used as the positive control and cells treated with 0.13% phenol was used as negative (toxic) control. The cells other than the toxic control was cultured in α-MEM, 10% FBS for 24 h. After 24 h, medium and test materials were removed from the wells; the cells were treated with 100 μL of MTT solution (1mg/ml in serum free α-MEM) and incubated for 2 h. The formazan crystals formed by metabolically

active cells was solubilized in 200 µL of isopropyl alcohol and colorimetrically assessed in a microplate reader (Biotek, USA) at 570 nm. The metabolic activity of the cells was calculated from the optical density values, using the formula:

$$\textbf{Percentage metabolic activity} = \frac{\textbf{OD test}}{\textbf{OD cell control}} \times \textbf{100}$$

iii. MTT assay using hPDL cells

The hPDL cells were seeded onto a 24-well cell culture plate (Nunc, Thermofischer) at a density of 3×10^4 cells/well and cultured for 24 h. Thereafter the medium was discarded and the sterile samples were carefully placed over the cell monolayer. The well with cells alone was taken as the cell control (negative control) and the well added with 0.13% phenol, as the positive control (toxic control). After 24 h the medium as well as phenol (in toxic control) from the wells containing the cells was discarded and the cells were incubated in 200 µL of freshly prepared MTT solution (1mg/mL) in the dark for 2 h. MTT assay was carried out to measure the mitochondrial cellular metabolism and is based on the capability of metabolically active hPDL cells to reduce the yellow water-soluble tetrazolium salt (MTT) to purple formazan crystals using the mitochondrial enzyme succinate dehydrogenase (SDH). The intensity of purple colour so formed is proportional to the number of metabolically active cells. After 2 h, the MTT solution was discarded and the formazan crystals formed was dissolved in isopropanol to measure the optical density (OD) spectrophotometrically at 570 nm. The percentage metabolic activity was calculated as per the formula:

$$\textbf{Percentage metabolic activity} = \frac{\textbf{ODtest}}{\textbf{ODcellcontrol}} \times \textbf{100}$$

The values were plotted as mean ± standard deviation

iv. Direct contact test using hPDL cells

For direct contact cytotoxicity evaluation, the hPDL cells were cultured in 24 well cell culture plates at 3×10^4 cells/well and cultured for 24 h. Then the medium was discarded, the samples (sterile discs of 4 mm diameter) were carefully placed over the cells and cultured for 24 h in α-MEM. The wells without the test materials were taken as the cell control (negative control) and those treated with 0.13% phenol were taken as the positive control. After 24 h, the wells were viewed under inverted phase contrast microscope (Nikon) and the cell response was graded, based on the morphology, cell lysis, cell detachment and vacuolization of the cells around the material. The grades were marked as: 0 - no cytotoxicity, 1 - slight cytotoxicity, 2 - mild cytotoxicity, 3 - moderate cytotoxicity and 4 - severe cytotoxicity.

v. Cell adhesion and spreading using hPDL cells

SEM evaluation : The morphology of hPDL cells on the membranes was evaluated by SEM. hPDL cells were seeded onto glass cover slips (control) and QC and CPQC membranes, at a cell density of 10^4 cells/cm^2 and cultured in αMEM, 10% FBS, 100 IU Penicillin/Streptomycin. The cells were fixed in 2% gluteraldehyde, at 24 and 48 h. The fixed cells were washed in PB solution containing 2 mM disodium hydrogen phosphate and sodium dihydrogen phosphate, 5 times. Then the samples were dehydrated using ascending concentration of ethanol – 30%, 50%, 70%, 90% and 100%, followed by critical point drying (HCP 1010) and gold sputter coating (HITACHI). The samples were viewed and SEM images were taken.

Actin cytoskeleton staining: The functional evaluation of the membranes was carried out using human periodontal ligament cells, isolated from human periodontal ligament tissues collected from discarded extracted teeth. Ethical committee approval was

obtained from the Institutional Ethics Committee, Sree Chitra Tirunal Institute of Medical Sciences and technology, Trivandrum. Primary periodontal ligament cells (hPDL cells) at passage 3 were trypsinised using 0.25% trypsin and seeded onto the membranes at a cell density of 10^4 cells /cm^2. The cells were cultured in αMEM, 10% FBS. At 24 and 48 h, the cells were fixed using 4% paraformaldehyde (PFA) for 1 h, washed with PBS, permeabilised using 0.1% triton X100 and incubated with Phalloidin-iFluor 555 Reagent (Abcam) for 1 h in darkness. After 1 h, the unbound dye was washed off using PBS and the cell nuclei was counterstained using Hoechst 33258 (0.05 µg/mL). The stained actin cytoskeleton was viewed and imaged in confocal laser scanning microscope CLSM (Nikon) at the excitation of 305 nm (for Hoechst 33258) and 555nm for Alexafluor conjugated phalloidin. A 3D stacked image of 100 µm thickness image was developed using the image analysis software (Fiji).

3.3.3 Statistical analysis

Data obtained for mechanical and cytocompatibility analysis were represented as means ± standard error (SE) with $n \geq 12$ samples/group for mechanical analysis, $n \geq 6$ for *in vitro* degradation, swelling and $n \geq 3$ samples/group for *in vitro* cytocompatibility studies. A one-way analysis of variance (ANOVA) with t test was performed in GraphPad Prism 6.01 and $p \leq .05$ was considered significant. (*) $p < 0.05$, (**) $p < 0.01$, (***) $p < 0.001$, (****) $p < 0.0001$ and no significant difference (p value > 0.05) denoted by ns.

CHAPTER 4

RESULTS

This chapter gives results obtained from the experiments on the synthesis and characterization of the materials developed in the study, namely - (i) Quaternized chitosan- Strontium doped hydroxyapatite composite (QC-SA) ; (ii) Quaternized chitosan-calcium phosphate *in situ* composite (CPQC) ; (iii) Cross-linked Thiolated PVA graded porous composite containing hydroxyapatite (TPVA-HA) and (iv) Thiolated Polyvinyl alcohol -Thiolated Chitosan-Hydroxyapatite composite (TPVA-TCS-HA). The results are divided into four sections each represents the results of specific experiments discussed in the materials and methods section in Chapter 3.

4.1 Quaternized chitosan – Strontium doped hydroxyapatite composite (QC-SA)

The objective of this section is to modify commercially available chitosan in order to impart high degree of solubility and blend it with calcium phosphate based minerals to achieve bioactivity suitable for the regeneration of defective bone.

4.1.1 Purification of Chitosan and its characterization

Purification of crude chitosan powder was carried out by dissolving in aqueous solution of acetic acid to remove insoluble impurities, followed by precipitation of purer chitosan by adjusting the pH to alkaline condition. The presence of heavy metals in purified chitosan, degree of deacetylation and number average molecular weight of purified chitosan were determined.

4.1.1.1 Analysis of heavy metals in purified chitosan by ICP-OES

The heavy metal content in any implantable material is restricted by relevant standards, National as well as International. This is true with chitosan also, particularly because it is a natural material of marine origin. The purity of chitosan material in the present work was assessed based on ASTM F2103-18, "*Standard Guide for Characterization and Testing of Chitosan Salts as Starting Materials Intended for Use in Biomedical and Tissue-Engineered Medical Product Applications*". The crude chitosan after the purification step (CS) was analyzed for heavy metal contents using ICP-OES, the results of which are summarized in Table 1.

Table 1: Heavy metal analysis of chitosan using ICP-OES

Material : Chitosan		***Sample ID :*** 'CS'
Element	***Content Level (ppm)***	***Detection limit (ppm)***
Silver (Ag)	BDL	0.0070
Arsenic (As)	BDL	0.0530
Bismuth (Bi)	BDL	0.0340
Cadmium (Cd)	BDL	0.0027
Copper (Cu)	19.54	0.0097
Mercury (Hg)	BDL	0.0610
Lead (Pb)	1.272	0.0420
Molybdenum (Mo)	BDL	0.0079
Tin (Sn)	BDL	0.0960
BDL indicates 'below detection limit'		

Only copper and lead were detectable in the sample. The detected quantities of metals are below the permissible limits as prescribed in the standard ASTM F1609. The Pb content was lower than the prescribed limit of 30 ppm. The total metal can be 50 ppm, and copper is not listed as a toxic heavy element.

4.1.1.2 Potentiometric titration for determining degree of deacetylation of purified chitosan (CS)

One of the important properties that affect the amine functionalization of chitosan is the number of free amine moieties in the polymer. Hence, quantification of the '*degree of deacetylation*' (DD) is important prior to derivatization of chitosan. The free amino groups in chitosan were determined from potentiometric titration. For the determination of DD via potentiometric titration method, the difference in volume of NaOH between two deflections points in the plot of derivative of potential (dE/dV) against volume of NaOH is utilized. The first deflection corresponds to the neutralization of H^+ in the solution provided by free HCl molecules and the second deflection corresponds to the complete neutralization of NH_3^+ in the polymer. The difference in volume of NaOH will be equivalent to the concentration of amine moiety in the polymer. Figure 2 shows plot of variation of potential against volume of NaOH and its derivative during the estimation of degree of deacetylation (DD). The two peaks were obtained at 20.2 mL and 21.3 mL, and substituting this in the equation for calculating degree of acetylation, the purified CS was found deacetylated to a level of 87.6%.

4.1.1.3 Molecular weight analysis of Chitosan

The number average molecular weight of the chitosan was calculated using Gel permeation chromatography (GPC) which is represented in Figure 7 (Along with the modified material). From the graph, the number average molecular weight of chitosan was found to be 1074 kDa with a polydispersity of 1.54.

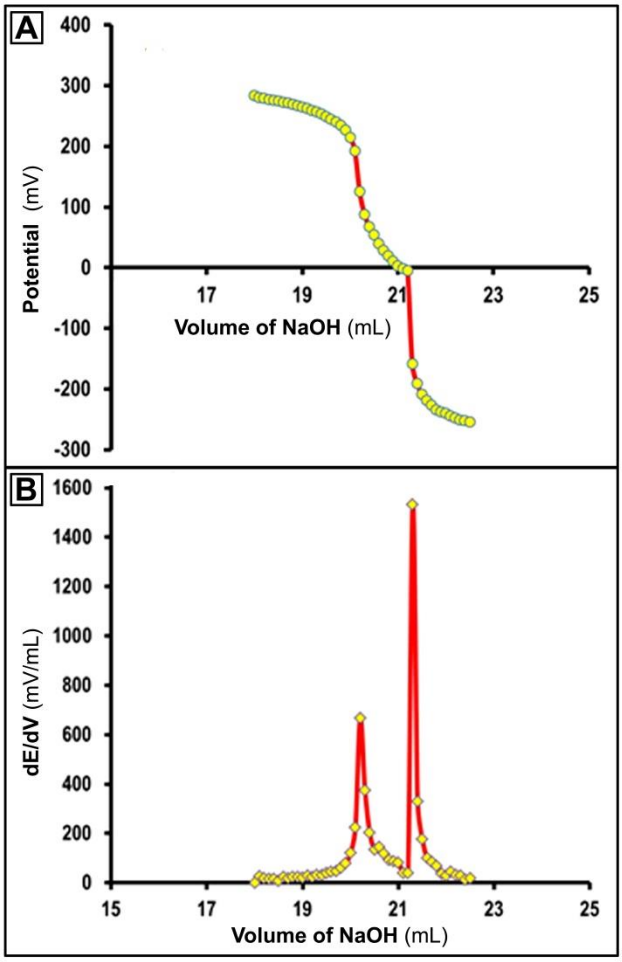

Figure 2: Plots representing [A] Potential versus volume of NaOH and [B] Derivative of potential versus volume of NaOH.

4.1.2 Preparation and characterization of quaternized chitosan (QC)

Quaternized chitosan was prepared by a ring opening reaction of Glycidyltrimethylammonium chloride (GTMAC) with acidic aqueous solution of chitosan at 80°C. Under this condition the glycidyl ring opens and get attached to the amine groups. Chitosan contains free amino groups as well as hydroxyl groups. Compared to hydroxyl groups, amino groups are more nucleophilic to open the glycidyl ring and the reagent gets covalently attached to the amino groups. The schematic representation of the reaction is given in the Figure 3. The structural analysis of the new material was done through FTIR and ^{1}H NMR.

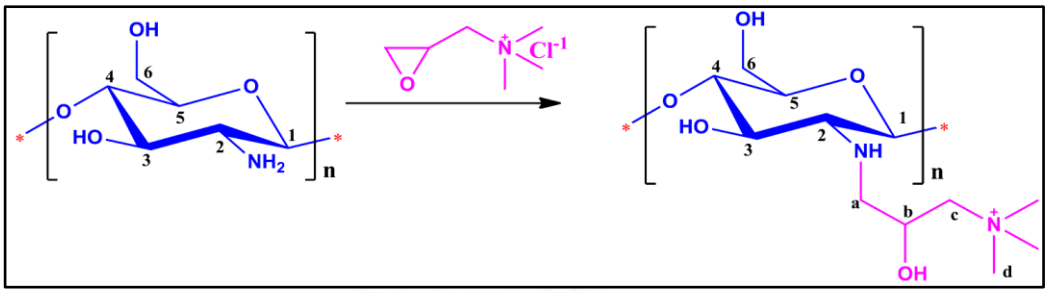

Figure 3: Schematic representation showing quaternization reaction of chitosan

4.1.2.1 Fourier transform infrared (FTIR) analysis of CS and QC

Chitosan consist of amino/acetamido group as well as both primary and secondary hydroxyl groups at the C-2, C-3 and C-6 positions. The conjugation of GTMAC to amine moieties of chitosan was confirmed by FTIR spectral analysis (Figure 4). The broad band at 3350 cm^{-1} represents the stretching band from both hydroxyl groups and residual amine groups. Peaks at 2920 cm^{-1} and 2876 cm^{-1} on the shoulder of the broad band indicate the symmetric and anti-symmetric stretching of C-H bond and amide I stretching from the residual N- acetyl groups along with N-H bending vibrations of primary amines are represented by a peak at 1627 cm^{-1}. The amide II band of residual amide bonds is observed at 1520 cm^{-1}. Peaks at 1414 cm^{-1} and 1379 cm^{-1} could be assigned to the CH_2 bending and CH_3 symmetrical deformation. The peak at 1150 cm^{-1} represents the C-O-C bridge, and those at 1067 cm^{-1} and 1024 cm^{-1} correspond to C-O stretching modes. Another characteristic peak from the CH bending out of the plane of the monosaccharide ring appeared at 900 cm^{-1}.

In quaternized chitosan (QC), most of the characteristic vibrations of chitosan are present. The peak at 1150 cm^{-1} is retained in the product showing that C-O-C bridge between the monomer units is not affected. Compared to CS, there is shift in the peaks 1627 cm^{-1} and 1520 cm^{-1}. The shift 1627 cm^{-1} to 1640 $cm^{-1}$and 1520 cm^{-1} to 1542 cm^{-1} may be due to the partial modification of primary amine groups [Zouet al.,2015].

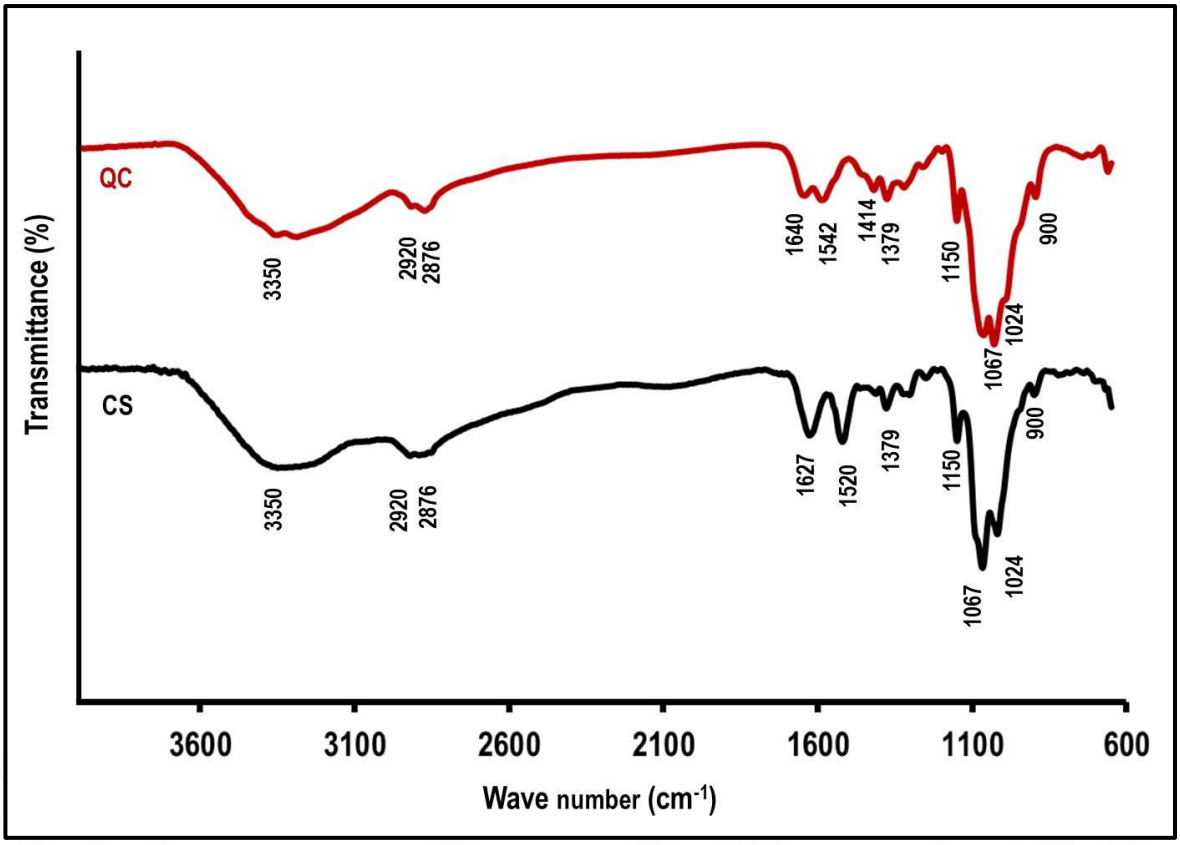

Figure 4: FTIR spectrum of chitosan (CS) and quaternized chitosan (QC)

4.1.2.2 ^{1}H- Nuclear Magnetic Resonance spectra (NMR) of CS and QC

The ^{1}H NMR spectrum of chitosan is shown in Figure 5. The methyl protons from the residual acetyl groups appeared at δ ~ 1.93 ppm. The characteristic peaks of protons from primary and secondary alcohol groups are present at δ ~ 1.27 and 1.28 ppm, the CH protons present in 3 to 6 positions are represented by peaks at δ ~ 3.05 ppm to 3.78 ppm. The amide proton from residual N- acetyl part is observed at δ ~ 8.08 ppm.

The ^{1}H NMR spectrum of quaternized chitosan represented in Figure 6 shows that the peak at δ ~ 1.94 ppm is retained, indicating that hydroxyl groups is not affected during the reaction. A new peak at δ ~ 3.14 ppm has appeared which corresponds to the methyl proton in +N $(CH_3)_3$ from the conjugated part. A peak at δ ~ 4.47 ppm appeared in the spectrum of QC is from the OH groups from the GTMAC part [Ruihua et al.,2012; Zou et al.,2015; Kalsi.,2007; Luo et al.,2010].

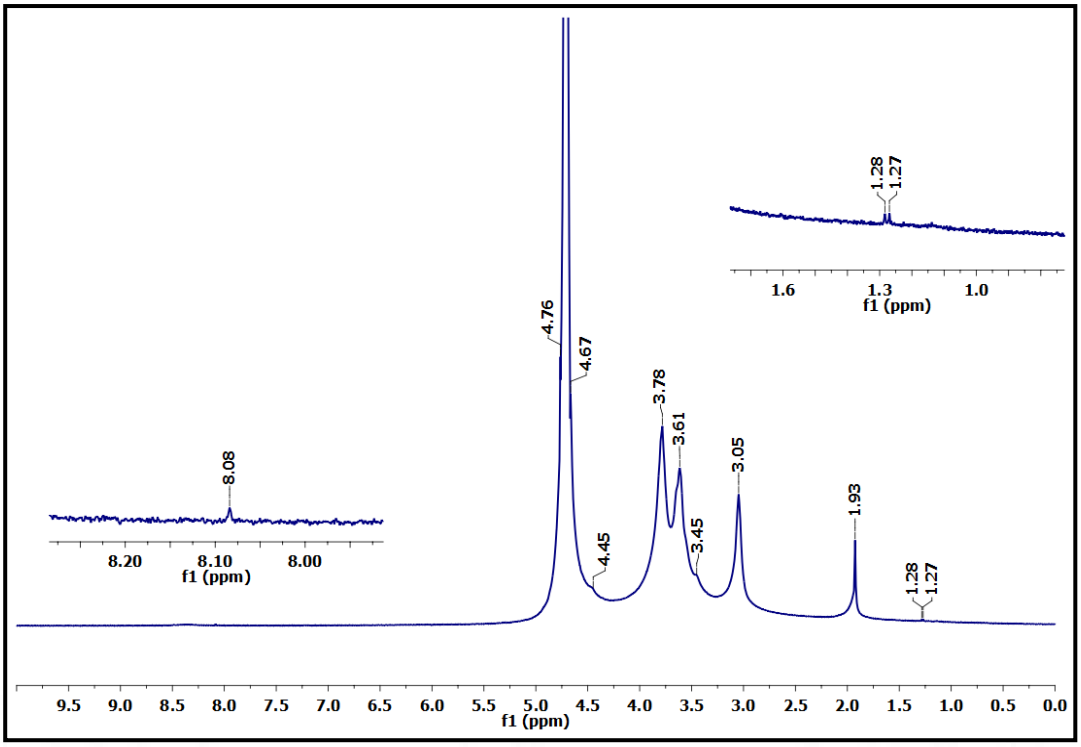

Figure 5: ^{1}H NMR spectrum of chitosan

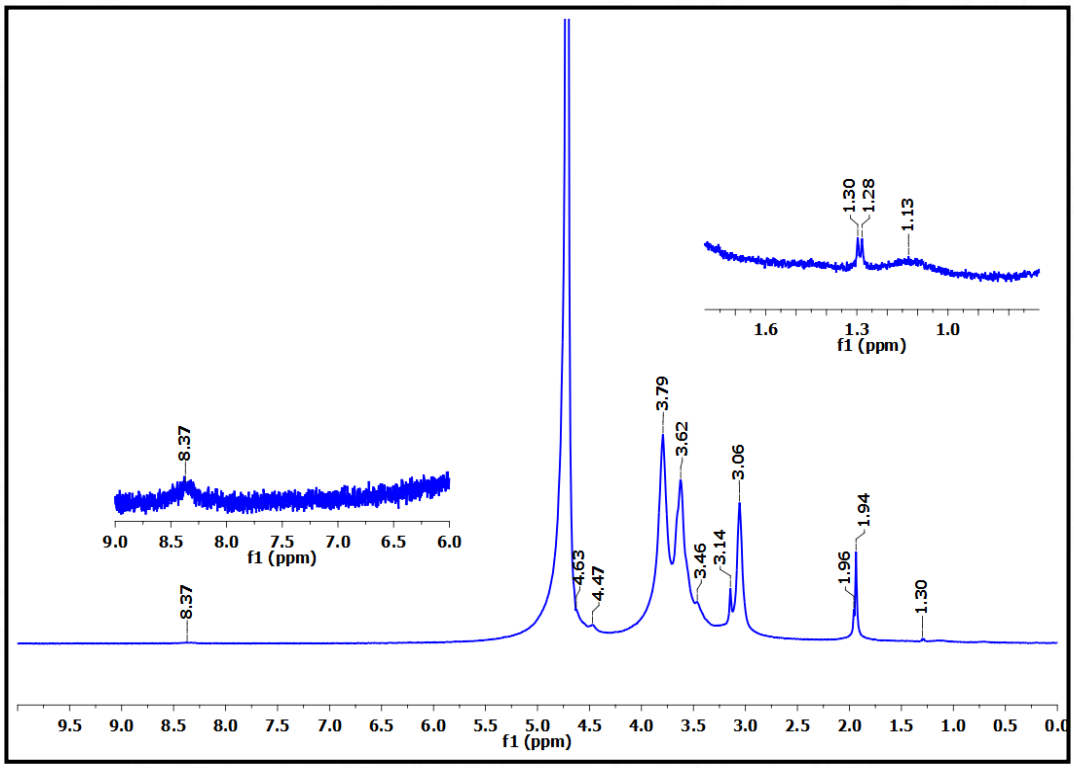

Figure 6: ^{1}H NMR spectrum of quaternized chitosan

4.1.2.3 Molecular weight analysis of Quaternised chitosan

The number average molecular weight of the quaternised chitosan was calculated using GPC and is depicted in Figure 7. From the graph, the number average molecular weight of quaternised chitosan was found to be 624 kDa and its polydispersity was found to be 1.60. This may be due to the possible chain scission that has occurred during the reaction of CS with GTMAC at 80°C for 7 h.

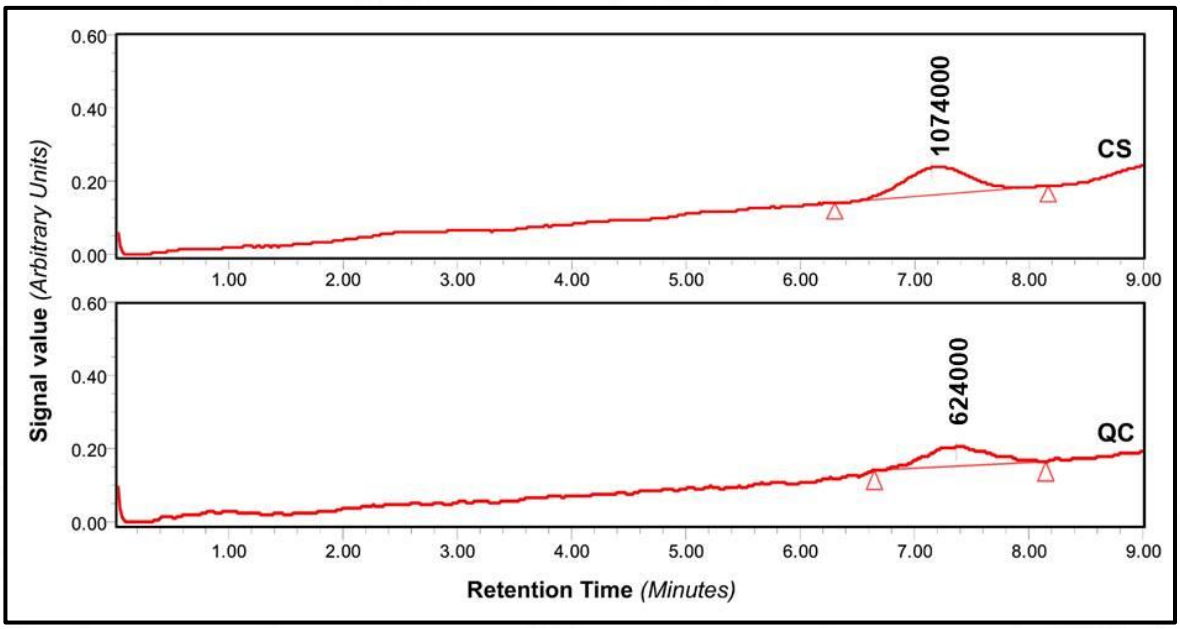

Figure 7 : GPC curve showing molecular weight distributions of CS and QC

. 4.1.2.4 Surface wettability of CS and QC

The surface wetting property of CS and QC analyzed through water contact angle measurements is shown in Figure 8. The contact angles obtained for CS and QC (above 90°) indicate the hydrophobic nature of the chitosan material. Yet, it is to be noted that the quaternization process have decreased the contact from 112±6° to 96±3°, which means a reduction in hydrophobicity

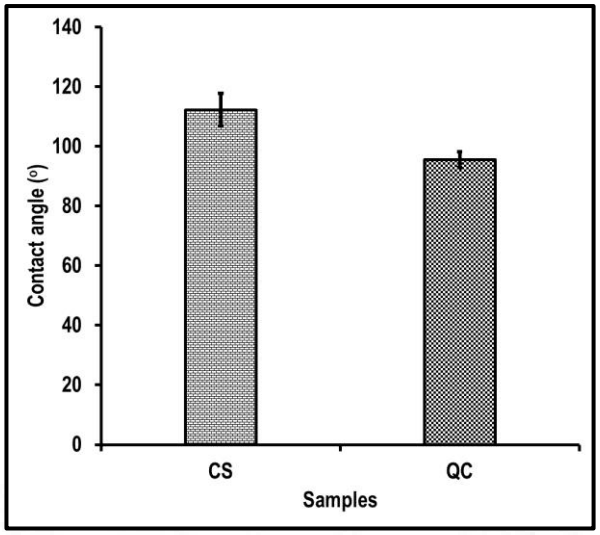

Figure 8 : Water contact angle of CS and QC materials.

4.1.3 Preparation of strontium doped hydroxyapatite (SA)

Strontium-containing apatite, along with hydroxyapatite (HA) was prepared through a wet co-precipitation through the reaction of calcium nitrate and strontium nitrate with ammonium dihydrogen orthophosphate in ammonia solution. Strontium nitrate was taken in a ratio so that the strontium content is10 mol% to calcium, a value which showed optimum bone remodeling enhancement [Chandran et al.,2016; Chandran et al.,2018]. The amount of ammonium dihydrogen orthophosphate was adjusted such that the ratio of combined alkali-metal ions to phosphorous, or the (Ca+Sr)/P molar ratio, is 1.67. The mixture of precipitates with 10% strontium-containing apatite (SA) in hydroxyapatite (HA), is formed. The precipitate was washed and spray dried to 10 micron size particles [Velayudhan et al., 2007]. The prepared SA was characterized by FTIR and XRD.

4.1.3.1 FTIR spectra of SA

The FTIR spectra of SA shows characteristic OH groups stretching at 3570 cm^{-1}, asymmetric C-O stretching in CO_3^{2-} at 1413 cm^{-1} (Figure 9). The absorption peaks at 1099 cm^{-1} and 1030 cm^{-1} corresponds to the asymmetric stretching vibrations of the P–O and

the peak observed at 960 cm^{-1} is assigned to the symmetric stretching mode of the P–O in $PO4^{3-}$ groups. The peaks at 605 cm^{-1} and 563 cm^{-1} are assigned to the bending vibrations of the O–P–O in $PO4^{3-}$ groups.

4.1.3.2 XRD analysis of SA

XRD pattern of SA was very similar to the hydroxyapatite and matched with the standard pattern of strontium calcium apatite (JCPDS – 0340484). The XRD spectra gave the characteristic peaks of apatites, which are indexed and shown in Figure 10. Some new peaks were seen in the spectra (marked * in Figure 10). A comparison of the peaks of SA with that of HA is given in Table 2.

Table 2: Comparison of the X-Ray diffraction data of HA and SA

HA		**SA**		**Remarks**
Peaks	**Plane**	**Peaks**	**Plane**	
21.81	2 0 0	21.71	2 0 0	
22.81	1 1 1	22.71	1 1 1	Reduced
25.83	0 0 2	25.73	0 0 2	
28.14	1 0 2	27.84	1 0 2	Shifted/ Reduced
28.94	2 1 0	28.85	2 1 0	
		31.06		Additional peak
31.76	2 1 1	31.66	2 1 1	
32.16	1 1 2	32.06	1 1 2	
32.87	3 0 0	32.76	3 0 0	
		33.87		Additional peak
34.08	2 0 2			Not in SA
		34.97		Additional peak
35.38	3 0 1	35.28	3 0 1	Reduced
39.10	2 1 2	39.10	2 1 2	
39.81	3 1 0	39.71	3 1 0	
41.82	3 1 1	41.81	3 1 1	
		43.53		Additional peak
43.73	1 1 3	43.82	1 1 3	
45.13	2 0 3			Not in SA
46.64	2 2 2	46.54	2 2 2	
48.05	3 1 2	47.95	3 1 2	
48.25	3 2 0	48.05	3 2 0	
49.46	2 1 3	49.25	2 1 3	

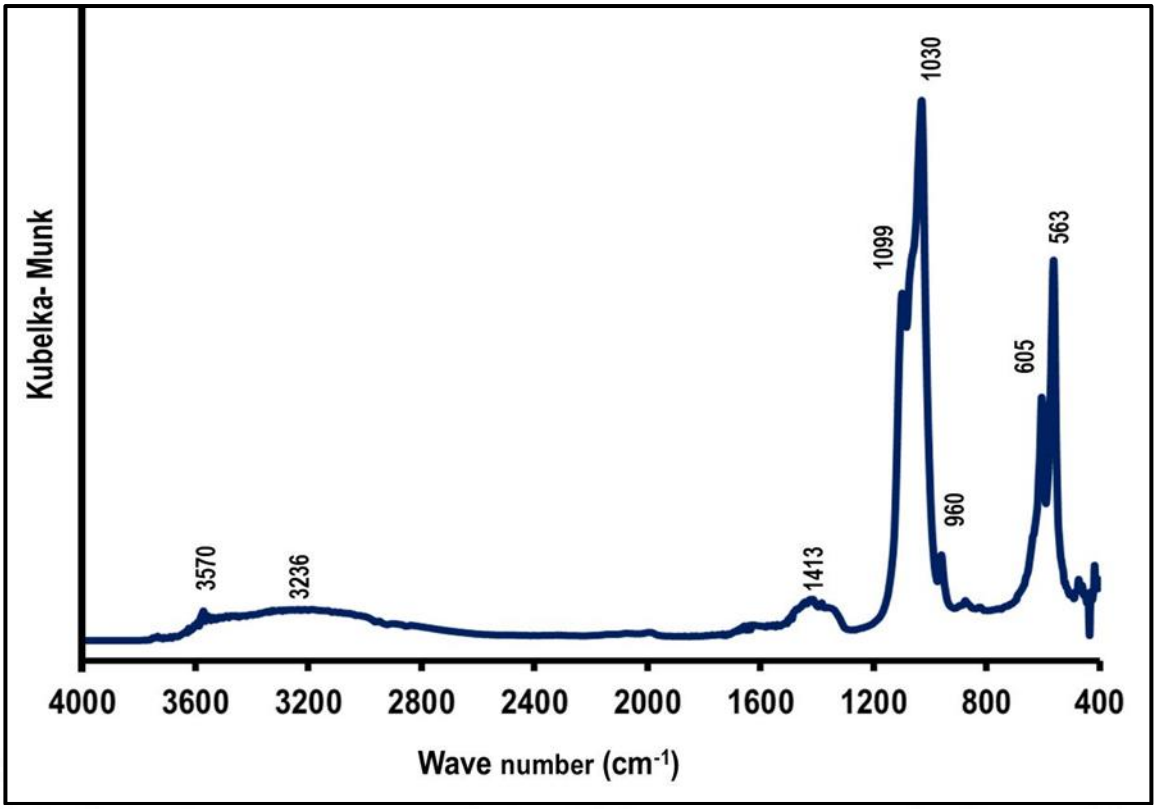

Figure 9: FTIR spectrum of SA

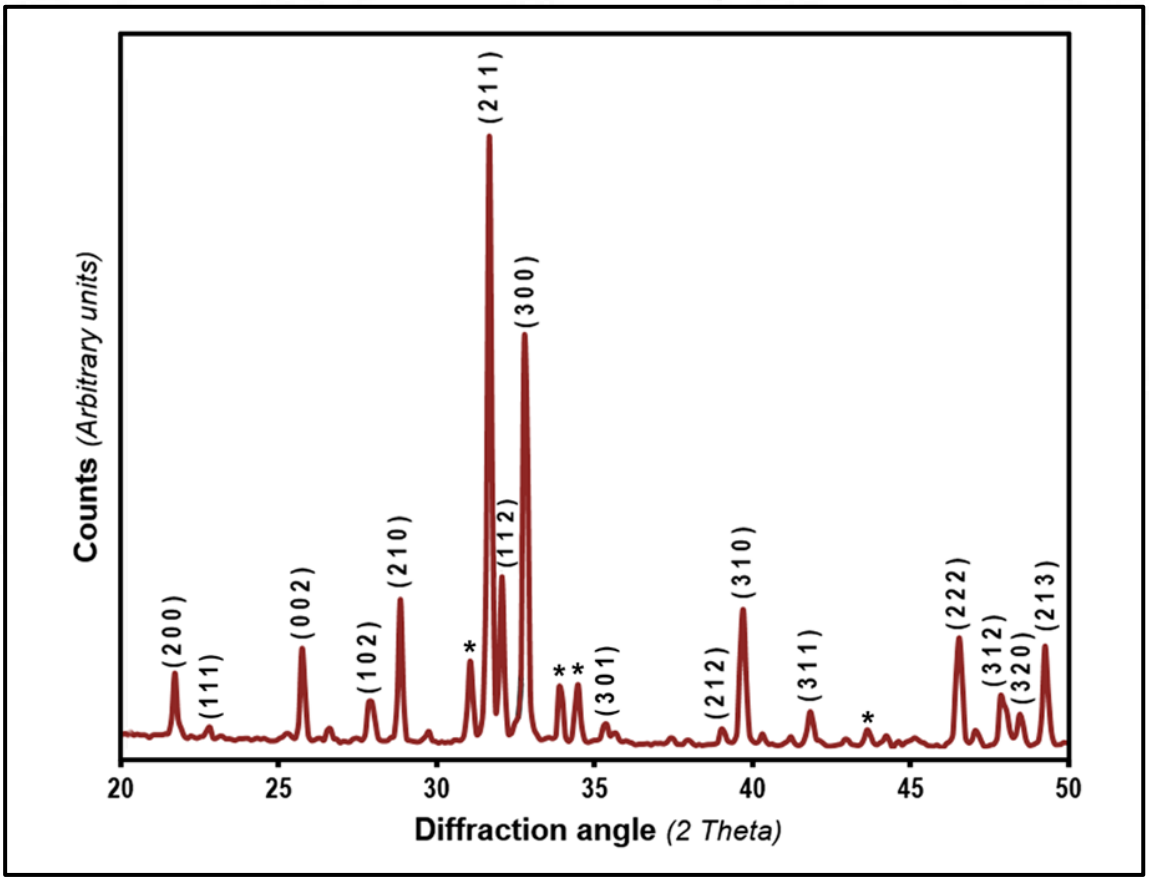

Figure 10: XRD spectrum of SA

4.1.4 Fabrication of porous, cytocompatible and biodegradable composite sheet from QC and SA.

4.1.4.1 FTIR spectra of QC and QC-SA composites

The FTIR spectra of QC (Figure 4) detailed in the section 4.1.2.1 showed a broad band corresponding to OH and NH_2 stretching at 3350 cm^{-1}, symmetric and anti-symmetric stretching peaks of C-H bond at 2920 cm^{-1} and 2876 cm^{-1}, amide I stretching from the residual N- acetyl groups along with N-H bending vibrations of primary amines at 1640 cm^{-1} and Amide II band of residual amide bonds is observed at 1542 cm^{-1}. The peaks of CH_2 bending and CH_3 symmetrical deformations were present at 1414 cm^{-1} and 1379 cm^{-1} and the characteristic of C-O-C bridge was seen at 1150 cm^{-1} and those of C-O stretching modes at 1067 cm^{-1} and 1024 cm^{-1} respectively. Characteristic peak from the CH bending out of the plane of the monosaccharide ring appeared at 900 cm^{-1}.

In the FTIR spectra of QC-SA-1.5 and QC-SA-2.0 composites (Figure 11), all the characteristic peak of quaternized chitosan is present. The only difference is the appearance of a peak at 1721 cm^{-1} when QC was composited with SA. It is interesting that the intensity of 1721 cm^{-1} peak increases with the amount of SA in the composite matrix.

4.1.4.2 Micromorphology of QC and QC-SA composites using SEM

The scanning electron microscopy images of the samples (QC-0, QC-SA-1.5 and QC-SA-2.0) at a magnification of 400X are shown in Figure 12. The quaternized chitosan sheet obtained through the lyophilization process appeared highly porous with thin reticulated wall structure (Figure 12A). Though the features are not highly uniform, the average porosity was assessed (using ImageJ) to be around 25 µm. The incorporation of strontium containing apatite (SA) nano particles has drastically changed the porous structure of the sheets. In QC-SA-1.5 and QC-SA-2.0 samples, organized honeycomb-like structures are

formed, as evident from the pictures 12B and 12C. The average pore diameter increased with the concentration of SA. There is an appreciable increase in the wall thickness also. QC-SA-2.0 samples showed an average pore diameter of 50 µm.

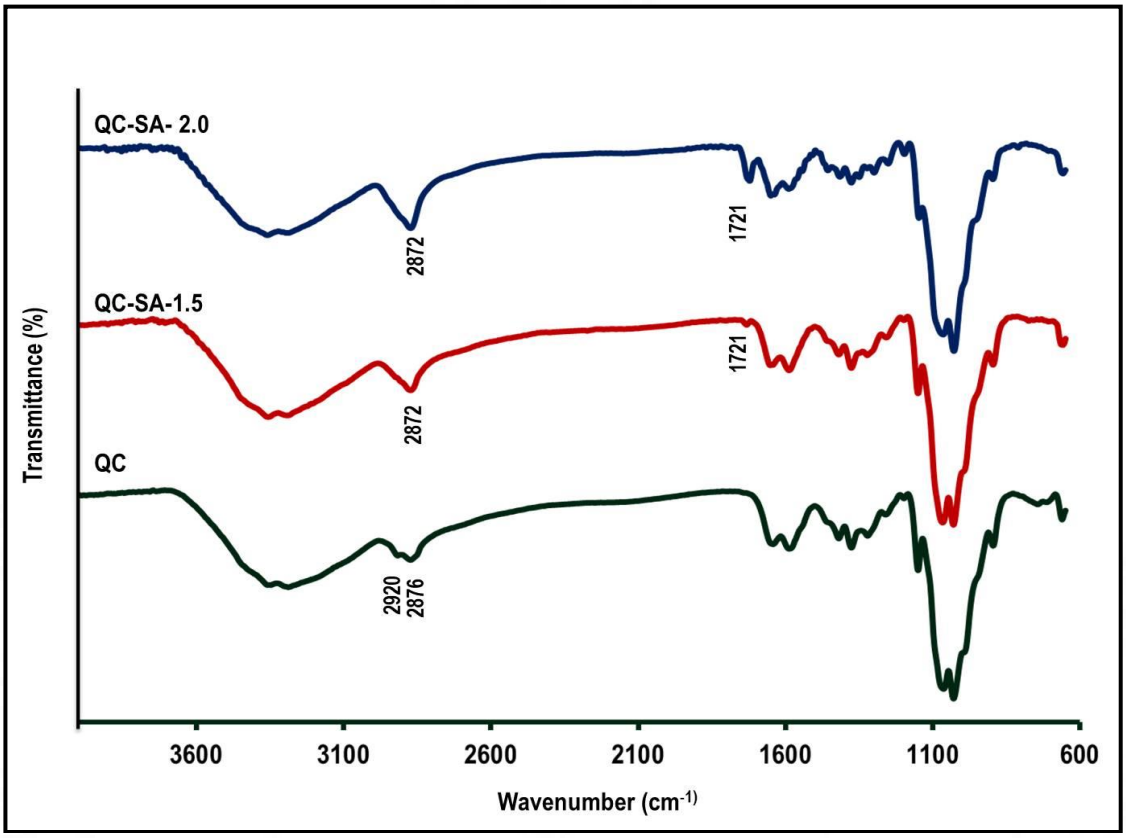

Figure 11 : FTIR spectra of QC and QC-SA composites

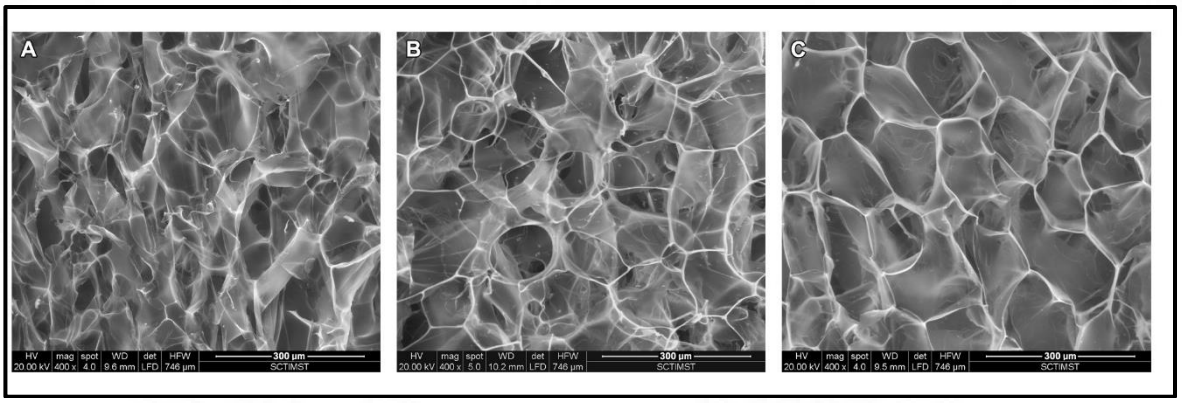

Figure 12: SEM micrograph showing reticulate wall structure of QC-SA-0, (B) QC-SA-1.5 and (C) QC-SA-2.0

4.1.4.3 Surface wettability of QC and QC-SA composites

The surface wetting property of QC and QC-SA composite sheets were analysed by water contact angle measurements, the results of which are given graphically in Figure 13. The samples for testing were made by flattening the porous membranes prepared with and without SA in QC material. The average contact angles obtained are: QC-SA-0: 117±1°; QC-SA-1.5: 117±5° and QC-SA-2.0: 107±5°. The higher value obtained for the QC material (QC-SA-0) compared to casted sheets (as given in Figure 8) may be due to the difference in sample preparation. The range of contact angle values shows that the composites are hydrophobic in nature. The addition of strontium doped hydroxyapatite has decreased the hydrophobic nature of the material.

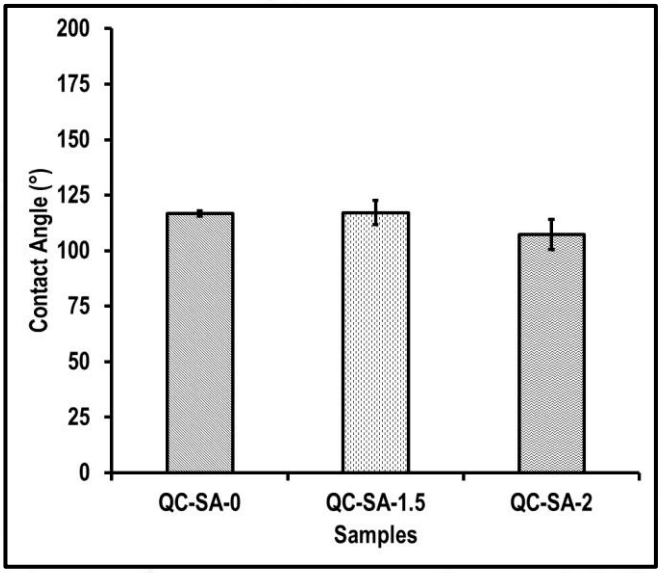

Figure 13: Water contact angle of QC and QC-SA composites

4.1.4.4 Mechanical Properties of QC and QC-SA composites

A material to be used as GBR/GTR sheets should have sufficient strength to withstand the local forces it is likely to experience in the final application. Depending upon the site of application, the requirement for tensile strength for bone tissue regeneration membranes will vary in the range of 0.1 kPa (for soft tissue) to 100 GPa [Das

and Zouani.,2014]. It is reported that hydroxyapatite–chitosan–gelatin sheets developed for a periodontal tissue regeneration application, have tensile strength in the range of 0.5 MPa and the values were considered sufficient to function as a barrier membrane [Sculean et al.,2008].

The mechanical properties of the sheets were evaluated by measuring the tensile strength and suture pull out strength as described in section 3.3.3.5. Figure 14 shows the mean tensile strength and suture pull out strength of quaternized chitosan with and without SA. The bare quaternized chitosan (QC-SA-0) showed tensile strength of 0.235±0.019 MPa, whereas tensile strengths of SA incorporated composites were 0.32±0.041 MPa for QC-SA-1.5 and 0.461±0.052 MPa for QC-SA-2.0 composites (Figure 14A). Compared to bare QC-SA-0, there is 36% to 96% increase in the strength respectively on converting the material to QC-SA-1.5 and to QC-SA-2.0.

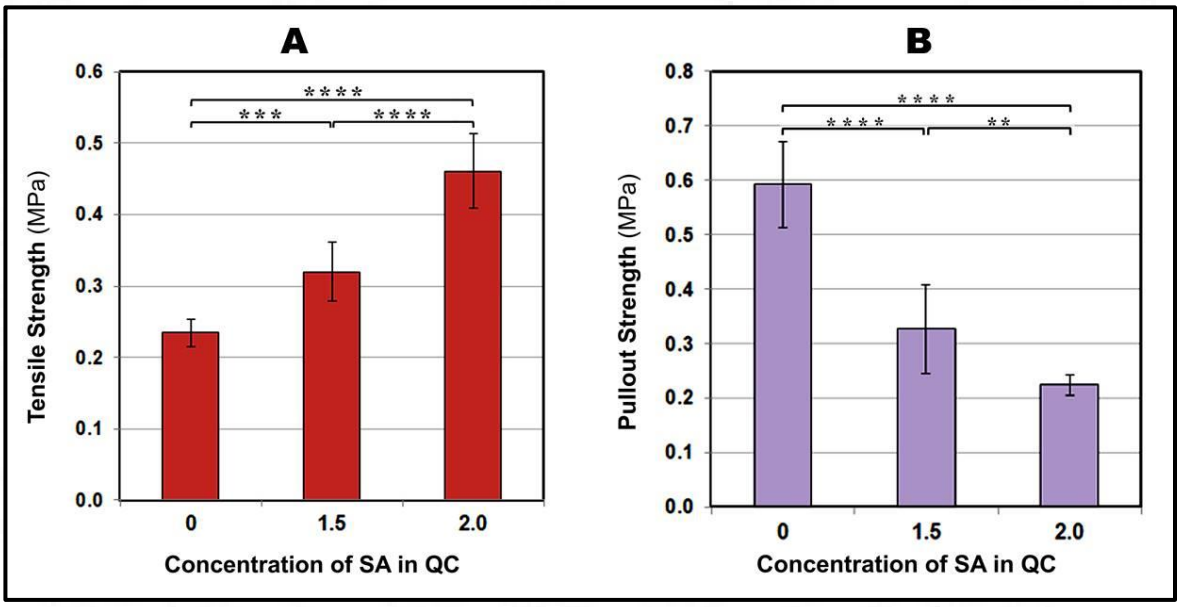

Figure 14 : Mechanical property evaluations of QC and QC-SA composites. [14A] Mean tensile strength and [14B] Mean suture pull out strength

Figure 14B compares the suture pull out strength of bare QC as well as the composite sheets. Contrary to the trend in tensile strength, the addition of SA is seen to

reduce the suture pull out strength. The value of 0.592±0.079 MPa for QC-SA-0 got reduced to 0.326±0.081 MPa and 0.225±0.019 MPa for the samples QC-SA-1.5 and QC-SA-2.0 respectively.

4.1.4.5 In vitro degradation studies of QC and QC-SA composites in PBS

In vivo degradation is essential for a GBR/GTR material so that it should give way for natural tissue to occupy the defect space after the intended function. Another requirement of GBR/GTR sheets is that the degradation should not lead to any toxic fragments [Sam and Pillai., 2014]. *In vitro* degradation studies of materials were carried out as described in section 3.3.3.3. Figure 15 shows weight loss of sheets measured at a definite time interval. All the compositions showed degradation and there is a steady increase in weight loss over the period, though not strictly linear. The degradation increased with the increase in concentration of strontium-containing nano apatite (SA) in the sheets. QC-SA-0 samples recorded a weight loss of 36.1% over 28 days period. The values for the samples QC-SA-1.5 and QC-SA-2.0 were 50% and 59.1% respectively.

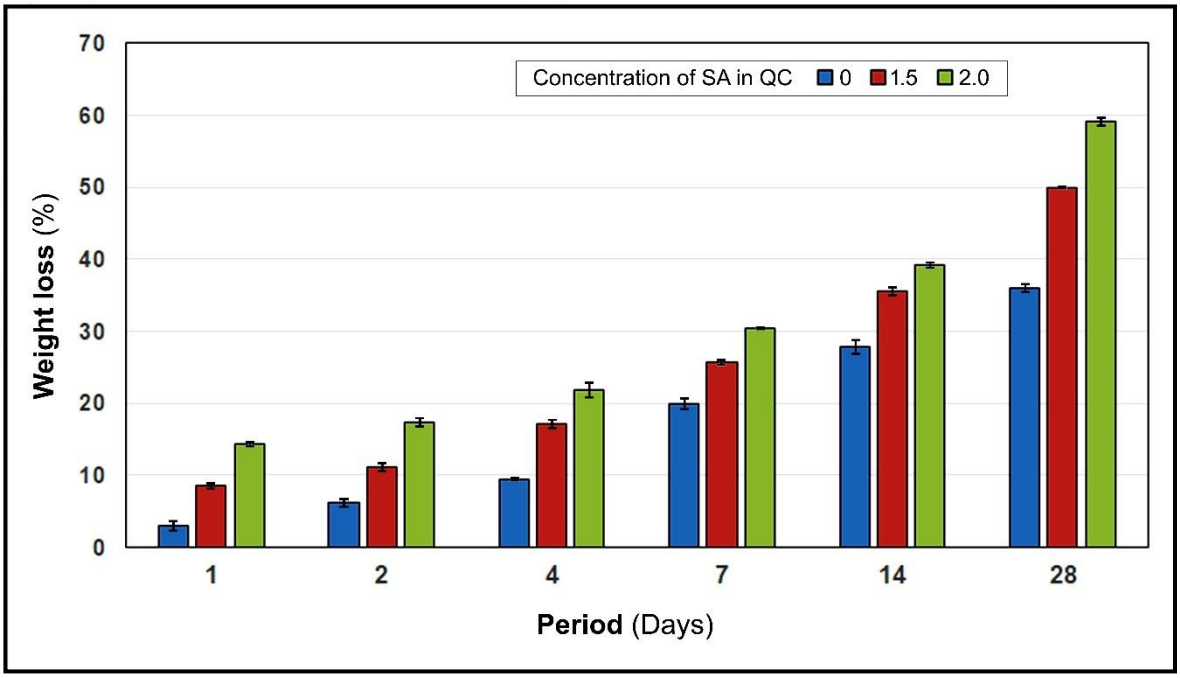

Figure 15: *In vitro* degradation behavior of QC and QC-SA composites

4.1.4.6 In vitro swelling of QC and QC-SA composites

The water uptake by membrane at different time points is represented in the Figure 16. The uptake gradually increases and reaches a maximum in 48 h and thereafter it diminishes. At any time point up to 24 h, the water uptake by QC-SA is higher compared to the bare QC membranes and its trend increases with increase in SA concentration. After that, the swelling of QC-SA decreases with increase in SA content.

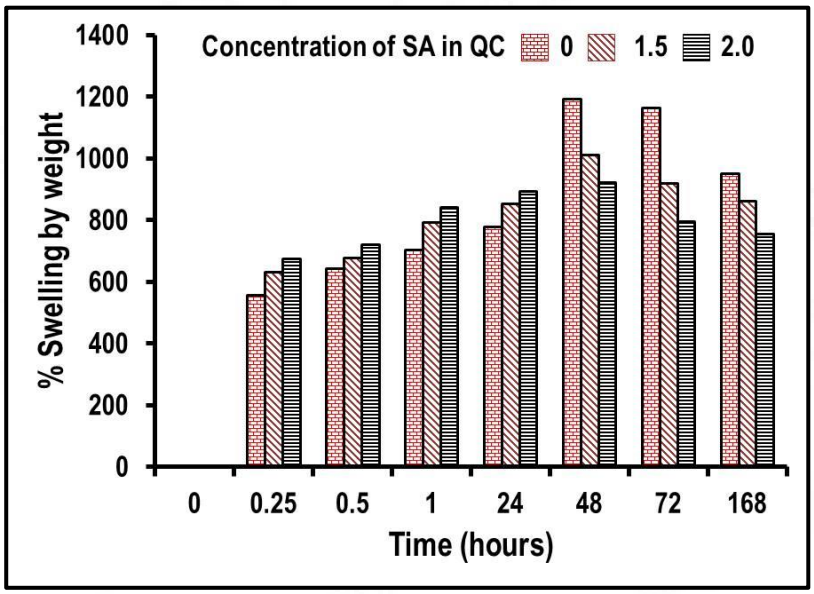

Figure 16 : *In vitro* swelling data of QC and QC-SA composites expressed in terms of weight gain when kept immersed in 1X PBS at 37±0.5°C.

4.1.4.7 In vitro cytocompatibility studies of QC and QC-SA composites using **hPDL cells**

The potential of the prepared materials for biomedical applications (as GTR membranes) was evaluated by doing *in vitro* cytocompatibility evaluation using hPDL cells as discussed in section 3.3.3.7 (iii and iv). Figure 17 A shows the optical micrographs showing hPDL cells cultured in direct contact with the materials. The cells were viable on all the materials and there was no morphological evidence of cell death or toxicity in any of the samples. The cells also retained their morphology and adhered well to culture wells even after 24 h of exposure. It was also observed that there was no vacuole formation or detachment of cells on contact with the test materials.

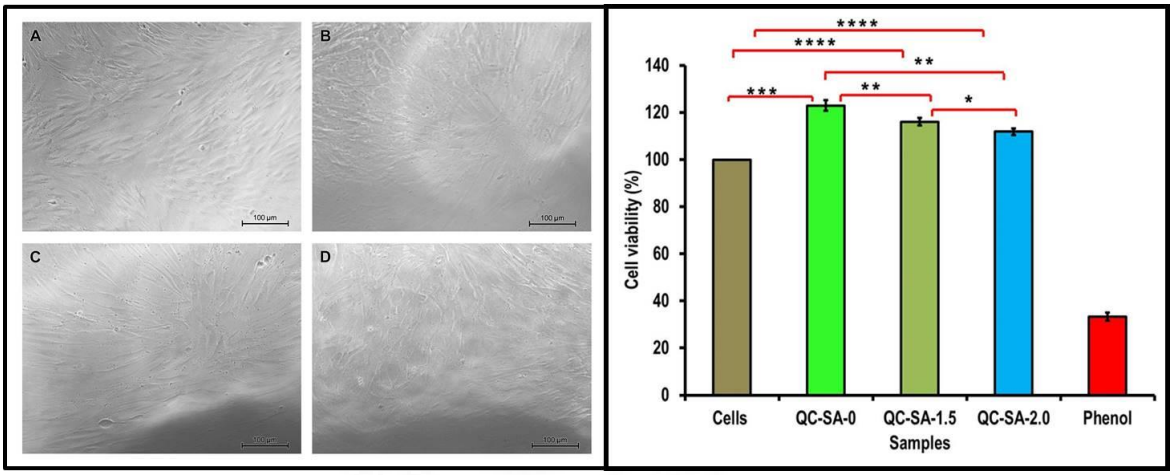

Figure 17: Results of the *in vitro* cytocompatibility studies of QC and QC-SA composites using human periodontal ligament (hPDL) cells. The left panel shows images of the direct contact culture at 24 h. [A] Cell alone (Control), [B] QC-SA-0, [C] QC-SA-1.5 and [D] QC-SA-2.0. The right panel shows cell viability of QC and QC-SA composites calculated through MTT assay. Phenol is taken as the positive control. The values are normalised with respect to the cell control (taken as 100%).

The right panel in Figure 17 represents the results of MTT assay using hPDL cells. The values for the test samples (QC-0, QC-SA-1.5 and QC-SA-2.0) are plotted along with the cell control and the positive control. All the test samples showed higher cell viability than the cell control. The QC-0 sample showed a value of 111.86% and the presence of SA particles enhanced it further, as 122.97% for the QC-SA-1.5 sample. However, for QC-SA-2.0 the value is 116.09%, indicating that higher SA content reduces the cell viability. Even this reduction keeps the cell viability above that of QC sample, which is higher than the acceptable value (80%) for *in vitro* cytocompatibility.

4.2 Quaternized chitosan- calcium phosphate in situ composite (CPQC)

The objective of this section is to develop bioactive composites based on quaternized chitosan immobilized with *in situ* precipitated calcium phosphate for the regeneration of defective bone.

4.2.1 Preparation and characterization of quaternized chitosan- calcium phosphate composite (CPQC)

The QC and CPQC composite were prepared in sheet form as described in section 3.2.7.1 Preparation of CPQC. and was analysed for its properies.The thickness of the sheet is of 0.5 mm.

4.2.1.1 FTIR analysis of QC and CPQC composites

FTIR spectra of QC contain the characteristic band corresponding to OH and NH2 stretching at 3350 cm^{-1}. The peaks at 2920 cm^{-1} and 2876 cm^{-1} appeared from the symmetric and anti-symmetric stretching of C-H bond (Figure 18). The C=O stretching from the residual N-acetyl part, commonly termed as amide I peak along with N-H bending vibrations of primary amine in quaternized chitosan is formed at 1640 cm^{-1}, Amide II band of residual amide bonds could be found at 1542 cm^{-1}. The two peaks at 1414 cm^{-1} and 1379 cm^{-1} corresponds to CH_2 bending and CH3 symmetrical deformations. The characteristic peak of C-O-C bridge is present at 1150 cm^{-1} is and C-O stretching modes are observed at 1067 cm^{-1} and 1024 cm^{-1}. Peak at 900 cm^{-1} is from the CH bending out of plane and is characteristic to monosaccharide ring. In the FTIR spectra of CPQC, all the peaks remain same as that quaternized chitosan except a new peak at 1725 cm^{-1}.

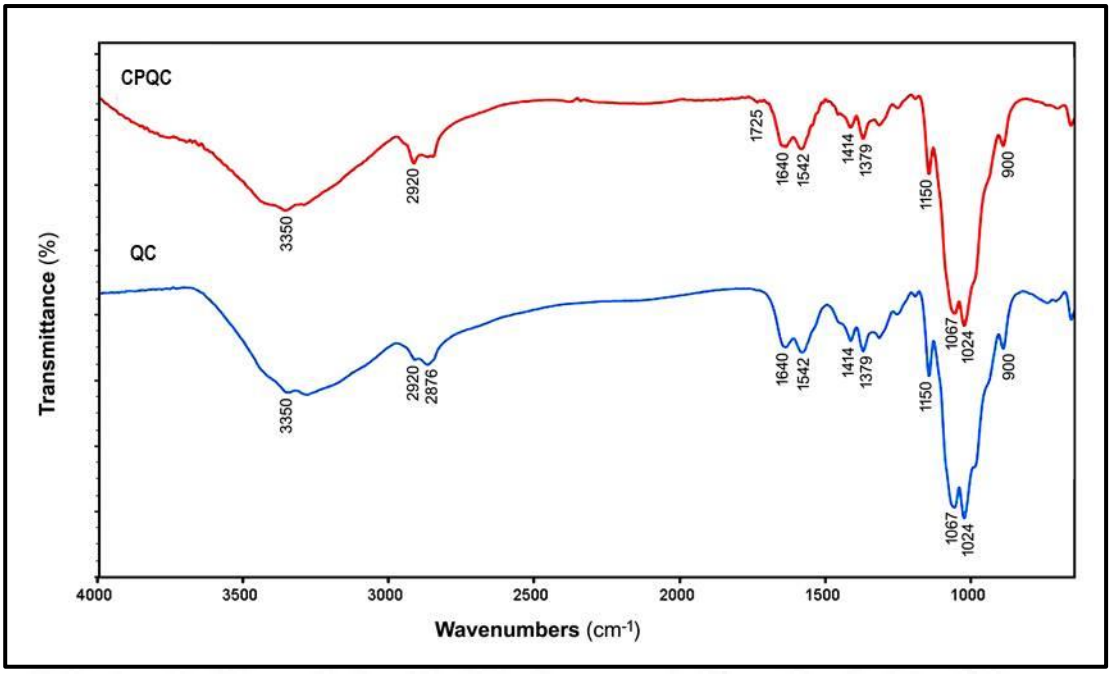

Figure 18: FTIR spectra of QC and CPQC composites

4.2.1.2 Phase identification of the in situ calcium phosphate by X-ray diffraction (XRD) analysis

The phase identification of the *in situ* deposited calcium phosphate was done by X-Ray diffraction technique. The XRD results obtained for QC and CPQC are shown in Figure 19. The bare QC material showed the typical XRD spectrum of an amorphous polymer. The XRD pattern of CPQC showed sharps peaks over the base spectrum of QC. The peaks seen in CPQC sample matches with the ICDD 09-0077 which corresponds to the brushite phase of calcium phosphate ($CaHPO_4.2H_2O$).

4.2.1.3 Micromorphology of QC and CPQC using SEM

The micro surface feature of the QC and CPQC composites analyzed at 50X and 1000 X magnifications are shown in Figure 20. Lyophilized composites of both QC and CPQC were porous and *in situ* precipitation has drastically changed the surface from non-ordered porous to an ordered porous structure. The average pore dimension

evaluated using ImageJ shows a decrease in pore diameter from 225 µm to 86 µm on converting QC to CPQC.

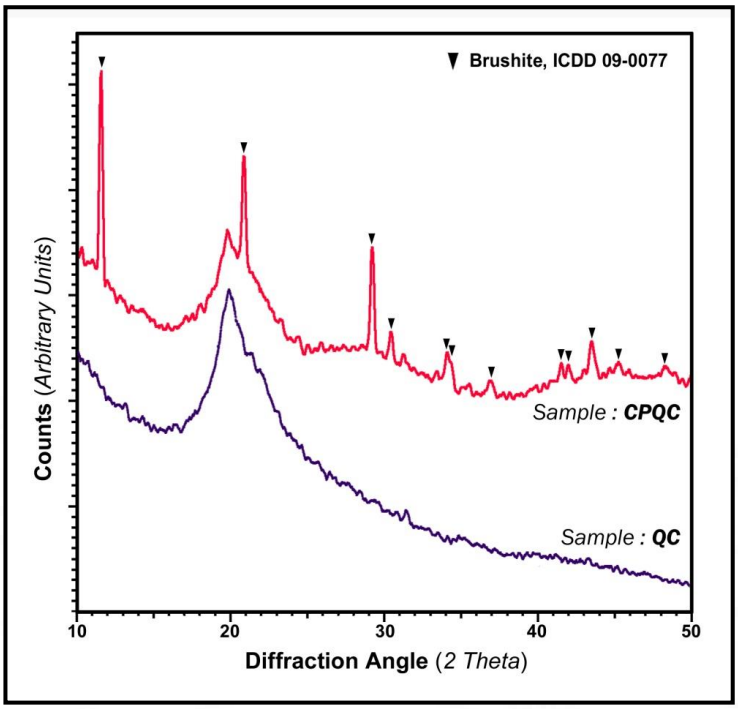

Figure 19: XRD spectra of quaternized chitosan (QC) membrane and Quaternized chitosan-calcium phosphate *in situ* composite (CPQC).

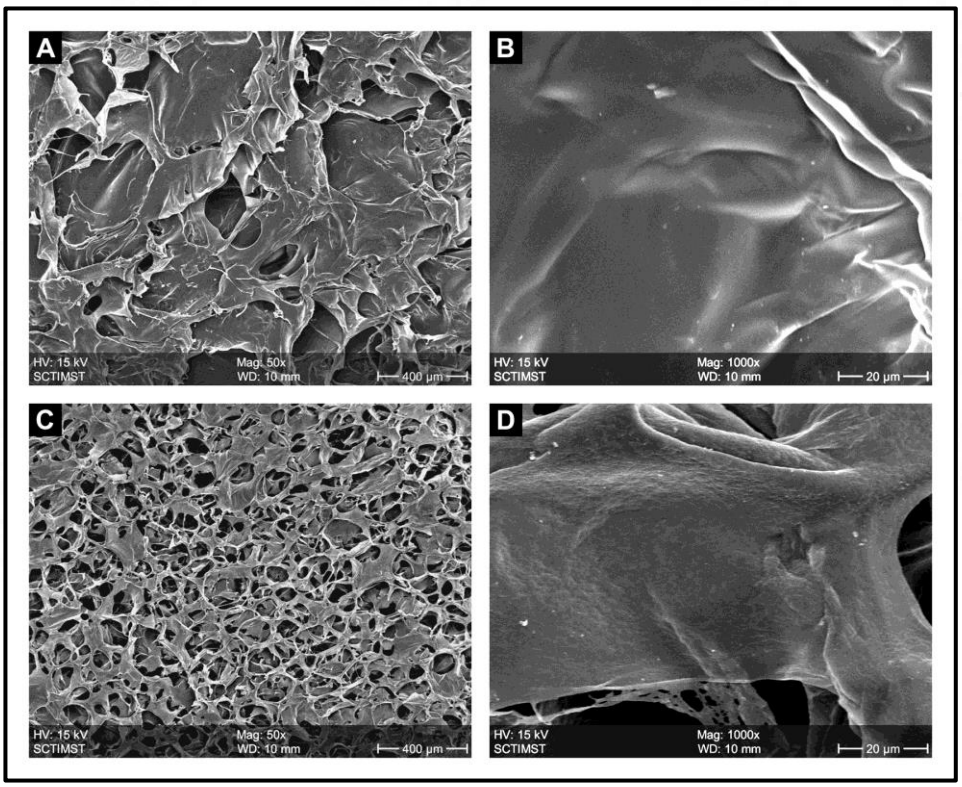

Figure 20: SEM micrograph showing QC surface at 50X [in A], its magnified image at 1000X [in B], CPQC surface at 50X [in C] and it's magnified image at 1000X [in D].

4.2.1.4 Surface wettability of QC and CPQC composites

The surface wetting property of the samples analyzed via water contact angle (Sessile drop method), measured immediately after dropping the liquid could be seen in Figure 21. The average water contact angles observed are 117±4° for QC and 111±2° for CPQC, indicating a hydrophobic nature. There is no significant decrease in contact angle on *in situ* precipitation of brushite, when measured instantly by sessile drop method. This will, however, turn out to be an apparent observation, and if the measurement is continued for some time, the value drastically decreases due to absorption of water.

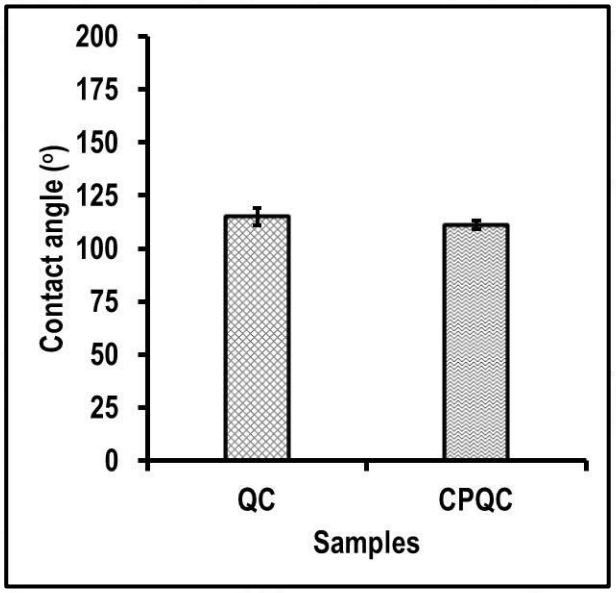

Figure 21: Contact angle of QC and CPQC composites

4.2.1.5 Mechanical Properties of QC and CQPC composites

For any material to be used as tissue regeneration membrane it should possess sufficient strength to withstand the force acting on it, based on the area of application. If the material is used as thin sheets for periodontal regeneration, it should behave like a barrier material between the periodontal defect and the gingival tissue during surgical flap procedure. The mechanical property evaluated by measuring the mean tensile strength and mean suture pull out strength are represented in the Figures 22 and 23.

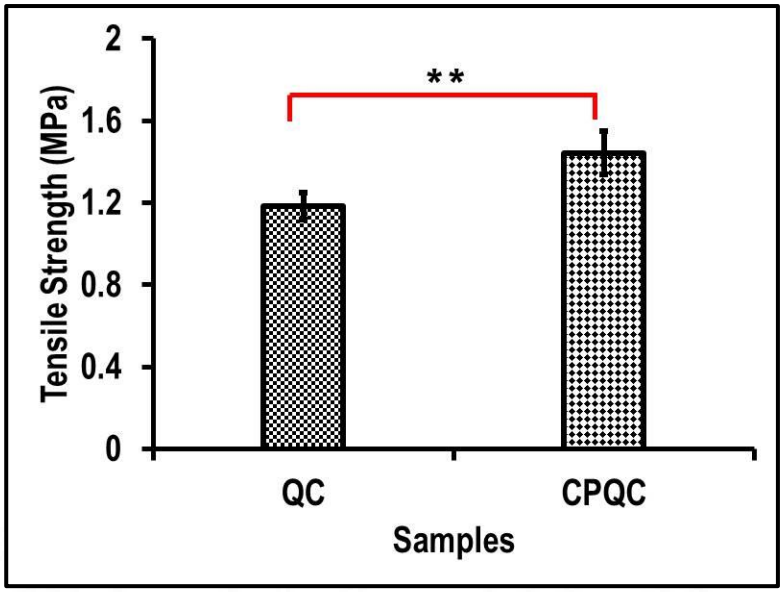

Figure 22: Tensile strength of QC and CPQC composites

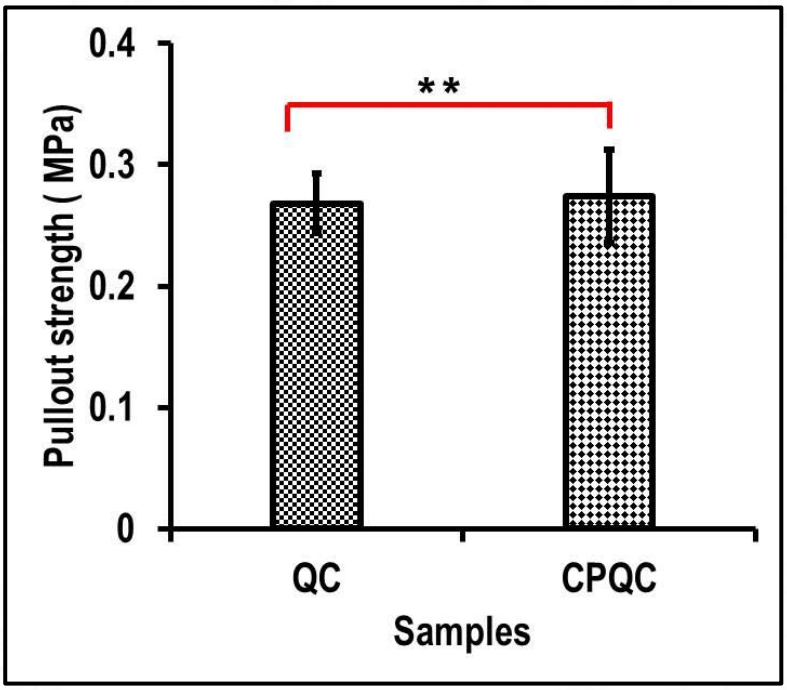

Figure 23: Suture pull out strength of QC and CPQC composites

It was observed that incorporation of calcium phosphate via *in situ* precipitation increased the strength from 1.139±0.123 MPa (for QC) to 1.418±0.111 MPa (for CPQC). It could be noted that there is 25% increase in strength when converted to composite membrane (Figure 22). Figure 23 compares the variation in suture pull out strength while

incorporating calcium phosphate into the polymer matrix. The suture pull out value of 0.2642±0.036 MPa for QC got reduced to 0.2329±0.053 MPa on conversion to CPQC.

4.2.1.6 In vitro swelling of QC and CQPC composites

The water uptake by membrane at different time points is represented in the Figure 24. The uptake gradually increases and reaches a maximum in 48 h and after that it decreases. At any time point the water uptake by CPQC is lower compared to the QC membranes. The difference in the uptake of water arises mainly from reduction in pore diameter in CPQC.

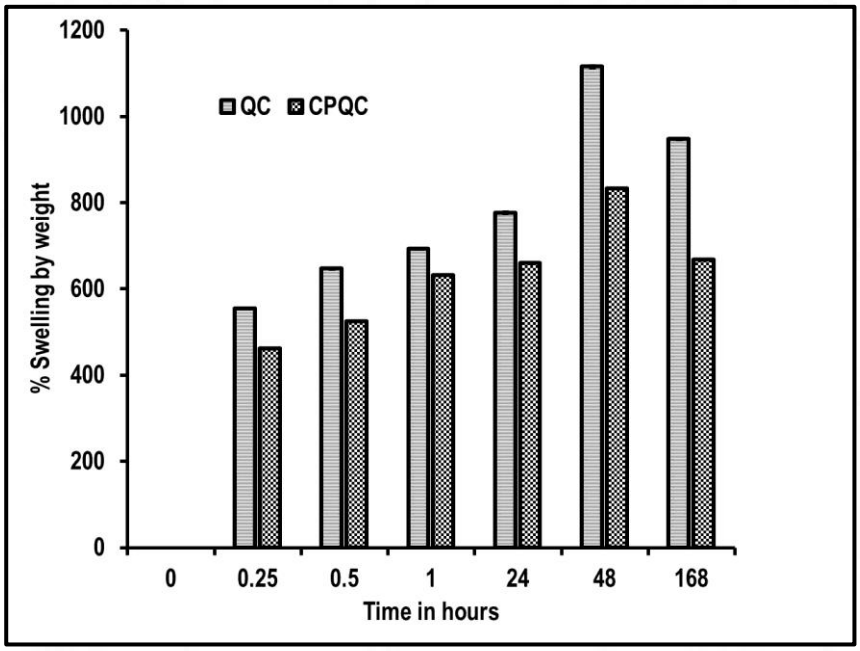

Figure 24: *In vitro* swelling data of QC and CPQC composites expressed in terms of weight gain when kept immersed in 1X PBS at 37 ± 0.5°C

4.2.1.7 In vitro degradation of QC and CQPC composites

Biodegradation of the material is of great concern in the area of tissue regeneration approaches. A tissue regeneration material should degrade with in a time period for providing space for newly formed tissue and should not release any toxic degradation by-products, as far as possible [Sam and Pillai., 2014]. In some parts of body, especially in

the case of periodontal defect, the use of biodegradable membranes will avoid a second surgical produce to remove the implanted material after local healing. The biodegradation of chitosan mainly occurs in the body by the enzymatic hydrolysis of β-1,4glycosidic bonds. The degraded products are simple amino sugars which get into the metabolic pathway and get eliminated from the body [Qasim et al.,2015].

The percentage degradation of composite materials based on weight loss in PBS at definite time intervals is shown in Figure 25. Both QC and CPQC showed a steady degradation and are able to degrade nearly to half its mass within 45 days. On comparing QC and CPQC, the degradation of CPQC is slightly less at all-time points. This shows that conversion of QC to a composite membrane CPQC decreased its degradation rate.

4.2.1.8 In vitro bioactivity of QC and CPQC composites

For a material to be used as bone regeneration material, its ability to bond with living bone via the formation of apatite layer (bone-mineral composition) over its surface is of great significance. This property can be tested *in vitro* by immersing in simulated body fluid (SBF), a solution with ionic concentration close to that of human blood plasma [Kokubo and Takadama., 2006]. A material having inherent bioactivity (or the ability to form bone-bonding) will consume Ca^{2+} and PO_4^{3-} from the SBF solution and in turn results in the growth of bone-like apatite crystals on its surface [Kokubo and Takadama., 2006]. This bioactive nature of material can be confirmed from SEM, EDS and XRD analysis. The surface morphology of the membranes after immersing in simulated body fluid for 3 days and 7 days are shown in the Figure 26(a) and (b). There are observable changes in surface morphology for both membranes. For QC (Pictures 26 A to D) a degradation of layers from the membranes could be observed rather than the formation of any growth layer indicating bioactivity. In the case of CPQC membrane, an appreciable

growth features are visible on the surface at 200X magnification. A higher magnification of 5000X reveals fine crystals of apatite, as reported in the literature (Pictures 26 E to H).

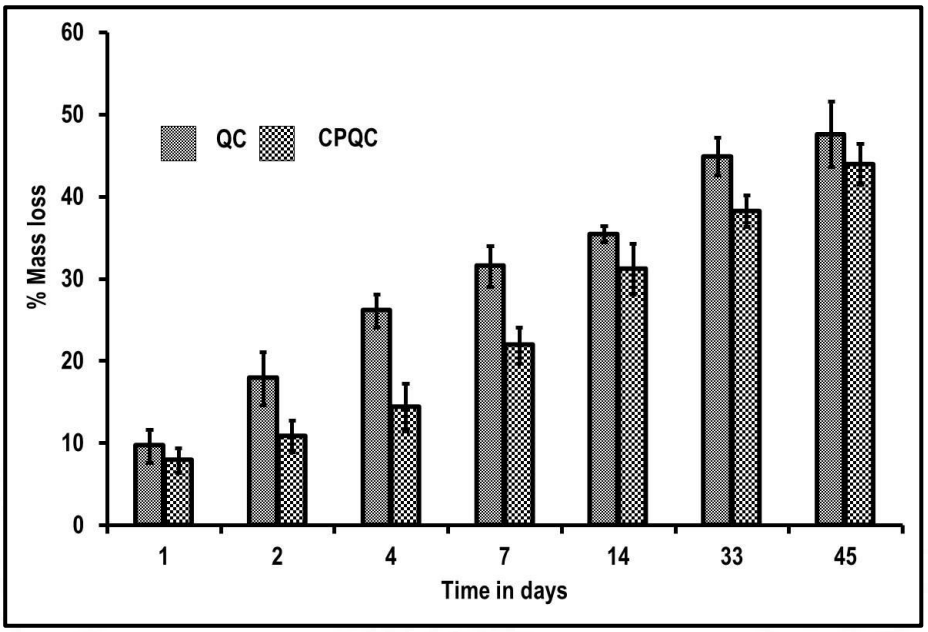

Figure 25: *In vitro* degradation behavior of QC and CPQC composites, based on the mass loss at different time periods in PBS.

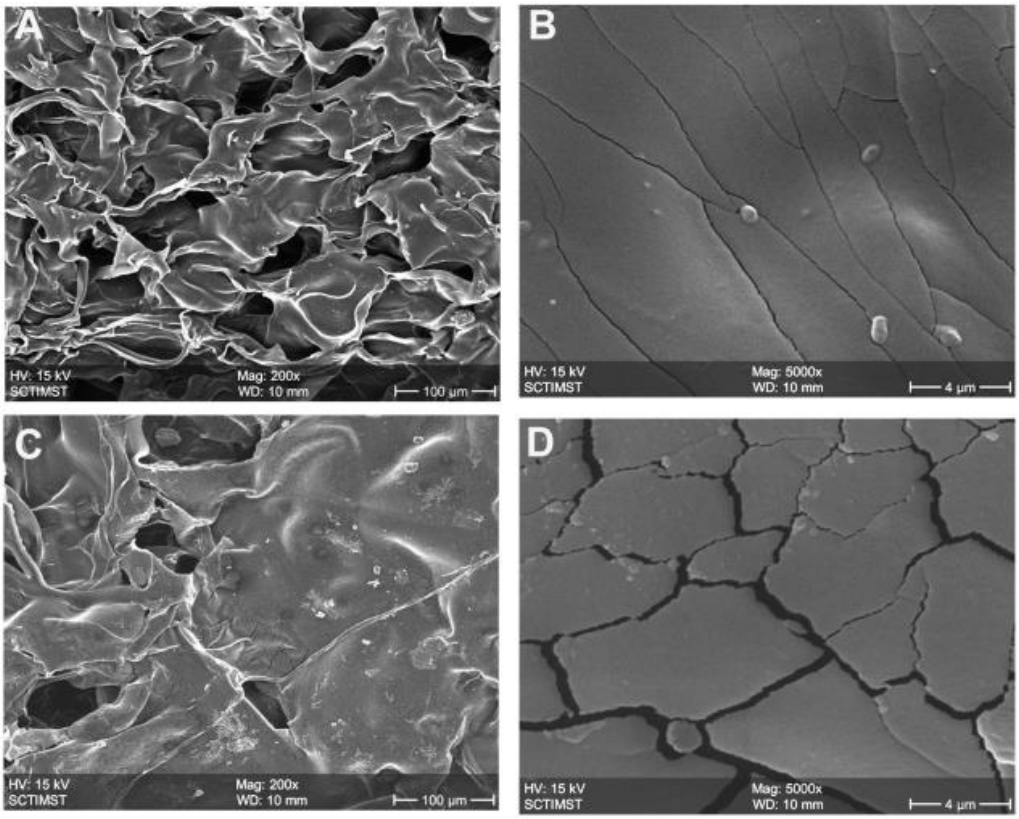

Figure 26(a): SEM images of the QC membrane surface after immersion in SBF. [A] After 3 days at 200X, [B] After 3 days at 5000X, [C] After 7 days at 200X and [D] After 7days at 5000X

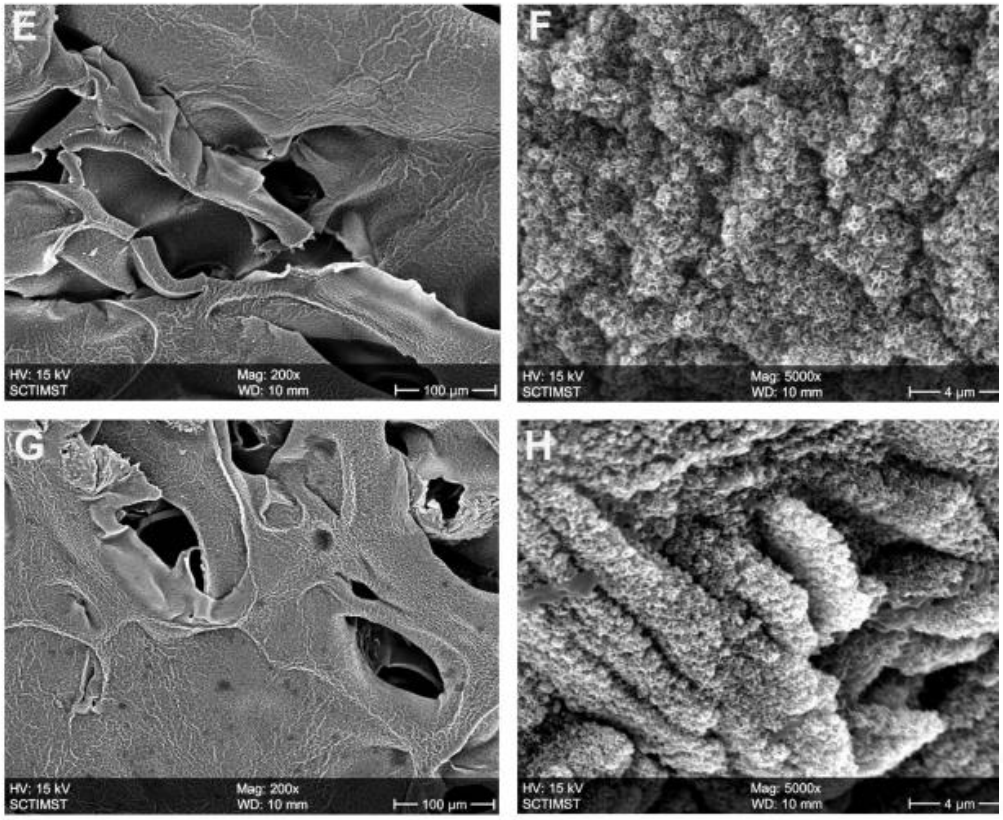

Figure 26(b): SEM images of the CPQC membrane surface after immersion in SBF. [E] After 3 days at 200X, [F] After 3 days at 5000X. [G] After 7 days at 200X, and [H] After 7 days at 5000X

In order to identify the chemical phase of the deposited particles on the composite surface, EDS (energy-dispersive X-ray spectroscopy) analysis and XRD analysis were done, the results of which are given as Figure 27 and Figure 28. The EDS analysis done on the deposited layer (Figure 27) shows the peaks of calcium and phosphorous. The Ca/P ratio from EDS is found to be 1.66, which is close to the theoretical Ca/P ratio of 1.67 in hydroxyapatite. The confirmation of the deposited material is further corroborated with the XRD analysis of the deposited layer. The XRD data of the CPQC sheets after *in vitro* bioactivity test using SBF (CPQC-B) showed in Figure 28 matches with the characteristic peak of hydroxyapatite (ICDD-09-0432). The CPQC sheet before immersion in SBF was used as the control material. The hydroxyapatite peaks are broadened in CPQC-B, indicating its amorphous nature. While comparing the XRD data of CPQC-B and CPQC, all the characteristics peaks of the brushite are submerged by the hydroxyapatite peaks

which also confirm that the deposit of hydroxyapatite over the surface is at least several microns thick.

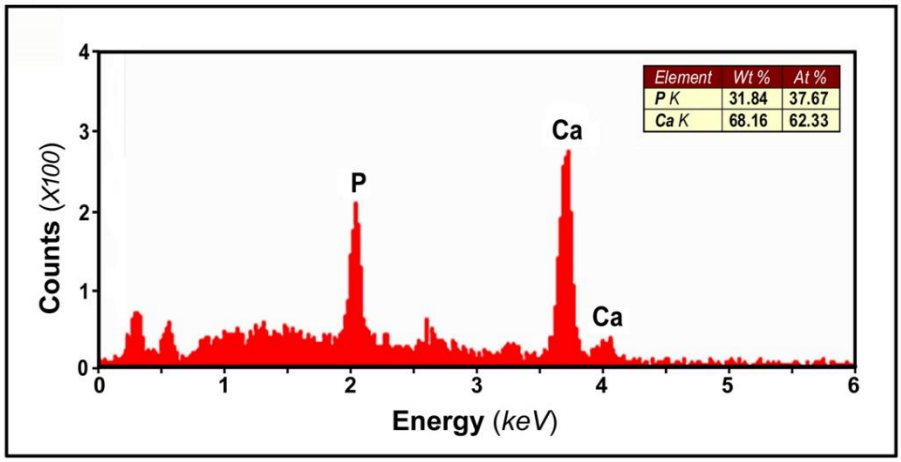

Figure 27: EDS analysis of the quaternized chitosan- calcium phosphate membrane surface after the bioactivity test. The presence of Ca and P in the newly formed layer is seen

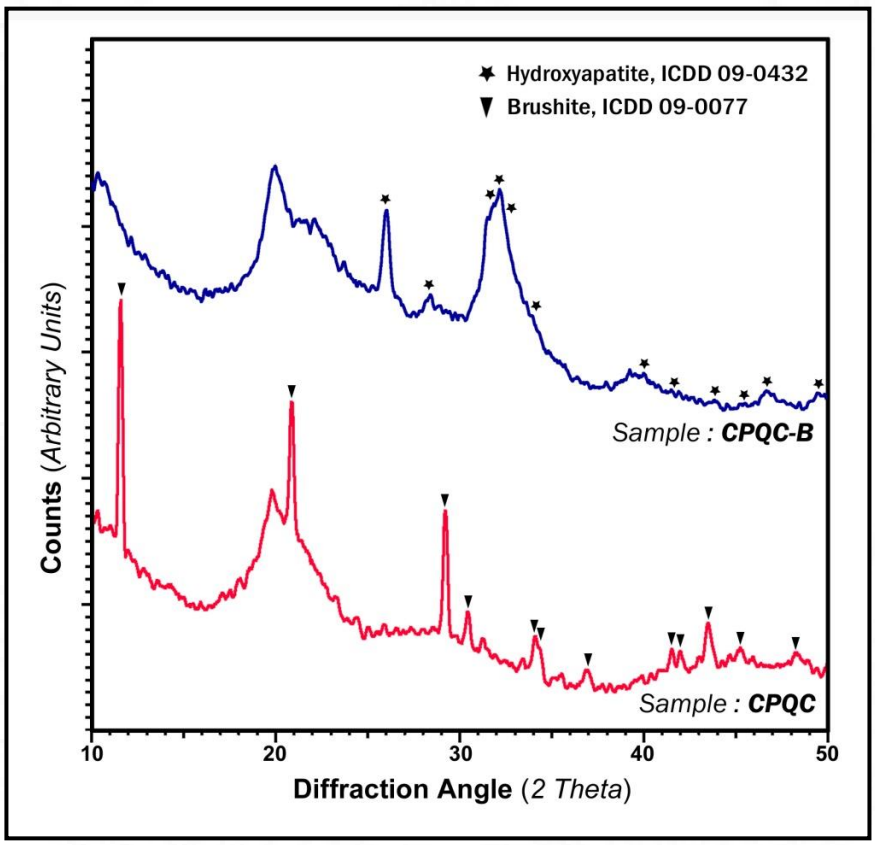

Figure 28: XRD spectra of the quaternized chitosan- calcium phosphate membrane before and after the *in vitro* bioactivity test. Surface after the bioactivity test (CPQC-B) shows broad peaks of hydroxyapatite, whereas in the sample before the test (CPQC) carries sharper peaks of brushite

4.2.1.9 In vitro cytocompatibility of QC and CQPC composites

Another important requirement of a material to be used for tissue regeneration purpose is that it should be compatible with host cells and tissues. The cytocompatibility of a material is assessed through MTT assay and direct contact tests, done *in vitro* using candidate cells.

i. MTT assay

Figure 29 represents the percentage cell viability values obtained when the QC and CPQC samples were evaluated using L929 cells along with cell control and toxic control (phenol). Both QC and CPQC showed more than 80% cell metabolic activity indicating the cytocompatibility. The cell viability in the presence of CPQC material (89%) was significantly less compared to that of QC membranes (112%).This decrease in the value may be likely due to the in situ precipitation of the nano-hydroxyapatite layer on the surface from culture media which can reduce the material compatibility towards L929 cells.

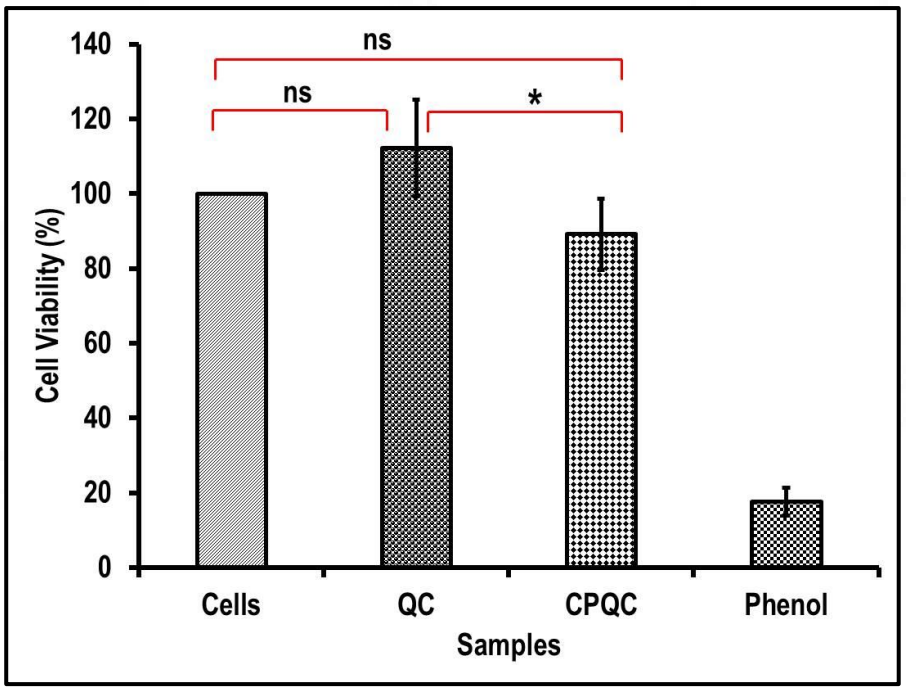

Figure 29: MTT assay done on QC & CPQC composites using L929 cells

ii. Direct contact

The above results of MTT assay was further supported by the images obtained from direct contact test shown in Figure 30. The L929 cells cultured in the presence of the test materials showed no evidence of cytotoxicity. The cells were attached, and maintained their morphology, both in the cell control and in the presence of the membranes, in comparison to the cells in positive control which showed cell death in the form of detached round cells.

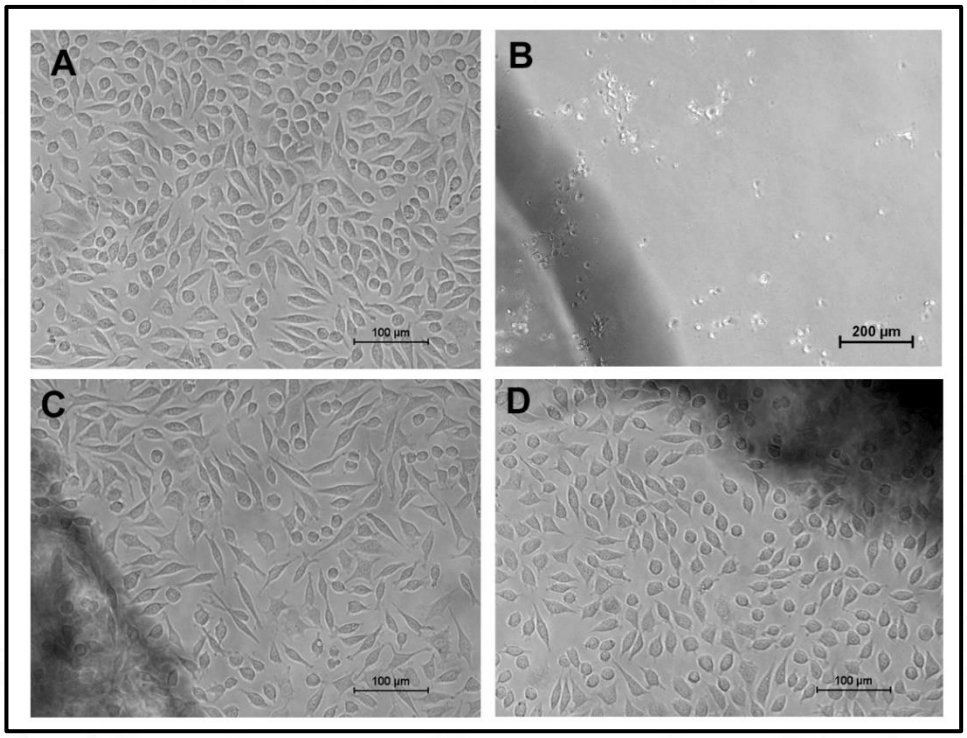

Figure 30: Direct contact test done using L929 cells for 24 h. [A] Cells alone, [B] Toxic control (Tin-stabilized PVC disk), [C] QC membrane and [D] CPQC membrane

iii. Cell adhesion and spreading

(a) Actin staining: The CLSM images of actin staining are shown in Figure 31. The CLSM images of the hPDL cells on the membranes showed typical spindle morphology as compared to the control cells cultured on cover glass. In addition, the periodontal

ligament fibroblasts cultured on the membranes showed a three dimensional distribution, showing migration of cells into the membranes.

(b) Environmental Scanning Electron Microscopy (ESEM) Evaluation: The ESEM images of hPDL cells cultured over the QC and CPQC membranes are shown in the Figure 32. The ESEM images of the hPDL cells on the membranes exhibited typical morphology and a three dimensional distributions, showing migration of cells into the membranes

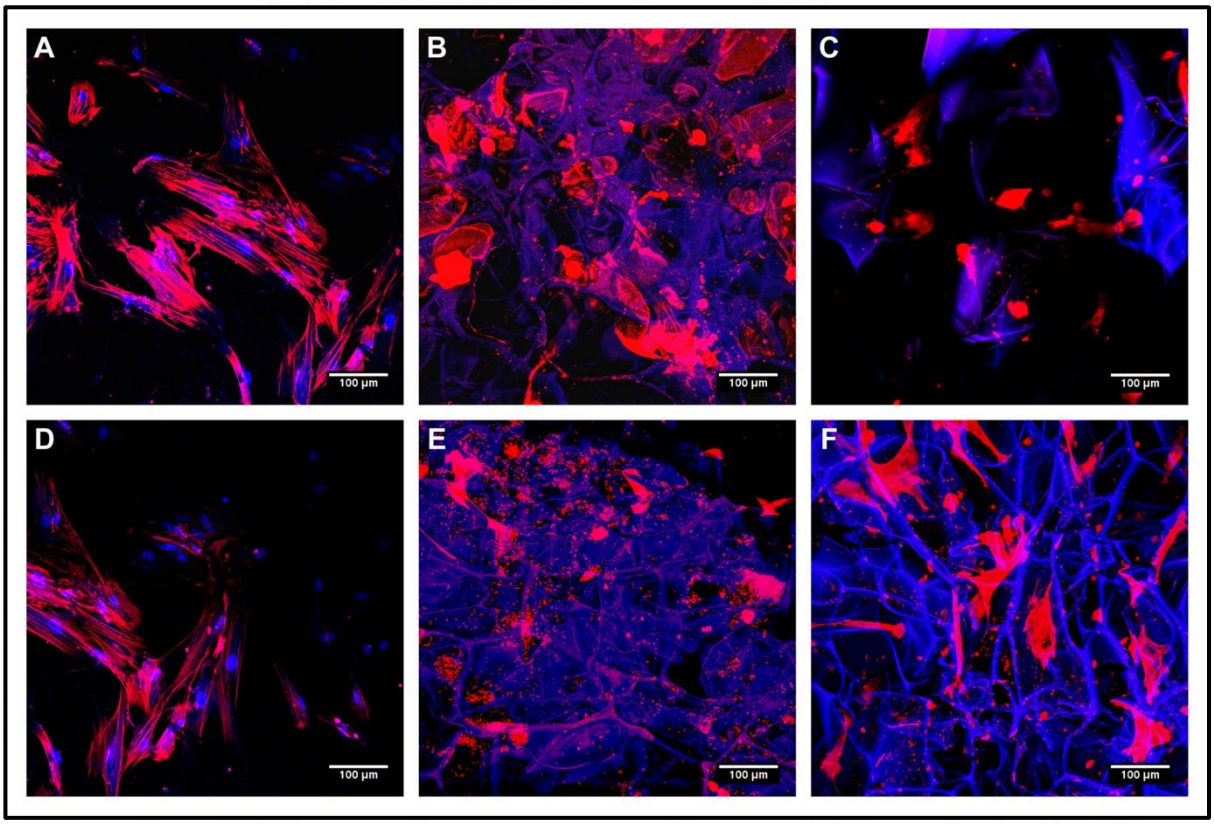

Figure 31: Confocal laser scanning microscopic images of QC and CPQC composite membranes cultured with hPDL cells for 24 and 48 h period, along with control material (cover glass). [A] Control - 24h, [B] QC -24h, [C] CPQC - 24h, [D] Control - 48h, [E] QC- 48h and [F] CPQC - 48h

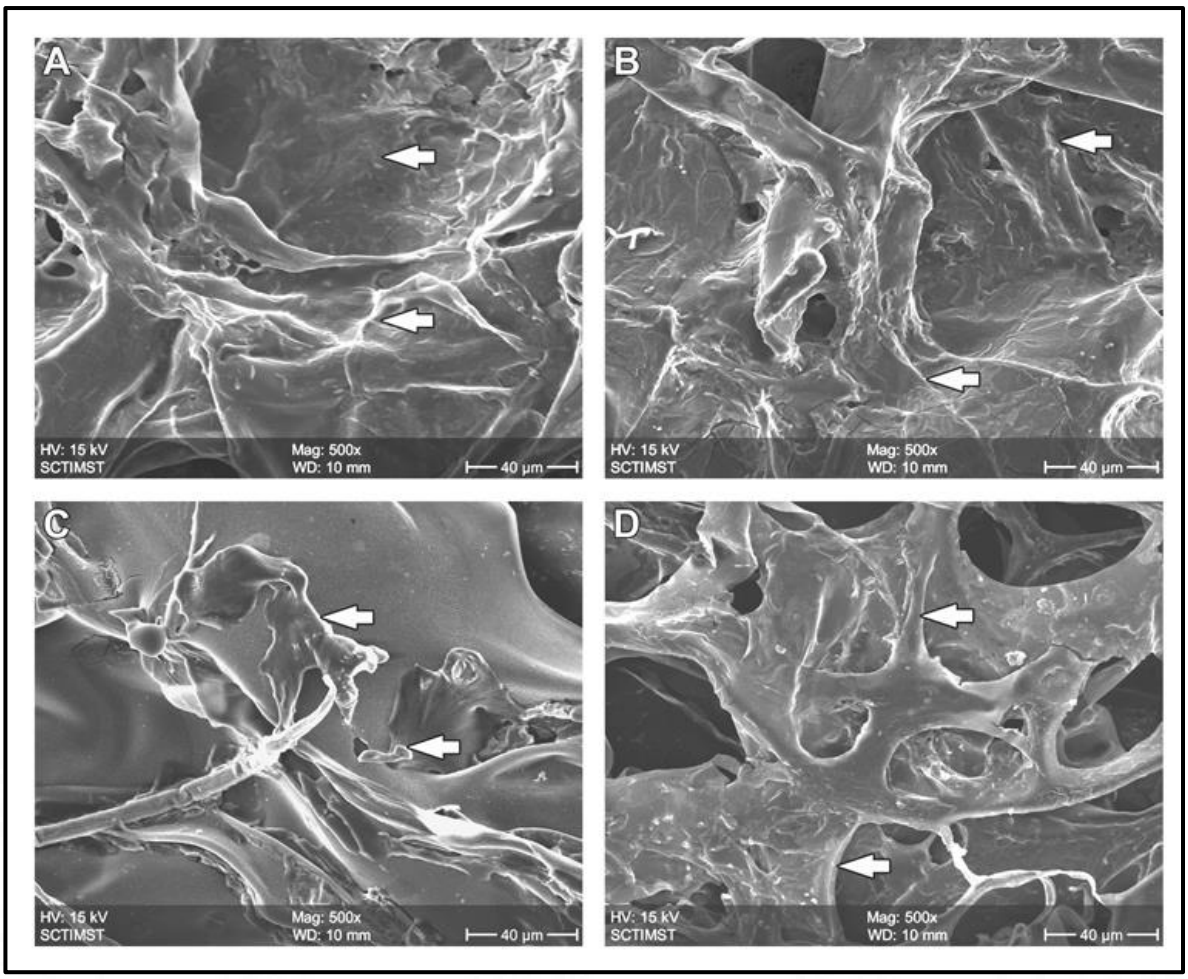

Figure 32: SEM images of the QC and CPQC membranes after culturing the material along with hPDL cells. [A] Surface of QC membrane after 24h; [B] Surface of CPQC membrane after 24h, [C] Surface of QC membrane after 48h and [D] Surface of CPQC membrane after 48h. The positions of the attached cell remnants are marked by left block arrows

4.3 Preparation of Thiolated Polyvinyl Alcohol - hydroxyapatite graded cross-linked composite (TPVA-HA)

The objective of this section is to modify polyvinyl alcohol and make composite structure with calcium phosphate based minerals to achieve bioactivity for the regeneration of defective bone.

4.3.1 Preparation and characterization of thiolated Polyvinyl Alcohol (TPVA)

Thiolated Polyvinyl Alcohol was prepared by acid catalyzed esterification reaction of polyvinyl alcohol with thioglycolic acid at 60°C. The esterification of PVA with thioglycolic acid is a type of nucleophilic acyl substitution (Figure 33). The reaction starts by the protonation of the carbonyl oxygen of thioglycolic acid followed by nucleophilic attack of OH group of PVA. Finally the ester bond is formed by the removal of water molecule followed by a proton. The schematic representation of the reaction is given in the figure 33.

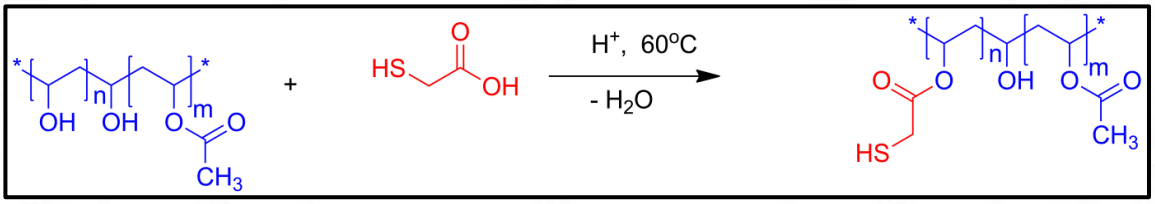

Figure 33: Schematic representation showing thiolation of PVA through esterification

4.3.1.1 Fourier transform Infrared spectrophotometer (FTIR) spectra of PVA & TPVA

The conjugation of thioglycolic acid to hydroxyl groups of polyvinyl alcohol (PVA) was confirmed by FTIR spectral analysis. Figure 34 represents FTIR spectra of PVA and its thiolated derivative, TPVA.

In PVA, a broad band was seen at 3280 cm^{-1} corresponding to the stretching from hydroxyl groups. The peaks at 2940 cm^{-1} and 2908 cm^{-1} represents the symmetric and anti-symmetric stretching vibrations of C-H in CH_2. The peaks at 1415 cm^{-1} and 1372 cm^{-1}

correspond to C-H bending vibrations and wagging C-H vibrations respectively and that at 1329 cm^{-1} to O-H bending vibrations. The C-O stretching peak could be observed at 1091 cm^{-1}. In TPVA, most of the characteristic vibrations of PVA are present. A new peak at 1715 cm^{-1} appeared which is due to the C=O stretching vibrations of ester linkage.

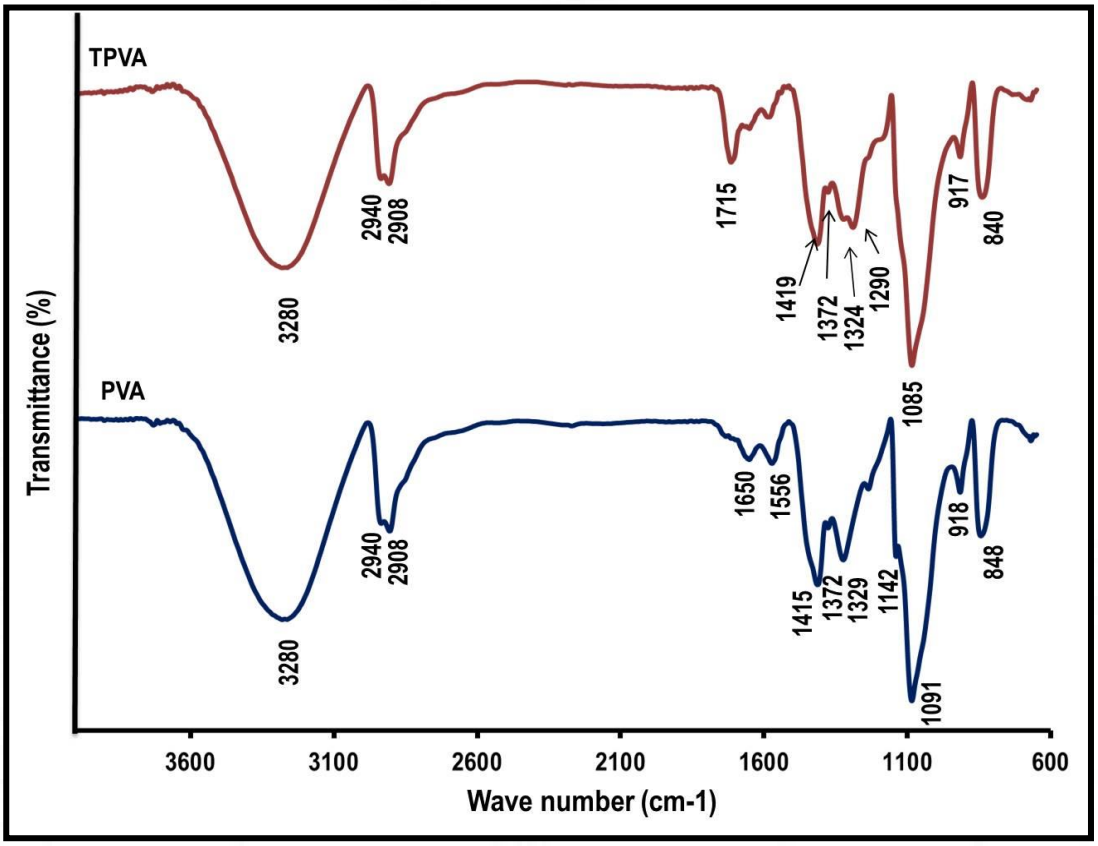

Figure 34: FTIR spectrum of PVA and TPVA

4.3.1.2 FT Raman spectra of PVA & TPVA

In the FT-Raman spectra of PVA (Figure 35), the broad part of the spectrum peaking at 3300 cm^{-1} is obviously due to the stretching from hydroxyl groups. The prominent peak at 2900 cm^{-1} is due to stretching vibrations (symmetric and asymmetric) of CH_2. Peaks at 1439 cm^{-1} and 1360 cm^{-1} are due to the bending vibrations of CH and OH. C-O stretching vibrations are present at 1141 cm^{-1} and 1088 cm^{-1}. The peaks seen at 852 cm^{-1} and 915 cm^{-1} are due to C-C stretching. In TPVA, most of the characteristic

vibrations of PVA are present. New peaks are formed at 1718 cm^{-1} due to C=O stretching from ester bonds and at 470 cm^{-1}because of the S-S stretching vibration.

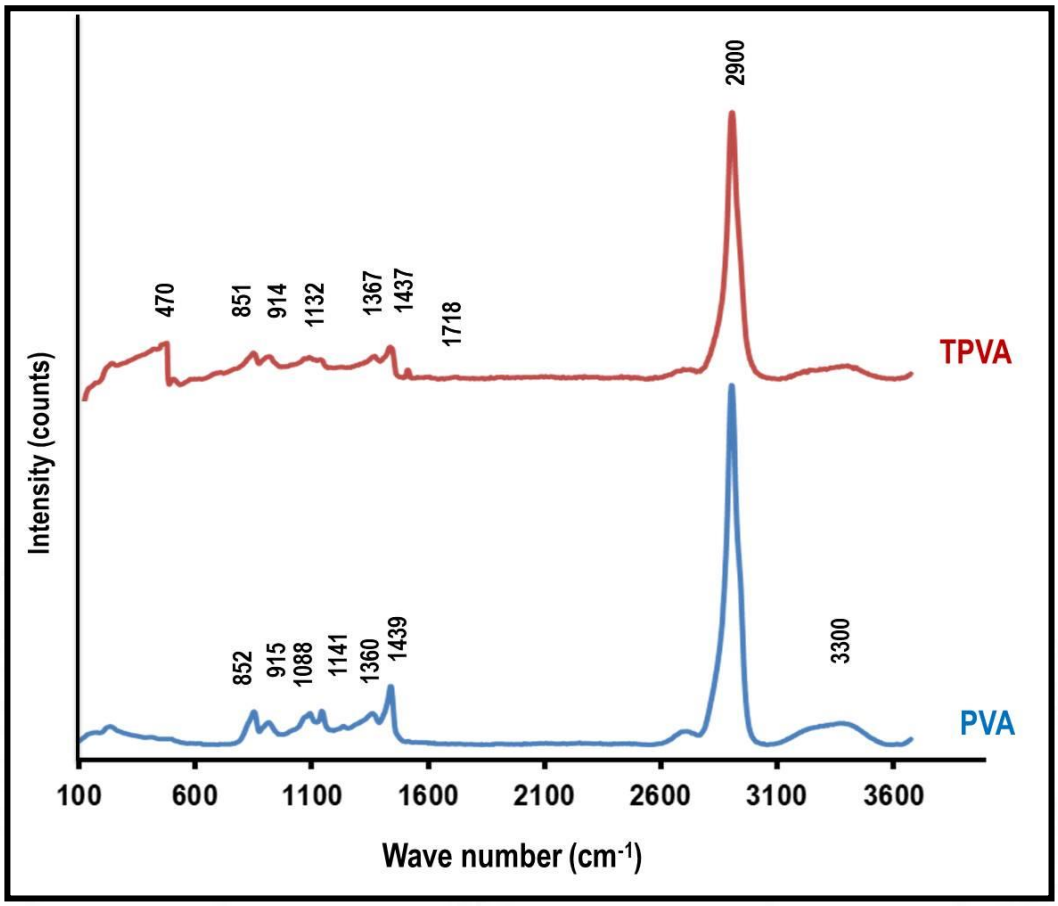

Figure 35: FT Raman spectrum of PVA and TPVA

4.3.1.3 ^{1}H- Nuclear Magnetic Resonance spectra (^{1}H NMR) of PVA & TPVA

Conjugation of thioglycolic acid to PVA polymer was further confirmed from the proton NMR spectra of PVA and TPVA. Figure 36 and 37 represents the proton NMR spectra of pure PVA and TPVA.

In figure 36, peaks at δ ~ 4.69 ppm, 4.49 ppm and 4.26 ppm could be assigned to the OH group of PVA. The peak at δ ~ 3.84 ppm is from the proton in CH part. Peaks at δ ~ 3.40 ppm and 3.51 ppm correspond to the H_2O. A sharp peak formed at 2.51 ppm is from the residual protons in DMSO solvent, peak at δ ~ 1.99 ppm is from the

methyl proton of residual acetyl part, and peaks at δ ~ 1.44 ppm, 1.39 ppm and 1.33 ppm are from the protons in CH_2 part.

All the characteristic peaks of polyvinyl alcohol are present in proton NMR spectra of TPVA except some new peaks appeared in the spectrum (Figure 37). A new peak at δ ~ 3.17 ppm is from the proton present in the carbon adjacent to the thiol group. Since PVA is produced by the hydrolysis of polyvinyl acetate, residual acetate groups will be present in the polymer and the peak δ ~ 1.99 ppm represents the methyl proton of residual acetyl part. The peaks at δ ~ 1.44 ppm, 1.39 ppm and 1.33 ppm represents the methylene proton [Kalsi.,2007, Dicharry et al.,2006]. Since the esterification of PVA will not replace all the OH groups in PVA, the proton NMR spectra of the product thiolated PVA will also contain most of the peaks in PVA. The notable feature is the appearance of new peaks from conjugated part (Figure 37). The new peak at δ ~ 3.17 ppm is from the methylene proton present adjacent to the thiol group. Since the proton NMR spectra of TPVA are not free from the peak of OH groups, it could be concluded that the esterification reaction is partial.

4.3.1.4 ^{13}C- Nuclear Magnetic Resonance spectra (^{13}C NMR) of PVA & TPVA

The ^{13}C NMR spectra of PVA and TPVA are shown in Figure 38 and 39 respectively. In the ^{13}C NMR spectra of PVA (Figure 38), the peak at δ ~ 40 ppm is the solvent peak (DMSO). Three peaks at δ ~ 64.20 ppm, 66.31 ppm, 68.09 ppm correspond to the carbon in CH-OH part and four peaks at δ ~ 45.19 ppm, 45.72 ppm, 45.17 ppm, 44.93 ppm correspond to the carbon in CH_2 part. The ^{13}C NMR spectra of TPVA (Figure 39) also showed similar spectra. The expected peaks in TPVA are the appearance of peaks at 28 ppm and 170 ppm from methylene carbon of TGA and carbonyl group in ester part. However, those peaks were not seen in ^{13}C NMR spectra of TPVA, to the reason may be the low degree of substitution.

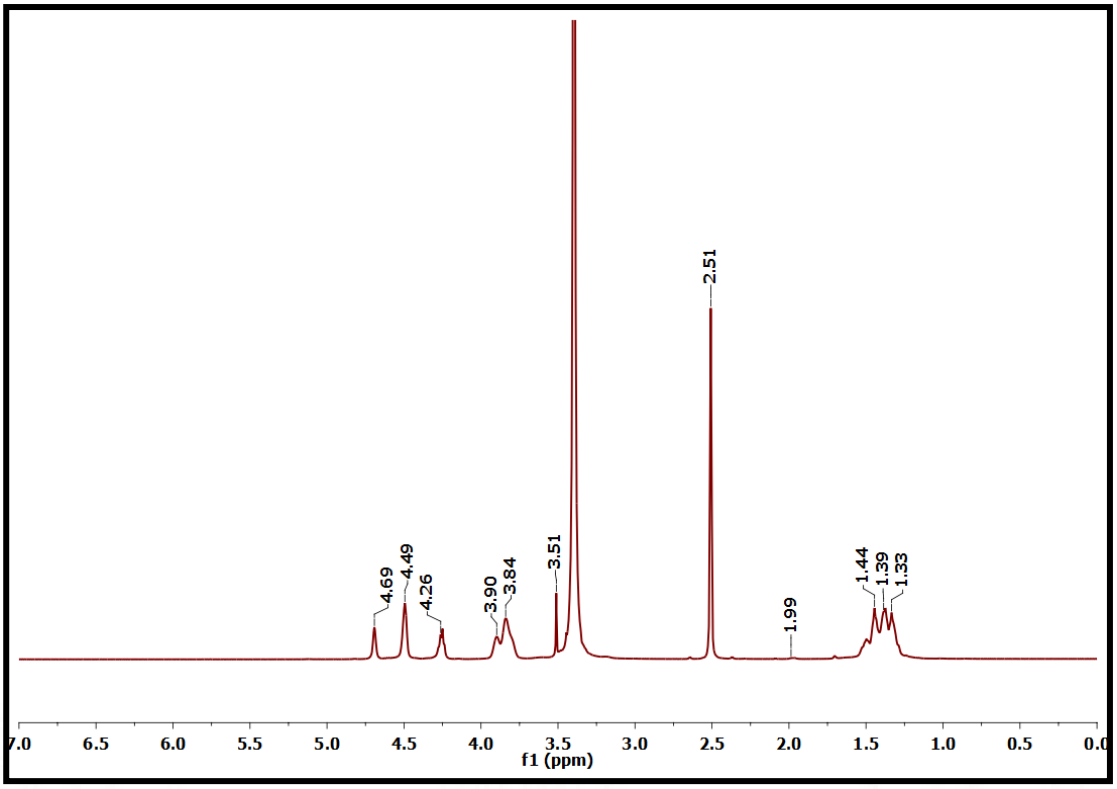

Figure 36: ^{1}H NMR spectrum of PVA

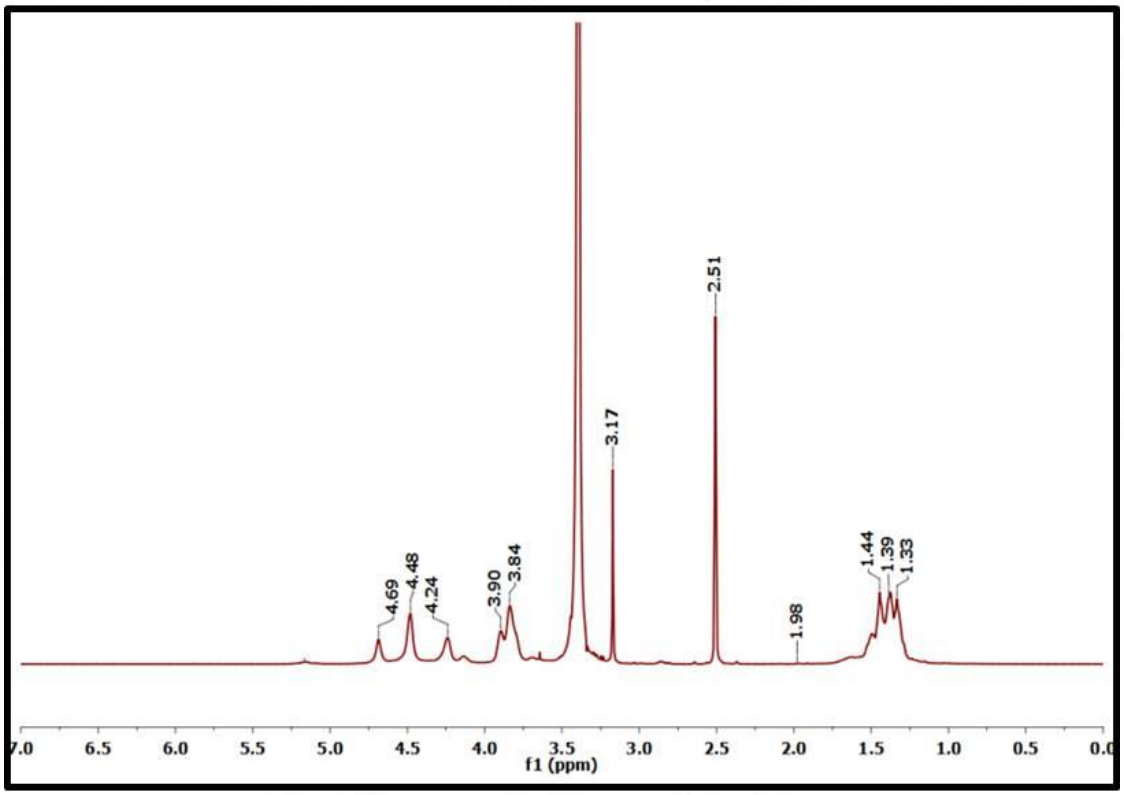

Figure 37: ^{1}H NMR spectrum of TPVA

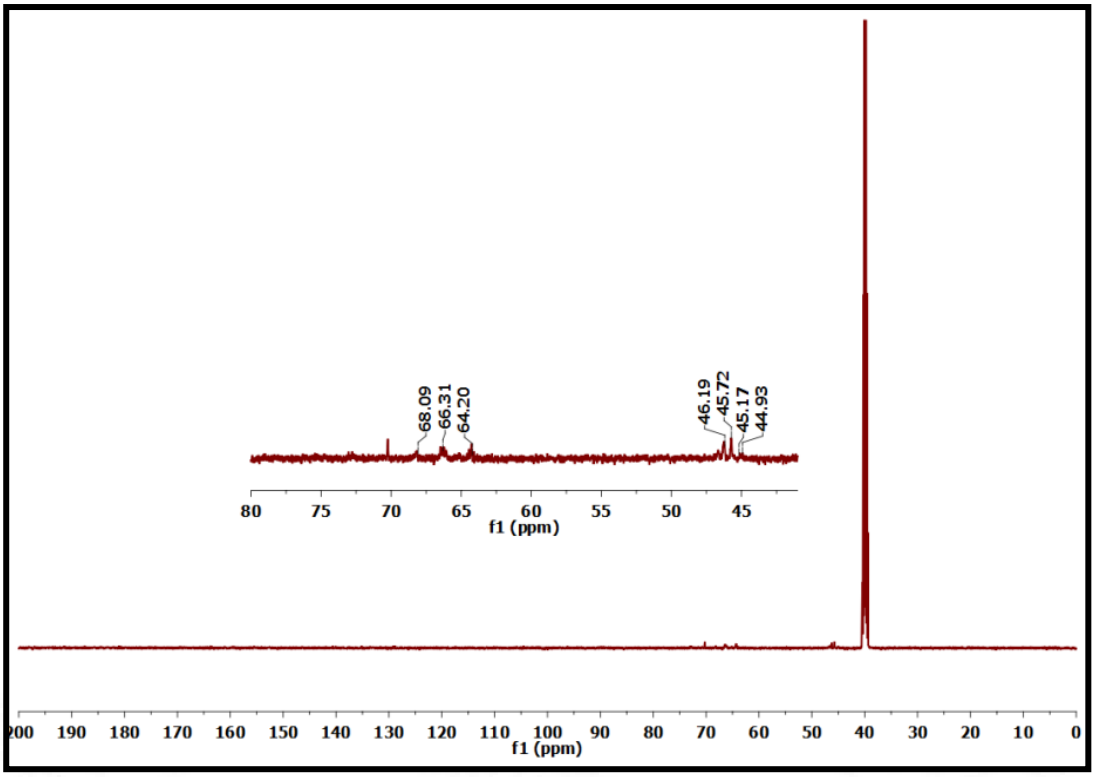

Figure 38: ^{13}C NMR spectrum of PVA

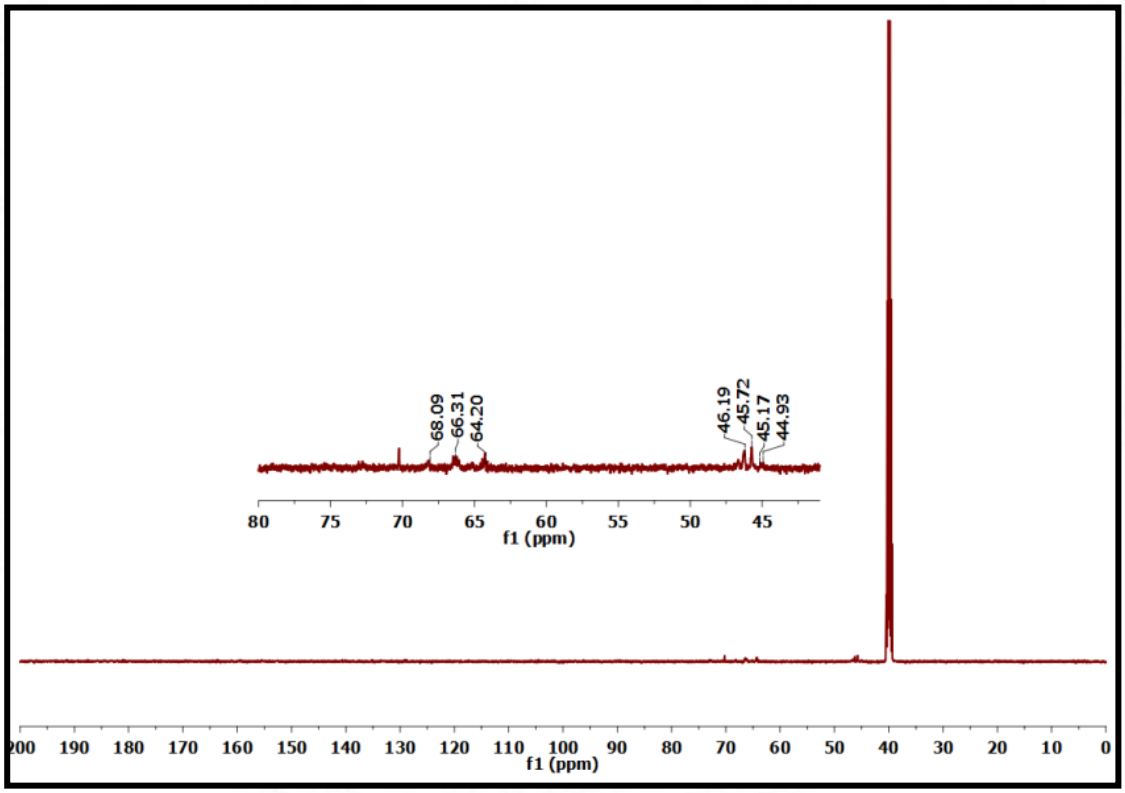

Figure 39: ^{13}C NMR spectrum of TPVA

4.3.1.5 Molecular weight analysis of PVA and TPVA by GPC

Figure 40 represents molecular weight analysis of PVA and TPVA determined using Gel Permeation Chromatography (GPC) analysis. PVA showed a number average molecular weight of 90048 (Figure 40) whereas the TPVA shows three prominent peaks at1008558, 107830 and 26466. The number average molecular weight of PVA and TPVA by GPC technique could be assigned as 90048 Da and 107830 Da respectively. The peak observed at 1008558 Da in TPVA sample (which is approximately about 10 times of the assigned molecular weight) indicates that the polymer has undergone a disulphide crosslinking by self-oxidation. This conclusion is supported by the FT-Raman data in which peak for S-S linkage appeared instead of S-H group.

4.3.1.6 Estimation of thiol content (Ellman assay & EDS analysis)

The thiol content in polymer is calculated by Ellman assay from the regression equation obtained from the standard curve based on cysteine standard (Figure 41). The thiol content per gram of the polymer was found to be 1.16 mmol and based on calculation from thiol content, the degree of substitution was found to be 6.2% and it matches with the maximum degree of substitution for thiolation of PVA reported in literature [Dicharry et al.,2006]. The result was further substantiated by the EDS analysis (Figure 42).

For a thiol-ene reaction to be considered, the number of thiol groups per gram of polymer has to be quantified. The thiol content per gram of polymer was calculated colorimetrically by Ellman assay [CE., 2002, Ellman.,1959]. It is simple and accurate method for the estimation of free thiol groups. The Ellman's reagent {5,5'-dithio-bis-(2-nitrobenzoic acid)}, commonly known as DTNB, reacts with free SH groups to produce an yellow colour and the absorbance of this yellow solution is measured spectrophotometrically at 412nm. Initially, a standard curve was plotted using cysteine standard to obtain a regression equation (Figure 41). Substituting the absorbance value

obtained with known concentration of TPVA in the regression equation average value of free thiol groups per gram of polymer was obtained. It was found that an average value of 1.16 mmol of free thiol per gram of TPVA polymer is available. Based on the thiol groups per gram, the degree of substitution was calculated to be approximately 6.20%. The percentage substitution was further confirmed from EDS analysis of TPVA (Figure 42) and found that the percentage substitution (6.22%) has good agreement with the values obtained from Ellman assay.

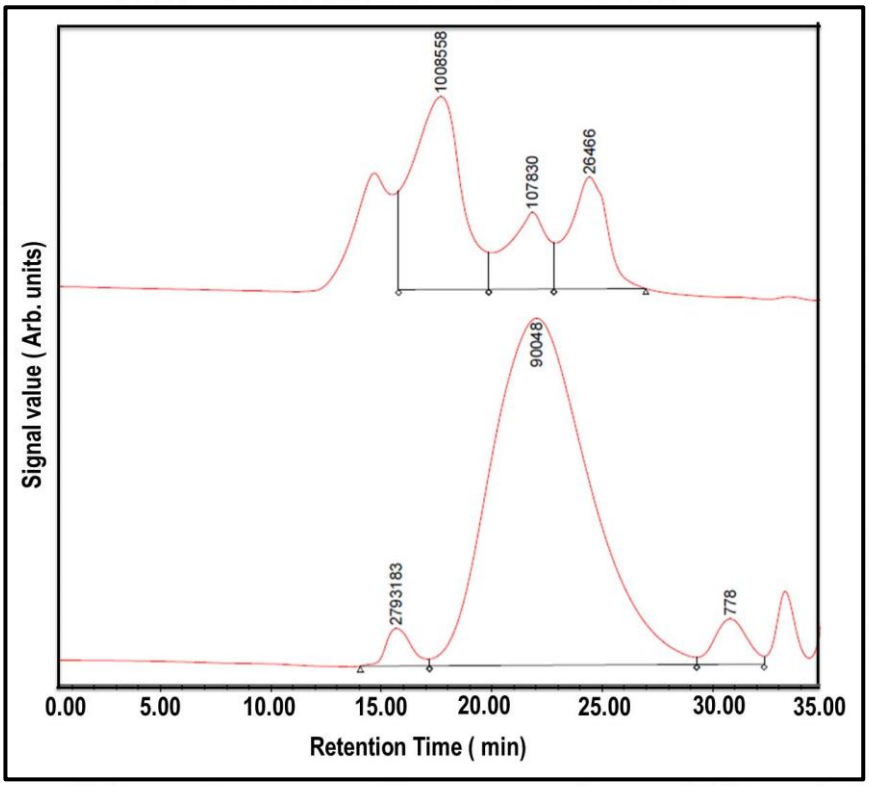

Figure 40: GPC curve showing the molecular weight distribution of PVA & TPVA

4.3.1.7 Surface wettability of PVA and TPVA

The surface wetting property of PVA and TPVA analyzed via water contact angle measurements is shown in Figure 43. The contact angle obtained for PVA (69±6°) and TPVA (23±2°) shows hydrophilic nature of the material which indicates that the thiolation has significantly increased the surface wettability of polyvinyl alcohol.

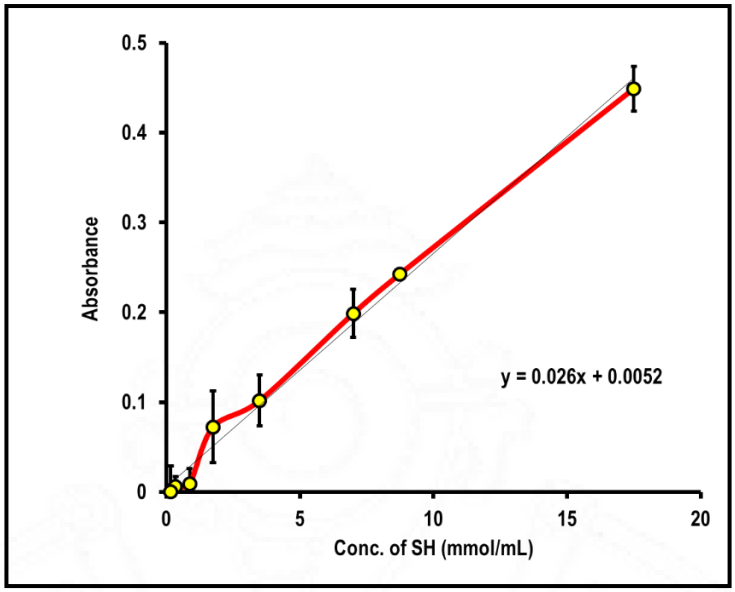

Figure 41:Thiol content versus concentration of TPVA

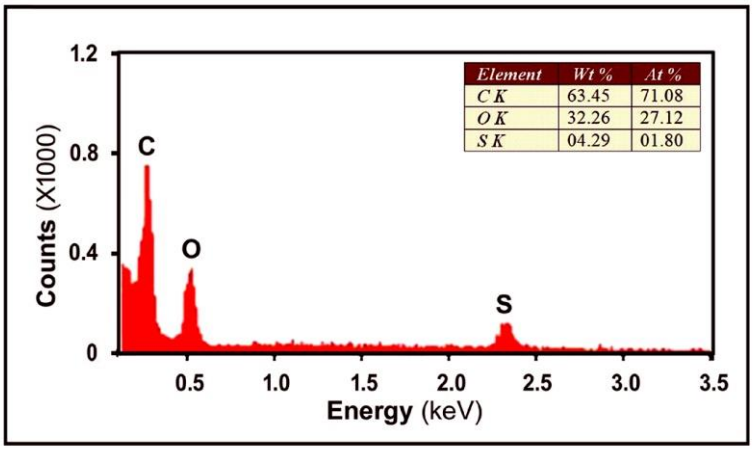

Figure 42 : EDS analysis of TPVA for the thiol content

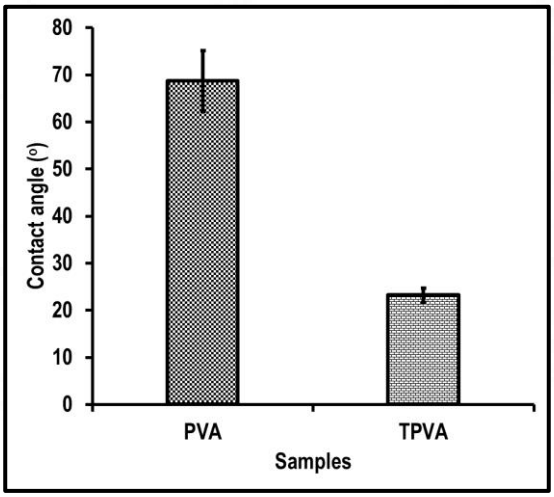

Figure 43 : Water contact angle of PVA and TPVA

4.3.2 Gel - preparation and characterization

Cross linked TPVA-PEGDA hydrogels were prepared by mixing a neutral solution of TPVA with PEGDA solution. The reactions between the thiol group in TPVA and C=C in PEGDA occur via base catalyzed thiol-ene Michael addition mechanism. Briefly the reaction starts by the abstraction of proton from thiol by base to form a thiol anion. The thiol anion attacks the C=C to form C-S bond. The schematic representation of the reaction is given in the Figure 44.

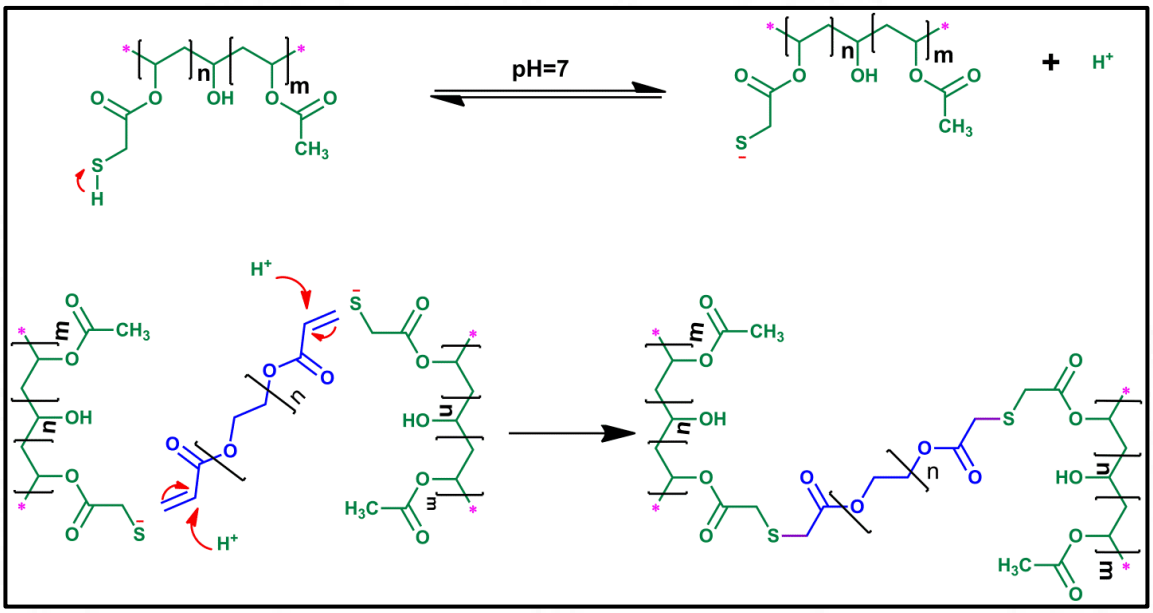

Figure 44: Schematic representation showing crosslinking mechanism during gel formation

4.3.2.1 Characterization of freeze dried Gel using FTIR

The formation of crosslinking between thiol and diene during gel formation was confirmed from the FTIR analysis and is shown in Figure 45. In the spectra of PEGDA, peaks at 1635 cm^{-1} and 1720 cm^{-1} correspond to the C=C and the ester C=O bonding, respectively. During the crosslinking with TPVA, the C=C of PEGDA will be used up and consequently the peak at 1635 cm^{-1}disappears from the gel.

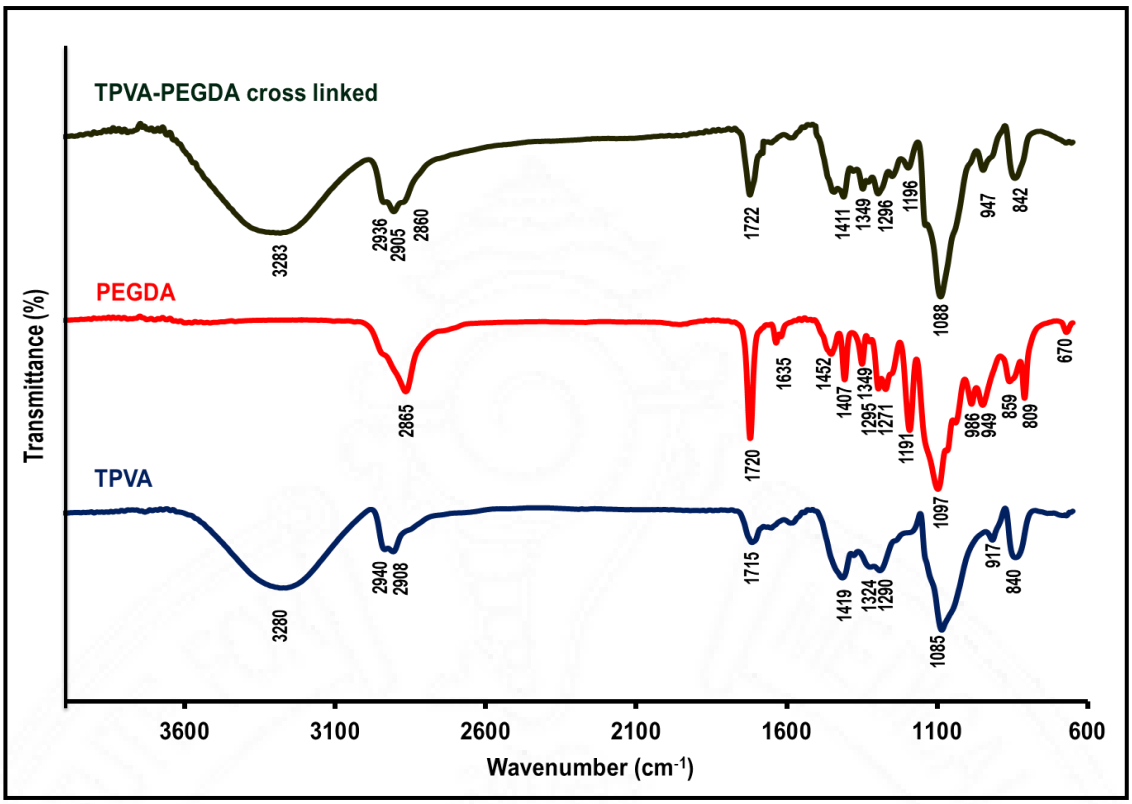

Figure 45 : FTIR spectra of (a) PEGDA, (b) TPVA (c) TPVA-PEGDA cross-linked gel

4.3.2.2 FT-Raman spectra of TPVA and TPVA cross linked

The crosslinking between PVA thiol and PEGDA during gel formation was confirmed from the FT-Raman analysis and is shown in Figure 46. In the spectra of PEGDA cross-linked TPVA, there is small increase in intensity of C=O stretching at 1718 cm^{-1} from newly added ester part from PEGDA and peak at 470 cm^{-1} completely disappeared in cross-linked one which also prove the complete utilization of thiol groups by dialkene so that there is no residual SH for oxidation to S-S.

The confirmation of crosslinking between TPVA and PEGDA is obtained from the FTIR analysis (Figure 45). The FTIR spectra of PEGDA contains absorption peaks from C=O stretch at 1720 cm^{-1} and C=C at 1635 cm^{-1} [Kalsi., 2007]. Similarly, in the case of TPVA, an ester carbonyl peak is present at 1715 cm^{-1}. After the crosslinking reaction, the ester carbonyl peaks got enhanced and the peaks due to C=C completely disappeared. This confirms the effective thiol-ene crosslinking. Additionally, FT-Raman spectra were also

recorded for cross-linked TPVA-PEGDA and TPVA (Figure 46). Comparing the spectra of TPVA and cross-linked TPVA-PEGDA, it could be seen that the S-S peak is absent in the cross-linked sample. This is because; all the thiol groups have reacted with the alkene without giving a chance for oxidation to S-S.

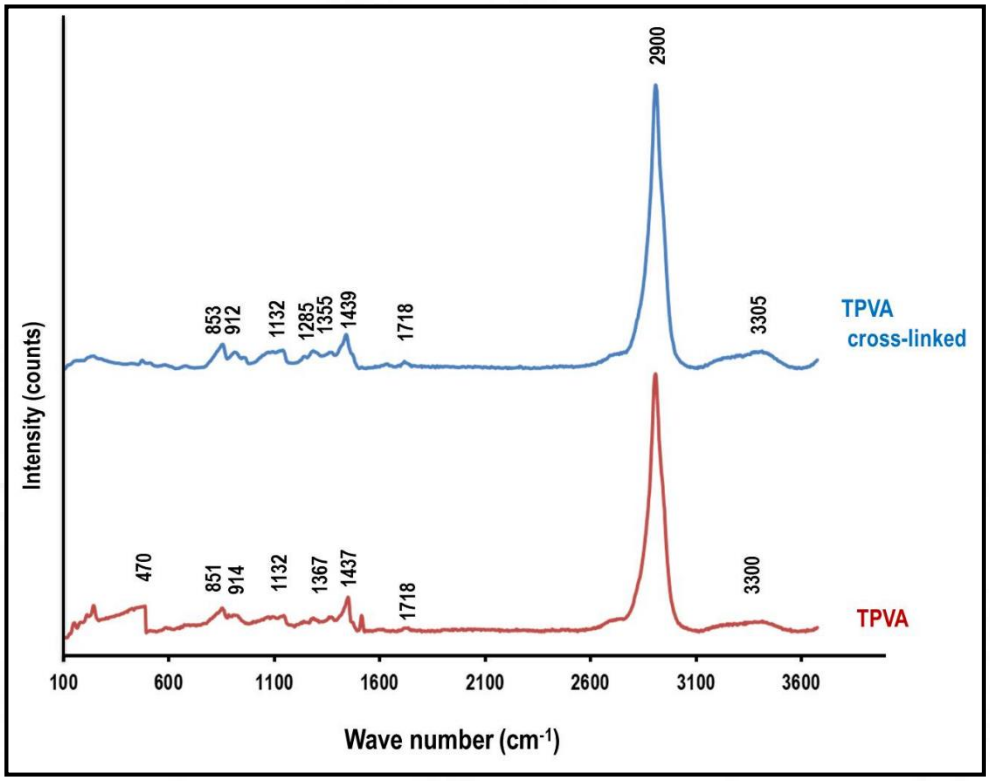

Figure 46: FT-Raman spectra of TPVA and TPVA crosslinked

4.3.2.3 Optimization of Gelling parameters

The parameters like pH of the medium, concentration of polymer solution, cross-linker concentration and time for gelation were optimized.

i. Effect of pH of the medium on gelation

The gel formation on mixing TPVA and PEGDA at different pH was evaluated (Figure 47). The TPVA-PEGDA cross linking without any photo-initiator will occur at neutral pH and alkaline pH. At a pH near to neutral condition or above neutral condition, thiol groups dissociate to provide thiolate anion needed for the crosslinking reaction.

ii. Effect of polymer concentration on gelation

The effect of thiolated polymer concentration on gelation is evaluated by mixing PEGDA with TPVA polymer solution of various concentrations. The results are shown in Table 3. Minimum concentration of polymer solution for gel formation is 3% (m/v) and below that concentration, the mixture behaves like a viscous fluid.

iii. Effect of cross linker concentration (mmol% to SH) on gelation

The effect of crosslinker concentration on gelation TPVA solution of fixed concentration is shown in Figure 48. The minimum amount of dialkene (in mmol%) to cross-link with the thiol group is found to be 6.25%, below which, the thiol-ene reaction is inefficient to produce a hydrogel.

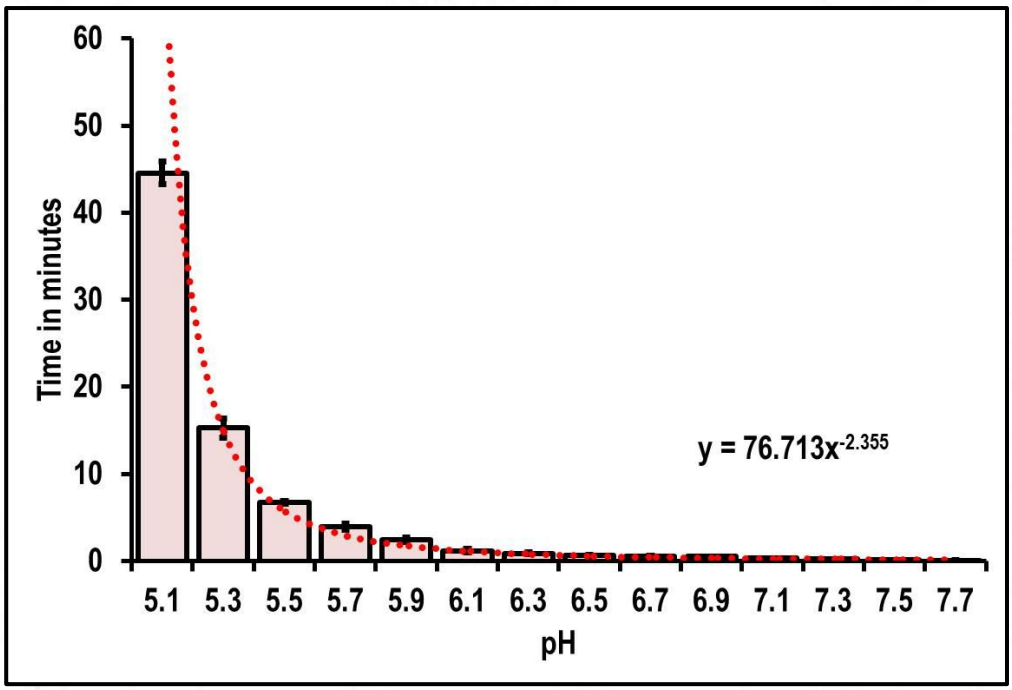

Figure 47: Effect of pH on gelation.

Table 3: Effect of polymer concentration on gelation

Concentration of TPVA solution (m/v %)	10	9	8	7	6	5	4	3	2	1	0.5	0.25
Gel formation	Yes	Yes	Yes	Yes	Yes	Yes	Yes	Yes	**No**	**No**	**No**	**No**

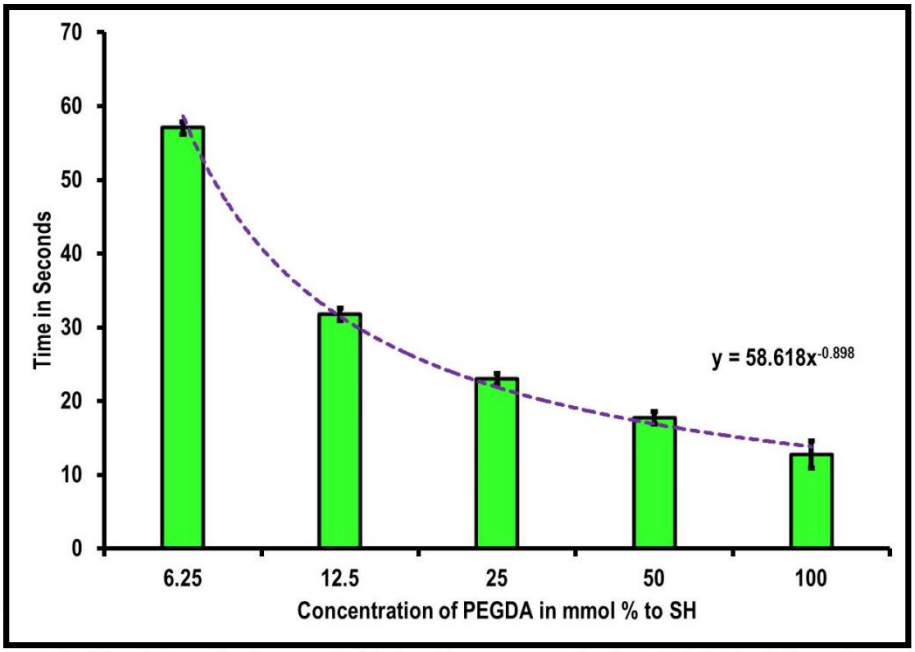

Figure 48: Effect of cross linker concentration on gelation

By considering all these factors, the gelling parameters were optimized as follows:

Concentration of TPVA polymer solution	5 w/v%
Concentration crosslinker (w.r.t. total thiol content)	50 mmol%
pH	~ 7

4.3.2.4 Preparation of hydroxyapatite (HA)

Hydroxyapatite was synthesized through a wet chemical precipitation method [Krishnan et al., 2016]. Calcium nitrate tetrahydrate and ammonium dihydrogen orthophosphate in the (Ca/P) molar ratio is 1.67 were made to react at aqueous alkaline (pH >10) condition at 80°C. The ammonium dihydrogen orthophosphate solution was added drop-wise to calcium nitrate solution to precipitate hydroxyapatite. Centrifugation was done to isolate the precipitate and washed several time till the precipitate is free from residual impurities. The final slurry obtained was spray-dried to obtain fine, free-flowing powder of hydroxyapatite

i. FTIR analysis of HA

FTIR spectra of HA shows characteristic OH groups stretching at 3570 cm^{-1}. The absorption peaks 1094 cm^{-1} and 1041 cm^{-1} correspond to the asymmetric stretching vibrations of the P–O and the peak observed at 962 cm^{-1} is due to the symmetric stretching mode of the P–O in PO_4^{3-} groups. The peaks at 603 cm^{-1} and 565 cm^{-1} could be assigned to the bending vibrations of the O–P–O in PO_4^{3-} groups.

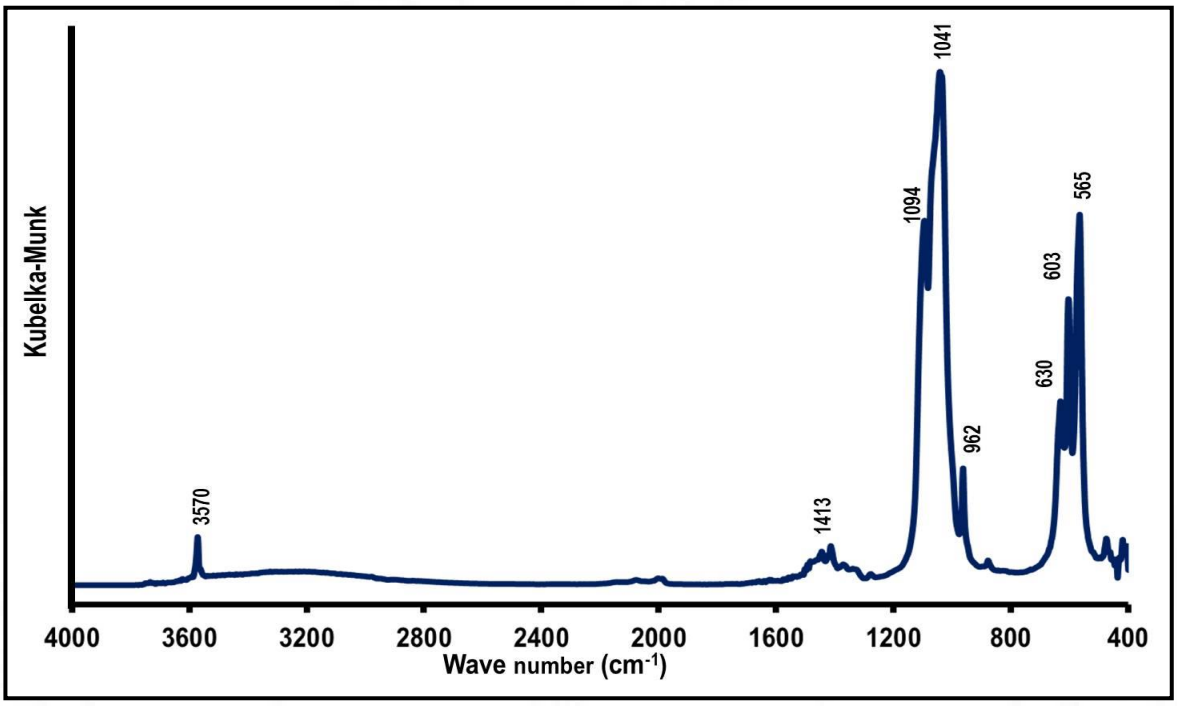

Figure 49: FTIR spectrum of hydroxyapatite

ii. XRD analysis of HA

X-ray diffraction pattern of HA match with the reported JCPDS data of hydroxyapatite (JCPDS 009-0432). All the characteristic peaks of HA between the 2θ value of 20 and 50 could be found in the spectrum (Figure 50). The 2θ values of the major peaks and the corresponding planes of the hydroxyapatite crystal (Miller indices) are given as - 25.59 (0 0 2), 27.76 (1 0 2), 28.46 (2 1 0), 31.43 (2 1 1), 31.59 (1 1 2), 32.57 (3 0 0), 33.72 (2 0 2), 34.9 (3 0 1), 38.8 (2 1 2), 39.44 (3 1 0), 41.46 (3 1 1), 43.2 (1 1 3), 44.7 (2 0 3), 46.36 (2 2 2), 47.58 (3 1 2) and 49.15 (2 1 3).

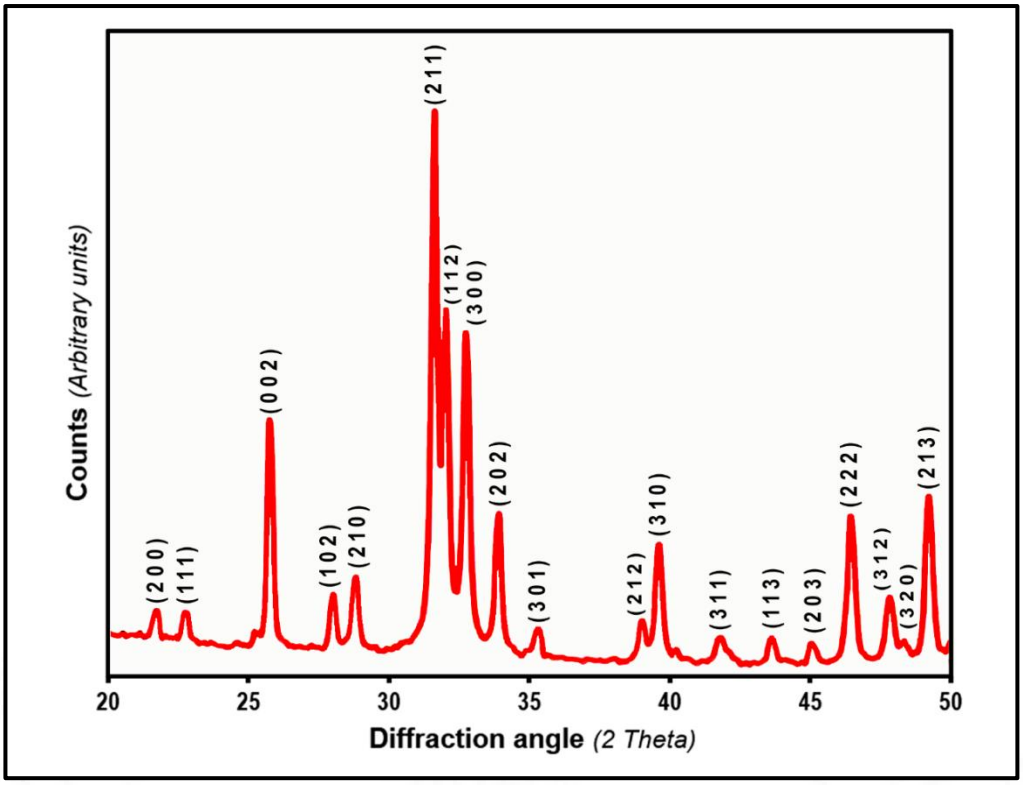

Figure 50: XRD characterization of hydroxyapatite

4.3.2.5 Fabrication and characterization of cross-linked TPVA-HA graded porous composite.

i. Phase analysis of TPVA-HA composites

In order to identify the material phases in the composites, the samples were subjected to X-Ray Diffraction (XRD). Figure 51 compares the XRD spectra of samples of PVA, TPVA and TPVA-HA composite. The XRD data of PVA and TPVA showed diffused background line without any specific molecular order, typical with amorphous polymer materials. The XRD pattern of TPVA-HA contained peaks along with the amorphous background of TPVA. The peaks obtained on the TPVA-HA sample matched with the standard XRD pattern for the hydroxyapatite (JCPDS 00-009-0432). Only major peaks could be identified compared to the HA powder in Figure 50 (which is due to the embedding inside the polymer) and they have a broadness indicating low particle size. To

conclude, the presence of the HA in freeze dried four layered membrane is confirmed from the XRD analysis.

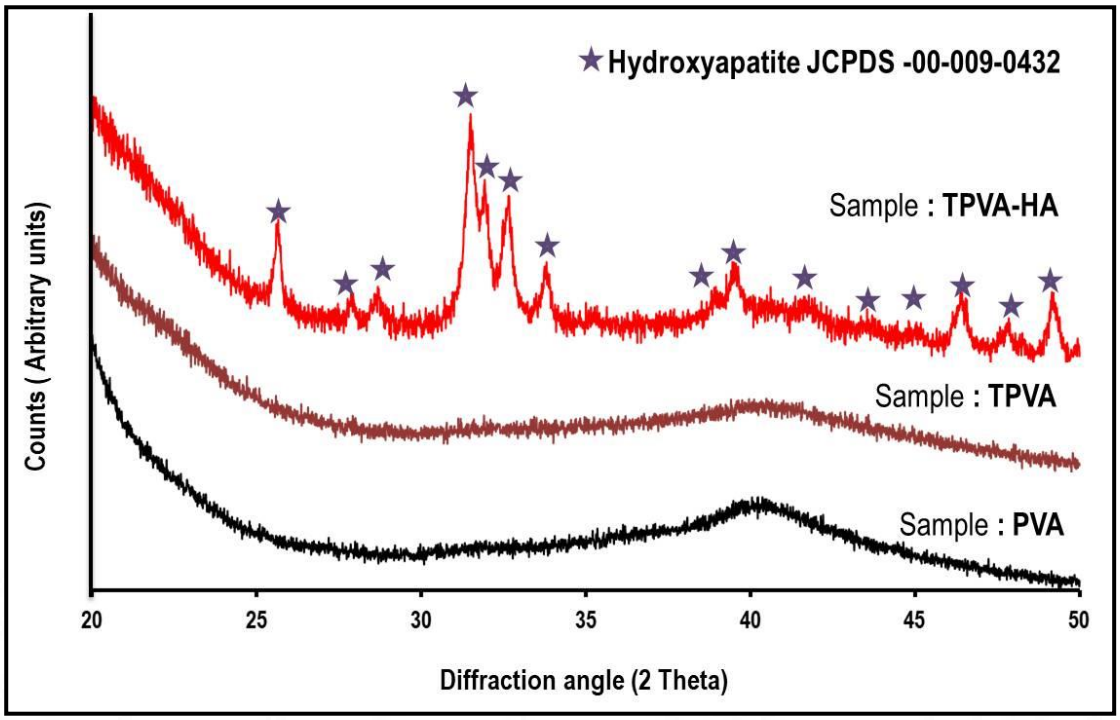

Figure 51: XRD spectra of Polyvinyl Alcohol (PVA), Thiolated Polyvinyl Alcohol (TPVA) and Thiolated PVA-HA composite (TPVA-HA)

ii. Micromorphology (SEM) of TPVA-HA composites

The micromorphology of the composite samples was visualized under scanning electron microscope at 1000X magnification, which could be found in Figure 52. Lyophilized sheets of TPVA and TPVA-HA composites show a non-porous surface feature. This is mainly due to thin skin like formation on its surface. The porous nature of material gets revealed when the thin skin over its surface degrades away.

iii. Surface wettability of TPVA-HA composites

The results of the water contact angle measurements of TPVA-HA composite along with TPVA and PVA are shown in Figure 53. Since the surface of the TPVA-HA has irregularities, sessile drop method cannot be applied and hence dynamic contact angle measurements were done. The average contact angle for PVA is 63.7° and those for TPVA

and TPVA-HA are 39.2° and 34.1°. PVA is hydrophilic and the composite material is seen highly hydrophilic in nature which arises from the thiol groups immobilized on the surface of PVA.

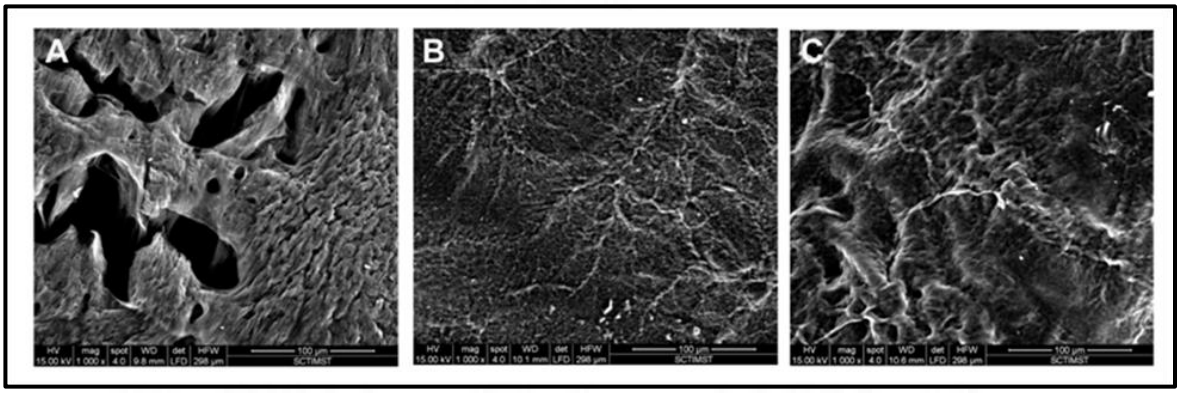

Figure 52: SEM micrograph showing surface features of [A] PVA, [B] TPVA and [C] TPVA-HA composite

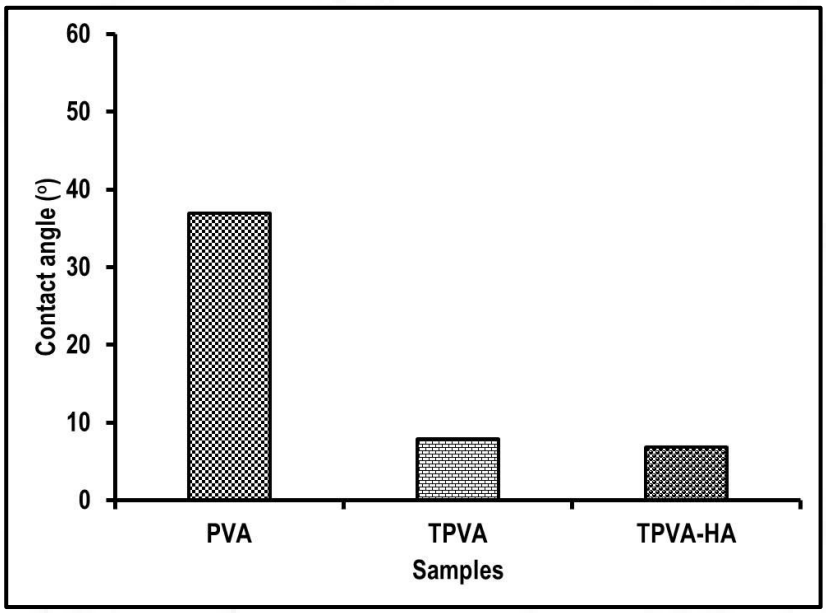

Figure 53: Contact angle measurements of Polyvinyl Alcohol (PVA), Thiolated Polyvinyl Alcohol (TPVA) and Thiolated PVA-HA composite (TPVA-HA)

iv. Mechanical Properties of TPVA-HA composites

The tensile strength and suture pullout strength of the composite in sheet form were evaluated to validate it for the use of GTR membrane. The results of mechanical property evaluation (tensile strength and suture pull out strength) using UTM are represented in the figure 54. It is observed that crosslinking of PVA via thiol-ene reaction

has increased its tensile strength from 0.538±0.201 MPa in PVA to 6.645±0.993 MPa in TPVA. Incorporation of hydroxyapatite further increased the strength of the composite to 9.25±0.925 MPa (Figure 54A).The suture pullout strength variation is just contrary to the results observed in tensile strength. Figure 54 B compares the mean suture pullout strength of composite and the control polymer samples. Similar to the tensile strength trend, the suture pullout strength of cross-linked TPVA is higher than the PVA. However, with the addition of HA a decrease in strength of about 37% was observed. The suture pullout strength of TPVA and TPVA-HA was 2.272±0.212 MPa to 1.435±0.236 MPa respectively.

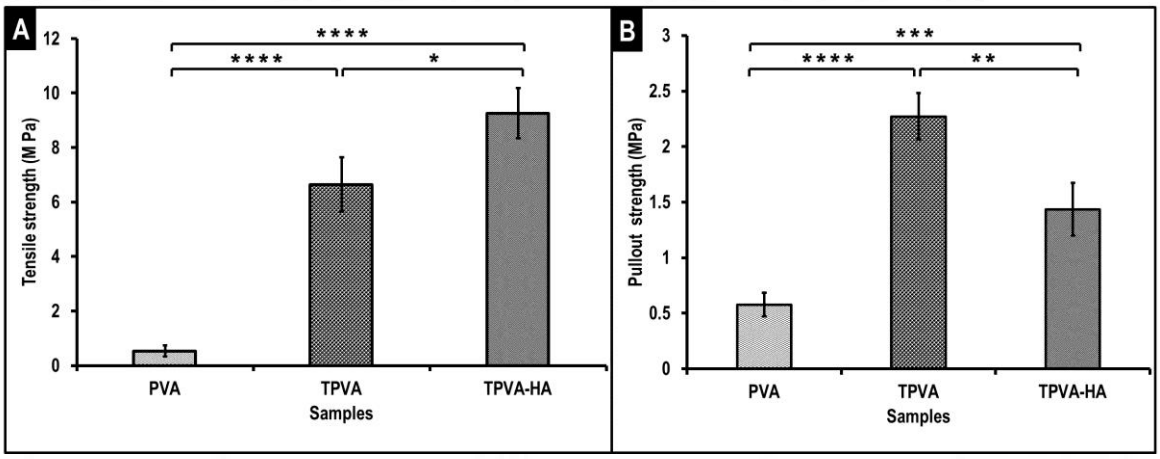

Figure 54: Mechanical property evaluation of PVA, TPVA and TPVA-HA
54A - Mean tensile strength and 54B - Mean suture pull out strength

v. In vitro swelling of TPVA-HA composites

(a) Water uptake: The results of the *in vitro* swelling studies on the materials in sheet form are shown in Figure 55. Compared to bare PVA, the cross linked TPVA and TPVA-HA showed more than 2.5 times swelling. This high rate of swelling mainly arises from the enhanced hydrophilicity of PVA when it was converted to its thiolated form.

(b) Volume swelling: *In vitro* swelling of the materials in sheet form was assessed based on its volume changes and the results are shown in Figure 56. For PVA sheets, the

dimensional change was negligible, however the dimensions of TPVA and TPVA-HA samples was higher and at any time point, TPVA-HA showed increased swelling.

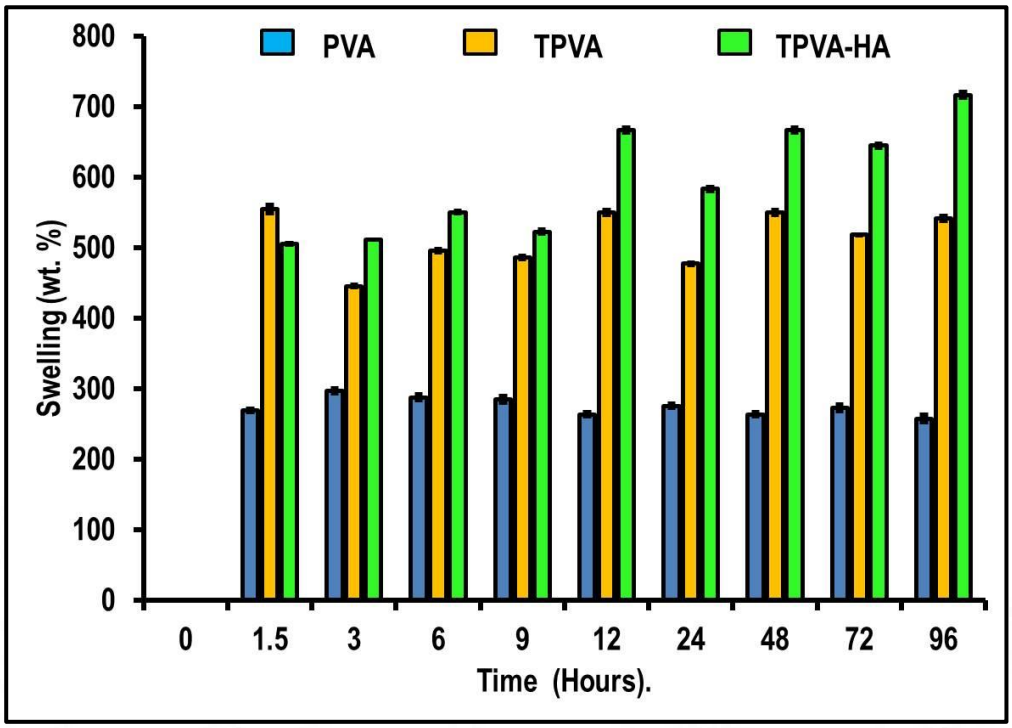

Figure 55 : *In vitro* swelling studies showing water uptake behavior of PVA, TPVA and TPVA-HA composites

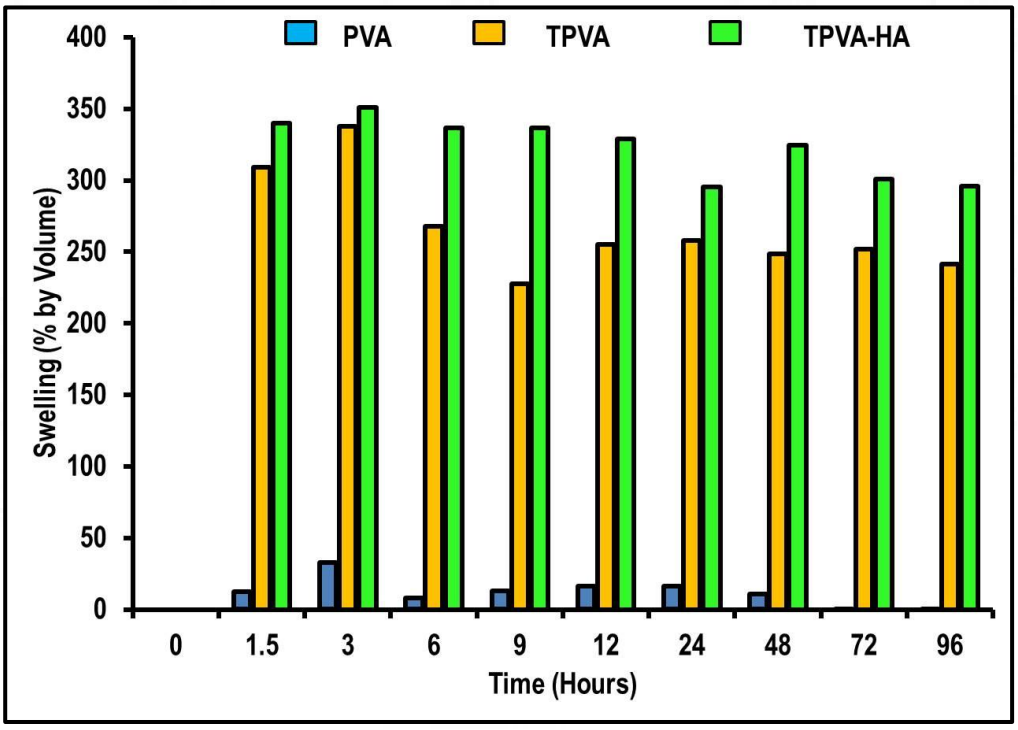

Figure 56 : *In vitro* swelling studies showing dimensional change in PVA, TPVA and TPVA-HA composites

vi. In vitro degradation of TPVA-HA composites

The percentage degradation of composite in sheet form was assessed by measuring the weight loss of PBS incubated samples at definite time intervals. The weight loss of samples on PBS ageing is shown in Figure 57.

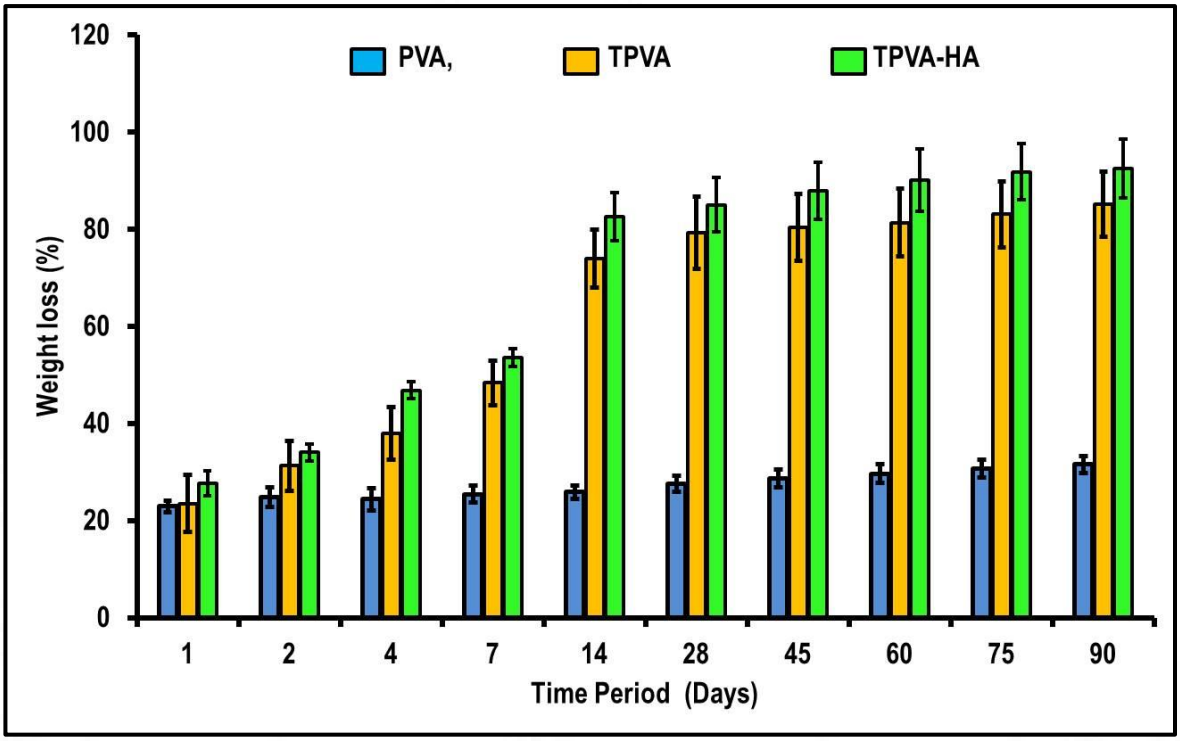

Figure 57 : *In vitro* degradation study showing percentage weight loss of PVA, TPVA and TPVA-HA composites during ageing in PBS

The results of the *in vitro* degradation studies in PBS shows that after 24 h, more than 20 wt.% weight loss occurred for all the samples. The weight loss was more prominent after 14 days, with the percentage values of 25%, 74% and 82% for PVA, TPVA and TPVA-HA composites respectively (Figure 57). The non-degrading behavior of PVA in PBS is clear from the data. The initial weight loss happens due to the leaching of small unbound molecules alone and do not represent the structural disruption. In PVA, there is no labile bond in the C-C back bone structure, which in turn prevents the lysis into small molecules. The degradation profile of TPVA and TPVA-HA composites are similar and the mass loss in PEGDA cross-linked TPVA occurs via ester degradation. There are ester bonds between PVA and TGA in TPVA backbone and between acrylate and PEG in

PEGDA. As chemical bonds are considered, ester bonds are more labile at physiological pH. This is the reason that TPVA and TPVA-HA showed more than 70% degradation within 2 weeks. The degraded product will be PVA, PEG and 2,2′-Thio-bis(acetic acid). Afterwards, up to a period of 3 months, the degradation is negligible. By that time all the ester bonds might have been cleaved away, leaving out the PVA back bone which is not prone to degradation through hydrolysis.

vii. In vitro bioactivity studies

The surface morphology of the sheets after immersing in simulated body fluid for 7 days is shown in the Figure 58. PVA shows a degradation of surface, and TPVA-HA carries apatite like deposition on its surface. Energy-dispersive X-ray spectroscopic (EDS) analysis of the deposited particle was carried out and the results are shown in Figure 59. The Ca/P ratio obtained from the EDS analysis was approximately 1.72.

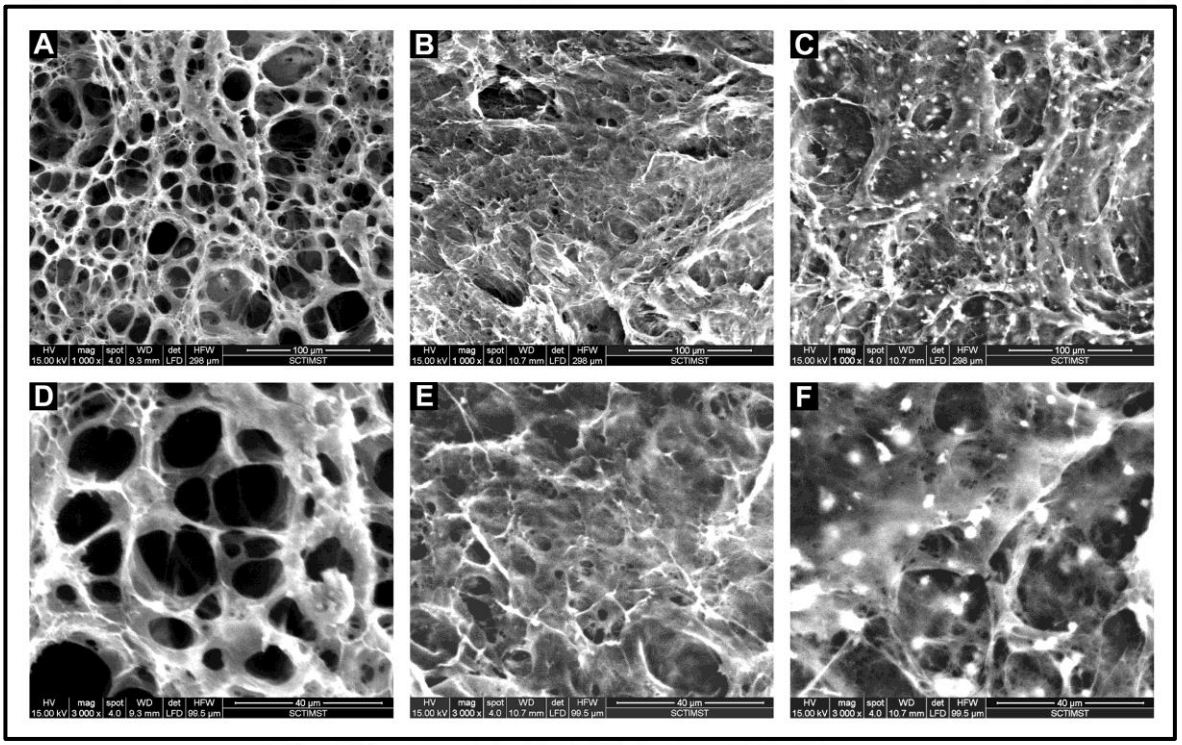

Figure 58: SEM images of the PVA, TPVA and TPVA-HA sheet surfaces after the *in vitro* bioactivity test, by immersing in SBF for 7 days. [A, B and C] represent the surfaces of PVA, TPVA and TPVA-HA sheets respectively at 1000X. [D, E and F] represent the same areas at 3000X.

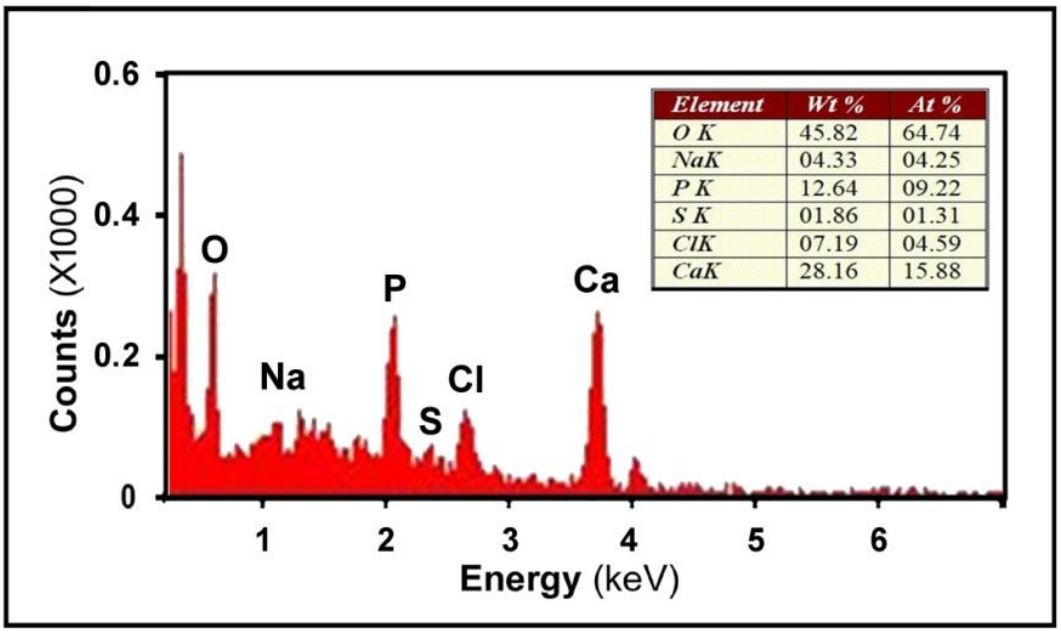

Figure 59: EDS analysis of the TPVA-HA sheets surface after the bioactivity test

viii. In vitro cytocompatibility

(a) Direct contact: The cytocompatibility of the materials with hPDL cells was evaluated using direct contact test (Figure 60). The hPDL cells cultured in the presence of the test materials showed no evidence of cytotoxicity. The cells were adherent and maintained their morphology, both in the cell control and in the presence of PVA, TPVA and TPVA-HA sheets.

(b) MTT assay: Figure 61 represents the results of MTT assay using hPDL cells showing percentage metabolic activity in the presence of PVA, TPVA and TPVA-HA materials. The hPDL cells exhibited a percentage metabolic activity > /= 100% in the presence of the materials and no significant difference were seen among the samples. The value for TPVA-HA was significantly higher compared to the hPDL cell control (Figure 61).

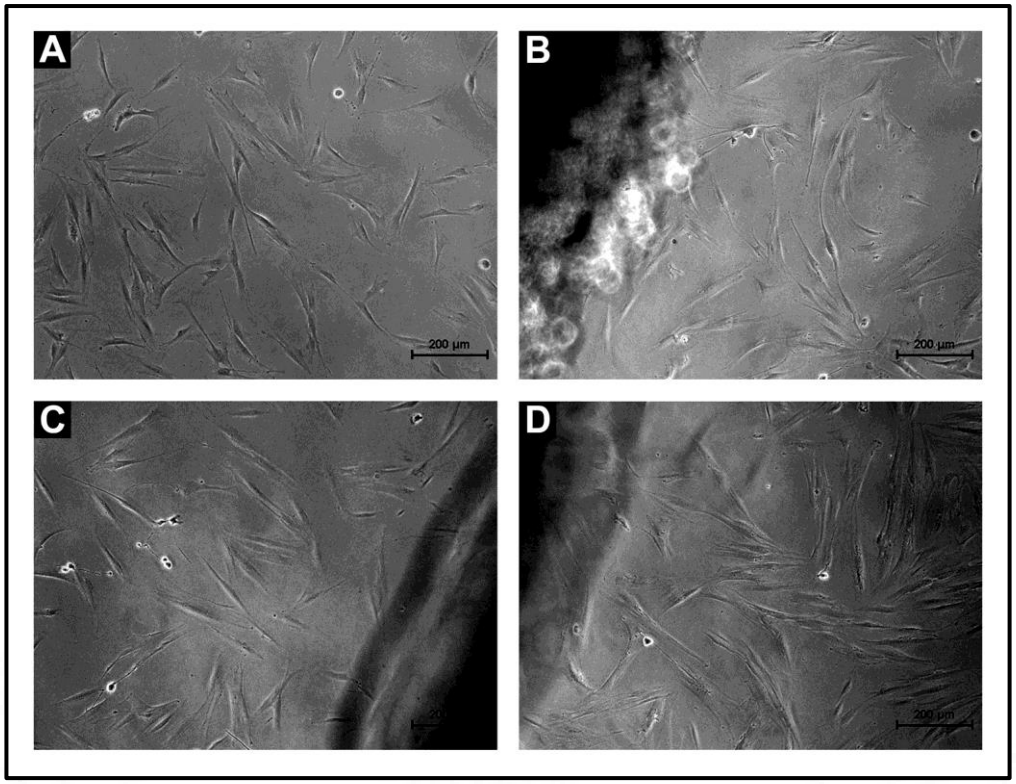

Figure 60 : Direct contact assay of materials using hPDL cells for 24 h.
[A] Cells alone, [B] PVA sheet [C] TPVA sheet and [D] TPVA-HA sheet

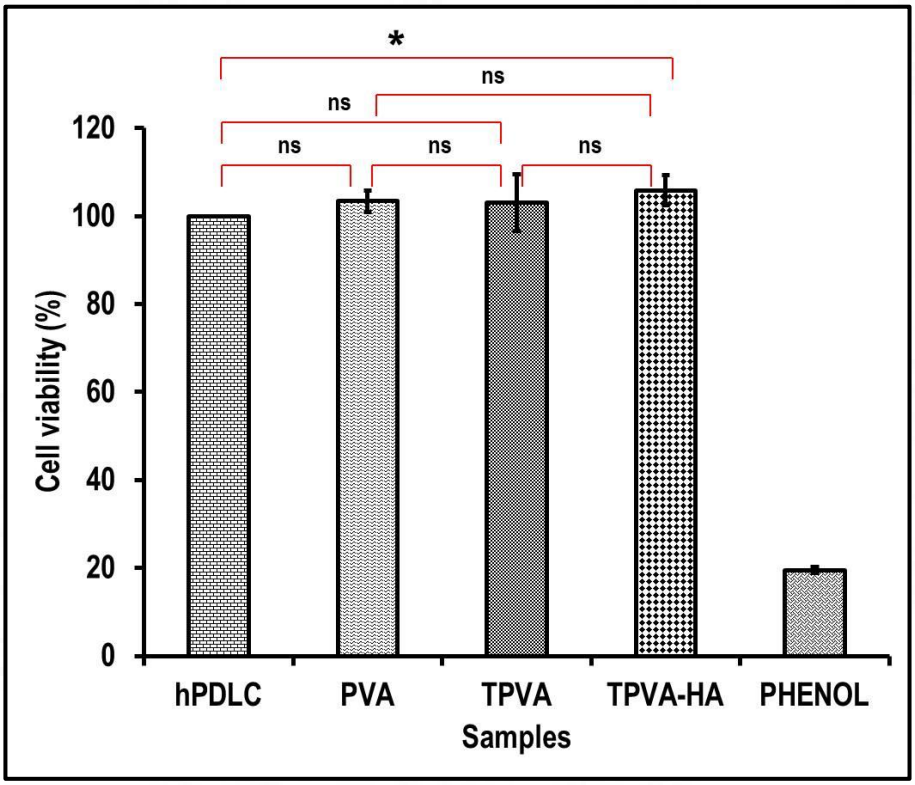

Figure 61: MTT assay of PVA, TPVA and TPVA-HA sheets using hPDL cells

(c) Cell adhesion and spreading by Actin staining: The confocal (CLSM) images of actin staining are shown in Figure 62. The CLSM images of the hPDL cells on the membranes showed typical spindle morphology as compared to the control cells cultured on cover glass. In addition, the periodontal ligament fibroblasts cultured on the membranes showed a three dimensional distribution, showing migration of cells into the membranes.

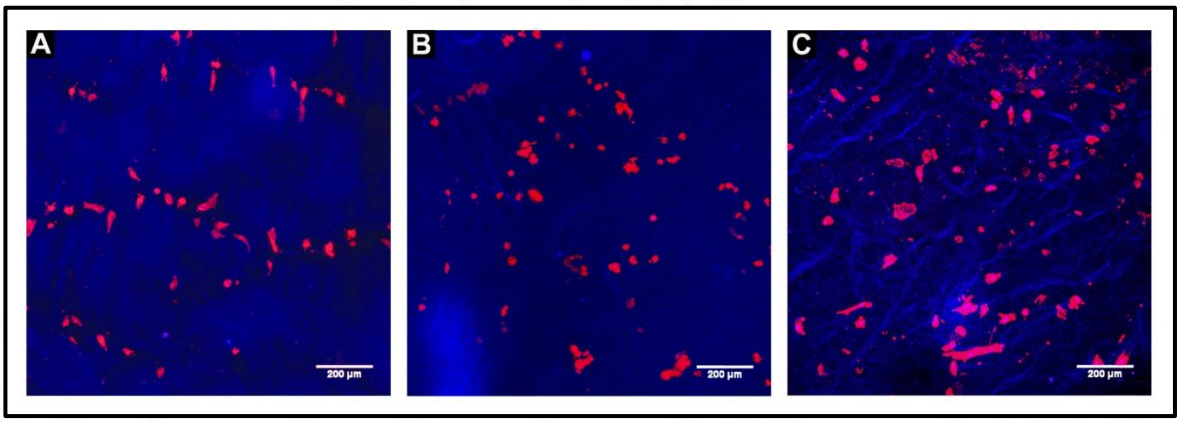

Figure 62: Confocal laser scanning microscopic images showing actin staining on sheets cultured with hPDL cells for 24 h. [A] PVA, [B] TPVA and [C] TPVA-HA

4.4 Preparation of Thiolated Polyvinyl Alcohol-Thiolated chitosan-Hydroxyapatite graded cross-linked composite membrane (TPVA-TCS-HA)

The objective of this section is to make combinational materials of modified chitosan and polyvinyl alcohol containing hydroxyapatite, with functionally graded structure which satisfies the essential requirements of guided tissue regeneration membranes.

4.4.1. Preparation and characterization of Thiolated chitosan (TCS)

Thiolated Chitosan (TCS) was prepared by EDC coupling reaction between the amine group of chitosan and the carboxylic acid group of thioglycolic acid (Figure 63). The amount of thiol group immobilized on the chitosan polymer estimated via Ellman's assay was approximately 170 µmol/gram of polymer. This corresponds to grafting efficiency of 1.5%.

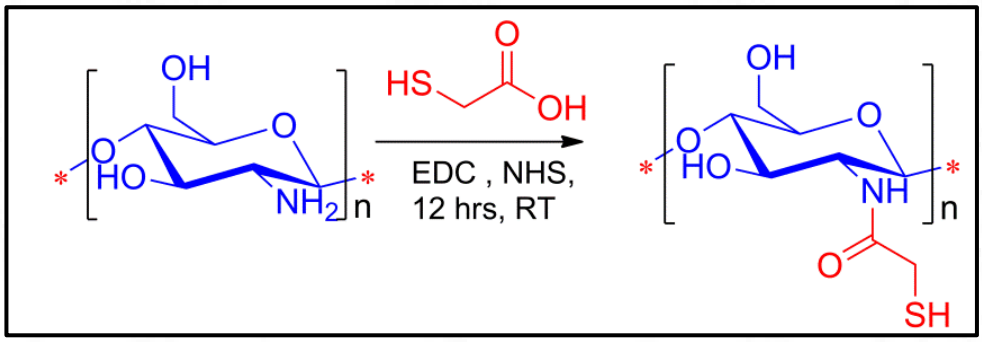

Figure 63: Schematic representation showing thiolation of chitosan through EDC coupling reaction

4.4.1.1 FTIR spectra of CS & TCS

The broad band at 3350 cm^{-1} represents the stretching band from both hydroxyl groups and residual amine groups. Peaks at 2920 cm^{-1} and 2876 cm^{-1} on the shoulder of the broad band indicate the symmetric and anti-symmetric stretching of C-H bond. The N-H bending vibration of primary amine together with amide I stretching from the residual

N- acetyl groups are represented by a peak at 1627 cm^{-1}. Amide II band of residual amide bonds is observed at 1520 cm^{-1} and Peak 1379 cm^{-1} could be assigned to the CH_3 symmetrical deformation. The peak at 1150 cm^{-1} represents the C-O-C bridge, and those at 1067 cm^{-1} and 1024 cm^{-1} correspond to C-O stretching modes. Another characteristic peak from the CH bending out of the plane of the monosaccharide ring appeared at 900 cm^{-1}.

Almost all the peaks in the spectra of chitosan is retained in thiolated chitosan (TCS) however, the notable difference is in of N-H bending and amide I and II region. The N-H bending intensity got decreased whereas at the same time, the intensities of amide peaks got enhanced. This is due to the conversion of amine to amide via EDC coupling.

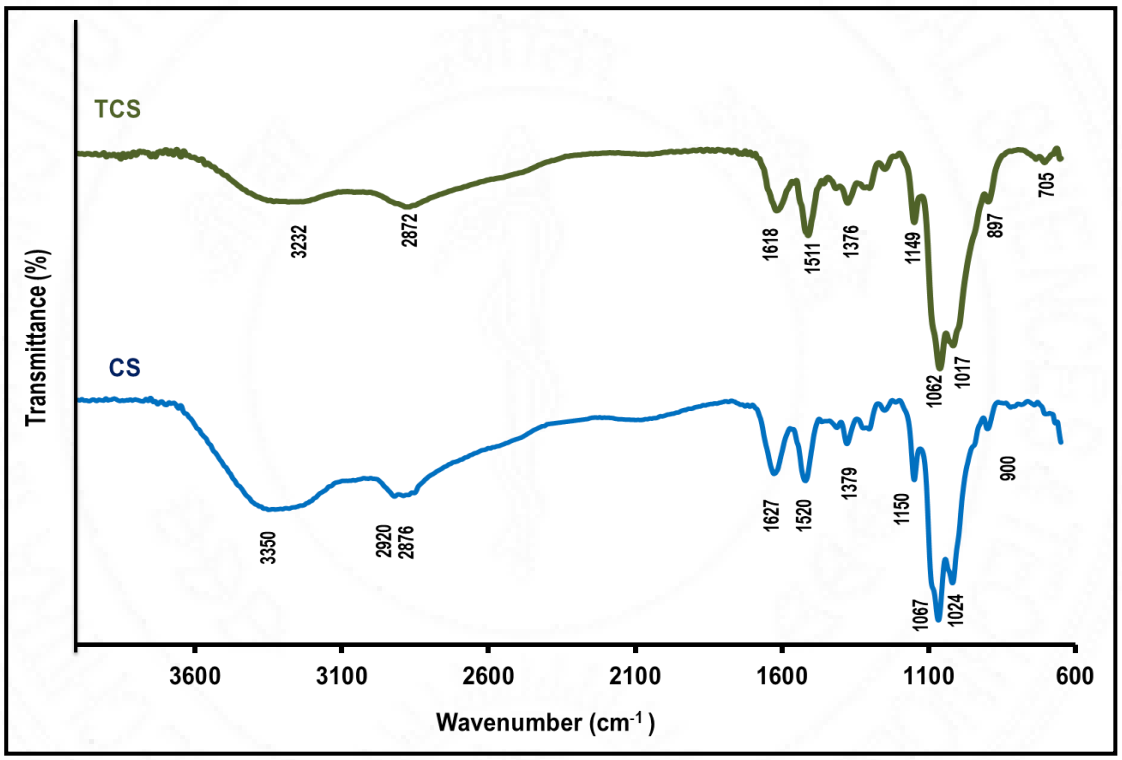

Figure 64: FTIR spectrum of CS and TCS

4.4.1.2 ^{1}H NMR spectra of CS & TCS

^{1}H NMR spectra of chitosan and its thiolated derivative (TCS) taken using DCl and D_2O solvents are shown in Figures 65 and 66 respectively. The proton NMR spectrum

of chitosan shows characteristics peaks at δ ~ 8.08 ppm corresponding to the amide proton, the methyl protons from the residual acetyl groups are observed at δ ~1.93 ppm. The characteristic peaks of protons from primary and secondary alcohol groups are observed at δ ~ 1.27 and 1.28 ppm, the CH protons present in 3 to 6 positions of pyranose ring are represented by peaks at δ ~ 3.45 ppm to 3.78 ppm. The peak at δ ~ 3.05 corresponds to the proton in C_2 carbon of pyranose ring [Ruihua et al.,2012; Zou et al.,2015; Kalsi.,2007; Luo et al.,2010]

In case of proton NMR spectra TCS (Figure 66), most of the peaks remain same, which indicates that only a small portion of the amine groups has undergone modification. The characteristic peak at δ ~ 0.70 ppm represents the α proton with respect to the thiol group. A small peak at δ ~ 1.49 ppm correspond to the SH proton. Peaks from 0.98 ppm to 1.15 ppm correspond to the protons in newly attached part. The remaining peaks correspond to those present in the proton NMR spectra of chitosan [Kalsi., 2007,Esquivel et al.,2015]. Using FTIR and NMR data, the effective thiolation of chitosan via amide linkage is thus confirmed. The percentage substitution measured from Ellman assay was found to be 1.5%.

4.4.1.3 Surface wettability of CS and TCS

The surface wetting property of CS and TCS analyzed via water contact angle measurements is shown in Figure 67. Thiolation of chitosan have significant effect on increasing the surface wettability. The contact angle obtained for TCS (58±12°) compared to CS (112±6°) reveals the induction hydrophilic nature through thiolation.

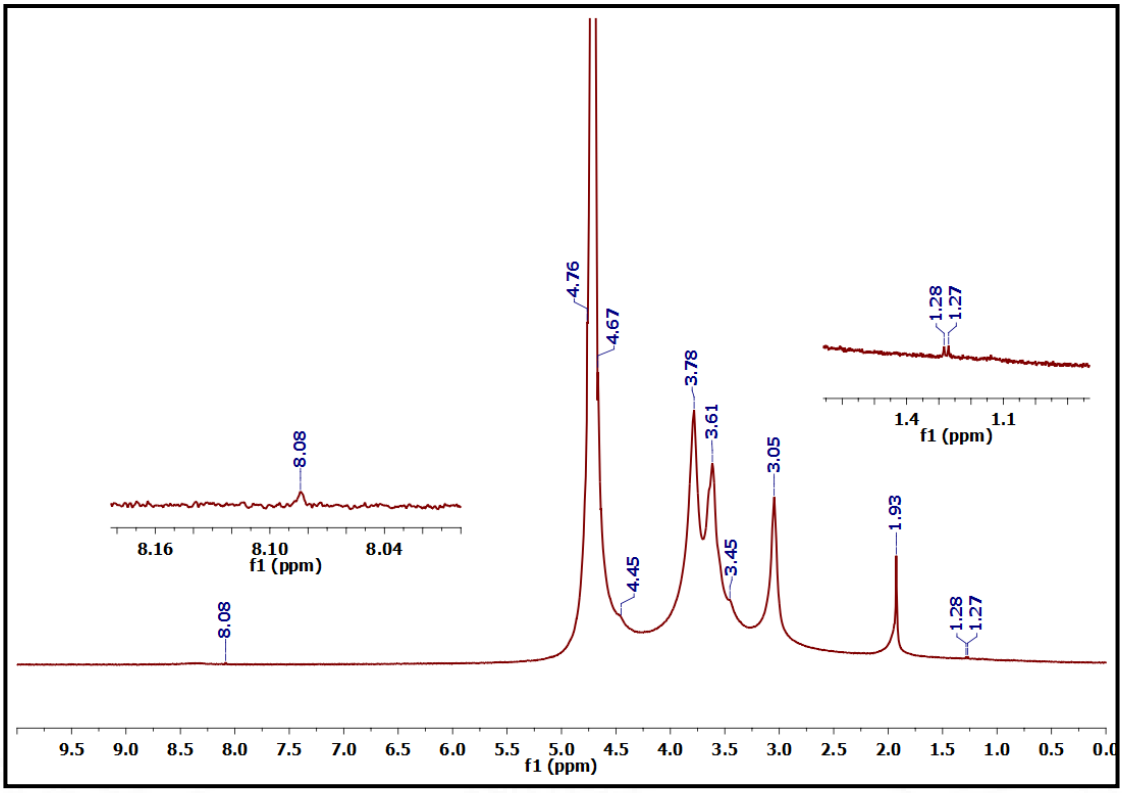

Figure 65: ^{1}H NMR spectrum of chitosan

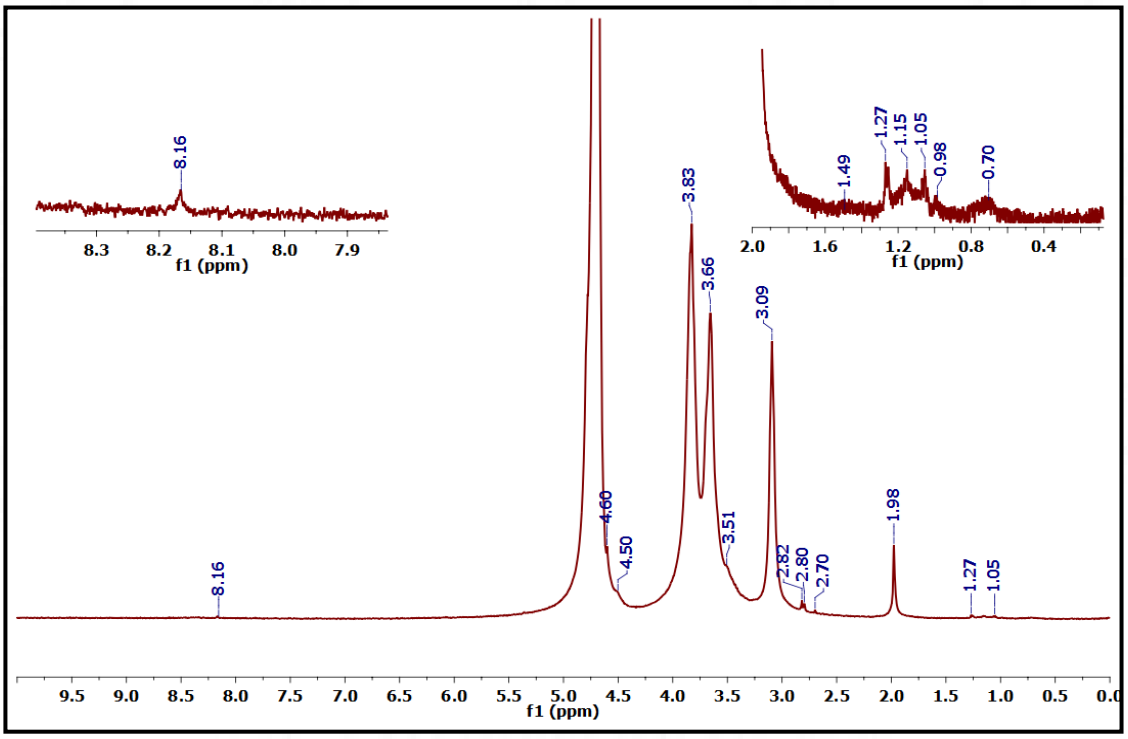

Figure 66: ^{1}H NMR spectrum of TCS

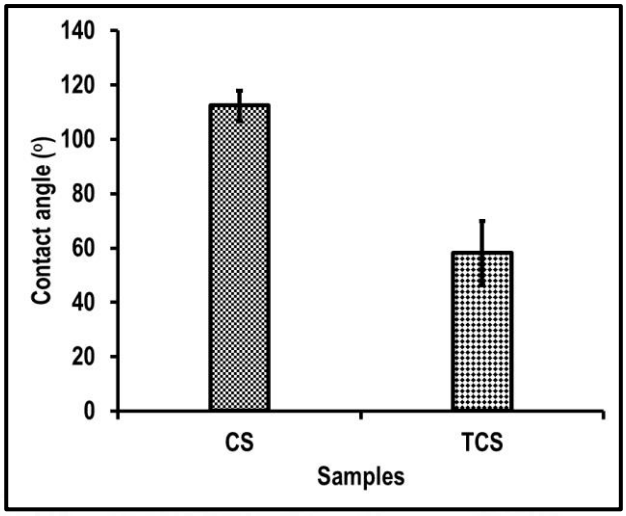

Figure 67 : Water contact angle measurements of CS and TCS

4.4.2 Preparation and characterization of cross-linked TPVA-TCS-HA graded porous composite.

The TPVA-TCS and TPVA-TCS-HA composite were prepared in sheet form as described in section 3.2.9.2 and was analysed for its physical properies.The thickness of the sheet was 0.5 mm.

4.4.2.1 XRD analysis of TPVA-TCS-HA composites

The composition of HA in each layer is similar to the four layered TPVA-HA composite except the presence of TCS. The amount of TCS was adjusted to 10% m/m compared to TPVA polymer in TPVA-TCS_{10}-HA and 5% m/m to TPVA polymer in TPVA-TCS_5-HA. The gel was then freeze dried to form dry composite material. The XRD patterns of the TPVA-TCS_{10}-HA and TPVA-TCS_5-HA were similar which contained the characteristic peaks of hydroxyapatite along with the amorphous polymer background (Figure 68).

The peaks seen in the diffraction pattern for the TPVA-TCS-HA (Figure 68) matches with the standard data for the hydroxyapatite (JCPDS 00-009-0432). The peaks obtained and their corresponding planes (as Miller indices) are 25.59 (0 0 2), 27.76 (1 0

2), 28.46 (2 1 0), 31.43 (2 1 1), 31.59 (1 1 2), 32.57 (3 0 0), 33.72 (2 0 2), 34.9 (3 0 1), 38.8 (2 1 2), 39.44 (3 1 0), 41.46 (3 1 1), 43.2 (1 1 3), 44.7 (2 0 3), 46.36 (2 2 2) and 47.58 (3 1 2). This proves that the HA added get incorporated in the membranes without any phase change.

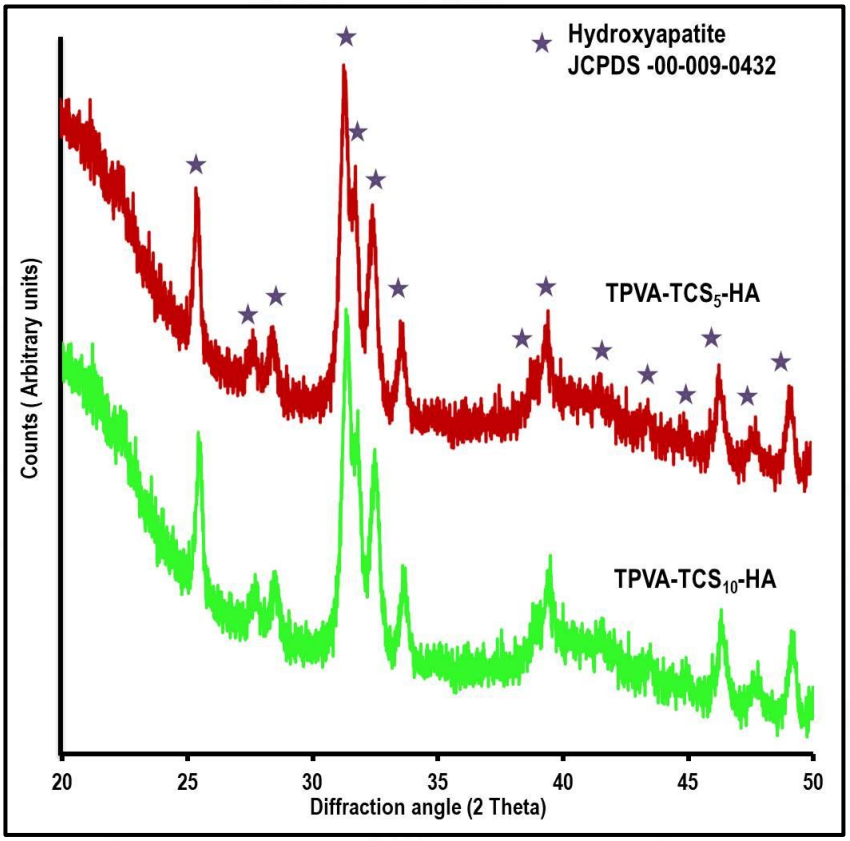

Figure 68: XRD spectra of TPVA-TCS_5-HA and TPVA-TCS_{10}-HA

4.4.2.2 Micromorphology of TPVA-TCS-HA composites using SEM

The micromorphology of the composite samples visualized under scanning electron microscope at 1000X magnification is shown in Figure 69. The TPVA-HA composite showed non-porous surface morphology. The incorporation of polymer TCS to TPVA-HA composite membranes did not alter its surface feature notably. Both the composites membranes (TPVA-TCS_5-HA and TPVA-TCS_{10}-HA) showed surface features without any pore, probably due to a thin skin-like formation on its surface.

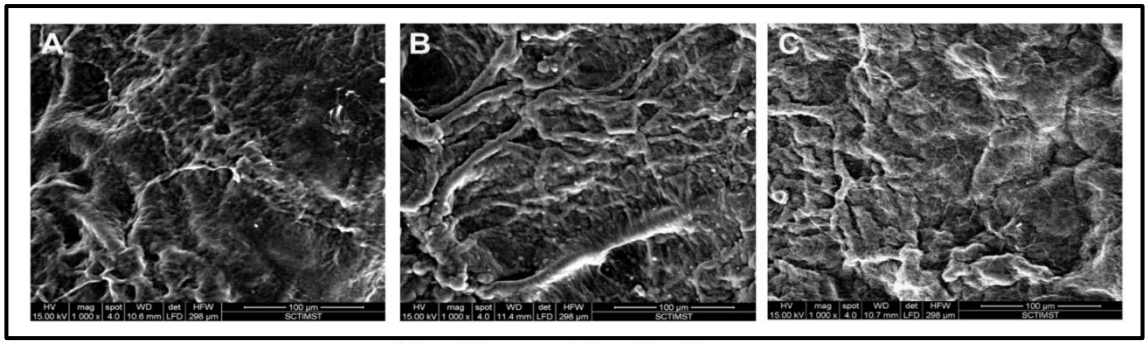

Figure 69: SEM micrograph showing surface feature of composites
[A] TPVA-HA, [B] TPVA-TCS_5-HA and [C] TPVA-TCS_{10}-HA

4.4.2.3 Surface wettability of TPVA-TCS-HA composites

The surface wetting property of TPVA-TCS-HA analyzed via water contact angle measurements is shown in Figure 70. The contact angle obtained reveal the hydrophilic nature of all the samples (TPVA-HA: 34.1°; TPVA-TCS_5-HA: 34° and TPVA-TCS_{10}-HA: 32.6°). The TPVA-TCS_{10}-HA composite has slightly higher wettability.

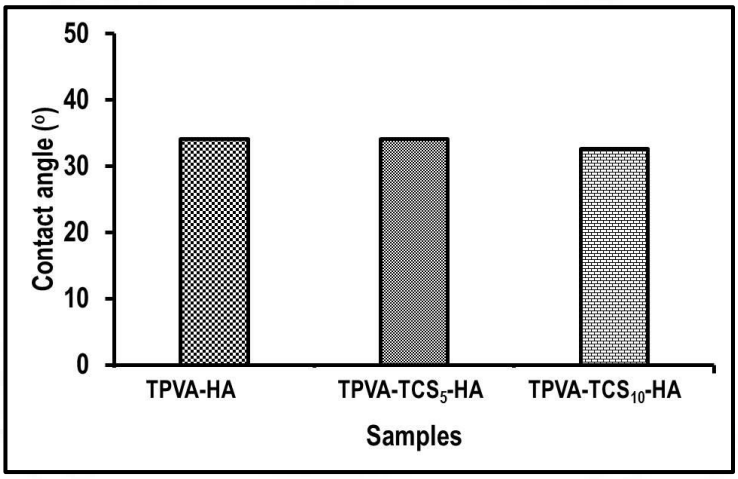

Figure 70: Contact angles of TPVA-TCS-HA composites

4.4.2.4 Mechanical Properties of TPVA-TCS-HA composites

The mechanical properties of the composites evaluated by measuring the mean tensile strength and mean suture pull out strength are represented in the Figure 71. The tensile strength of TPVA-HA composite (9.25±0.925 MPa) got decreased (6.34±0.411

MPa) by the addition of 5% TCS. Further, a 10% TCS addition caused further drop in the tensile strength (3.46±0.418 MPa).

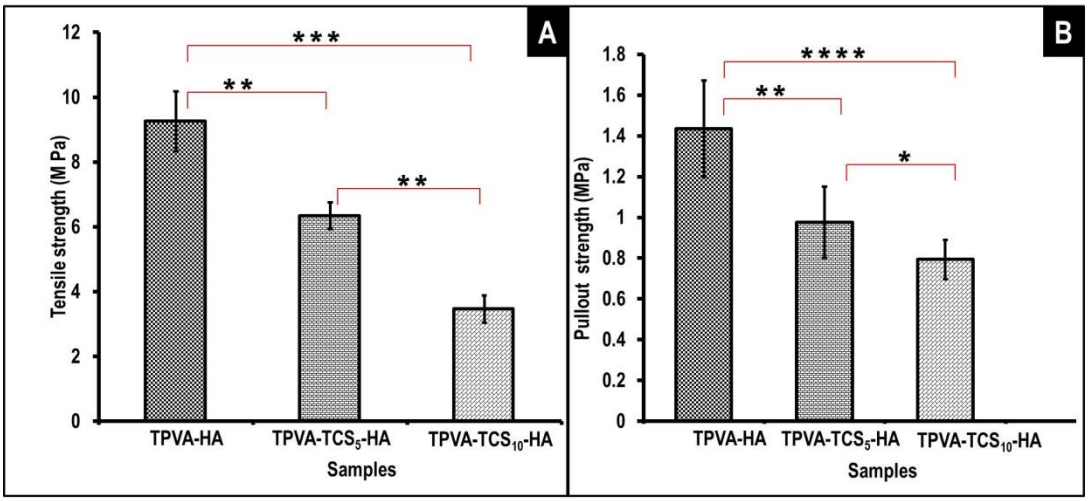

Figure 71: Mechanical property evaluation of TPVA-TCS-HA composite.
71A - Mean tensile strength and 71B - Mean suture pull out strength

4.4.2.5 In vitro degradation of TPVA-TCS-HA composites

The *in vitro* degradation of composites was analyzed by measuring the weight loss of samples at different time periods (Figure 72). The results show that after 24 h, more than 20 wt.% weight loss was observed for all the samples. The weight loss was more prominent after 14 days with weight loss of 82%, 72% and 66% for TPVA-HA, TPVA-TCS_5-HA and TPVA-TCS_{10}-HA respectively.

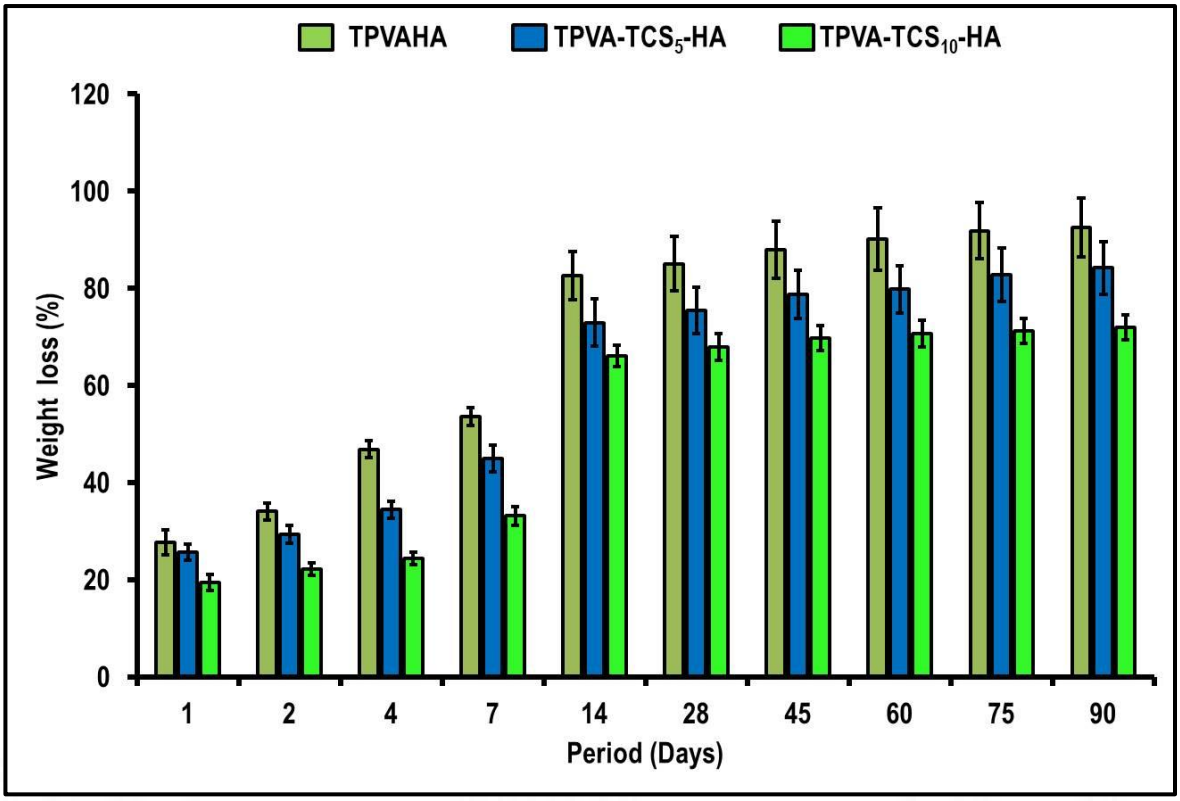

Figure 72: *In vitro* degradation studies in PBS - Weight loss of the composites

4.4.2.6 In vitro swelling of TPVA-TCS-HA composites

i. Water uptake

In vitro swelling of the composites is shown in Figure 73. Compared to TPVA-HA composite, both TCS added composites (TPVA-TCS-HA) showed decrease in water uptake.

ii. Volume swelling

In vitro swelling of the composites based on its volume change is shown in Figure 73B. Similar to swelling studies based on water uptake, the dimensional change at each time point of TCS added composites were lower than TPVA-HA composites. This is due to decreased uptake of water by composite in presence of TCS.

The water uptake studies on TPVA-TCS-HA showed that the absorption of water has been reduced in presence of TCS (Figure 73A). The reduction in water uptake is proportional to the amount of TCS added. Similarly, the volume swelling has been

considerably reduced in the presence of TCS (Figure 73B). At a concentration of 10% m/m TCS with respect to the TPVA polymer, the swelling based on water uptake and volume change got reduced and was similar to values obtained for PVA. This can be attributed to the slight decrease in hydrophilicity of TPVA (23±2° to 33±6°) during the addition of TCS (figure 74).

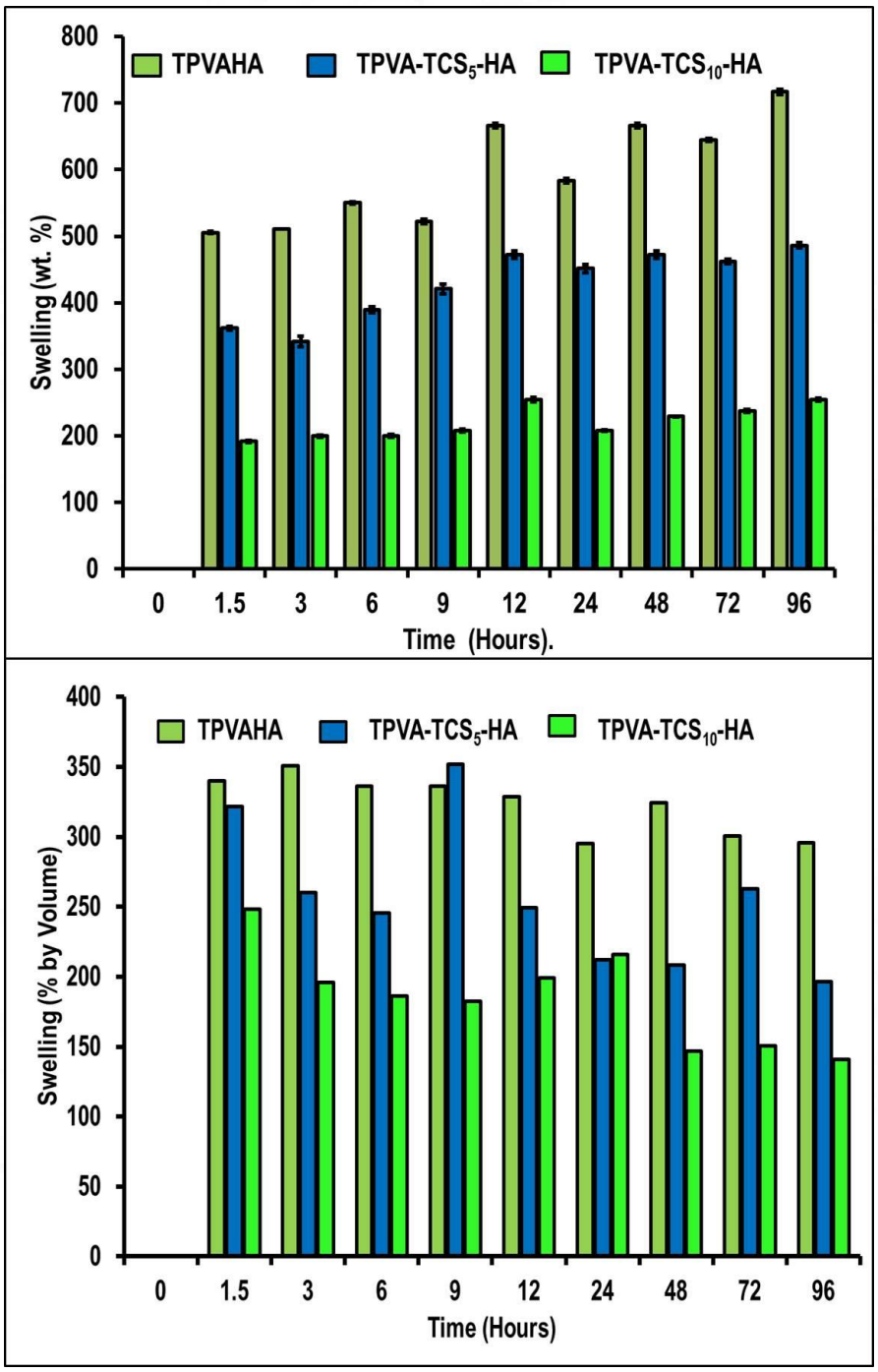

Figure 73: *In vitro* swelling of TPVA-TCS-HA composites.
[A] Swelling based on water uptake, and [B] Swelling based on dimension change

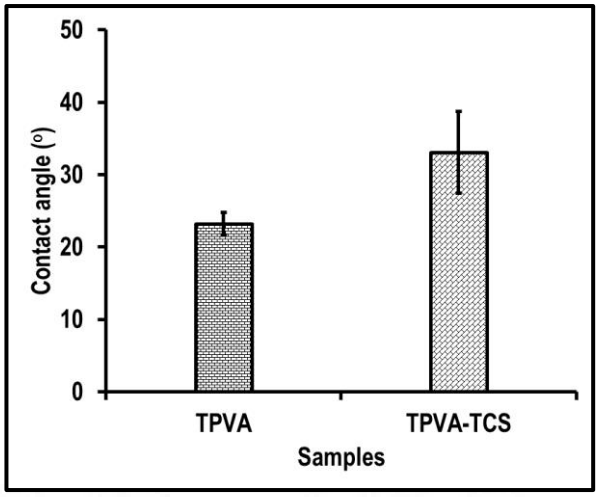

Figure 74 : Comparison of the water contact angles of TPVA and TPVA-TCS.

4.4.2.7 In vitro bioactivity of TPVA-TCS-HA composites

The depositions on the surface the sheets after immersing in simulated body fluid for 7 days have been explored and the corresponding SEM images are shown in the Figure 75. Typical apatite-like deposition has formed for TPVA-TCS_5-HA (75 B & D), on its surface and inside the pores. Compared to TPVA-HA, the growth is more and hence it could be concluded that the bioactivity get enhanced in presence of TCS.

Energy-dispersive X-ray spectroscopic (EDS) analysis of the deposited particle is also done and is shown in Figure 76. The Ca/ P ratio obtained from EDS peaks was approximately 1.7.

4.4.2.8 In vitro cytocompatibility of TPVA-TCS-HA composites

The preliminary cytocompatibility tests such as MTT assay and direct contact was done using hPDL cells.

i. MTT assay

Figure 77 represents the results of MTT assay using hPDL cells. All the samples were non-cytotoxic and show more than 100% metabolic activity (or more cell growth) after 24 h. There were no significant differences between the viability values of the

samples. However, the samples had significantly higher values in comparison with the hPDL cell control.

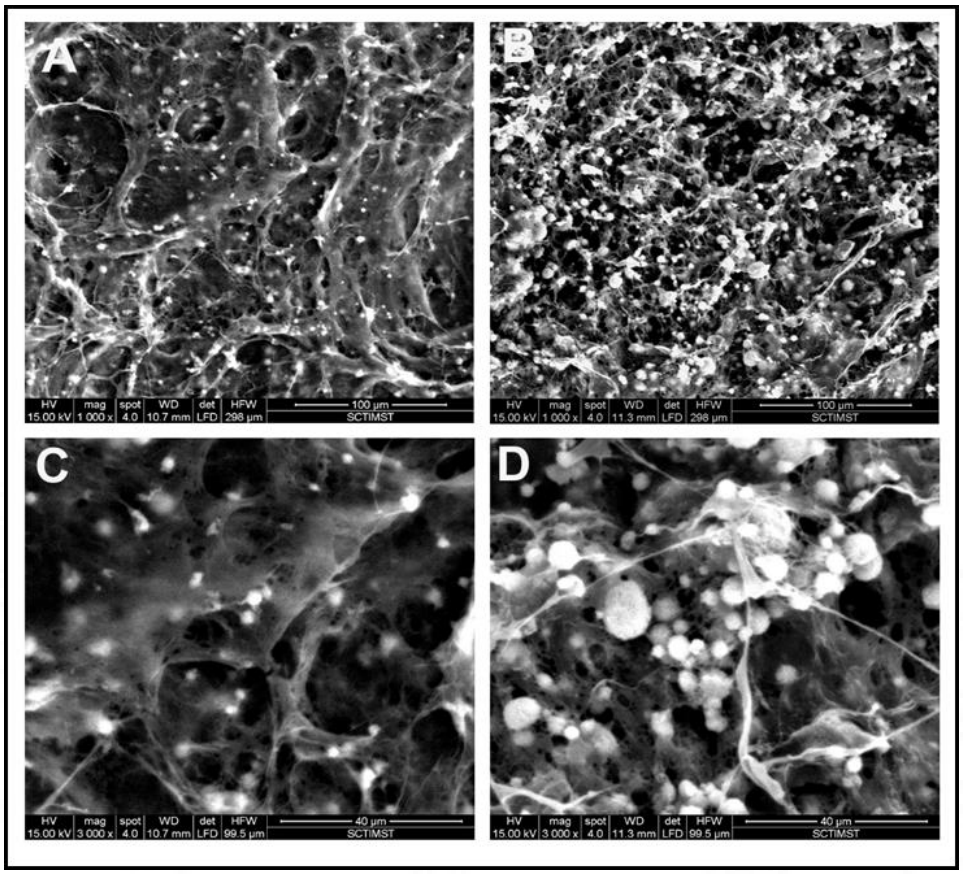

Figure 75: SEM images of sheet after *in vitro* bioactivity test for 7 days [A} TPVA-HA at 1000X, [C] TPVA-HA at 3000 X, [B] TPVA-TCS_5-HA at 1000X and [D] TPVA-TCS_5-HA at 3000X

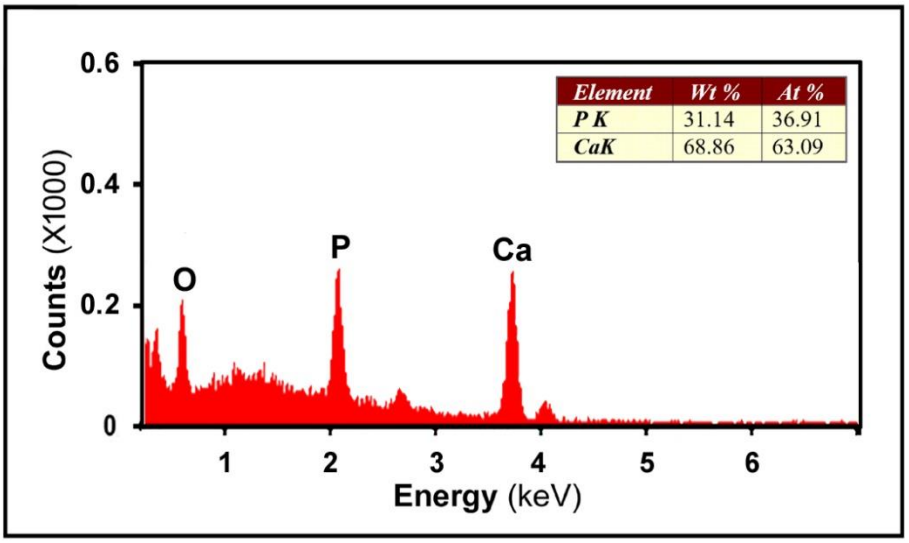

Figure 76: EDS analysis of the TPVA-TCS-HA surface after the *in vitro* bioactivity test

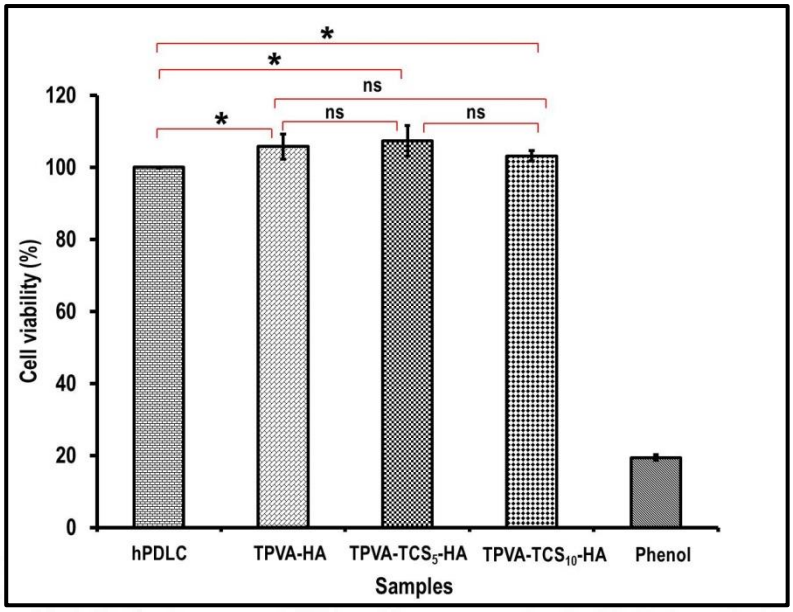

Figure 77: MTT assay done on TPVA-TCS-HA composites using hPDL cells

ii. Direct contact

The results of MTT assay was further supported by the images obtained from direct contact test shown in Figure 78. The hPDL cells cultured in the presence of the test materials showed no evidence of cytotoxicity. The cells were seen attached, and maintained their morphology in both cell control and over TPVA-TCS-HA sheets.

iii. Cell adhesion and spreading- Actin staining

The confocal microscopic (CLSM) images of actin staining of the hPDL cell cultured over the samples are shown in the Figure 79. The hPDL cells on the membrane samples showed typical spindle morphology. In addition, the periodontal ligament fibroblasts cultured on the membranes showed a three dimensional distribution, showing migration of cells into pores of the membranes.

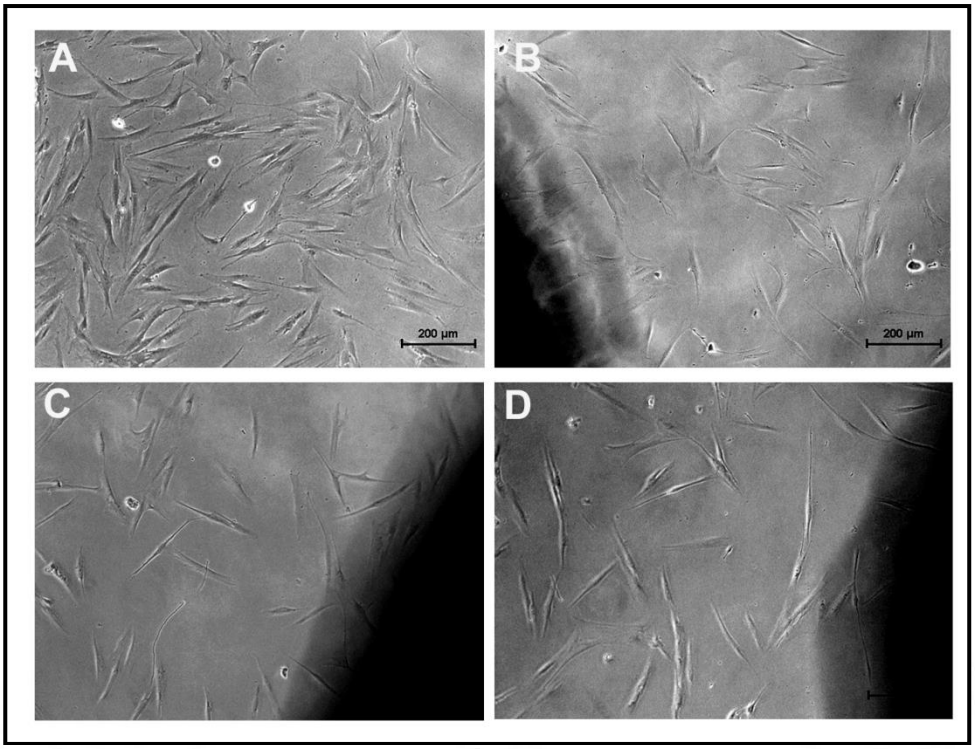

Figure 78: Direct contact test done using hPDL cells for 24 h.
[A] Cells alone, [B] TPVA-HA, [C] TPVA-TCS_5-HA, and [D] TPVA-TCS_{10}-HA

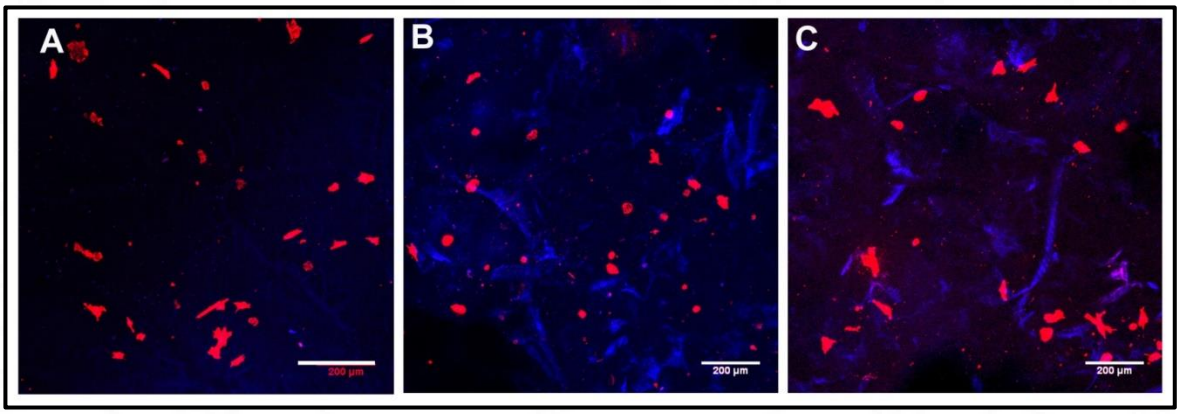

Figure 79: Confocal laser scanning microscopic images of composite sheets cultured with hPDL cells for 24 h. [A] TPVA-HA, [B] TPVA-TCS_5-HA, [C] TPVA-TCS_{10}-HA Scale bar 200µm

CHAPTER 5

DISCUSSION

This chapter contains the interpretation of the results obtained in chapter 4 and a discussion based on the current knowledge in this area. A brief analysis about the significance of the study is presented (Section 5.1), followed by the major findings of the study discussed under four subsequent sections. These sections include evaluation of (i) Quaternized chitosan-strontium hydroxyapatite composite, (ii) Quaternized chitosan-calcium phosphate *in situ* composite, (iii) Thiolated PVA-hydroxyapatite composite and (iv) Thiolated PVA-thiolated chitosan-hydroxyapatite composite. Each section analyzes the properties of prepared composite materials and its suitability for biomedical applications.

Section 5.2 discusses about the purification and characterization of natural polymer chitosan and its modification to quaternized chitosan (QC) which is its water soluble derivative. It also deals with the preparation and characterization of strontium hydroxyapatite (SA) by wet precipitation reaction. Additionally, the preparation and characterization of QC-SA composite with two different composition of SA by freeze drying method are discussed. The suitability of the prepared composite material as tissue guiding membrane for biomedical applications is also evaluated. In Section 5.3 the preparation and characterization of quaternized chitosan immobilized with *in situ* precipitated calcium phosphate for regeneration applications is discussed. Section 5.4 deals with the modification of synthetic polymer polyvinyl alcohol to its thiolated derivative - thiolated polyvinyl alcohol (TPVA), preparation and characterization of hydroxyapatite (HA) by wet precipitation reaction followed by preparation and characterization of functionally graded TPVA-HA composite as tissue regeneration material. Section 5.5 discusses about the preparation and characterization of thiolated

chitosan (TCS) followed by preparation and characterization of thiolated PVA - thiolated chitosan graded composite with HA and its evaluation for suitability as tissue regeneration membrane for biomedical applications.

5.1. Significance of the study

Recent advances in tissue regeneration techniques show remarkable achievements in tissue repair and regeneration. The state-of-the-art smart biomaterials are engineered so as to respond to the internal or external stimuli such as temperature, ionic strength, pH etc. to promote tissue regeneration or repair of damaged tissue to restore the normal functioning [Holzapfel et al., 2013]. Another approach is mimicking the extra cellular matrix (ECM). ECM is a natural biologic matrix with a variety of polysaccharides, proteoglycans, glycosaminoglycans, fibrous proteins and adhesion proteins in a well-organized three-dimensional form to support cell adhesion, proliferation and function [Nguyen et al.,2016]. ECM mimicking substitutes can be designed from natural molecular structures (like collagen, gelatin, silk fibroin, alginates, deacetylated chitin /chitosan) etc.), as well as synthetic macromolecules (polyanhydrides, polyesters polyamides, polyethers, polyphosphazenes, polyurethanes etc.). The functionalization of natural or synthetic polymers to obtain desired property includes quaternization, pegylation, acrylation, carboxymethylation, etherification, thiolation, crosslinking and so on. Even though a wide range of natural polymers are available abundant and cost-effective, limited understanding of their complex structural composition and concern over the immunogenicity and pathogen transmission, demanded the development of synthetic polymer of scaffolds. Tissue regeneration scaffolds are three-dimensional porous materials designed to perform functions like (i) enhanced cell material interaction, cell adhesion and ECM deposition; (ii) allowing transport of gases, nutrients, and regulatory factors for cell survival, proliferation, and differentiation; (iii) controlled biodegradation without producing toxic

leachants to provide space for newly formed tissues; and (iv) minimal degree of inflammation (preferably, no reaction)[Fuchs et al.,2001].

One of the current challenges in regenerative medicine is to fabricate biomaterial structures that can effectively mimic the cell–ECM interactions, preferably using affordable natural or synthetic polymer. There are certain cues through with the cell interact and communicates with the ECM which include chemical, mechanical and topographical [Chen et al., 2018]. The chemical cues include biological molecules, wettability and surface energy. Surfaces of moderate hydrophilicity are preferred by most of the animal cells. In terms of surface energy, polymer surface with low surface free energy can suppress cell behaviors whereas high surface free energy improves cell adhesion [Feng et al., 2005, Inoue et al., 2013, Iwata et al.,2004]. The mechanical cues of polymer surface have a great role in controlling cell behavior. In general, the stiffness of ECM in *in vivo* ranges from 0.1 kPa in brain tissues and 100 GPa in bone tissues. Coming to topographical cues, the micro surface features also significantly influence the cell-material interaction [Liu and Wang., 2014]. Generally, the topography of materials can be divided into two - regular surface topography and random surface topography. The random surface features (porosity, roughness, pore dimension) significantly affect the protein adsorption and thereby cell interaction with the material. It is reported in literature that porous surface with approximately 14 μm pore dimension enhances cell attachment and spreading [Lim et al., 2007].

The significance of the present work is that it takes the challenge of converting affordable natural or synthetic polymer through chemical modification. It was possible to design materials with degradability and bioactivity and fabricate them in appropriate form with porous sheet structure, so as to make them fit for guided bone regeneration applications.

5.2 Preparation and characterization of quaternized chitosan- strontium hydroxyapatite composite (QC-SA)

Chitosan, is obtained by the partial deacetylation of chitin found in the exoskeletons of crustaceans, mollusks, insects and fungi [Aranaz et al.,2010; Dash et al.,2011]. It is a polycationic polymer having the basic unit of glucosamine and N-acetyl glucosamine. Chitosan is soluble only in acidic medium which is a major limitation for its use in biomedical products wherein solubility is needed [Elieh-Ali-Komi and Hamblin., 2016]. The various reactive functional groups in chitosan are amino/acetamido group, as well as the primary and secondary hydroxyl groups at the C-2, C-3 and C-6 positions, open up scopes for chemical modification of chitosan. Water soluble derivatives of chitosan are usually obtained by chemical modification such as acetylation, quaternization, carboxymethylation, generation of N-trimethyl chitosan etc. [Pokhrel and Yadav., 2019].

Since chitin for the preparation of chitosan is obtained from the shells of marine organism, it is important to ensure its purity after deacetylation to chitosan. The ICP-OES data of purified chitosan shows that the amount of heavy metals is below the permissible limits as specified in the standard ASTM F2103 (Table 1).

Prior to the functionalization or modification of chitosan, properties like degree of deacetylation and molecular weight were determined, as these two parameters greatly influence the degradability as well as solubility. Potentiometric titration method is simple in terms of performance and calculation for determining degree of deacetylation of chitosan [Czechowska-Biskup et al., 2012]. In this method, chitosan solution is titrated against NaOH, and a curve with two inflexion points is obtained on plotting potential against volume. The first one is during the complete neutralization of H^+ in the solution. Thereafter the protonated amine is attacked by the OH^{-1} from NaOH and the potential

slowly changes. At the complete neutralization of protonated amine, second large deflection in potential is observed (Figure 2A).Determination of the first derivative helps in precise reading of volume. The derivative graph of potential against volume of NaOH (Figure 2B) shows two main peaks corresponding to the two major deflections. The difference in volume of NaOH between two peaks is equal to number of protonated amine and the calculated degree of deacetylation is 87.6%.

Molecular weight of purified chitosan can be determined by techniques like Gel Permeation Chromatography (GPC), Static Light Scattering (SLS) and intrinsic viscosity measurement. Among these various techniques, molecular weight determination by gel permeation chromatography is quite simple method. The number average molecular weight of the chitosan was calculated and is represented in Figure 7 (Along with the modified material). From the graph, the number average molecular weight of chitosan was found to be 1074 kDa with a polydispersity of 1.54.

For chemical modification of chitosan, the quaternization was selected and the effectiveness of quaternization was proved by FTIR and ^{1}H NMR. The FTIR spectra of chitosan (CS) (Figure 4) contains peaks corresponding to both OH and NH_2 at 3350 cm^{-1}, symmetric and anti-symmetric stretching of CH_2 at 2920 cm^{-1} and 2876 cm^{-1}, N-H bending of primary amine combined with the amide I peak of residual acetyl groups is obtained at 1627 cm^{-1}. The amide II peaks from N-H of residual N- acetyl part is seen in the region 1520 cm^{-1}, peaks at 1414 cm^{-1} and 1379 cm^{-1} can be assigned to the CH_2 bending and CH_3 symmetrical deformation, peak at 1150 cm^{-1} is due to the C-O-C bridge and those at 1067 cm^{-1} and 1024 cm^{-1} correspond to C-O stretching modes [Ruihua et al.,2012; Zou et al.,2015; Kalsi., 2007; Luo et al.,2010]. Another characteristic peak from the CH bending out of the plane of the monosaccharide ring appeared at 900 cm^{-1}. In quaternized chitosan (QC), most of the characteristic vibrations of chitosan are present.

The peak at 1150 cm^{-1} is retained in the product showing that C-O-C bridge between the monomer units is not affected. Compared to CS, there is shift in the peaks 1627 cm^{-1} and 1520 cm^{-1}. The shift 1627 cm^{-1} to 1640 $cm^{-1}$and 1520 cm^{-1} to 1542 cm^{-1} may be due to the partial modification of primary amine groups [Zouet al.,2015].

From Figure 4, it could be learnt that quaternized chitosan (QC) shares most of the IR peaks with unmodified chitosan (CS) except shift and reduction in intensity of the N-H bending peaks. In the quaternized product, the amide I got resolved and attain prominence at 1640 cm^{-1}. The decrease in N-H bending absorption of primary amine is due to the consumption of primary amine by the GTMAC reagent to form the quaternized product [Ruihua et al.,2012; Zou et al.,2015; Kalsi.,2007; Luo et al.,2010]. Similarly, the amide II peak at 1520 cm^{-1} is shifted to 1542 cm^{-1}. These shift in amide I and II as well as decrease in N-H bending are presumably from the amine modification. Other peaks of CS remain unaltered in QC which proves the chemical modification has occurred only through the amine moiety.

Further confirmation of modification via amine groups is obtained from the comparison of proton NMR spectra of CS and QC (Figure 5 and 6). The proton NMR spectrum of chitosan shows characteristics peaks at $\delta \sim 8.08$ corresponding to the amide proton, the methyl protons from the residual acetyl groups are observed at $\delta \sim 1.93$ppm. The characteristic peaks of protons from primary and secondary alcohol groups are observed at $\delta \sim 1.27$ and 1.28ppm, the CH protons present in 3 to 6 positions of pyranose ring are represented by peaks at $\delta \sim 3.05$ ppm to 3.78 ppm. [Ruihua et al.,2012; Zou et al.,2015; Kalsi., 2007; Luo et al.,2010]. The quaternization reaction occurs through ring opening and conjugation of GTMAC by more nucleophilic amino groups in chitosan. It was inferred from the NMR spectra that the peaks corresponding to hydroxyl groups remain unaffected whereas the new peaks corresponding to groups in the GTMAC

appeared after quaternization. The protons in hydroxyl groups (δ~1.3ppm) remained unaffected which proves that the hydroxyl groups are free after the reaction. Peaks at δ~3.14 ppm and δ~4.47 ppm appeared which corresponds to methyl of $^{+}N(CH_3)_3$ and OH groups from the GTMAC part [Ruihua et al.,2012; Zou et al.,2015; Kalsi., 2007; Luo et al.,2010]. From the FTIR and NMR data, it is clear that the effective conjugation of GTMAC has occurred in the chitosan through the amine moieties. All the spectral data of the materials were comparable with those reported in literature [Ruihua et al.,2012; Zou et al.,2015; Kalsi., 2007; Luo et al.,2010].

The molecular weight of the quaternised chitosan, calculated using GPC (Figure 7) shows a number average molecular weight of 624 kDa and its polydispersity was found to be 1.60. This reduction in molecular weight may be due to the possible chain scission that has occurred during the reaction of CS with GTMAC at 80°C for 7 h. The surface wetting property of CS and QC analyzed through water contact angle measurements (Figure 8) shows an increase in hydrophilicity on modifying the chitosan via quaternisation.

The formation of Sr-doped hydroxyapatite (SA) formation via wet chemical precipitation was confirmed from the XRD and FTIR studies (Figure 9 and 10). The XRD peak pattern obtained for the SA matches with the standard spectrum of 10% Sr doped HA Similar results were obtained from the FTIR studies also. The FTIR evaluation of the QC-SA composite (Figure 11) showed an additional peak at 1721 cm^{-1} along with the peaks of quaternized chitosan. In amides, the lone pair electron in the nitrogen enters into resonance with the C=O and results in the weakening of the C=O bond strength. This is the reason why in amides the carbonyl stretching (amide I) appear in low frequency region. When QC was composited with SA, the lone pair electron in the N atom of NH_2 will form coordinate bond with the Ca and Sr atom in ceramic part. This additional

coordinate bond reduces the resonance effect and thus results in the shift of amide I back to high frequency region. It is evident from the FTIR spectra that increase in SA concentration increases the intensity of amide I at 1721 cm^{-1} [Kalsi., 2007; Xianmiao et al., 2009].

Micromorphological analysis of the freeze-dried sheets with SA and those without SA showed high degree of porosity which can provide suitable microenvironments to support cell growth and function. Compared to the sheets without apatite, QC-SA-1.5 and QC-SA-2 showed well-ordered structure (Figure 12). The porosity and pore structure of a layer obtained by lyophilization will depend on ice crystals formed during the freezing step [Kawasaki et al.,2019]. During the lyophilization process, phase separation and ice formation occurs. The addition of the hydrophilic SA particles may lead to more clumping together with chitosan material through surface charges, leaving out space for more water accumulation and consequent increase in porosity.

For a material to be used as GBR/GTR sheets, it should have sufficient strength to withstand the force experiences on it. Depending upon the area of application, the tensile strength will vary in the range of 0.1 kPa for soft tissue to 100 GPa for bone tissue regeneration [Das and Zouani., 2014]. For a periodontal tissue regeneration application, it is reported that hydroxyapatite–chitosan–gelatin sheets have tensile strength in the range of 0.5MPa and the values were considered sufficient to function as a barrier membrane, for periodontal defect repair [Sculean et al., 2008]. In the composite samples with SA (QC-SA-2) the tensile strength got enhanced to 0.461±0.052 MPa compared to the 0.235±0.019 MPa in bare QC.

The suture pull-out strength of a bioactive sheet becomes significant as they are needed to be sutured over the defect area. The suture pull-out test results show a gradual decrease in strength when the concentration of strontium apatite is increased. When QC is

made into composite sheets with the strontium-containing apatite, the particles are distributed at the sub-surface, in between the polymeric chains. It will help in reinforcing the sheet walls, making them stiffer and bigger. The suture thread is thin, the effective pressure experienced at the sheets and suture interface will be far greater compared to force experienced during the tensile strength measurement. Therefore, it will easily pierce through the composite sheets compared to the QC. In QC- SA samples, the pore-sizes go bigger and so do the thicknesses of the walls. The enhanced thickness of the walls leads to higher tensile strength whereas, in suture pull-out, the number of walls opposing the moving suture will be less when SA content is higher and hence the lowering of pull-out strength. The surface wettability evaluated by contact angle measurement showed hydrophobic nature (> 90°C) by definition. Interesting part of this analysis is after a few seconds contact angle decreases to hydrophilic range by the protonation of quaternary ammonium groups immobilized over chitosan by absorbing water [Sarmento et al., 2011].

In vivo degradation is essential for a GBR/GTR material so that it should give way for natural tissue to occupy the defect space after the intended function. Another requirement of GBR/GTR sheets is that the degradation should not produce any toxic fragments [Sam and Pillai., 2014]. In the *in vitro* degradation study (figure 15), it was observed that the weight loss increases with the concentration of SA particles in composite sheet. This is associated to the preferential attack of water at the polymer–particle interface and the resultant leaching of SA to the solution, as the interaction between the SA and QC is basically non-covalent in nature. The SEM images indicate that the incorporation of SA increase the pore size in the sheets. This favors high water uptake into the sheets and consequent higher degradation rate. Similar results were reported for other biodegradable polymers reinforced with hydroxyapatite. The initial increase in swelling for QC-SA composite compared to QC (figure 16) is due to the increase in pore size on

compositing with SA. More the entry of water into the composite, more will be degradation compared to others in the group. Once it starts degrading, it cannot hold that much amount of water and hence after 48 h the swelling of QC-SA membrane decreases below that of QC. The results of both MTT assay and direct contact test, confirm that the cytocompatibility of the sheets towards hPDL cells and suggests the suitability of composite membrane for periodontal applications.

5.3 Preparation and characterization of quaternized chitosan-calcium phosphate composite (CPQC)

The QC-SA composites meet almost all the essential requirements for a tissue regeneration membrane in terms of structural features, mechanical properties, biodegradability and cytocompatibility. However, from the material perspective, the bioactive apatite particles are not readily miscible with the viscous polymer and hence utmost care should be given in blending to get a uniform distribution. It will be an advantage if bioactivity could be induced to the composite by *in situ* precipitation of bioactive particles.

In QC-SA system described above, the composite was prepared by mixing polymer solution (QC) with calcium-strontium phosphate (SA) powder followed by freeze drying. For making bioactive composites, rather than adding insoluble calcium phosphate powder to the polymer, it is better to add the precursor ions during preparation so that the calcium phosphate can be immobilized in the polymer surface by precipitation in an alkaline environment. Towards this purpose, quaternized chitosan was made into solution in water and calculated amount of calcium nitrate and phosphoric acid mixture was added to ensure the homogenous distribution of polymeric chains and ions. The precursor ionic mixture was prepared in such a way that the molar ratio between calcium and phosphate ions is in the ratio 1.67, which is the theoretical value for the bone mineral. The amount of

the ions in the mixture added was adjusted so that the precipitated calcium phosphate will be 10% w/w to the dry weight of quaternized chitosan. On immersing the porous polymer block with the precursor ions into aqueous ammonia, the Ca^{2+} and PO_4^{3-} ions diffuses down and due to the alkaline pH, it gets precipitated as calcium phosphate.

The confirmation of the calcium phosphate as brushite phase was obtained from the XRD analysis (Figure 19). While comparing the spectra obtained for QC and CPQC, sharp peaks were obtained for the CPQC and all the peaks matched with the standard XRD pattern for 'brushite' phase (ICDD-09-0077). The peaks at 2θ values 11.46, 21.27, 23.13, 29.12, 34.80, 36.81, 41.39, 50.04, correspond to the (0 2 0), (1 2 $\bar{1}$), (0 4 0), (1 4 1), (1 2 1), (2 2 $\bar{2}$), (1 5 $\bar{2}$), (1 $\bar{4}$ 3) planes respectively of the brushite crystal [Binitha and Pradyumnan.,2013]. Even though the ions of Ca^{2+} and PO_4^{3-} were taken in the stoichiometry of hydroxyapatite, the final precipitated phase was brushite (dicalcium phosphate). This might have happened due to the fact that the local environment in the polymeric matrix is slightly acidic, and brushite is the thermodynamically stable phase at that conditions [Mekmene et al.,2009].The presence of brushite, in fact, can supply more calcium ions locally and can lead to faster bone remodeling *in vivo* [Theiss et al.,2005]

The spectrum indicates additional co-ordinate interaction between nitrogen atom in QC and Ca atom in the calcium phosphate present in the CPQC composites (similar to that in the case of QC-SA composite system, discussed earlier). The additional peak in the FTIR spectrum of CPQC (Figure 18), at 1725 cm^{-1} is due to shift in amide I of residual acetyl part due to the restricted resonance in amide bond [Xianmiao et al.,2009]

It is clear that the topographical cues can greatly influence the cell adhesion and spreading. The microtopography of QC differ drastically during *in situ* precipitation (CPQC sample) as evident form SEM images of QC and CPQC composites (Figure 20A and 20C) clearly shows that there is abrupt change in pore dimension as well as pore size.

The *in situ* precipitation of the brushite particles has given an ordered pore structure to the CPQC membrane compared to the random pores in QC. Also it is notable that the pore diameter has reduced to half its size in presence of brushite particles. The decreased pore size and its ordered nature in presence of calcium phosphate particles must be due to the formation of new co-ordinate bond interactions between Ca^{2+} and the residual amine moieties of chitosan. The additional interaction that occurs between the residual amine in quaternized chitosan with the Ca^{2+} ions in brushite is similar to the coordinate bond and hydrogen bond interaction in chitosan-nanohydroxyapatite composite membranes [Xianmiao et al.,2009]. Another factor that controls the pore size is the *in situ* precipitation, wherein porous sheets with precursor ions are immersed in alkaline solution. The precipitation occurs by the diffusion of alkaline solution into the membrane followed by nucleation of the calcium phosphate phase. Large pores accommodate more solution compared to smaller ones and hence precipitation will be more in large pores. Therefore, the large pores will be reduced more compared to smaller ones. For any material to be used as tissue regeneration membrane it should have sufficient strength to withstand the force acting on it based on the area of application. If the material is used as thin sheets for periodontal regeneration, it should behave like a barrier material between the periodontal defect area and the gingival tissue during surgical flap procedure.

On comparing the tensile strength variation between QC and CPQC membranes, there is 25% increase in strength when converted to composite membrane (Figure 22). This significant increase mainly arises from factors like decrease in pore size, change from a non-ordered pore morphology to highly ordered porous structure and extra coordinate bond interaction between Ca^{2+} and the amine groups in the CPQC membrane compared to QC [Xianmiao et al., 2009]. In case of tensile strength, uniform distribution of calcium phosphate particles has reinforced the QC polymer matrix and resulted in better

mechanical strength which is similar to the QC-SA system. Compared to QC-SA system, the distribution of calcium phosphate was more homogenous in CPQC which resulted in higher tensile strength for CPQC than QC-SA.

Suture pull out strength evaluation is important when the material has to be sutured during the clinical application. In the comparison of suture pull out strength (Figure 23), the value has decreased slightly for CPQC. The more the uniform distribution of calcium phosphate particles, the more will be the stiffness of the material. In contrary to QC-SA system, the pore size decreases during *in situ* precipitation but the suture pull out strength relation is same as QC-SA. Since the suture thread is thin material, the stress experienced at the interface of the suture and polymer composite sheet will be very high compared to the distribution of tension throughout the material during the tensile strength measurement. As force increases the suture material easily pierce through the test material. The physicochemical properties like wettability and surface energy can greatly affect the cell adhesion and spreading over a biomaterial. Any material that comes in contact with the body fluid will either absorb or repel water (known as hydrophilicity or hydrophobicity, respectively). As mentioned earlier, materials of moderate hydrophilic nature will be more appropriate for proper cell adherence and proliferation. The static water contact angle measured by sessile drop method, observing immediately after dropping) showed an average water contact angle of 111±2° for CPQC and 117±4° for QC surface (Figure 21). There is no significant decrease in contact angle on *in-situ* precipitation of brushite. This indicates that the effect of brushite on altering the wettability and surface energy is minimal (or even negligible) compared to bare QC. By definition, water contact angle greater than 90° is considered as hydrophobic, and hence the material could be apparently graded as hydrophobic in nature. Interestingly, this hydrophobicity is a transient phenomenon which last for only 10 seconds. Thereafter, the

water contact value drastically decreases and the drop gets flattened. The matrix absorbs the drop readily and behaves like a perfect hydrophilic material. This lag in exhibiting hydrophilic behavior is due to the time required for the protonation of quaternary ammonium group [Sarmento et al.,2011]. According to the structural aspects and the soaking characteristics, material can be considered as hydrophilic.

The further proof of hydrophilic nature of the material is obtained from the *in vitro* water uptake study (Figure 24) shows the water uptake of the material at different time period. In the case of the mentioned samples, the water uptake increased progressively, reached its maximum by 48 hours and thereafter decreased. At any time point, the water uptake by the CPQC was slightly lesser than that of the bare QC material. This small decrease in uptake can be correlated to two factors - topography and wettability. During the conversion of QC to CPQC, the pore size has reduced to half its original value which would have restricted the uptake of water. The contact angle measurement showed that the wettability increased slightly. The effect of topography change must be more prominent than the surface wettability increase, and that may be the reason for lesser water uptake by the CPQC material compared to bare QC material. The considerable decrease in swelling of QC and CPQC after 48 h immersion in 1X PBS saline must be due the possible degradation of the polymer and the release of unbound particles from the material. This is evident from the degradation data, wherein more than 10% weight loss occurred in the case of composite matrix at 48 h exposure to PBS saline. The combined effect of topography and surface wettability has made the water uptake by the CPQC material lower than the control QC.

Biodegradation of the material is of great concern in the area of tissue regeneration approaches. A tissue regeneration material to be used either for hard or soft tissue should degrade with in a time period for providing space for newly formed tissue and should

release toxic degradation by products [Sam and Pillai.,2014]. In some parts of body, especially for periodontal defect repair, the use of biodegradable membranes will avoid the second surgical produce. The biodegradation of chitosan mainly occurs in the body by the enzymatic hydrolysis of β-1,4 glycosidic bonds. The degraded products are simple amino sugars which get into the metabolic pathway and get eliminated from the body [Qasim et al.,2015]. Comparing the degradation profile of QC and CPQC, both are degradable and the percentage mass loss for CPQC is lower than QC due to the presence of calcium phosphate (Figure 25). In CPQC, the reduced pore dimension and reduced water uptake resulted in slow rate of degradation in CPQC compared to QC. From water uptake study, it is clear that the altered pore structure has reduced the entry of water molecules into the composite. The degradation of the QC mainly occurs via hydrolysis of glycosidic linkage and that of the brushite occur via resorption process. The coordinate bond interaction between the calcium ions from brushite and the residual amine groups of the quaternized chitosan also resulted in lowering the degradation of CPQC.

For a material to be used as bone regeneration material, its ability to bond with living bone via the formation of apatite layer (bone-mineral composition) over its surface is of great significance. This ability can be tested *in vitro* by using simulated body fluid (SBF), a solution with ionic concentration close to that of human blood plasma [Kokubo and Takadama., 2006]. A material having inherent bioactivity will consume Ca^{2+} and PO_4^{3-} from the SBF solution and in turn results in the growth of bone-like apatite crystals on its surface [[Kokubo and Takadama., 2006]. This bioactive nature of material can be confirmed from SEM, EDS and XRD analysis. On comparing the surface features of QC and CPQC after 3 days and 7 days immersion in SBF, globular deposits of amorphous carbonated hydroxyapatite is only formed over CPQC (Figure 26 a and 26 b). The magnified surface images of CPQC at 3 days (Figure 26 (b) E and F) and 7 days (Figure

26(b) G and H) showed chrysanthemum like surface morphology which is similar to typical hydroxyapatite layer growth [Kokubo and Takadama., 2006]. This was seen to grown as a thick layer after 7 days immersion in SBF (Figure 26 (b) H). The surface of QC shows degradation instead of bioactivity, presumably due to the absence of calcium phosphate in the polymer matrix (Figure 26 (a) A to D). Results of *in vitro* swelling study have shown decrease in water uptake after 48 h which can be correlated to the degradation of the composites. For QC control material, the surface has degraded and can be visualized from SEM image (Figure 26 (a) A to D). Comparing the results, it is clear that CPQC composite is sufficiently bioactive for bone regeneration than bare QC. The EDS analysis over the deposited layer (Figure 27) showed peaks of calcium and phosphorous. The Ca/P ratio from EDAX is found to be 1.66, which is close to the Ca/P ratio of 1.67 in hydroxyapatite. The confirmation of the deposited material as amorphous carbonated hydroxyapatite is further corroborated from the XRD analysis of the deposited layer. The broad peaks obtained in the XRD data of the CPQC sheets after *in vitro* bioactivity test using SBF (CPQC-B) shown in Figure 28 matches with the characteristic peak of hydroxyapatite (ICDD-09-0432). The CPQC sheet before immersion in SBF was used as the control material. The hydroxyapatite peaks are broadened in CPQC-B, which proves its amorphous nature. While comparing the XRD data of CPQC-B and CPQC, all the characteristics peaks of the brushite is submerged by the hydroxyapatite peaks which also confirms the thick deposit of hydroxyapatite over the surface.

Another important requirement of a material to be used for tissue regeneration purpose is the biocompatibility of the material and its degradation products. The cytocompatibility is assessed through MTT assay and direct contact tests. The results show that both QC and CPQC or its leachants are non-cytotoxic in nature. In direct contact test using L929 cells, it was observed that there were no morphological changes to

the cells when they came in contact with the composite material CPQC and the control material bare QC (Figure 30). The metabolic activity of cells are quantitatively evaluated using MTT assay which shows more than 80% cells in contact with the QC and CPQC sheets were viable (Figure 29).The *in vitro* cytocompatibility of these materials were further evaluated using hPDL cells. The results of both actin staining and cell adhesion using ESEM analysis indicated better interaction of the material with the hPDL cells (Figure 31 and Figure 32) It was observed that the cells maintained their typical morphology and had three dimensional distributions over the materials indicating its cytocompatibility.

5.4 Preparation and characterization of Thiolated Polyvinyl Alcohol-Hydroxyapatite composite

The QC-SA and CPQC composites discussed in the preceding sections meet most of the requirements for a tissue regeneration material. The inability of QC-SA composites to induce apatite deposition *in vitro* has been resolved by the *in situ* CPQC system. However, one of the downsides of the above methods is the inability to make a graded structure. Thiolated Polyvinyl Alcohol-hydroxyapatite composite has been developed so that the graded structure could be generated easily. The material can be laid layer by layer, wherein the composition of each layer can be precisely tuned and the desired structure can be designed. Also, this work signifies how a synthetic polymer could be modified to impart bioactivity and degradability.

The synthetic polymer polyvinyl alcohol (PVA) was selected for this investigation and modified suitably to a cross linkable form. The modification reaction is a simple acid catalyzed esterification reaction which can also be easily scaled up to commercial production. The modified PVA can be easily and quickly crosslinked using ‘click’ approach without any free radical initiator. The crosslinking reaction occurs due to the

click reaction between thiol groups and alkene. 'Click reactions' are usually characterized by high yields, stereospecific, regiospecific and has very high thermodynamic driving force.

In this study, PVA of number average molecular weight 98 KDa was modified to thiolated PVA by acid catalyzed esterification using thioglycolic acid. The effective conjugation via ester linkage was confirmed from spectroscopic techniques like FTIR, FT-Raman, ^{1}H NMR and ^{13}C NMR spectroscopy. In the FTIR spectra of PVA, (Figure 34) a broad spectrum at 3280 cm^{-1} represents the stretching band from hydroxyl groups. The peaks at 2940 cm^{-1} and 2908 cm^{-1} on the shoulder of the broad band represents the symmetric and anti-symmetric stretching vibrations of C-H in CH_2 and the C-H bending vibrations are observed at 1415 cm^{-1}.The peaks at 1372 cm^{-1} correspond to the wagging C–H vibrations, 1329 cm^{-1} corresponds to O-H bending vibrations and 1091 cm^{-1} corresponds to the C-O stretching [Kalsi., 2007; Dicharry et al., 2006]. In the FTIR spectrum of TPVA (Figure 34), all the characteristic peaks of PVA are retained, however a new peak at 1715 cm^{-1} was observed which corresponds to the C=O stretching from the ester linkages formed by the conjugation of thioglycolic acid to PVA [Kalsi., 2007; Dicharry et al.,2006]. Since the S-H stretching vibrations are weak in FTIR, FT-Raman analysis of PVA and TPVA samples were carried out. The Raman spectra of PVA (figure 35) shows a broad peak at 3300 cm^{-1} which corresponds to OH stretching and peak at 2900 cm^{-1} represents the symmetric CH, CH_2 and anti-symmetric CH_2 stretching. Peaks at 1439 cm^{-1} and 1360 cm^{-1} are due to the bending vibrations of CH and OH. C-O stretching vibrations are present at 1141 cm^{-1} and 1088 cm^{-1}. The peaks seen at 852 cm^{-1} and 915 cm^{-1} are due to C-C stretching. In TPVA, most of the characteristic vibrations of PVA are present (figure 35). New peaks are formed at 1718 cm^{-1} due to C=O stretching from ester bonds and at 470 cm^{-1} because of the S-S stretching vibration. This is because; the thiol

groups have a tendency for self-oxidation to form S-S [Nagy., 2013]. In the case of PVA thiol, SH groups are in oxidized form that is why the thiol peak is absent in both FT-Raman and FTIR spectra.

Further confirmation of thiol modification via esterification was obtained from the comparison of proton NMR spectra of PVA and TPVA (Figure 36 and 37). The proton NMR spectra of PVA showed peaks at δ= 4.69ppm, 4.49 ppm and 4.26 ppm which corresponds to the OH group of PVA. Another peak at δ= 3.84 ppm represents C-H proton in the carbon containing hydroxyl group. The peak at δ= 3.40 ppm and a shoulder at 3.51 ppm corresponds to the H_2O and a sharp peak at 2.51 ppm is from the residual protons in DMSO solvent [Kalsi., 2007; Dicharry et al.,2006]. Since PVA is produced by the hydrolysis of polyvinyl acetate, residual acetate groups will be present in the polymer and the peak δ= 1.99 ppm represents the methyl proton of residual acetyl part. The peaks at δ =1.44 ppm, 1.39 ppm and 1.33 ppm represents the methylene proton [Kalsi., 2007, Dicharry et al.,2006]. Since the esterification of PVA will not replace all the OH groups in PVA, the proton NMR spectra of the product thiolated PVA will also contain most of the peaks in PVA. The exception is the appearance of new peaks from conjugated part (Figure 30). A new peak at δ= 3.17 ppm is from the methylene proton present adjacent to the thiol group. Since the proton NMR spectra of TPVA are not free from the peak of OH groups, it can be concluded that the esterification reaction is partial. Comparison of ^{13}C NMR spectra of PVA and TPVA (Figure 38 and 39) also proves that the thiol substitution is partial. For PVA , the peaks at δ = 40 ppm is the solvent peak (DMSO) and three peaks at δ = 64.20 ppm, 66.31 ppm, 68.09 ppm corresponds to the carbon in CH-OH part and the four peaks at δ= 45.19 ppm, 45.72 ppm, 45.17 ppm, 44.93 ppm corresponds to the carbon in CH_2 part [Kalsi., 2007]. The expected peaks in TPVA are the appearance of peaks at 28 ppm and 170 ppm from methylene carbon of TGA and carbonyl group in ester part.

However, those peaks were not seen in ^{13}C NMR spectra of TPVA, which is due to the low degree of substitution.

The molecular weight analysis by GPC technique (figure 40) showed a number average molecular weight of 90048 Da for PVA and 107830 Da for TPVA. A major peak is observed at 1008558 Da which is approximately about 10 times of molecular weight of TPVA. The presence of this peaks showed that the polymer has undergone a disulphide crosslinking by self-oxidation which is proved by the FT-Raman data in which peak for S-S linkage appeared instead of S-H group. For a thiol-ene reaction to be considered, the number of thiol groups per gram of polymer has to be quantified. The thiol content per gram of polymer was calculated colorimetrically by Ellman assay [CE., 2002, Ellman., 1959]. It is simple and accurate method for the estimation of free thiol groups. The Ellman's reagent {5,5'-dithio-bis-(2-nitrobenzoic acid)}, commonly known as DTNB, reacts with free SH groups to produce an yellow colour and the absorbance of this yellow solution is measured spectrophotometrically at 412nm. Initially, a standard curve was plotted using cysteine standard to obtain a regression equation (Figure 41). Substituting the absorbance value obtained with known concentration of TPVA in the regression equation average value of free thiol groups per gram of polymer was obtained. It was found that an average value of 1.16 mmol of free thiol per gram of TPVA polymer is available. Based on the thiol groups per gram, the degree of substitution was calculated to be approximately 6.2%. The percentage substitution was further confirmed from EDS analysis of TPVA (Figure 42) and found that the percentage substitution (6.22%) has good agreement with the values obtained from Ellman assay.

In order to develop the composite with graded concentration of hydroxyapatite (HA), gel-based approach was utilized. Four layered membranes of TPVA with each layer having specific wt.% of HA in diminishing order (10%, 5%, 2.5% and 0%) were made by

layer by layer gel casting. As already discussed in Chapter 3, the TPVA gel with HA was prepared by mixing a dispersion of TPVA and HA with PEGDA cross linker at neutral pH. The reaction proceeds by base catalyzed Michael addition reaction. The pKa value of the SH in thioglycolic acid was 10.55 and which got reduced to ≈ 7.9 when it is converted to an ester with PVA [Paquette et al., 2009]. At pH above 7.9, the thiol will completely ionize to produce S^- , H^+ ions and at a pH below 7.9, it will be partially ionized. At a pH value closer to 7, ionization will be more hence more will be the thiol anion which will be readily attacked by the alkene. The mechanism of the crosslinking reaction is given in Figure 44. The confirmation of crosslinking between TPVA and PEGDA is obtained from the FTIR analysis (Figure 45). The FTIR spectra of PEGDA contains absorption peaks from C=O stretch at 1720 cm^{-1} and C=C at 1635 cm^{-1} [Kalsi., 2007]. Similarly, in the case of TPVA, an ester carbonyl peak is present at 1715 cm^{-1}. After the crosslinking reaction, the ester carbonyl peaks got reinforced and the peaks due to C=C got completely disappeared. This confirms the effective thiol-ene crosslinking. Additionally, FT-Raman spectra were also recorded for cross-linked TPVA-PEGDA and TPVA (Figure 46). Comparing the spectra of TPVA and cross-linked TPVA-PEGDA, the S-S peak is absent in the cross-linked one. This is because, all the thiol groups have reacted with the alkene and hence there is no oxidation to S-S. The various parameters which influence the crosslinking reactions such as concentration of TPVA, concentration of crosslinker, pH and time for gelation were optimized. Considering the pH, more the concentration of thiol anion, lesser will be the gelling time. This is evident from Figure 47 which shows that at low pH, more time for gelation is needed and at a pH less than 5.1, there is no gelation even after hours of mixing. From this it is clear that for sufficient ionization of SH in the TPVA, the pH of solution should be greater than 5. As the pH approaches 7, the SH groups are ionized to a higher extend and it makes the crosslinking very fast and it will

take only a few seconds. The effect of concentration of TPVA polymer solution shown in Table 3 indicates that a minimum concentration 3 w/v% of TPVA polymer solution is required for the formation of a gel which can maintain a three dimensional shape. Below 3 w/v%, rather than forming a gel it behaves like a viscous liquid. Crosslinker concentration also have role in adjusting the gelling time. Gelling time can be reduced by reducing the concentration of the cross linker PEGDA (Figure 48). At a concentration equal to or less than of 3.125 mmol% to the total thiol content in the polymer, no gelling was observed, and only a viscous solution was formed. By considering all these factors the concentration of TPVA polymer solution selected was 5 w/v%, crosslinker concentration of 50 mmol% to total thiol content and a pH near to 7.

FTIR and XRD spectra (Figures 49 and Figure 50) of the in-house synthesized HA confirm its chemical structure. The presence of the HA in freeze dried four layered membrane is confirmed from the XRD analysis of TPVA-HA, TPVA and PVA samples. While comparing the spectra obtained for PVA, TPVA and TPVA-HA (Figure 51), both PVA and thiol modified PVA showed a typical pattern of amorphous polymer while the TPVA-HA composite showed peaks of hydroxyapatite along with the pattern observed for the polymer sample. The peaks obtained on the TPVA-HA sample matched with the standard XRD pattern for the hydroxyapatite (JCPDS 00-009-0432). The 2θ values of the major peaks and the corresponding planes of the hydroxyapatite crystal (Miller indices) are given as - 25.59 (0 0 2), 27.76 (1 0 2), 28.46 (2 1 0), 31.43 (2 1 1), 31.59 (1 1 2), 32.57 (3 0 0), 33.72 (2 0 2), 34.9 (3 0 1), 38.8 (2 1 2), 39.44 (3 1 0), 41.46 (3 1 1), 43.2 (1 1 3), 44.7 (2 0 3), 46.36 (2 2 2), 47.58 (3 1 2) and 49.15 (2 1 3). Considering the topography of the samples, PVA, TPVA and TPVA-HA showed a non-porous surface which is mainly due to a skin like formation over its surface by the polymer (Figure 52). The porous nature will be only become evident when the thin skin over its surface

degrades away. The tensile strength and suture pullout strength of the composite in sheet form were evaluated as material can be used in membrane form also. On comparing the tensile strength of TPVA and TPVA-HA sheets with the control material PVA, there is a 12-fold increase in strength when PVA was thiolated and cross-linked with PEGDA (Figure 54 A). This significant enhancement in tensile strength is due to the cross-linked structure. When bare PVA is considered, the hydrogen bond interaction plays a major role in holding the polymeric chains. After thiolation and crosslinking, along with the non-covalent interaction of hydrogen bonding, covalent crosslinking has also formed between the chains. This bonding interactions tightly keep the polymer chains together and that is the reason why this increase in tensile strength [Rynkowska et al.,2019]. The tensile strength of TPVA- HA composite membrane got enhanced by 1.4 times of that of TPVA. This can be correlated to the additional attractive interactions between the Ca^{2+} ions and –OH in the hydroxyapatite particles with the residual OH groups in the TPVA polymer via hydrogen bonds and coordinate interactions [Wei et al.,2016; Pineda-Castillo et al.,2018] All these attractive interactions collectively increase the strength of composite membranes.

In the case of suture pullout, (Figure 54 B), the tear strength of TPVA is higher than PVA. The suture pull out strength of TPVA-HA composites got decreased by 22%. The increase in suture pull out strength of TPVA compared to PVA is from the covalent crosslinking between polymeric chains and its magnitude is far greater than non-covalent hydrogen bond interaction in pure PVA. Since suture is thin material, pressure exerted at the interface of thread and polymer will be very high and that is why suture pull out strength is less compared to tensile strength. In TPVA-HA composite, even though additional attractive interactions are there, the pressure exerted at interface of thread and polymer over-ride them.

In vitro degradation studies in PBS shows that after 24 h, more than 20 wt.% weight loss was observed for all the samples. The weight loss was more prominent after 14 days with the percentage values of 25%, 74% and 82% for PVA, TPVA and TPVA-HA composites respectively (Figure 57). This shows the non-degrading behavior of PVA in PBS. The initial weight loss is only due to the leaching of small unbound molecules and do not represent the true degradation. As PVA is considered, there is no labile bond in the C-C back bone structure, which in turn prevents the lysis in small molecules. The degradation of TPVA and TPVA-HA composites are quite similar, and the mass loss in PEGDA cross-linked TPVA occurs via ester degradation. There are ester bonds between PVA and TGA in TPVA backbone and between acrylate and PEG in PEGDA. As chemical bonds are considered, ester bonds are more labile at physiological pH. That is why TPVA and TPVA-HA has undergone more than 70% degradation within 2 weeks. The degraded product will be PVA, PEG and 3-((carboxymethyl)thio) propanoic acid. Afterwards, up to a period of 3 months, the degradation is negligible. By that time all the ester bonds might have been cleaved away, leaving out the PVA back bone which is not prone to degradation through hydrolysis.

In order to evaluate the surface wettability, contact angle measurements were done. Since the surface of the TPVA-HA has irregularities, sessile drop method cannot be applied to measure contact angle. The dynamic contact angle measurements of TPVA-HA composite using TPVA and PVA as control material shows that the composite material is highly hydrophilic in nature (Figure 53). This high hydrophilic character arises from the thiol groups immobilized on the surface of PVA (figure 43). Since the composite as well as the thiolated PVA are highly hydrophilic, it can absorb water to a great extent and this is evident from the swelling studies based on weight gain and dimensional change (Figure 55 and 56). The percentage water uptake by TPVA and its composite with HA is almost

twice that of bare PVA sheets, as the introduction of thiol moieties has made the polymer hydrophilic. From the analysis of dimensional swelling, it could be understood that PVA had insignificant increase in size, but TPVA and TPVA-HA composites samples grew in volume nearly 300 times. However, with time, the swollen samples were seen to shrink, which can be attributed to the degradation of the materials.

In vitro bioactivity studies showed that there was no apatite deposition over the surfaces for both PVA and TPVA (Figure 58). This is understandable as there are no specific functional groups in these polymers to induce apatite formation. In case of TPVA-HA composites, spherical globules of apatite crystal can be seen over and into the surface of the material after 7 days of immersion in SBF. Compared to the CPQC composite system discussed in part 5.3, the rate of deposition of apatite crystal for TPVA-HA composites is slow. This is mainly due to the difference in the solubility of HA and brushite (dicalciumphosphate) in the surrounding medium. Another interesting feature of TPVA-HA graded composite is that the bioactivity is directed to one side (i.e., side of membrane having high concentration of HA) as evident from the *in vitro* results (Figure 58). There was no bioactivity on other side of the graded composite without HA. The graded composite prepared via layer by layer gel casting gives a gradation in bioactivity to the composite. This will help in the guided regeneration purpose proposed. Further confirmation of the deposited layer is obtained from EDS analysis of the particles (Figure 59). The EDS data shows a Ca/P ratio of 1.72 for the apatite-like deposition which is within the range of apatitic ratios [Heydary et al., 2015].

The *in vitro* cytotoxicity of materials evaluated via MTT assay and direct contact test using hPDL cells proves that materials are non-cytotoxic in nature. Direct contact test using hPDL cells shows that there is no morphological changes to the cells which are in contact with the composite material (TPVA-HA) as well as the control materials (TPVA

and PVA) (Figure 60).The quantification of cell viability based on MTT assay shows that more than 100% cells that were in contact with the PVA, TPVA and TPVA-HA sheets were viable (Figure 61).The cell adhesion and spreading study using confocal microscopy further substantiate the results of MTT and direct contact assay (Figure 62).

5.5 Preparation and characterization of Thiolated Chitosan-Thiolated Polyvinyl Alcohol-Hydroxyapatite Composite

In the previous section, it is seen that TPVA-HA composite is fast degrading and of graded bioactive nature, high swelling in terms of mass and volume in PBS, sufficient mechanical strength and cytocompatibility. In order to manipulate and tune the degradation TPVA-HA composite according to physiological requirement, thiolated chitosan (TCS) was added. The rationale behind the selection of thiolated chitosan was its solubility at physiological pH and the antibacterial property reported recently [Geisberger et al.,2013; Esquivel et al.,2015]. The crosslinking mechanism in the TPVA-HA-PEGDA matrix is thiol-ene reaction, the addition of thiolated chitosan is advantageous as the thiol groups in chitosan can also participate in the crosslinking reaction [Wen et al.,2017]. This can ensure proper immobilization of chitosan thiol chains in the polymer composite matrix by covalent bonds.

The purified chitosan was selected and the amine moieties were selectively modified using thioglycolic acid using EDC-NHS coupling to form amide bond between the amino groups of chitosan and the carboxylic acid group of thioglycolic acid (Figure 63). The effective functionalization was confirmed from FITR and proton NMR analysis. In FTIR spectra of chitosan and thiolated chitosan (Figure 64),

The broad band at 3350 cm^{-1} represents the stretching band from both hydroxyl groups and residual amine groups. Peaks at 2920 cm^{-1} and 2876 cm^{-1} on the shoulder of the broad band indicate the symmetric and anti-symmetric stretching of C-H bond. The N-

H bending vibration of primary amine together with amide I stretching from the residual N- acetyl groups are represented by a peak at 1627 cm^{-1}. Amide II band of residual amide bonds is observed at 1520 cm^{-1} and Peak 1379 cm^{-1} could be assigned to the CH_3 symmetrical deformation. The peak at 1150 cm^{-1} represents the C-O-C bridge, and those at 1067 cm^{-1} and 1024 cm^{-1} correspond to C-O stretching modes. Another characteristic peak from the CH bending out of the plane of the monosaccharide ring appeared at 900 cm^{-1}.

As thiolated chitosan is considered, the new linkage through which the TGA molecules are connected is by the amide linkage. Most of the peaks in thiolated chitosan seem to be similar to that of the parent compound chitosan and the changes observed are for N-H bending, amide I, amide II absorptions. The N-H bending intensity has got decreased due to the consumption of primary amine to form amide linkage with TGA. The intensities of both amide I and amide II peaks got enhanced. This is due to the new amide linkage formed after the reaction [Esquivel et al., 2015]. The further confirmation of thiol modification is obtained from the proton NMR spectra of TCS. The proton NMR spectrum of bare chitosan (Figure 65) shows characteristic peaks of amide proton, methyl protons from residual acetyl part, primary and secondary alcohol groups at $\delta \sim 8.08$ ppm, $\delta \sim 1.93$ ppm, $\delta \sim 1.27$ ppm and 1.28 ppm. The CH protons present from 3 to 6 positions of pyranose ring are observed at $\delta \sim 3.45$ ppm to 3.78 ppm. Another peak at $\delta \sim 3.05$ corresponds to the proton in C2 carbon of pyranose ring [Ruihua et al., 2012; Zou et al.,2015; Kalsi., 2007; Luo et al.,2010]. After modification using TGA (Figure 66), a new peak appeared at $\delta \sim 0.70$ ppm from an α proton with respect to the thiol group. A peak at $\delta \sim 1.49$ ppm is the characteristic peak of SH proton from the conjugated part. Peaks from 0.98 ppm to 1.15 ppm correspond to the protons in newly attached part. The remaining peaks correspond to the peaks present in the proton NMR spectra of chitosan [Kalsi., 2007,Esquivel et al.,2015]. Using FTIR and NMR data, the effective thiolation of chitosan

via amide linkage is thus confirmed. The percentage substitution measured from Ellmann assay was found to be 1.5%.

The preparation of composite containing TCS is similar to the TPVA-HA preparation, here a mixture of TPVA, TCS and HA was mixed with PEGDA cross linker to develop the composite gel. The composition of HA in each layer is similar to the four layered TPVA-HA composite except the presence of TCS. The amount of TCS was adjusted to 10 % m/m compared to TPVA polymer in TPVA-TCS_{10}-HA and 5% m/m to TPVA polymer in TPVA-TCS_5-HA.The gel was then freeze dried to form dry composite material. The XRD pattern of the TPVA-TCS_{10}-HA and TPVA-TCS_5-HA was similar and it shows the characteristic peaks of hydroxyapatite along with the amorphous polymer background. The peaks obtained for the TPVA-TCS-HA (Figure 68) matches with the standard XRD pattern for the hydroxyapatite (JCPDS 00-009-0432). The peaks obtained and their corresponding planes (as Miller indices) are 25.59 (0 0 2), 27.76 (1 0 2), 28.46 (2 1 0), 31.43 (2 1 1), 31.59 (1 1 2), 32.57 (3 0 0), 33.72 (2 0 2), 34.9 (3 0 1), 38.8 (2 1 2), 39.44 (3 1 0), 41.46 (3 1 1), 43.2 (1 1 3), 44.7 (2 0 3), 46.36 (2 2 2) and 47.58 (3 1 2). This proves the incorporation of HA without any phase change.

In the surface morphology analysis, the SEM images of TPVA-TCS_{10}-HA and TPVA-TCS_5- HA did not show any difference in surface feature. The addition of TCS to the matrix has no influence in the surface topography (Figure 69).

The increase in weight percent of TCS from 5% to 10% relative to TPVA polymer has reduced the tensile strength nearly by half (Figure 71 A).This can be attributed to the limited availability of C=C double bond for TPVA crosslinking as out of the total C=C double bond available from PEGDA, one part bonds with thiol from TPVA and other with thiol from TCS [Wen et al., 2017]. This distribution of alkene between the TPVA and TCS reduces the attractive interaction between the PVA chains in polymer matrix and

hence results in the reduction of overall tensile strength. In the case of suture pullout (Figure 71B), the tear strength of TPVA-TCS_{10}-HA and TPVA-TCS_5-HA are lower than that of the TPVA-HA composites. The decrease in strength is proportional to the increase in the amount of TCS in the matrix. This decrease in suture pull out strength can also be correlated to the decreased crosslinking between the TPVA chains by PEGDA in presence of TCS.

Similar to TPVA-HA graded composite, TCS incorporated composite is also fast degrading. In vitro degradation studies in PBS shows that after 24 h, more than 20 wt.% weight loss was observed for all the samples. The weight loss was more prominent after 14 days with weight loss of 82%, 72% and 66% for TPVA-HA, TPVA-TCS_5-HA and TPVA-TCS_{10}-HA respectively. At any given time point, the degradation of the composite in presence of TCS is less compared to TPVA-HA (Figure 72). This can be related to the chemical linkages in the composite. In TPVA-HA composites, all the chemical linkages in the polymeric part are ester bond. Those bonds have same rate of degradation at physiological pH and degrade into alcohol and carboxylic acid. The TPVA-TCS-HA composite contains ester linkage in PEGDA, TPVA part and amide bonds in TCS part. If the hydrolysis rate of esters and amides are considered, rate for hydrolysis of amide bond is less than that of an ester bond. This is the reason why the rate of degradation has decreased for TCS containing composite compared to TPVA-HA.

The surface wettability evaluation through contact angle measurements on TPVA-TCS- HA composites shows that both compositions with TCS are highly hydrophilic. The water uptake studies on TPVA-TCS-HA showed that the absorption of water has been reduced in presence of TCS (Figure 73A). The reduction in water uptake is proportional to the amount of TCS added. Similarly, the volume swelling has been considerably reduced in the presence of TCS (Figure 73B). At a concentration of 10% m/m TCS with respect to

the TPVA polymer, the swelling based on water uptake and volume change got reduced and was similar to values obtained for PVA. The presence of TCS along with TPVA in the composite reduces the hydrophilicity slightly and is evident from figure 74.

In vitro bioactivity studies, the side of the composite membrane with no HA did not show any apatite deposition and the side with 10% HA has shown apatite formation. These results were similar to that for TPVA-HA composites. Comparing the SEM images of TPVA-HA and TPVA-TCS-HA, bioactivity (indicated by the apatite growth) got enhanced in presence of TCS (Figure 75). The EDS analysis on spherical deposits formed over the bioactive side gave a Ca/P ratio of 1.70 (Figure 76) which is close to the Ca/P values obtained for HA [Heydary et al., 2015].

The results of direct contact assay shows no morphological changes to the cells and they retained their characteristic morphology which was further supported by the MTT assay in which more than 100% cells were viable (Figure 77 and 78).The cell adhesion and spreading study using confocal microscopy on TPVA-TCS-HA samples further substantiate the results of MTT and direct contact assay, that the materials are highly cell compatible (Figure 79).

5.6 Comparison of the GBR/GTR membranes developed.

In the present work, four candidate membranes for GBR/GTR applications have been developed. In order to choose the apt membrane to translate to a clinically useful product, different aspects about the material to be considered, from the synthesis to the biocompatibility.

The first aspect is the process viability. It covers the preparation of the basic polymeric material, modification processes and fabrication steps of the composites. In general, all the processes selected for the work are simple chemical reactions in aqueous

media, avoiding organic solvents and complex reaction steps. Comparing quaternization of chitosan and thiolation of PVA, both the reactions are simple but the levels of efforts differ for the preparation of final finished membrane. Considering the yield in membrane form and structural integrity, TPVA based systems were found to be better since the gradation and immobilization of bioactive component can be precisely tuned, because the click reaction is utilized for crosslinking the polymeric chains. The order of material viability is TPVA-HA ~ TPVA-TCS-HA > CPQC > QC-SA.

The second factor for comparison is mechanical strength, in terms of tensile strength and pull out strength. Mechanical aspects are important because the material will experience tensile and shear forces during the application. TPVA based system (both TPVA-HA and TPVA-TCS-HA) is chemically cross-linked, which imparted the material relatively higher tensile strength and pull out strength compared to QC based system. The order of tensile strength is TPVA-HA > TPVA-TCS_5-HA > TPVA-TCS_{10}-HA > CPQC > QC-SA and that for pull out strength is TPVA-HA > TPVA-TCS_5-HA >TPVA-TCS_{10}-HA > CPQC = QC-SA.

The *in vitro* swelling based on water uptake measurements shows that TPVA-TCS-HA system has less uptake compared to other materials and the order of mass swelling is as follows: TPVA-HA (716%) > CPQC (668%) > TPVA-TCS_5-HA (486%) >TPVA-TCS_{10}-HA (254%). As the *in vitro* degradation is considered, membranes based on chitosan and TPVA is degradable and the degradation for a period of 28 days follows the order TPVA-HA (85%) > TPVA-TCS_5-HA (75%) >TPVA-TCS_{10}-HA (67%) > QC-SA (59%) > CPQC (36%).

The porosity of the composite membranes is important, considering the final application. TPVA based systems showed apparently nonporous surface morphology while the QC based systems were porous. CPQC composite had an average pore size of is

86 µm and QC-SA had 50 µm. It has been identified that the TPVA systems have porous internally and the surface forms a skin over it closing the pores. Once degradation starts, the membranes will expose the pores.

The *in vitro* bioactivity of the membranes has been tested in terms of the ability to induce apatite deposition in simulated body fluid. Except QC-SA material, all others showed good bioactivity, *in vitro*. The order of bioactivity based on micro morphological analysis is as follows: CPQC > TPVA-TCS-HA > TPVA-HA. The cytocompatibility of all materials assed via *in vitro* cytotoxicity assay indicated that none of the composites are cytotoxic.

The TPVA-HA system is apparently good in many respects, except for the *in vitro* bioactivity compared to TPVA-TCS-HA. Considering swelling and degradation TPVA-TCS-HA is better. This work demonstrates the usefulness of the quaternized chitosan material for GBR/GTR applications. Also, it is notable that *in situ* precipitation of bioactive calcium phosphate in QC is a novel attempt. Yet, the level of purity required for chitosan is high to get rid of immune reactions, which makes the material more expensive than PVA. Making TPVA through click reaction should also be highlighted, which avoid the final purification steps of the membranes for implantation. Therefore, the TPVA material seems to be promising for guided bone regeneration applications.

CHAPTER 6

SUMMARY AND CONCLUSIONS

The purpose of the study is to develop – candidate tissue regeneration materials which can be used for guided regeneration. When bone tissues are lost and the area is laden with soft tissues in the vicinity, the healing may affected despite the grafting/filling of the defect. Guidance structures which isolate the area and provide proper scaffolding to blood vessels to grow will greatly enhance the regaining of the local tissue architecture. These are made as sheets or membranes and placed over the grafted site. The material development was based on natural and synthetic polymers **(**chitosan and poly vinyl alcohol) which are abundant, economical, biocompatible and easily modifiable. The aim of the study is to modify these polymers and to develop bioactive and functionally graded structures which can be used as membranes for guided tissue regeneration of bone defects. The various objectives set in order to achieve the proposed aim were (i) To modify the polymer chitosan to impart higher solubility and make composite structure with calcium phosphate based minerals to achieve bioactivity (ii) To modify polyvinyl alcohol and make graded composite structure with calcium phosphate based minerals to achieve bioactivity (iii) To make combinational materials containing modified chitosan and polyvinyl alcohol, with functionally graded structure satisfying the essential requirements of guided tissue regeneration membranes.

The work plan, the methods and the results are presented in the preceded chapters and the significances are discussed.

6.1 Summary

The first part of the study dealt with the purification and modification of chitosan to its quaternized derivative and the development of strontium hydroxyapatite incorporated quaternized chitosan membranes. The study involves a detailed analysis of physico-mechanical characterization of the material and its suitability for the intended applications. The prepared membranes satisfied almost all the essential requirements, however they lacked bioactivity which further led to the design of *in situ* calcium phosphate precipitated composite. Bioactive membranes based on quaternized chitosan were prepared via *in-situ* precipitation method. The incorporation of calcium phosphate via *in situ* precipitation has enhanced the tensile properties of quaternized chitosan whereas decreased the suture pull out strength. The chemical phase was analyzed using XRD and elemental analysis by ICP-OES. The bioactive nature of the material was confirmed from *in vitro* immersion in simulated body fluid. The *in vitro* cytocompatibility of membranes evaluated using L929 and hPDL cells further confirms the suitability of materials for GBR/GTR applications.

The second objective of the study was to modify polyvinyl alcohol and make graded composite structure with calcium phosphate based minerals to achieve bioactivity. PVA was successfully thiolated and the effective functionalization was confirmed by NMR, FTIR and FT-Raman techniques. Click approach was adopted, by which the free radical initiators are avoided for crosslinking the polymer system. Composite crosslinked membranes were prepared with synthesized hydroxyapatite distributed in graded pattern. Each cross-linked layer was made using thiol-ene click approach. The cross linking was further confirmed by spectroscopic techniques. Mechanical properties evaluation showed improved tensile strength and suture pullout strength for crosslinked graded membranes. The incorporation of calcium phosphate provided bioactivity to membranes, as assessed *in*

vitro. The more liable ester bonds in the crosslinked polymer matrix made the material a fast degrading one revealed by the *in vitro* biodegradation studies. The cytocompatible, biodegradable, graded bioactive structure of membranes allows the composite to be used for GBR /GTR application.

The objective of third part was to make combinational materials containing modified chitosan and polyvinyl alcohol, with functionally graded structure and function. Thiolated derivative of chitosan was successfully prepared by EDC coupling reaction and structural modification was confirmed from spectroscopy techniques like FTIR and proton NMR studies. Graded composite membranes of thiolated PVA-HA was modified with thiolated chitosan in two different weight ratios of TCS to TPVA. The incorporation of thiolated chitosan has modified the composite in all aspects such as mechanical, *in vitro* degradation, swelling and bioactivity. The graded composite membrane showed bioactivity at *in vitro* conditions. *In vitro* cytocompatibility evaluation by MTT, direct contact and actin staining studies further proved that the TCS addition has not compromised the cytocompatibility of the base materials.

6.2 Conclusions

Based on the results and the inference from the study, it can be concluded that

1. Quaternisation and thiolation were utilized to modify polymer chitosan and PVA respectively.
2. Successfully converted quaternized chitosan to composite membrane through lyophilization of quaternized chitosan- Sr-HA suspension and *in situ* precipitation of chitosan sheets containing calcium and phosphate ions.

3. High degrees of bioactivity and enhanced physicochemical properties were achieved in quaternized chitosan- calcium phosphate composite prepared via *in situ* precipitation.
4. Thiolation of PVA and chitosan paved a click crosslinking approach for preparing graded composite material, with base catalyzed Michael addition, which avoids free radical initiators and other reagents for crosslinking.
5. Graded composites were obtained by freeze drying of layer by layer cross-linked gel and covalent cross linking effectively increased the mechanical properties.
6. Compared to amide functionalities in chitosan, the ester linkages in TPVA-HA composite made the material fastly degrading.
7. The effect of thiolated chitosan in TPVA-HA matrix on varying its physico chemical aspects was successfully evaluated.
8. The presence of thiolated chitosan altered the physicochemical properties of TPVA without changing the compatibility of composites.
9. All the four composites have their own relevance in application, depending on the polymeric back bone and composting technique. The appropriate polymeric system can be selected based on the need.
10. The TPVA based material seems to be promising for GBR/GTR applications because of tunable structure and biodegradation property.

6.3 The leads obtained from the work

- Quaternized chitosan composite fabricated via *in situ* precipitation can enhance bioactivity and degradability of the material.
- Layer by layer crosslinking technique can be utilized to generate graded composite systems.

- Extension of click chemistry for synthesis can generate safer material which could be converted to graded composites in terms of function and structure.
- Utilization of modified nature-derived polymer in combination with synthetic polymers can impart biomimetic property and degradability for tissue regeneration application.

6.4 Future perspectives

1. *In situ* calcium phosphate immobilized CPQC composite material showed good bioactivity in *in vitro* studies. *In situ* approach can be extended to TPVA-HA and TPVA-TCS-HA systems so as to produce uniformly distributed composite material.
2. The ester linkages in thiolated PVA limits the *in situ* precipitation of calcium phosphate in alkaline condition, hence ester linkages to be modified with ether linkage or urethane linkage.
3. The variation of physico-chemical properties to be evaluated with different functional linkages.
4. The TPVA-HA and TPVA-TCS-HA materials could be used in injectable form for filling bone defects.
5. The materials developed could be tested in animal models for pre-clinical proof.

BIBLIOGRAPHY

1. Aaboe, M., Pinholt, E.M., Hjørting-Hansen, E., Solheim, E. and Prætorius, F., 1993. Guided tissue regeneration using degradable and nondegradable membranes in rabbit tibia. Clinical Oral Implants Research, 4(4), pp.172-176.
2. Agusti, G., Jordan, O., Andersen, G., Doelker, É. and Chevalier, Y., 2015. Radiopaque iodinated ethers of poly (vinyl iodobenzyl ether) s: Synthesis and evaluation for endovascular embolization. Journal of Applied Polymer Science, 132(14)
3. Altman, G. H., Diaz, F., Jakuba, C., Calabro, T., Horan, R. L., Chen, J., Lu, H., Richmond, J. & Kaplan, D. L., 2003. Silk based biomaterials. Biomaterials, 24, pp. 401–416.
4. Ba Linh, N.T., Lee, K.H. and Lee, B.T., 2013. Functional nanofiber mat of polyvinyl alcohol/gelatin containing nanoparticles of biphasic calcium phosphate for bone regeneration in rat calvaria defects. Journal of Biomedical Materials Research Part A, 101(8), pp.2412-2423.
5. Bell, A., Templeman, D. and Weinlein, J.C., 2016. Nonunion of the femur and tibia: an update. The Orthopedic clinics of North America, 47(2), pp.365-375.
6. Bernkop-Schnürch, A., Hornof, M. and Zoidl, T., 2003. Thiolated polymers—thiomers: synthesis and in vitro evaluation of chitosan–2-iminothiolane conjugates. International journal of pharmaceutics, 260(2), pp.229-237.
7. Binitha, M.P. and Pradyumnan, P.P., 2013. Dielectric property studies of biologically compatible brushite single crystals used as bone graft substitute.
8. Blumenthal, N.M., 1988. The use of collagen membranes to guide regeneration of new connective tissue attachment in dogs. Journal of periodontology, 59(12), pp.830-836.
9. Boland, E. D., Espy, P. G. and Bowlin, G. L. , 2004. Tissue engineering scaffolds. In Encyclopaedia of Biomaterials and biomedical engineering. Wenk G. E.; Bowlin, G. L. (Edi). pp 1633-1635. Richmong, Verginia , USA.
10. Bottino, M.C., Pankajakshan, D. and Nör, J.E., 2017. Advanced scaffolds for dental pulp and periodontal regeneration. Dental Clinics, 61(4), pp.689-711.
11. Bowers, G.M., Chadroff, B., Carnevale, R., Mellonig, J., Corio, R., Emerson, J., Stevens, M. and Romberg, E., 1989. Histologic evaluation of new attachment apparatus formation in humans: Part I. Journal of Periodontology, 60(12), pp.664-674.
12. Boyne, P.J., 1969. Restoration of osseous defects in maxillofacial casualties. The Journal of the American Dental Association, 78(4), pp.767-776.
13. Britto, D. de, Assis, O.B.G., 2007. A novel method for obtaining a quaternary salt ofchitosan, Carbohydr. Polym. 69, pp.305–310.
14. Buser, D., 2009. Years of guided bone regeneration in implant dentistry, 2010. New Malden: Quintessence Publishing Co Ltd.

15. Cao, W. and Hench, L.L., 1996. Bioactive materials. Ceramics international, 22(6), pp.493-507.

16. Capuccini, C., Torricelli, P., Boanini, E., Gazzano, M., Giardino, R. and Bigi, A., 2009. Interaction of Sr-doped hydroxyapatite nanocrystals with osteoclast and osteoblast-like cells. Journal of Biomedical Materials Research Part A,89, pp. 594–600.

17. Caridade, S.G., Monge, C., Almodóvar, J., Guillot, R., Lavaud, J., Josserand, V., Coll, J.L., Mano, J.F. and Picart, C., 2015. Myoconductive and osteoinductive free-standing polysaccharide membranes. Acta biomaterialia, 15, pp.139-149.

18. Caton, J., Nyman, S. and Zander, H., 1980. Histometric evaluation of periodontal surgery II. Connective tissue attachment levels after four regenerative procedures. Journal of Clinical Periodontology, 7(3), pp.224-231.

19. CE, K., 2002. Thiolated polymers: stability of thiol moieties under different storage conditions. Scientia Pharmaceutica, 70(4), pp.331-339.

20. Chandran, S., Babu, S.S., Varma, H.K. and John, A., 2016. Osteogenic efficacy of strontium hydroxyapatite micro-granules in osteoporotic rat model. Journal of biomaterials applications, 31(4), pp.499-509.

21. Chandran, S., Shenoy, S.J., Nair, R.P., Varma, H.K. and John, A., 2018. Strontium Hydroxyapatite scaffolds engineered with stem cells aid osteointegration and osteogenesis in osteoporotic sheep model. Colloids and Surfaces B: Biointerfaces, 163, pp.346-54

22. Chapple, I.L., Van der Weijden, F., Doerfer, C., Herrera, D., Shapira, L., Polak, D., Madianos, P., Louropoulou, A., Machtei, E., Donos, N. and Greenwell, H., 2015. Primary prevention of periodontitis: managing gingivitis. Journal of clinical periodontology, 42, pp.S71-S76.

23. Chatani, S., Nair, D.P. and Bowman, C.N., 2013. Relative reactivity and selectivity of vinyl sulfones and acrylates towards the thiol–Michael addition reaction and polymerization. Polymer Chemistry, 4(4), pp.1048-1055.

24. Chen, L., Yan, C. and Zheng, Z., 2018. Functional polymer surfaces for controlling cell behaviors. Materials Today, 21(1), pp.38-59.

25. Cheng, K., Blusztajn, A., Shen, D., Li, T.S., Sun, B., Galang, G., Zarembinski, T.I., Prestwich, G.D., Marbán, E., Smith, R.R. and Marbán, L., 2012. Functional performance of human cardiosphere-derived cells delivered in an in situ polymerizable hyaluronan-gelatin hydrogel. Biomaterials, 33(21), pp.5317-5324.

26. Cho, T.J., Gerstenfeld, L.C. and Einhorn, T.A., 2002. Differential temporal expression of members of the transforming growth factor β superfamily during murine fracture healing. Journal of bone and mineral research, 17(3), pp.513-520

27. Chou, Y.C., Cheng, Y.S., Hsu, Y.H., Yu, Y.H. and Liu, S.J., 2016. A bio-artificial poly ([D, L]-lactide-co-glycolide) drug-eluting nanofibrous periosteum for segmental long bone open fractures with significant periosteal stripping injuries. International journal of nanomedicine, 11, p.941.

28. Colnot, C., 2009. Skeletal cell fate decisions within periosteum and bone marrow during bone regeneration. Journal of Bone and Mineral Research, 24(2), pp.274-282.

29. Colnot, C., Zhang, X. and Tate, M.L.K., 2012. Current insights on the regenerative potential of the periosteum: molecular, cellular, and endogenous engineering approaches. Journal of Orthopaedic Research, 30(12), pp.1869-1878.

30. Cui, J., Liang, J., Wen, Y., Sun, X., Li, T., Zhang, G., Sun, K. and Xu, X., 2014. In vitro and in vivo evaluation of chitosan/β-glycerol phosphate composite membrane for guided bone regeneration. Journal of Biomedical Materials Research Part A, 102(9), pp.2911-2917.

31. Czechowska-Biskup, R., Jarosińska, D., Rokita, B., Ulański, P. and Rosiak, J.M., 2012. Determination of degree of deacetylation of chitosan-comparision of methods. Progress on Chemistry and Application of Chitin and its Derivatives, 17, pp.5-20

32. Dahlin C, Gottlow J, Linde A, Nyman S., 1990. Healing of maxillary and mandibular bone defects using a membrane technique. An experimental study in monkeys. Scand J Plast Reconstr Surg Hand Surg; 24(1), pp. 13-9

33. Dahlin, C., Linde, A., Gottlow, J. and Nyman, S., 1988. Healing of bone defects by guided tissue regeneration. Plast Reconstr Surg, 81, pp.672-676.

34. Das, R.K. and Zouani, O.F., 2014. A review of the effects of the cell environment physicochemical nanoarchitecture on stem cell commitment. Biomaterials, 35(20), pp.5278-5293.

35. DiAngelis, A.J., Andreasen, J.O., Ebeleseder, K.A., Kenny, D.J., Trope, M., Sigurdsson, A., Andersson, L., Bourguignon, C., Flores, M.T., Hicks, M.L. and Lenzi, A.R., 2012. International Association of Dental Traumatology guidelines for the management of traumatic dental injuries: 1. Fractures and luxations of permanent teeth. Dental Traumatology, 28(1), pp.2-12.

36. Dicharry, R.M., Ye, P., Saha, G., Waxman, E., Asandei, A.D. and Parnas, R.S., 2006. Wheat Gluten− Thiolated poly (vinyl alcohol) blends with improved mechanical properties. Biomacromolecules, 7(10), pp.2837-2844

37. Domard, A., Rinaudo, M., Terrassin, C., 1986. New method for the quaternization of chitosan, Int. J. Biol. Macromol, 8, pp. 105–107.

38. Einhorn, T.A., 1998. The cell and molecular biology of fracture healing. Clinical Orthopaedics and Related Research®, 355, pp.S7-S21.

39. Elbert, D.L., Pratt, A.B., Lutolf, M.P., Halstenberg, S. and Hubbell, J.A., 2001. Protein delivery from materials formed by self-selective conjugate addition reactions. Journal of Controlled Release, 76(1-2), pp.11-25.

40. Elieh-Ali-Komi, D. and Hamblin, M.R., 2016. Chitin and chitosan: production and application of versatile biomedical nanomaterials. International journal of advanced research, 4(3), p.411.

41. Elliott, D.S., Newman, K.J.H., Forward, D.P., Hahn, D.M., Ollivere, B., Kojima, K., Handley, R., Rossiter, N.D., Wixted, J.J., Smith, R.M. and Moran, C.G., 2016. A unified theory of bone healing and nonunion: BHN theory. The bone & joint journal, 98(7), pp.884-891.

42. Ellman, G.L., 1959. Quantitation of sulfhydrl DTNB, Ellman's reagent. Arch Biochem Biophys, 82, pp.70-7

43. Esquivel, R., Juárez, J., Almada, M., Ibarra, J. and Valdez, M.A., 2015. Synthesis and characterization of new thiolated chitosan nanoparticles obtained by ionic gelation method. International Journal of Polymer Science, 2015.

44. Feng, W., Zhu, S., Ishihara, K. and Brash, J.L., 2005. Adsorption of fibrinogen and lysozyme on silicon grafted with poly (2-methacryloyloxyethyl phosphorylcholine) via surface-initiated atom transfer radical polymerization. Langmuir, 21(13), pp.5980-5987.

45. Florjanski, W., Orzeszek, S., Olchowy, A., Grychowska, N., Wieckiewicz, W., Malysa, A., Smardz, J. and Wieckiewicz, M., 2019. Modifications of Polymeric Membranes Used in Guided Tissue and Bone Regeneration. Polymers, 11(5), p.782.

46. Fratzl, P. and Weinkamer, R., 2007. Nature's hierarchical materials. Progress in materials Science, 52(8), pp.1263-1334.

47. Fu, L., Wang, Z., Dong, S., Cai, Y., Ni, Y., Zhang, T., Wang, L. and Zhou, Y., 2017. Bilayer poly (lactic-co-glycolic acid)/nano-hydroxyapatite membrane with barrier function and osteogenesis promotion for guided bone regeneration. Materials, 10(3), pp.257.

48. Fuchs, J.R., Nasseri, B.A. and Vacanti, J.P., 2001. Tissue engineering: a 21st century solution to surgical reconstruction. The Annals of thoracic surgery, 72(2), pp.577-591.

49. Gaina, C., Ursache, O., Gaina, V., and Ionita, D., 2012. Study on the Chemical Modification of Poly(Vinyl Alcohol) with 4-Maleimidophenyl Isocyanate. Polym. Plast. Technol. Eng., 51, pp. 65–70.

50. Geisberger, G., Gyenge, E.B., Hinger, D., Käch, A., Maake, C. and Patzke, G.R., 2013. Chitosan-thioglycolic acid as a versatile antimicrobial agent. Biomacromolecules, 14(4), pp.1010-1017.

51. Ghosh, K., Ren, X.D., Shu, X.Z., Prestwich, G.D. and Clark, R.A., 2006. Fibronectin functional domains coupled to hyaluronan stimulate adult human dermal fibroblast responses critical for wound healing. Tissue engineering, 12(3), pp.601-613.

52. Giannitelli, S.M., Basoli, F., Mozetic, P., Piva, P., Bartuli, F.N., Luciani, F., Arcuri, C., Trombetta, M., Rainer, A. and Licoccia, S., 2015. Graded porous polyurethane foam: A potential scaffold for oro-maxillary bone regeneration. Materials Science and Engineering: C, 51, pp.329-335.

53. Gohil, M., Bhattacharya, A. and Ray, P., 2006. Studies on the cross-linking of poly(vinyl alcohol). J. Polym. Res. 13, pp.161–169.

54. Gottlow, J., Nyman, S., Karring, T. and Lindhe, J., 1984. New attachment formation as the result of controlled tissue regeneration. Journal of clinical periodontology, 11(8), pp.494-503.

55. Guda, T., Walker, J.A., Singleton, B.M., Hernandez, J.W., Son, J.S., Kim, S.G., Oh, D.S., Appleford, M.R., Ong, J.L. and Wenke, J.C., 2013. Guided bone regeneration in long-bone defects with a structural hydroxyapatite graft and collagen membrane. Tissue Engineering Part A, 19(17-18), pp.1879-1888.

56. Guo, D.G., Hao, Y.Z., Li, H.Y., Fang, C.Q., Sun, L.J., Zhu. H., Wang, J., Huang, X.F., Ni, P.F. and Xu, K.W., 2013. Influences of Sr dose on the crystal structure

parameters and Srdistributions of Sr-incorporated hydroxyapatite. Journal of Biomedical Materials Research Part B:Applied Biomaterials,101(7), pp.1275-83.

57. Gupta, B., Anjum, S. and Ikram, S., 2013. Preparation of thiolated polyvinyl alcohol hydrogels. Journal of applied polymer science, 129(2), pp.815-821.
58. Halima, N.B., 2016. Poly (vinyl alcohol): review of its promising applications and insights into biodegradation. RSC advances, 6(46), pp.39823-39832.
59. Hassan, C.M. and Peppas, N.A., 2000. Structure and Applications of Poly(vinyl alcohol) Hydrogels Produced by Conventional Crosslinking or by Freezing/Thawing Methods. Adv. Polym. Sci., 153,pp.37-65.
60. Hench, L.L. and Polak, J.M., 2002. Third-generation biomedical materials. Science, 295(5557), pp.1014-1017.
61. Hench, L.L., 1991. Bioceramics: from concept to clinic. Journal of the american ceramic society, 74(7), pp.1487-1510.
62. Hench, L.L., Splinter, R.J., Allen, W.C. and Greenlee, T.K., 1971. Bonding mechanisms at the interface of ceramic prosthetic materials. Journal of biomedical materials research, 5(6), pp.117-141.
63. Heydary, H.A., Karamian, E., Poorazizi, E., Heydaripour, J. and Khandan, A., 2015. Electrospun of polymer/bioceramic nanocomposite as a new soft tissue for biomedical applications. Journal of Asian Ceramic Societies, 3(4), pp.417-425.
64. Hildebrand, H.F., 2013. Biomaterials–a history of 7000 years. BioNanoMaterials, 14(3-4), pp.119-133.
65. Holzapfel, B.M., Reichert, J.C., Schantz, J.T., Gbureck, U., Rackwitz, L., Nöth, U., Jakob, F., Rudert, M., Groll, J. and Hutmacher, D.W., 2013. How smart do biomaterials need to be? A translational science and clinical point of view. Advanced drug delivery reviews, 65(4), pp.581-603.
66. Hoyle, C.E., Lowe, A.B. and Bowman, C.N., 2010. Thiol-click chemistry: a multifaceted toolbox for small molecule and polymer synthesis. Chemical Society Reviews, 39(4), pp.1355-1387.
67. Huang, Y. C. & Mooney, D. J., 2005. Gas foaming to fabricate polymer scaffolds in tissue engineering. In: Scaffoldings in tissue engineering, Ma X P., Elisseeff J., (Ed.), PP 159,Taylor and Francis group. CRC press, 206, pp. 61-72.
68. Hurley L, Stinchfield F, Bassett A, Lyon W: The role of soft tissues in osteogenesis. An experimental study of canine spine fusions. J Bone Joint Surg Am 1959, 41:1243-1254.
69. Hutmacher, D., Hürzeler, M.B. and Schliephake, H., 1996. A review of material properties of biodegradable and bioresorbable polymers and devices for GTR and GBR applications. International Journal of Oral & Maxillofacial Implants, 11(5).
70. Inoue, Y., Nakanishi, T. and Ishihara, K., 2013. Elastic repulsion from polymer brush layers exhibiting high protein repellency. Langmuir, 29(34), pp.10752-10758.
71. Iwata, R., Suk-In, P., Hoven, V.P., Takahara, A., Akiyoshi, K. and Iwasaki, Y., 2004. Control of nanobiointerfaces generated from well-defined biomimetic polymer brushes for protein and cell manipulations. Biomacromolecules, 5(6), pp.2308-2314.

72. Jacob, S.A. and Amudha, D., 2017. Guided Tissue Regeneration: A Review. J Dent Health Oral Disord Ther, 6(3), p.00197.

73. Jamuna-Thevi, K., Suleiman, M.J. and Sabri, S.N., 2016. Strength improvement of a functionally graded and layered composite membrane for guided bone regeneration in orthopedics. Materials Today: Proceedings, 3, pp.S120-S128

74. Kalsi, P.S., 2007. Spectroscopy of organic compounds. New Age International.

75. Karring, T., Isidor, F., Nyman, S. and Lindme, J., 1985. New attachment formation on teeth with a reduced but healthy periodontal ligament. Journal of clinical periodontology, 12(1), pp.51-60.

76. Karring, T., Nyman, S. and Lindhe, J., 1980. Healing following implantation of periodontitis affected roots into bone tissue. Journal of clinical periodontology, 7(2), pp.96-105.

77. Kast, C.E. and Bernkop-Schnürch, A., 2001. Thiolated polymers—thiomers: development and in vitro evaluation of chitosan–thioglycolic acid conjugates. Biomaterials, 22(17), pp.2345-2352.

78. Kast, C.E., Frick, W., Losert, U. and Bernkop-Schnürch, A., 2003. Chitosan-thioglycolic acid conjugate: a new scaffold material for tissue engineering?. International journal of pharmaceutics, 256(1-2), pp.183-189.

79. Kawasaki, H., Shimanouchi, T. and Kimura, Y., 2019. Recent development of optimization of lyophilization process. Journal of Chemistry, 2019.

80. Kim, M.S., Choi, Y.J., Noh, I. and Tae, G., 2007. Synthesis and characterization of in situ chitosan-based hydrogel via grafting of carboxyethyl acrylate. Journal of Biomedical Materials Research Part A: 83(3), pp.674-682.

81. Kim, M.Y. and Lee, J., 2011. Chitosan fibrous 3D networks prepared by freeze drying. Carbohydrate polymers, 84(4), pp.1329-1336.

82. Knaul J.Z., Hudson, S.M. and Creber K.A.M., 1999. Crosslinking of chitosan fibers with dialdehydes: Proposal of a new reaction mechanism. J Polym Sci, Part B: Polym Phys., 37, pp.1079-94.

83. Knaul, J.Z., Kasaii, M.R., Bui, V.T. and Creber, K.A., 1998. Characterization of deacetylated chitosan and chitosan molecular weight review. Canadian Journal of Chemistry, 76(11), pp.1699.

84. Kokubo, T. and Takadama, H., 2006. How useful is SBF in predicting in vivo bone bioactivity? Biomaterials, 27(15), pp.2907-2915.

85. Krishnan, V., Bhatia, A. and Varma, H., 2016. Development, characterization and comparison of two strontium doped nano hydroxyapatite molecules for enamel repair/regeneration. Dental Materials, 32(5), pp.646-659.

86. Kuo, S.M., Chang, S.J., Chen, T.W. and Kuan, T.C., 2006. Guided tissue regeneration for using a chitosan membrane: an experimental study in rats. Journal of Biomedical Materials Research Part A: An Official Journal of The Society for Biomaterials, The Japanese Society for Biomaterials, and The Australian Society for Biomaterials and the Korean Society for Biomaterials, 76(2), pp.408-415.

87. Lallana, E., Riguera, R. and Fernandez-Megia, E., 2011. Reliable and efficient procedures for the conjugation of biomolecules through Huisgen azide–alkyne cycloadditions. Angewandte Chemie International Edition, 50(38), pp.8794-8804.

88. Lee, E.J., Shin, D.S., Kim, H.E., Kim, H.W., Koh, Y.H. and Jang, J.H., 2009. Membrane of hybrid chitosan–silica xerogel for guided bone regeneration. Biomaterials, 30(5), pp.743-750.

89. Leong, M. F.; Rasheed, M. Z.; Lim, T. C. & Chian, K. S., 2008. Invitro cell infiltration and invivo cell in filtration and vascularization in fibrous highly porous poly (D,L-Lactic acid) scaffold fabrication by electrospining technique. J. Biomed. Res. A, 91, pp. 231-240.

90. Li, W. J. & Tuan R. S. (2009). Fabrication and application of nanofibrous scaffolds in tissue engineering. Curr. Protoc. Cell. Biol. 25 Unit 25.2

91. Li, Y., Feng, Z., Hao, L., Huang, L., Xin, C., Wang, Y., Bilotti, E., Essa, K., Zhang, H., Li, Z. and Yan, F., 2020. A Review on Functionally Graded Materials and Structures via Additive Manufacturing: From Multi-Scale Design to Versatile Functional Properties. Advanced Materials Technologies, 5(6), p.1900981.

92. Li, Z.Y., Lam, W.M., Yang, C., Xu, B., Ni, G.X., Abbah, S.A., Cheung, K.M.C.K., Luk, D.K. and Lu, W.W., 2007.Chemical composition, crystal size and lattice structuralchanges after incorporation of strontium into biomimetic apatite. Biomaterials, 28, pp.1452–60.

93. Liao, S., Wang, W., Uo, M., Ohkawa, S., Akasaka, T., Tamura, K., Cui, F. and Watari, F., 2005. A three-layered nano-carbonated hydroxyapatite/collagen/PLGA composite membrane for guided tissue regeneration. Biomaterials, 26(36), pp.7564-7571.

94. Lim, J.Y., Dreiss, A.D., Zhou, Z., Hansen, J.C., Siedlecki, C.A., Hengstebeck, R.W., Cheng, J., Winograd, N. and Donahue, H.J., 2007. The regulation of integrin-mediated osteoblast focal adhesion and focal adhesion kinase expression by nanoscale topography. Biomaterials, 28(10), pp.1787-1797.

95. Lindhe, J., Nyman, S. and Karring, T., 1984. Connective tissue reattachment as related to presence or absence of alveolar bone. Journal of clinical periodontology, 11(1), pp.33-40.

96. Liou, S.M.K.C.C., Chuang, C.L. and Wang, Y.J., 2001. Studies of the effects of PVA-AE on dentinal bonding of HEMA. Journal of Medical and Biological Engineering, 21(4), pp.243-248.

97. Listgarten, M.A. and Rosenberg, M.M., 1979. Histological study of repair following new attachment procedures in human periodontal lesions. Journal of periodontology, 50(7), pp.333-344

98. Liu, X. and Wang, S., 2014. Three-dimensional nano-biointerface as a new platform for guiding cell fate. Chemical Society Reviews, 43(8), pp.2385-2401.

99. Loubaki, E., Ourevitch, M. and Sicsic, S., 1991. Chemical modification of chitosan by glycidyl trimethylammonium chloride. Characterization of modified chitosan by 13C-and 1H-NMR spectroscopy. European Polymer Journal, 27(3), pp.311-317.

100. Loubaki, E., Ourevitch, M., Sicsic, S., 1991. Chemical modification of chitosan by glycidyltrimethylammonium chloride. Characterization of modified chitosan by ^{13}C-and ^{1}H-NMR spectroscopy, Eur. Polym. J. 27, pp.311–317.

101. Lu, C., Miclau, T., Hu, D., Hansen, E., Tsui, K., Puttlitz, C. and Marcucio, R.S., 2005. Cellular basis for age-related changes in fracture repair. Journal of orthopaedic research, 23(6), pp.1300-1307.

102. Luo, J., Wang, X., Xia, B. and Wu, J., 2010. Preparation and characterization of quaternized chitosan under microwave irradiation. Journal of Macromolecular Science, Part A: Pure and Applied Chemistry, 47(9), pp.952-956.

103. Ma, Z., Kotaki, M., Inai, R. & Ramakrishna, S., 2005. Potential of nanofiber matrix as tissue-engineering scaffolds, Tissue Engineering, 11, pp.101–109.

104. Malkoch, M., Vestberg, R., Gupta, N., Mespouille, L., Dubois, P., Mason, A.F., Hedrick, J.L., Liao, Q., Frank, C.W., Kingsbury, K. and Hawker, C.J., 2006. Synthesis of well-defined hydrogel networks using click chemistry. Chemical Communications, (26), pp.2774-2776.

105. Mandal, B. B. & Kundu, S. C., 2009. Cell proliferation and migration in silk fibroin 3D scaffolds. Biomaterials, 30, pp.2956-2965.

106. Mandal, B. B. & Kundu, S. C. (2009b). Osteogenic and adipogenic differentiation of rat bone marrow cells on non-mulberry and mulberry silk gland fibroin 3D scaffolds. Biomaterials, 30, 5019–5030.

107. Mansour H, Sadahira C, Souza A, Mansur A (2008). FTIR spectroscopy characterization of poly (vinylalcohol) hydrogel with differenthydrolysis degree and chemically with glutaraldehyde. Mat. Sci. Eng. C. 28:539–548.

108. Martien, R., Loretz, B., Thaler, M., Majzoob, S. and Bernkop-Schnürch, A., 2007. Chitosan–thioglycolic acid conjugate: an alternative carrier for oral nonviral gene delivery?. Journal of biomedical materials research Part A, 82(1), pp.1-9.

109. Mather, B.D., Viswanathan, K., Miller, K.M. and Long, T.E., 2006. Michael addition reactions in macromolecular design for emerging technologies. Progress in Polymer Science, 31(5), pp.487-531.

110. Matsumoto, K., Nakamura, T.A.I.S.U.O., Shimizu, Y.A.S.U.H.K.O., Ueda, H., Sekine, T., Yamamoto, Y., Kiyotani, T.E.I.S.U.Y.A. and Takimoto, Y.U.K.I.N.O.B.U., 1999. A novel surgical material made from collagen with high mechanical strength: a collagen sandwich membrane. ASAIO journal (American Society for Artificial Internal Organs: 1992), 45(4), pp.288-292.

111. Matthews, J. A.; Wnek, G. E.; Simpson, D. G. & Bowlin G. L. (2002). Electrospinning of collagen nanofibers. Biomacromolecules 3, 232-238.

112. Melcher, A.H., 1976. On the repair potential of periodontal tissues. Journal of periodontology, 47(5), pp.256-260.

113. Melcher, A.H., McCulloch, C.A.G., Cheong, T., Nemeth, E. and Shiga, A., 1987. Cells from bone synthesize cementum-like and bone-like tissue in vitro and may migrate into periodontal ligament in vivo. Journal of periodontal research, 22(3), pp.246-247.

114. Menger, M.M., Laschke, M.W., Orth, M., Pohlemann, T., Menger, M.D. and Histing, T., 2020. Vascularization Strategies in the Prevention of Nonunion Formation. Tissue Engineering Part B: Reviews.

115. Metters, A. and Hubbell, J., 2005. Network formation and degradation behavior of hydrogels formed by Michael-type addition reactions. Biomacromolecules, 6(1), pp.290-301.

116. Mikos, A.G. Lu, L., Temenoff, J.S. and Temmser, J.K. 2004. Synthetic Bioresorbable polymer scaffolds. In: An introduction to material in medicine, Ratner B D, Hoffman A S, Schoen F J, Lemons J E, (Ed.). pp 743, Elsevier Academic Press. USA.

117. Mikos, A. G., Sarakinos, G., Leite, S. M., Vacanti, J. P. and Langer, R. 1993. Laminated three-dimensional biodegradable foams for use in tissue engineering. Biomaterials, 14, pp.323-330.

118. Min, Z. and Shigehiro, H., 1995. Novel N-unsaturated fatty acyl and N-trimethylacetyl derivatives of chitosan. Carbohydr Polym, 26, pp.205-209

119. Miyazaki, S., Ishii, K. and Nadai, T., 1981. The use of chitin and chitosan as drug carriers. Chem. Pharm. Bull., 29, pp. 3067-69.

120. Nagy, P., 2013. Kinetics and mechanisms of thiol–disulfide exchange covering direct substitution and thiol oxidation-mediated pathways. Antioxidants & redox signaling, 18(13), pp.1623-1641.

121. Nauth, A., McKee, M.D., Einhorn, T.A., Watson, J.T., Li, R. and Schemitsch, E.H., 2011. Managing bone defects. Journal of orthopaedic trauma, 25(8), pp.462-466.

122. Nguyen, A.T., Sathe, S.R. and Yim, E.K., 2016. From nano to micro: topographical scale and its impact on cell adhesion, morphology and contact guidance. Journal of Physics: Condensed Matter, 28(18), p.183001.

123. Nielsen, F.F., Karring, T. and Gogolewski, S., 1992. Biodegradable guide for bone regeneration: polyurethane membranes tested in rabbit radius defects. Acta Orthopaedica Scandinavica, 63(1), pp.66-69

124. Nimmo, C.M., Owen, S.C. and Shoichet, M.S., 2011. Diels− Alder click cross-linked hyaluronic acid hydrogels for tissue engineering. Biomacromolecules, 12(3), pp.824-830.

125. Nyman, R., Magnusson, M., Sennerby, L., Nyman, S. and Lundgren D., 1995. Membrane guided bone regeneration. Segmental radius defects studied in the rabbit. Acta Orthop Scand, 66, pp.169-173.

126. Nyman, S., Karring, T., Lindhe, J. and Plantén, S., 1980. Healing following implantation of periodontitis-affected roots into gingival connective tissue. Journal of clinical periodontology, 7(5), pp.394-401.

127. Nyman, S., Lindhe, J., Karring, T. and Rylander, H., 1982. New attachment following surgical treatment of human periodontal disease. Journal of clinical periodontology, 9(4), pp.290-296

128. Ogiso, B., Hughes, F.J., Melcher, A.H. and McCulloch, C.A., 1991. Fibroblasts inhibit mineralised bone nodule formation by rat bone marrow stromal cells in vitro. J Cell Physiol., 146, pp.442-450.

129. Ohkawa, K., Cha, D., Kim, H., Nishida, A. & Yamamoto, H., 2004. Electrospinning of Chitosan. Macromolecular Rapid Communications, 25, pp.1600-1605.

130. Ossipov, D.A. and Hilborn, J., 2006. Poly (vinyl alcohol)-based hydrogels formed by "click chemistry". Macromolecules, 39(5), pp.1709-1718.

131. Owston, H.E., Moisley, K.M., Tronci, G., Russell, S.J., Giannoudis, P.V. and Jones, E., 2020. Induced Periosteum-Mimicking Membrane with Cell Barrier and Multipotential Stromal Cell (MSC) Homing Functionalities. International journal of molecular sciences, 21(15), pp.5233

132. Paquette, L.A., Crich, D., Fuchs, P., Molander, G., Van Dyke, A.R. and Jamison, T.F., 2009. Encyclopedia of reagents for organic synthesis. Van Dyke, AR; Jamison, TF.

133. Park, Y.J., Lee, Y.M., Lee, J.Y., Seol, Y.J., Chung, C.P. and Lee, S.J., 2000. Controlled release of platelet-derived growth factor-BB from chondroitin sulfate–chitosan sponge for guided bone regeneration. Journal of controlled release, 67(2-3), pp.385-394.

134. Petti, S., Glendor, U. and Andersson, L., 2018. World traumatic dental injury prevalence and incidence, a meta-analysis—One billion living people have had traumatic dental injuries. Dental traumatology, 34(2), pp.71-86.

135. Pighinelli, L. and Kucharska, M., 2013. Properties of microcrystalline chitosan-calcium phosphate complex composite. Journal of Biomaterials and Nanobiotechnology, 2013

136. Pineda-Castillo, S., Bernal-Ballén, A., Bernal-López, C., Segura-Puello, H., Nieto-Mosquera, D., Villamil-Ballesteros, A., Muñoz-Forero, D. and Munster, L., 2018. Synthesis and characterization of poly (vinyl alcohol)-chitosan-hydroxyapatite scaffolds: a promising alternative for bone tissue regeneration. Molecules, 23(10), pp.2414.

137. Pitaru, S., Tal, H., Soldinger, M., Grosskopf, A., Noff, M., 1988. Partial regeneration of periodontal tissues using collagen barriers. Initial observations in the canine. J Periodontol, 59, pp.380-386.

138. Pitaru, S., Tal, H., Soldinger, M. and Noff, M., 1989. Collagen membranes prevent apical migration of epithelium and support new connective tissue attachment during periodontal wound healing in dogs. Journal of periodontal research, 24(4), pp.247-253

139. Plikk, P., Målberg, S. & Albertsson A. C., 2009. Design of resorbable porous tubular co-polyester scaffolds for use in nerve regeneration. Biomacromolecules, 10(5), pp. 1259-64

140. Pokhrel, S. and Yadav, P.N., 2019. Functionalization of chitosan polymer and their applications. Journal of Macromolecular Science, Part A, 56(5), pp.450-475.

141. Pompe, W., Worch, H., Epple, M., Friess, W., Gelinsky, M., Greil, P., Hempel, U., Scharnweber, D. and Schulte, K.J.M.S., 2003. Functionally graded materials for biomedical applications. Materials Science and Engineering: A, 362(1-2), pp.40-60.

142. Pounder, R.J., Stanford, M.J., Brooks, P., Richards, S.P. and Dove, A.P., 2008. Metal free thiol–maleimide 'Click'reaction as a mild functionalisation strategy for degradable polymers. Chemical communications, (41), pp.5158-5160.

143. Qasim, S.B., Delaine-Smith, R.M., Fey, T., Rawlinson, A. and Rehman, I.U., 2015. Freeze gelated porous membranes for periodontal tissue regeneration. Acta biomaterialia, 23, pp.317-328.

144. Queiroz, T.P., Hochuli-Vieira, E., Gabrielli, M.A.C. and Cancian, D.C.J., 2006. Use of bovine bone graft and bone membrane in defects surgically created in the cranial vault of rabbits. Histologic comparative analysis. International Journal of Oral & Maxillofacial Implants, 21(1).

145. R.A.A. Muzzarelli, F. Tanfani, (1985) The N-permethylation of chitosan and the preparation of N-trimethyl chitosan iodide, Carbohydr. Polym., 5, pp.297–307.

146. Ratner, B.D., 2019. Biomaterials: Been there, done that, and evolving into the future. Annual review of biomedical engineering, 21, pp.171-191.

147. Reneker, D. H. & Chun, I. (1996). Nanometer diameter fibres of polymer, produced by electrospinning Nanotechnology, 7, 216-223.

148. Ritsilä, V.A., Santavirta, S., Alhopuro, S., Poussa, M., Jaroma, H., Rubak, J.M., Eskola, A., Hoikka, V., Snellman, O. and Osterman, K., 1994. Periosteal and perichondral grafting in reconstructive surgery. Clinical orthopaedics and related research, (302), pp.259-265.

149. Roberto-Rodrigues, M., Fernandes, R.M.P., Senos, R., Scoralick, A.C.D., Bastos, A.L., Santos, T.M.P., Viana, L.P., Lima, I., Guzman-Silva, M.A. and Kfoury-Júnior, J.R., 2015. Novel rat model of nonunion fracture with vascular deficit. Injury, 46(4), pp.649-654.

150. Rodriguez, I.A., Selders, G.S., Fetz, A.E., Gehrmann, C.J., Stein, S.H., Evensky, J.A., Green, M.S. and Bowlin, G.L., 2018. Barrier membranes for dental applications: A review and sweet advancement in membrane developments. Mouth Teeth, 2(1), pp.1-9.

151. Ruihua, H., Bingchao, Y., Zheng, D. and Wang, B., 2012. Preparation and characterization of a quaternized chitosan. Journal of Materials Science, 47(2), pp.845-851.

152. Rynkowska, E., Fatyeyeva, K., Marais, S., Kujawa, J. and Kujawski, W., 2019. Chemically and Thermally Crosslinked PVA-Based Membranes: Effect on Swelling and Transport Behavior. Polymers, 11(11), p.1799.

153. Sam, G. and Pillai, B.R.M., 2014. Evolution of barrier membranes in periodontal regeneration-"are the third generation membranes really here?. Journal of clinical and diagnostic research: JCDR, 8(12), p.ZE14.

154. Sarmento, B., Goycoolea, F.M., Sosnik, A. and das Neves, J., 2011. Chitosan and chitosan derivatives for biological applications: chemistry and functionalization.

155. Saul, J.M. and Williams, D.F., 2013. Handbook of Polymer Applications in Medicine and Medical Devices: 12. Hydrogels in Regenerative Medicine. Elsevier Inc. Chapters.

156. Schenk RK, Buser D, Hardwick WR, Dahlin C: Healing pattern of bone regeneration in membrane-protected defects: a histologic study in the canine mandible. Int J Oral Maxillofac Implants 1994, 9:13-29.

157. Schoof, H.; Apel, J.; Heschel, I. & Rau, G. (2001). Control of pore structure and size in freeze-dried collagen sponges. J. Biomed Mater Res. 58, 352–7.

158. Sculean, A., Nikolidakis, D. and Schwarz, F., 2008. Regeneration of periodontal tissues: combinations of barrier membranes and grafting materials–biological

foundation and preclinical evidence: a systematic review. Journal of clinical periodontology, 35, pp.106-116.

159. Sen, M.K. and Miclau, T., 2007. Autologous iliac crest bone graft: should it still be the gold standard for treating nonunions?. Injury, 38(1), pp.S75-S80.

160. Shi, R., Bi, J., Zhang, Z., Zhu, A., Chen, D., Zhou, X., Zhang, L., Tian, W. 2008. The effect of citric acid on the structural properties and cytotoxicity of the polyvinyl alcohol/starch films when molding at high temperature. Carbohydr. Polym, 74, pp. 763–770.

161. Shin, S.Y., Park, H.N., Kim, K.H., Lee, M.H., Choi, Y.S., Park, Y.J., Lee, Y.M., Ku, Y., Rhyu, I.C., Han, S.B. and Lee, S.J., 2005. Biological evaluation of chitosan nanofiber membrane for guided bone regeneration. Journal of periodontology, 76(10), pp.1778-1784.

162. Stewart, S., Bryant, S.J., Ahn, J. and Hankenson, K.D., 2015. Bone regeneration. In translational regenerative medicine (pp. 313-333). Academic Press.

163. Su, W.T., Chiou, W.L., Yu, H.H. and Huang, T.Y., 2016. Differentiation potential of SHEDs using biomimetic periosteum containing dexamethasone. Materials Science and Engineering: C, 58, pp.1036-1045.

164. Sukigara, S., Gandhi, M., Ayutsede, J., Micklus, M. & Ko, F. (2003). Regeneration of Bombyx mori silk by electrospinning—part 1: processing parameters and geometric properties. Polymer, 44, 5721–5727.

165. Suresh Kumar, N., Padma Suvarna, R., Chandra Babu Naidu, K., Banerjee, P., Ratnamala, A. and Manjunatha, H., 2020. A review on biological and biomimetic materials and their applications. Applied Physics A, 126, pp.1-18.

166. Tang, Y., Zhao, K., Hu, L. and Wu, Z., 2013. Two-step freeze casting fabrication of hydroxyapatite porous scaffolds with bionic bone graded structure. Ceramics International, 39(8), pp.9703-9707.

167. Tarlochan, F., 2012. Functionally graded material: a new breed of engineered material. J Appl Mech Eng, 1, pp.1-2.

168. Teng, S.H., Lee, E.J., Yoon, B.H., Shin, D.S., Kim, H.E. and Oh, J.S., 2009. Chitosan/nanohydroxyapatite composite membranes via dynamic filtration for guided bone regeneration. Journal of Biomedical Materials Research Part A: 88(3), pp.569-580

169. Teodorescu, M., Bercea, M. and Morariu, S., 2019. Biomaterials of PVA and PVP in medical and pharmaceutical applications: Perspectives and challenges. Biotechnology advances, 37(1), pp.109-131.

170. Theiss, F., Apelt, D., Brand, B., Kutter, A., Zlinszky, K., Bohner, M., Matter, S., Frei, C., Auer, J.A. and Von Rechenberg, B., 2005. Biocompatibility and resorption of a brushite calcium phosphate cement. Biomaterials, 26(21), pp.4383-4394.

171. Toh, W.S., Lee, E.H., Guo, X.M., Chan, J.K., Yeow, C.H., Choo, A.B. and Cao, T., 2010. Cartilage repair using hyaluronan hydrogel-encapsulated human embryonic stem cell-derived chondrogenic cells. Biomaterials, 31(27), pp.6968-6980.

172. Tsui-Chu, Y., Cheng-Chun, C. and Chin-Fung, L, 2005. Antibacterial activity of N-alkylated disaccharide chitosan derivatives. Int J Food Microbiol, 97, pp. 237-45.

173. Tubbs, R.K., 1966. Sequence distribution of partially hydrolyzed poly (vinyl acetate). Journal of Polymer Science Part A-1: Polymer Chemistry, 4(3), pp.623-629.

174. Velayudhan, S., Ramesh, P., Varma, H.K., Schmitt, S. and Friedrich, K., 2007. Stamp forming of hydroxyapatite filled ethylene vinyl acetate co-polymers: Process optimization using a right angle V-mould. Composites Part A: Applied science and manufacturing,38(6), pp.1621-9.

175. Villar, C.C. and Cochran, D.L., 2010. Regeneration of periodontal tissues: guided tissue regeneration. Dental Clinics, 54(1), pp.73-92.

176. Wang, H.L. and Carroll, W.J., 2001. Guided bone regeneration using bone grafts and collagen membranes. Quintessence international, 32(7).

177. Wang, M., Nasiri, A.R., Broadus, A.E. and Tommasini, S.M., 2015. Periosteal PTHrP regulates cortical bone remodeling during fracture healing. Bone, 81, pp.104-111.

178. Wei, Q., Wang, Y., Li, X., Yang, M., Chai, W. and Wang, K., 2016. Study the bonding mechanism of binders on hydroxyapatite surface and mechanical properties for 3DP fabrication bone scaffolds. Journal of the mechanical behavior of biomedical materials, 57, pp.190-200.

179. Wei, Y., Zhang, X., Song, Y., Han, B., Hu, X., Wang, X., Lin, Y. and Deng, X., 2011. Magnetic biodegradable Fe3O4/CS/PVA nanofibrous membranes for bone regeneration. Biomedical Materials, 6(5), pp.055008.

180. Wen, Y., Li, F., Li, C., Yin, Y. and Li, J., 2017. High mechanical strength chitosan-based hydrogels cross-linked with poly (ethylene glycol)/polycaprolactone micelles for the controlled release of drugs/growth factors. Journal of Materials Chemistry B, 5(5), pp.961-971.

181. Wenshui, X., Ping, L., Jiali, Z. and Jie, C., 2011. Biological activities of chitosan and chitooligosaccharides. Food Hydrocolloids,25, pp.170-79.

182. Wu, Z., Li, L., Mu, Y. and Wan, X., 2017. Synthesis and Adhesive Property Study of a Mussel-Inspired Adhesive Based on Poly (vinyl alcohol) Backbone. Macromolecular Chemistry and Physics, 218(16), pp.1700206.

183. Xianmiao, C., Yubao, L., Yi, Z., Li, Z., Jidong, L. and Huanan, W., 2009. Properties and in vitro biological evaluation of nano-hydroxyapatite/chitosan membranes for bone guided regeneration. Materials Science and Engineering: C, 29(1), pp.29-35.

184. Xu, J., Filion, T.M., Prifti, F. and Song, J., 2011. Cytocompatible Poly (ethylene glycol)-co-polycarbonate Hydrogels Cross-Linked by Copper-Free, Strain-Promoted Click Chemistry. Chemistry–An Asian Journal, 6(10), pp.2730-2737.

185. Xu, K., Cantu, D.A., Fu, Y., Kim, J., Zheng, X., Hematti, P. and Kao, W.J., 2013. Thiol-ene Michael-type formation of gelatin/poly (ethylene glycol) biomatrices for three-dimensional mesenchymal stromal/stem cell administration to cutaneous wounds. Acta biomaterialia, 9(11), pp.8802-8814.

186. Yu, F., Cao, X., Zeng, L., Zhang, Q. and Chen, X., 2013. An interpenetrating HA/G/CS biomimic hydrogel via Diels–Alder click chemistry for cartilage tissue engineering. Carbohydrate polymers, 97(1), pp.188-195.

187. Yu, Y., Deng, C., Meng, F., Shi, Q., Feijen, J. and Zhong, Z., 2011. Novel injectable biodegradable glycol chitosan-based hydrogels crosslinked by Michael-type addition reaction with oligo (acryloyl carbonate)-b-poly (ethylene glycol)-b-oligo (acryloyl carbonate) copolymers. Journal of Biomedical Materials Research Part A, 99(2), pp.316-326.

188. Yvon, H.J., 2017. Raman spectroscopy for analysis and monitoring. Raman Data and Analysis, 1, 2.

189. Zeng, S., Fu, S., Guo, G., Liang, H., Qian, Z., Tang, X. and Luo, F., 2011. Preparation and characterization of nano-hydroxyapatite/poly (vinyl alcohol) composite membranes for guided bone regeneration. Journal of biomedical nanotechnology, 7(4), pp.549-557.

190. Zhang, X., Xie, C., Lin, A.S., Ito, H., Awad, H., Lieberman, J.R., Rubery, P.T., Schwarz, E.M., O'Keefe, R.J. and Guldberg, R.E., 2005. Periosteal progenitor cell fate in segmental cortical bone graft transplantations: implications for functional tissue engineering. Journal of Bone and Mineral Research, 20(12), pp.2124-2137.

191. Zheng, J., Smith Callahan, L.A., Hao, J., Guo, K., Wesdemiotis, C., Weiss, R.A. and Becker, M.L., 2012. Strain-promoted cross-linking of PEG-based hydrogels via copper-free cycloaddition. ACS macro letters, 1(8), pp.1071-1073.

192. Zitzmann, N.U., Naef, R. and Schärer, P., 1997. Resorbable versus nonresorbable membranes in combination with Bio-Oss for guided bone regeneration. International Journal of Oral & Maxillofacial Implants, 12(6).

193. Zou, X., Zhao, X. and Ye, L., 2015. Synthesis of cationic chitosan hydrogel and its controlled glucose-responsive drug release behavior. Chemical Engineering Journal, 273, pp.92-100.

APPENDIX

1. Phosphate buffered Saline – 1 L , pH7.4

NaCl	8 g
KCl	0.2 g
Na_2HPO_4	1.15 g
KH_2PO_4	0.2 g
H_2O	1 L (Deionised)

2. Simulated body fluid - 1L, pH7.4

Sodium Chloride: 8.05g

Sodium carbonate: 0.355g

Potassium Chloride: 0.225 g

Dipotassium hydrogen phosphate: 0.261g

Magnesium Chloride hexahydrate: 0.311g

1 M Hydrochloric acid: 35 ml

Calcium Chloride Dihydrate: 0.55 g

Sodium Sulphate: 0.072 g

Tris: 6.60 g

CURRICULUM VITAE

PERSONAL DETAILS

Name	:	Adarsh R.K.
Date of birth	:	04/04/1990
Address	:	Santhi Bhavan, Kallar P. O., Vithura, TVPM-695551
Phone number	:	8893037899
E-mail	:	adarshkallar44@gmail.com

PRESENT OCCUPATION;

Currently working as Technical assistant in Drug Testing Laboratory, Drug Control Department, Thiruvananthapuram since 20th November 2020.

ACADEMIC PROFILE

Bachelor of Science (BSc) Chemistry	University of Kerala, March, 2012
Master of Science (MSc) Chemistry	University of Kerala, July 2014
Ph D	Since June 2016

RESEARCH EXPERIENCE

- Worked as **Project assistant** at **Polymer division** in an Inspire funded project entitled **"Polymeric *Nano capsules for targeted protein delivery*"** (15/11/2014 to 27/06/2016)
- Joined for **PhD program** at **Division of Bioceramics** (joined on 29/06/2016)
- Worked as **Project assistant** at **Division of Bioceramics** (11/08/2016 to 23/05/2017).
- Worked as **JRF** at **Division of Bioceramics** (25/05/2017 to 24/05/2019)
- Worked as **SRF** at **Division of Bioceramics** (25/05/2019 to 19/11/2020)

EXPERTISE WIH EQUIPMENTS

1. X-ray diffractometer
2. Fourier Transform Infrared spectrometer
3. UV-Visible spectrophotometer
4. Fluorimeter
5. *Gel permeation chromatography*
6. High-performance liquid chromatography
7. Goniometer

PUBLICATION DETAILS:

- **PhD Programme**

1. Alex G. Varghese, **Adarsh R K,** Nishad KV and Manoj Komath*, *In vitro* evaluation of the enamel remineralization potential of a dentifrice containing nano calcium strontium apatite, Trends Biomater. Artif. Organs 33 (2019) 56.
2. **R K Adarsh**, Najeema Sulaiman S, Sadasivan A, Joseph R, Komath M*. Porous membranes of quaternized chitosan composited with strontium-based nanobioceramic for periodontal tissue regeneration. Journal of Biomaterials Applications. 2022;36(7):1254-68.)
3. **Adarsh R K**, Das EC, Gopan GV, Rajan RK, Komath M*. Quaternised chitosan composites with in situ precipitated nano calcium phosphate for making bioactive and degradable tissue engineering scaffolds. Journal of Polymer Research. 2022;29(7):1-9.
4. **R K. Adarsh**, Eva C. Das, Gopika V. Gopan, Shivaram Selvam, and Manoj Komath*. Functionally Graded Bioactive Composites Based on Poly(vinyl alcohol) Made through Thiol−Ene Click Reaction. ACS omega. 2022;7(33):29246-29255

- **MSc. Chemistry Programme (Published 1 paper)**

1. Ratheesh S Nair, Ani Deepthi*, **Adarsh K**, Sidharth Chopra. A comparative study on the isolation and cerium (IV) ammonium nitrate mediated oxidative transformation of oleanolic acid and ursolicacid. Indian Journal of Chemistry. 2016; 55:598-603A

- **INSPIRE project period (Published 3 papers)**

1. Girija Seetharaman, **Adarsh R. Kallar**, Vineeth Vijayan, Jayabalan Muthu, Shivaram Selvam*, Design, preparation and characterization of pH-responsive prodrug micelles with hydrolyzable anhydride linkages for controlled drug delivery. Journal of colloid and interface science. 2017;492: 61-72

2. **Adarsh R. Kallar**, Jayabalan Muthu, Shivaram Selvam*, Bioreducible amino acid-derived polymeric nanoparticles for delivery of functional proteins. Colloids and Surfaces B: Biointerfaces. 2018;164:396-405
3. Anjana V. Latha, Manikandan Ayyappan, **Adarsh R. Kallar**, Reesha V. Kakkadavath, Sunita P. Victor, Shivaram Selvam. Fluorescence imaging of nitric oxide in living cells using o-phenylenediamine-rhodamine based polymeric nanosensors. Materials Science and Engineering: C. 2020 Mar 1;108:110463

ACHIEVEMENTS

Best poster presentation award, National Conference on Recent Trends In Materials Science and Technology (NCMST 2019); 18-20 December; IIST Valiamala Thiruvananthapuram.

CONFERENCES ATTENDED

1. International conference on BioMaterials, BioEngineering, and BioTheranostics (BioMET 2018) 24th-28th July, 2018;Vellore Institute of Technology, Vellore. (Poster Presentation)
2. First Indian Materials Conclave and 30th Annual General Meeting of MRSI; 12 - 15 Feb 2019; Indian Institute of Science, Bengaluru, India. (Poster Presentation)
3. 3rd International conference on advanced functional materials (ICAFM2019);9-10 December 2019; CSIR-NIIST, Thiruvananthapuram.
4. National Conference on Recent Trends In Materials Science and Technology (NCMST 2019); 18-20 December; IIST Valiamala Thiruvananthapuram (Best Poster award)